



ESCUELA POLITÉCNICA NACIONAL

DOCTORADO EN CIENCIAS DE LA MECÁNICA

**AGRO-INDUSTRIAL RESIDUES AND IRON OXIDE
NANOPARTICLES FOR THE REMOVAL OF CAFFEINE
AND TRICLOSAN IN BATCH ADSORPTION AND
FILTRATION/BIONFILTRATION PROCESSES**

**DOCTORAL THESIS FOR AWARDING THE DEGREE OF DOCTOR OF
MECHANICAL SCIENCE**

CRISTINA ELIZABETH ALMEIDA NARANJO

ADVISOR: VÍCTOR H. GUERRERO

**CO-ADVISORS: CRISTINA ALEJANDRA VILLAMAR
CAMILO ZAMORA-LEDEZMA**

Quito, August 2023

DECLARACIÓN DE AUTORÍA

Yo, Cristina Elizabeth Almeida Naranjo, declaro bajo juramento que el trabajo aquí descrito es de mi autoría; que no ha sido previamente presentado para ningún grado o calificación profesional; y, que he consultado las referencias bibliográficas que se incluyen en este documento.

A través de la presente declaración cedo mis derechos de propiedad intelectual correspondientes a este trabajo, a la Escuela Politécnica Nacional, según lo establecido por la Ley de Propiedad Intelectual, por su Reglamento y por la normatividad institucional vigente.

Cristina Elizabeth Almeida Naranjo

Versión Aprobada para Defensa Oral

To my dad, who now has his own wings, and to my earthly angels: Amira, Wladimir, Andrea, Mishelle, and Teresa, for being the love and inspiration of my life.

To all the other people who were given wings by the pandemic and those who suffered their departure.

Versión Aprobada para Defensa Oral

ACKNOWLEDGEMENT

To God, for allowing me to achieve this goal even in difficult times.

To my advisor and co-advisors, for their unwavering commitment and invaluable contributions to my growth as a researcher. Special gratitude goes to Alejandra, who has consistently shown me the beauty of research and helped me see beyond the obvious. Her guidance, support, and unwavering friendship have been indispensable, enabling me to experience research from different parts of the world.

To the manuscript reviewers, for generously dedicating their time, willingness, and providing valuable comments.

To the Faculties of Mechanical Engineering, Chemical Engineering, and Environmental Engineering, with a special mention to the latter two. Despite not being their doctoral student, they have always been ready to offer assistance. My professors and colleagues have generously shared their knowledge, and I extend my gratitude to Francis for her constant support and care. A heartfelt thanks to Salomé, Orlando, Karina, and Patricia for their dedication, hard work, and goodwill. I am also grateful to Camilito, Mr. Byron, Mr. Wilson, and Mr. Luchito for their unwavering assistance. Edwin, thank you for sharing your doctorate experiences with me.

To my family:

To my Amira, who serves as my constant motivation. Despite not fully comprehending my pursuits, she continues to believe in me, even during times of mistakes and limited time. To my daddy, your love, unwavering support, teachings, and enduring inspiration have shaped me. Wlady, your infinite patience, love, and support have been my pillars throughout this journey. To my mom, thank you for your backing and for standing by me as I chase my dreams. My younger sisters, undoubtedly my strongest allies, I am grateful for your unwavering support. To Mery and Willer, your presence for Amira has granted me the time to pursue my aspirations.

To my friends:

Pauly, Gaby, Andre, Lois, Mayritas, Mony, Lucy, Belén, and César, your words of encouragement and affection have been a constant source of strength. A special mention to Andre, George, and Vladi, who have illuminated even my darkest moments.

To my students:

Mayrita, Jennifer T., Joha, Jeniffer C., Vane, Henry, Gene, Bryan, Nicole, Fabricio, Mauri, Gonzalo, and Francisco, your pivotal role in this journey cannot be overstated. Your diligence, hard work, patience, and warmth have been an integral part of this process.

Contents

Abstract	1
Presentation	6
1. Literature review	8
1.1. Emerging contaminants	8
1.1.1. Pharmaceuticals and Personal Care Products (PPCPs).....	10
1.1.2. Pesticides	11
1.1.3. Steroid hormones.....	11
1.1.4. Other emerging contaminants.....	12
1.1. Alternatives to remove ECs	15
1.1.1. Adsorption process in the removal of ECs	17
1.2. Materials used to remove ECs from water in the batch adsorption process.....	17
1.2.1. Conventional materials	18
1.2.2. Inorganic non-conventional materials	22
1.2.3. Organic non-conventional materials.....	25
1.2.4. Nanomaterials.....	30
1.3. Technologies using materials to remove ECs from wastewater.....	37
1.3.1. Filtration technologies	37
1.3.2. Biofiltration	38
2. Hypotheses and Objectives	44
2.1. Hypotheses.....	44
2.2. General Objective	44
2.3. Specific objectives	44
2.4. Research challenges.....	45
3. Optimization of variables to remove caffeine and triclosan in batch adsorption processes using residues and composites.....	47
2.1. Batch adsorption processes using agro-industrial residues	47
Article 1. Caffeine/triclosan removal from synthetic solutions using rice husk in batch and fixed bed columns	49
Article 2. Peanut shells: characterization and performance in adsorption of caffeine and triclosan	65
3.4. Batch adsorption processes using residues and their magnetic composites	77
Article 3. Caffeine removal from synthetic wastewater using magnetic fruit peel composites: material characterization, isotherm and kinetic studies	78
Article 4. Triclosan/Caffeine removal using coconut fiber, corn cob, and magnetic corn cob in batch process and filter bed columns.....	93
4. Optimization of operational parameters and configuration in continuous filtration processes used to remove contaminants from water	115
Article 5. Caffeine and triclosan removal using corn cob biofilters (large columns)	117

Article 6. Caffeine adsorptive performance and compatibility characteristics (<i>Eisenia foetida</i> (<i>Savigny</i>)) of agro-industrial residues potentially suitable for vermifilter beds	134
Article 7. Performance of wood chips/peanut shells biofilters used to remove organic matter from domestic wastewater	147
5. Conclusions and outlook.....	158
REFERENCES	160

Versión Aprobada para Defensa Oral

List of Tables

Table 1.	Physical and chemical characteristics of some ECs and their concentrations in water bodies.	14
Table 2.	Conventional materials used for ECs removal from synthetic water in the batch adsorption process.	20
Table 3.	Inorganic non-conventional materials in ECs removal using synthetic water in the batch adsorption process.	23
Table 4.	Organic non-conventional materials used for EC removal from synthetic water in the batch adsorption process.	27
Table 5.	Nanoparticles used in ECs removal using synthetic water in the batch adsorption process.	34
Table 6.	Filtration/Biofiltration technologies using materials to remove ECs from wastewater.	41
Table 7.	Characteristics of caffeine and triclosan.	48
Table 8.	Kinetics model parameters for caffeine and triclosan adsorption.	59
Table 9.	Adsorption isotherm model parameters for caffeine and triclosan adsorption.	61
Table 10.	Adsorption isotherm model parameters for caffeine and triclosan adsorption.	63
Table 11.	Adsorption isotherm model parameters for caffeine and triclosan adsorption.	63
Table 12.	Chemical composition of peanut shells.	69
Table 13.	Parameters for non-linear adsorption kinetic models for caffeine and triclosan removal.	74
Table 14.	Parameters for the non-linear Langmuir, Freundlich and Sips adsorption models for caffeine and triclosan removal.	76
Table 15.	Chemical composition of peanut shells.	81
Table 16.	Surface area, pore volume and pore diameter of adsorbents.	84
Table 17.	Kinetic parameters calculated from pseudo-first-order, pseudo-second-order and Elovich models for the adsorption of caffeine.	88
Table 18.	Kinetic parameters calculated from intraparticle diffusion model for caffeine adsorption.	89
Table 19.	Isotherm parameters calculated from Langmuir, Freundlich, and Sips models.	91
Table 20.	Results of caffeine removal onto different adsorbents.	92
Table 21.	Physical-chemical characteristics of residues.	97
Table 22.	BET analysis of materials.	98
Table 23.	Parameters for the kinetics models fitted for the data obtained for triclosan removal using the CC and CF.	102
Table 24.	Isotherm model using CC and CF in the triclosan removal.	102
Table 25.	Parameter values for the kinetics and isotherm models fitted to the data about triclosan removal using iron oxide and composites.	106
Table 26.	Parameter values for intraparticle diffusion model fitted to the data about triclosan removal using CC, iron oxide and composites.	107
Table 27.	Main results of adsorption experiments in fixed bed columns.	112
Table 28.	Bohart-Adams parameters for caffeine and triclosan adsorption.	113
Table 29.	Physicochemical characteristics of corn cob.	121
Table 30.	Surface area, pore volume and pore diameter of agro-industrial residues.	138
Table 31.	Kinetic parameters for the pseudo-first-order and pseudo-second-order on CAF.	141

Table 32.	Isotherm parameters for the Langmuir and Freundlich models on CAF adsorption at different dose of agro-industrial residues (C0= 30 mg/L, RH dose= 4.0, 8.5 and 50 g/L, PS dose= 10, 17 and 35 g/L, CC dose= 11, 15 and 17 g/L, CF dose= 4, 10 and 12 g/L, for small, medium, and large particles, respectively).....	142
Table 33.	Synthetic domestic wastewater physicochemical characteristics.....	149
Table 34.	Operational strategy for each biofilter. The biofiltration typology (BM, BPM, BEM, HB) and a subscript corresponding to the nominal hydraulic loading rate (0.5, 1.0, 1.5 m ³ /m ² -d) were used to identify each biofilter.	151
Table 35.	Organic support material physicochemical characteristics	152
Table 36.	Compatibility evaluation of peanut shells on <i>Eisenia foetida</i> and <i>Schoenoplectus californicus</i>	153

Versión Aprobada para Defensa Oral

List of Figures

Figure 1.	Routes of entry of ECs into the environment, its behavior and effects.....	9
Figure 2.	Stages/characteristics/technologies or processes used in conventional WRRF. Kestemont & Depiereux, (2013)	16
Figure 3.	Adsorption mechanisms.....	17
Figure 4.	Alternatives to remove ECs	18
Figure 5.	Mechanisms for the EC removal in the batch adsorption process.....	37
Figure 6.	Experimental model.....	46
Figure 7.	Structure of natural fibers	47
Figure 8.	Point of zero charge for the small, medium, and large RH particles.....	54
Figure 9.	TGA curve of rice husk adsorbent. Inset: physical-chemical characterization and proximal analysis.....	54
Figure 10.	SEM analysis, nitrogen adsorption/desorption isotherms of RH, and pore radius distribution.	55
Figure 11.	FTIR spectra for a) caffeine, and b) triclosan, before and after the caffeine/triclosan adsorption. RH small= 120 – 150 μm , RH medium= 300 – 600 μm , RH large= 800 – 2,000 μm	56
Figure 12.	Optimal dose/contact time: a)/b) caffeine removal and c)/d) triclosan removal.	57
Figure 13.	Kinetic models for caffeine and triclosan adsorption in three particle sizes. Black points= experimental data, red line= pseudo-first-order model, blue line= pseudo-second-order model, green line= Elovich model.	58
Figure 14.	Intraparticle diffusion kinetics for adsorption of caffeine and triclosan.	60
Figure 15.	Isotherm models for caffeine and triclosan adsorption in three particle sizes.....	61
Figure 16.	Effect of particle size and contaminant type on breakthrough curve	62
Figure 17.	Thermogravimetric analysis of peanut shell.	69
Figure 18.	FTIR spectra of peanut shell before and after adsorption of caffeine and triclosan. bca= before caffeine adsorption, aca= after caffeine adsorption, bta= before triclosan adsorption, ata= after triclosan adsorption.....	71
Figure 19.	SEM images of small, medium, and large particles, nitrogen adsorption-desorption isotherm and pore radius distribution of small particles	72
Figure 20.	Optimal dose of peanut shells and contact time for the removal of a), c) caffeine and b), d) triclosan. Green line: small particles, blue line: medium particles and red line: medium particles. Caffeine/triclosan concentration= 30 mg/L, stirring rate= 150 rpm.	73
Figure 21.	Adsorption kinetics (a, b) and isotherm models (c, d) for caffeine and triclosan.....	75
Figure 22.	a) Raman spectra and b) FT-IR spectra of adsorbent materials.	82
Figure 23.	XRD analysis of adsorbent materials.....	83
Figure 24.	SEM images and EDS of materials. a) Orange peel, b) banana peel, c) orange peel composite, e) banana peel composite. d) and f) EDS of orange peel composite and banana peel composite, respectively.	85
Figure 25.	Optimal conditions for caffeine removal: a) optimal dose, b) optimal contact time. Black line: orange peel, cyan line: banana peel, blue line: magnetite, orange line: orange peel composite, green line: banana peel composite.	87
Figure 26.	Photographs of the magnetic separation of the composites from the aqueous phase after caffeine adsorption.....	87

Figure 27.	Pseudo-first-order, pseudo-second-order and Elovich kinetic models for adsorption of caffeine.....	89
Figure 28.	Intraparticle diffusion kinetics for adsorption of caffeine.....	90
Figure 29.	Langmuir, Freundlich and Sips isotherm models for adsorption of caffeine.....	91
Figure 30.	SEM images of residues, iron oxide nanoparticles and CC composites.....	98
Figure 31.	a) SEM composite 4CC:1IO, b) TEM iron oxide nanoparticles and c) SAED of iron oxide nanoparticles.....	99
Figure 32.	a) FT-IR and b) Raman spectra of the materials studied.....	100
Figure 33.	Optimal adsorption conditions for triclosan adsorption. a) Optimal dose, b) Optimal contact time. Green line: CC adsorption, orange line: CF adsorption.....	101
Figure 34.	a) Optimal contact time and optimal dose using iron oxide nanoparticles, b) Optimal dose using CC composites; for the triclosan removal.....	104
Figure 35.	a) Kinetics model fitting, b) isotherm model fitting for triclosan removal using iron oxide nanoparticles.....	105
Figure 36.	Fittings to the (a) kinetics, and (b) isotherm models for triclosan removal using CC composites.....	106
Figure 37.	Intraparticle diffusion kinetics for adsorption of triclosan.....	108
Figure 38.	Bangham diffusion model for triclosan.....	109
Figure 39.	Fractional Uptake of triclosan in CC, composites and IO.....	110
Figure 40.	Boyd's diffusion of triclosan in CC, composites and IO.....	111
Figure 41.	Effect of particle size and contaminant type on breakthrough curves.....	113
Figure 42.	Filtration typologies scheme.....	119
Figure 43.	Raw corn cob particles by size. a) Small CC (0.8-2.0 cm), b) Medium CC (2.0-3.5 cm), c) Large CC (3.5-5.7 cm) used in filters.....	120
Figure 44.	FTIR and photography of CC before and after caffeine removal. The CC subscripts represent the location of that material inside the filter.....	122
Figure 45.	a) SEM image and results of BET analysis, b) nitrogen adsorption-desorption isotherm and pore size distribution (inset) for the CC particles (0.8-2.0 cm).....	123
Figure 46.	Filter performance in the removal of caffeine function of time.....	125
Figure 47.	Filter performance in the removal of caffeine. Means with a common letter are not significantly different ($p < 0.05$).....	125
Figure 48.	CC at the saturation with caffeine using an HRL=1 m ³ /m ² -d. a) SPF (204 h), b) MPF (168 h), c) MxPF (138 h) and d) LPF (150 h).....	126
Figure 49.	pH performance in the removal of caffeine by particle size. Dot fuchsia lines= optimal pH range to the microorganism development.....	127
Figure 50.	Hydraulic conductivity and head losses in the removal of caffeine. Black line= 1 m ³ /m ² -d, blue line= 2 m ³ /m ² -d, green line= 4 m ³ /m ² -d. Dot fuchsia lines= optimal range of hydraulic conductivity to avoid clogging.....	129
Figure 51.	Filter performance in the removal of triclosan.....	130
Figure 52.	pH performance in the removal of triclosan. Dot fuchsia lines= optimal pH range to the microorganism development.....	130
Figure 53.	a) Control: MPF feed with drinking water b) MPF at the saturation with triclosan c) MPF duplicated. HRL=2 m ³ /m ² -d.....	131
Figure 54.	a) Hydraulic conductivity and b) head losses in the removal of caffeine and triclosan. Particle size= medium and HLR= 2 m ³ /m ² -d.....	132

Figure 55.	a) Physicochemical composition and b) proximal analysis of agro-industrial residues.	137
Figure 56.	SEM images before CAF adsorption, and FTIR spectra before (blue line) and after CAF adsorption (black line) by agro-industrial residues (small particle size).....	138
Figure 57.	a) – d) Effect of the agro-industrial residue dose and contact time on the CAF adsorption by agro-industrial residue. e) – h) Contact time of the optimal dose = 180 min. Optimal timing dose = optimal dose.	139
Figure 58.	Comparison of CAF removal efficiency using optimal conditions of agro-industrial residue dose and contact time.....	140
Figure 59.	Mortality of <i>Eisenia foetida</i> by each agro-industrial residue.	143
Figure 60.	Influence of components from each agro-industrial residue on the <i>Eisenia foetida</i> growth. ...	145
Figure 61.	Experimental scheme. BM = Biofilter with microorganisms, BEM = Biofilter with microorganisms and <i>Eisenia foetida</i> , BPM = Biofilter with microorganisms and <i>Schoenoplectus californicus</i> , HB = Biofilter with microorganisms, <i>Eisenia foetida</i> and <i>Schoenoplectus californicus</i>	150
Figure 62.	COD effluent concentrations (box-plot) and removal within biofilters (bar chart). a) BM, b) BPM, c) BEM and d) HB. * = Significant statistical differences between hydraulic rates, ** = Significant statistical differences between the biofilter type.....	154
Figure 63.	VS effluent concentrations (box-plot) and removal within biofilters (bar chart). a) BM, b) BPM, c) BEM and d) HB. * = Significant statistical differences between hydraulic rates.	154
Figure 64.	Biofilm, earthworm behavior and allometric measurements within BEMs. a) Biofilm, white box = 0.5 m ³ /m ² -d, light grey box = 1.0 m ³ /m ² -d and grey box = 1.5 m ³ /m ² -d; b) Live weigh, white box = 0.5 m ³ /m ² -d, light grey box = 1.0 m ³ /m ² -d and grey box = 1.5 m ³ /m ² -d; c) Individuals number per age, white box = 0.5 m ³ /m ² -d ¹ Hydraulic rate, light grey box = 1.0 m ³ /m ² -d and grey box = 1.5 m ³ /m ² -d. A= adult earthworms, J = juvenile earthworms, C = cocoons. In the X axis, B= individuals quantity before operation, E= individuals quantity at the end of operation; d) Apical height, white box = 0.5 m ³ /m ² -d, light grey box = 1.0 m ³ /m ² -d and grey box = 1.5 m ³ /m ² -d. Basal diameter, striped white box = 0.5 m ³ /m ² -d, striped light grey box = 1.0 m ³ /m ² -d, striped light grey box = 1.5 m ³ /m ² -d and relative abundance, striped white bar = 0.5 m ³ /m ² -d, striped light grey bar = 1.0 m ³ /m ² -d, striped light grey bar.....	156
Figure 65.	Phenols concentration vs. allometric measurements. a) BPM apical height, b) BPM basal diameter, c) BPM leaves number, d) HB apical height, e) HB basal diameter and f) HB leaves number.	156
Figure 66.	Hydraulic conductivity and head losses. a) BM, b) BPM, c) BEM and d) HB. Black line = 0.5 m ³ /m ² -d Hydraulic loading rate, green line = 1.0 m ³ /m ² -d Hydraulic loading rate and blue line = 1.5 m ³ /m ² -d Hydraulic loading rate.....	157

Abstract

Emerging contaminants, characterized by their low concentration, persistence, and limited regulation, pose global concern due to their potential adverse effects on aquatic life, ecosystems, and human health. Notable examples of emergent pollutants encompass caffeine and triclosan, with caffeine serving as a biomarker and triclosan identified as a toxic endocrine disruptor. Typically, adsorption-based removal techniques have been used to capture both pollutants, mainly employing activated carbon, despite its cost. Also, some organic and inorganic residues have been experimented with but with limited efficiency. This research is aimed to study the preparation, characterization, and environmental applications of agro-industrial residues alongside iron oxide nanoparticles to remove caffeine and triclosan from the aqueous phase. The studied residues encompassed rice husks (RH), peanut shells (PS), coconut fibers (CF), and corn cobs (CC) and were prepared by washing, drying, milling, and sieving. At the same time, iron oxide nanoparticles and composites were synthesized through precipitation. ASTM standards and instrumental techniques like SEM, TEM, BET, FTIR, TGA, and XRD were used for the physical and chemical characterization of the adsorbent materials. Moreover, the particle size, adsorbent dosage, nanoparticle impregnation, and contact duration underwent adjustment in batch adsorption processes, whereas hydraulic loads and filter bed heights were optimized in fixed-bed processes; the latter to find out the optimal experimental conditions and the adsorbents for efficient removal of caffeine and triclosan. Data obtained underwent fitting to conventional models, including kinetics isotherms (batch tests) and breakthrough curves (continuous tests). Additionally, OECD methods were used to evaluate the toxicity of agro-industrial residues using *Eisenia foetida* (Savigni). Experimentally, triclosan's heightened ease of elimination compared to caffeine, irrespective of the selected residue, achieves an adsorption capacity up to 124.7 times higher. This attribute stems from triclosan's lipophilic nature. On the other hand, the efficiency in removing both contaminants was evident with smaller particles (120 -150 μm) due to the higher material surface area. However, these particles presented challenges in continuous adsorption and filtration because of clogging issues (hydraulic conductivity < 100 mm/h). The particle size of the adsorbent was pivotal in fixed-bed column functionality, influencing the available surface area, void fraction, and wastewater pathway. Furthermore, impregnating nanoparticles on agro-industrial residues (at a 1:4 ratio) amplified the adsorption capacity across the batch processes (caffeine 1.7 times, triclosan 6.2 times) and the fixed-bed columns (extended saturation periods: caffeine = 225 min, triclosan = 550 min). The optimal dosage of nanoparticles and composites resulted in lower (between 3.75 and 25 times) than that of the control (CC). Regarding residue toxicity, while coconut fiber demonstrated remarkable caffeine removal (>94%), it showed the highest toxicity (14d-LC50=82%), unlike corn cob, which displayed no toxicity. This toxicity correlation is rooted in the waste's composition, notably the impact of lignin's recalcitrance in carbon availability compared to cellulose and hemicellulose. Consequently, corn cob emerged as a suitable filter medium, achieving over 90% efficiency in caffeine and triclosan removal using a 2 $\text{m}^3/\text{m}^2\text{-d}$ hydraulic load and 2.0 to 3.5 cm particle size. Also, promising results were observed in peanut shells, a prospective adsorbent employed in preliminary evaluations encompassing biofilters, vermifilters, constructed wetlands, and hybrids. These systems demonstrated effective organic matter removal (>80%) with earthworms and plants augmenting biofilter performance (efficiency and hydraulic characteristics).

Based on these results, this research presents a robust and cost-efficient avenue to address the challenges stemming from emerging pollutants across diverse applications and contexts and consequently, filters/biofilters could be trailed within the pharmaceutical wastewater treatment and community settings, extending their utility even by treating agricultural waters with pesticide profiles akin to the contaminants studied.

Keywords: Emerging contaminants, magnetic composites, biofiltration technologies, wastewater treatment.

Versión Aprobada para Defensa Oral

List of abbreviations

EC= emerging contaminant
WRRF=Water Resource Recovery Facility, before named: wastewater treatment plants
nd= non detected
S.O.= Synthetic origin
N.O.= natural origin
CT=contact time [h]
RT=residence time [h]
T= temperature [°C]
AD= adsorbent dose [g/L]
[EC]= Emerging contaminant concentration [mg/L]
FR=Flow rate [mL/min]
HLR= Hydraulic loading rate [cm/h]
GAC= Granular activated carbon
DEET= N,N-diethyl-toluamide
CWs= Constructed wetlands
PT= Plant type
ET= Earthworm type
ED=Earthworm density (worms/m³)
CC= Corn cob
RH= Rice husk
PS= Peanut shells
CF= Coconut fiber

Versión Aprobada para Defensa Oral

List of published articles that were used in writing up the thesis

1. **Almeida-Naranjo, C.E.**, Guerrero, V.H., Villamar-Ayala, C. A. (2023), Emerging contaminants and their removal from aqueous media using conventional/non-conventional adsorbents: A glance at the relationship between materials, processes, and technologies. <https://doi.org/10.3390/w15081626>.
2. **Almeida-Naranjo, C. E.**, Frutos, M., Tejedor, J., Cuestas, J., Valenzuela, F., Rivadeneira, M. I., ... & Guerrero, V. H. (2021). Caffeine adsorptive performance and compatibility characteristics (*Eisenia foetida* (Savigny)) of agro-industrial residues potentially suitable for vermifilter beds. *Science of The Total Environment*, 149666. <https://doi.org/10.1016/j.scitotenv.2021.149666>.
3. **Almeida-Naranjo, C. E.**, Aldás, M. B., Cabrera, G., & Guerrero, V. H. (2021). Caffeine removal from synthetic wastewater using magnetic fruit peel composites: Material characterization, isotherm and kinetic studies. *Environmental Challenges*, 5, 100343. <https://doi.org/10.1016/j.envc.2021.100343>.
4. Tejedor, J., Córdor, V., **Almeida-Naranjo, C. E.**, Guerrero, V. H., & Villamar, C. A. (2020). Performance of wood chips/peanut shells biofilters used to remove organic matter from domestic wastewater. *Science of The Total Environment*, 139589. <https://doi.org/10.1016/j.scitotenv.2020.139589>.
5. **Almeida-Naranjo, C. E.**, Guachamín, G., Guerrero, V. H., & Villamar, C. A. (2020). *Heliconia stricta* Huber Behavior on Hybrid Constructed Wetlands Fed with Synthetic Domestic Wastewater. *Water*, 12(5), 1373. <https://doi.org/10.3390/w12051373>.
6. Chicaiza, C., Huaraca, L., **Almeida-Naranjo, C. E.**, Guerrero, V. H., & Villamar, C. A. (2020). Improvement of organic matter and nutrient removal from domestic wastewater by using intermittent hydraulic rates on earthworm-microorganism biofilters. *Water Science and Technology*, 82(2), 281-291. <https://doi.org/10.2166/wst.2020.139>.
7. León, G. R., Aldás, M. B., Guerrero, V. H., Landáuzuri, A. C., & **Almeida-Naranjo, C. E.** (2019). Caffeine and irgasan removal from water using bamboo, laurel and moringa residues impregnated with commercial TiO₂ nanoparticles. *MRS Advances*, 4(64), 3553-3567. <https://doi.org/10.1557/adv.2020.33>.

List of articles under review that were used in writing up the thesis

1. **Almeida-Naranjo, C.E.**, Cuestas, J., Guerrero, V.H., Villamar-Ayala, C. A., Caffeine and triclosan removal from synthetic solutions using rice husk in batch and fixed bed columns (Under review in the journal: *Polymers*).
2. **Almeida-Naranjo, C.E.**, Frutos M., Guerrero, V.H., Villamar-Ayala, C. A., Peanut shells: characterization and performance in adsorption of caffeine and triclosan (Preparing to be submitted).

Additional scientific productivity on thesis-related topics

1. Almeida-Naranjo, C. E., Morillo, B., Aldás, M. B., Garcés, N., Debut, A., & Guerrero, V. H. (2023). Zinc removal from synthetic waters using magnetite/graphene oxide composites. *Remediation Journal*, 33(2), 135-150. <https://doi.org/10.1002/rem.21743>.
2. **Almeida-Naranjo, Cristina E.** and Guerrero, Victor H. (2022). Aerogels for Contaminant Removal from Water in Aerogels properties and applications. Nova Publishers. <https://doi.org/10.52305/WJOG8919>.
3. León, H., **Almeida-Naranjo, C.**, Aldás, M. B., & Guerrero, V. H. (2021, May). Methomyl removal from synthetic water using natural and modified bentonite clays. In *IOP Conference Series: Earth and Environmental Science* (Vol. 776, No. 1, p. 012002). IOP Publishing. 10.1088/1755-1315/776/1/012002.

Prologue

Scientific research is becoming increasingly crucial in an era marked by escalating environmental challenges and a growing global demand for sustainable solutions. Water, the lifeblood of our planet, is facing unprecedented threats from pollution, population growth, and climate change. As these challenges mount, the imperative to develop advanced technologies capable of safeguarding our water resources becomes undeniable. This doctoral thesis stands at the intersection of innovation and environmental stewardship, presenting a comprehensive exploration of novel water purification and treatment approaches by applying non-conventional materials.

At the heart of this work lies the innovative application of non-conventional materials sourced from agricultural wastes. By ingeniously repurposing these abundant and often underutilised resources with nanoparticles, a sustainable foundation is established for synthesising novel composites. This approach adds value to agricultural byproducts and addresses the critical need for eco-friendly materials.

The findings obtained in this thesis result from a systematic approach undertaken to design, synthesise, and characterise these novel materials. A comprehensive understanding of the materials' properties and performance was achieved through a meticulous combination of experimental procedures and analytical techniques.

This doctoral journey is embodied in a series of journal articles, each representing a distinct contribution to the field. These articles, authored by the Ph.D. candidate, have been published in reputable scientific journals and have undergone rigorous peer review. They collectively underscore the research's significance, highlighting the findings' practical applicability and scientific rigour.

This thesis is not merely a collection of academic exercises but a testament to the power of interdisciplinary collaboration, scientific curiosity, and unwavering dedication. It underscores the potential of non-conventional materials to revolutionise water treatment methodologies and offers a sustainable path forward by integrating agricultural waste-derived materials. As we navigate the complex challenges of the 21st century, this work stands as a beacon of innovation and hope, illuminating a route towards cleaner, safer, and more resilient water systems of filtration and biofiltration. I do not doubt that the reader of this thesis will find insights and inspiration in the great field of materials and sustainability.

Dr. Santiago D. Vaca J.

Versión Aprobada para Defensa Oral

Presentation

Globally, a staggering volume of approximately 3,600 km³/year of wastewater is generated, with a substantial 56% of this discharge occurring into the environment devoid of any form of treatment. Within this context, Latin America and the Caribbean collectively contribute to 22% of this global wastewater output. Within this regional scope, Ecuador plays a role, generating approximately 0.48 km³/year of wastewater. Regrettably, merely a meager 35% of this wastewater receives any form of treatment, underlining a pressing concern (Malik et al., 2015; Mateo-Sagasta et al., 2015).

The escalation in the daily usage and consumption of an array of chemical compounds has led to an increased prevalence of diverse contaminants within wastewater. Just half a century ago, the identification of emerging contaminants (ECs) in several water resources heralded a new era. These ECs, encompassing residues from pharmaceutical and personal care products, pesticides, hormones, and more, constitute a class of non-regulated substances distinguished by their enduring presence in the environment with persistence periods reaching up to 328 days, and their relatively low concentrations, ranging from ng/L to µg/L (Portinho et al., 2017). Despite their seemingly diluted nature, the potential toxic effects of ECs on aquatic organisms have spurred burgeoning concern, particularly their impacts on the endocrine system. Traditional water resource recovery facilities (WRRFs) have demonstrated limited efficacy in the removal of ECs. Furthermore, it is worth noting that conventional wastewater treatment processes, systems, and technologies are frequently unavailable or inadequate for developing countries, thus necessitating tailored solutions for each unique context (Couto et al., 2015).

A viable alternative arises in the form of the adsorption process employing activated carbon. However, the substantial expenses associated with this adsorbent (ranging from 0.13 to 0.74 USD/m³), coupled with the diminished efficiency encountered during the regeneration process, has spurred a quest for alternative adsorbents (Mallek et al., 2018; Paredes-Laverde et al., 2018). Enter agro-industrial residues, such as rice husk, peanut shells, coconut fiber, corn cob, and fruit peels/seeds, which emerge as compelling contenders for the role of ECs removal agents (M. S. Tanyildizi, 2011). This proposition is underpinned by several factors: their cost-effectiveness or even zero-cost nature, their abundant availability (often with undefined utility), and their established efficacy (surpassing 70% removal rates) in eliminating other contaminants such as heavy metals (e.g., Fe⁺³, Cu⁺², Cd⁺², Zn⁺²) and dyes (Mallek et al., 2018; Paredes-Laverde et al., 2018). The remarkable efficacy of agro-industrial residues can be attributed to the presence of lignocellulosic materials, as affirmed by prior studies (Mo et al., 2018; Pode, 2016).

In Ecuador, a nation renowned for its agricultural pursuits (contributing 8% to the GDP), the production of agricultural goods, including sugar cane, bananas, corn, rice, and oranges, yields a substantial output of around 23 million tons annually. This agricultural endeavor generates a considerable volume of agro-industrial residues, totaling approximately 2.2 million tons each year. Regrettably, a mere 8.5% of this waste finds repurpose through composting and anaerobic digestion for energy generation (MPCEIP & GIZ, 2021). Therefore, the prospect of repurposing these residues for ECs removal emerges as a noteworthy alternative.

Despite the considerable research undertaken on the utilization of agro-industrial residues for the removal of various contaminants, a significant portion of such studies involve the implementation of specific treatments, whether physical or chemical, to enhance their efficacy (Anastopoulos, Katsouromalli, et al., 2020). However, limited attention has been directed towards delineating the advantages associated with the application of raw residues in both environmental and economic terms (Almeida-Naranjo et al., 2021). Consequently, a comprehensive exploration of the potential of unprocessed or environmentally-friendlier modified residues is warranted. Among the spectrum of possibilities, a cost-effective avenue emerges in the form of iron oxide nanoparticle impregnation. These nanoparticles, characterized by straightforward synthesis, biocompatibility, and an augmentative effect on the adsorption capacity of agro-industrial residues, offer a practical solution. Moreover, their magnetic attributes facilitate the separation of residues from aqueous mediums, enhancing their overall functionality (Suhada et al., 2016).

In the present scenario, an excess of 80,000 ECs has been identified within the environment, necessitating the selection of a representative molecule to encapsulate this group (Luo et al., 2014; Yang et al., 2017). Caffeine, naturally occurring in numerous plant species and prevalent in widely consumed beverages like coffee and certain medications, serves as a prototype molecule for pharmaceutical products (anthropic

marker) (Rodríguez-Narvaez et al., 2017). Its omnipresence in the environment further suggests the coexistence of other potentially more toxic substances. Given caffeine's elevated water solubility (21,600 mg/L at 20°C) and relatively low biocompatibility ($\log K_{ow} = -0.07$), its high consumption rates render it one of the ECs featuring the most significant concentrations in the environment. Concentrations ranging from 0.1 to 20 $\mu\text{g/L}$ have been detected in wastewater treatment plant effluents (Álvarez-Torrellas et al., 2016). While aquatic species like *Astyanax altiparanae* exhibit adverse effects from caffeine concentrations as low as 27.5 $\mu\text{g/L}$, the polychaete *Diopatra neapolitana* demonstrates negative reactions even at lower concentrations (0.5 - 18 $\mu\text{g/L}$) (Muñoz-Peñuela et al., 2022; Vieira et al., 2022). In contrast, triclosan, another representative EC, showcases distinct physical-chemical attributes, including low solubility (10 mg/L at 25°C) and high biocompatibility ($\log K_{ow} = 4.3$). This compound, recognized for its antimicrobial properties, finds extensive utilization in various personal care products such as soap, toothpaste, talc, and disinfectants (Dhillon et al., 2015). Triclosan's classification as an endocrine disruptor has been corroborated by negative effects observed in diverse fish species at concentrations as low as 0.56 $\mu\text{g/L}$. Alarmingly, wastewater treatment plant effluents have exhibited concentrations up to three times this threshold. Furthermore, the recent global COVID-19 pandemic has indirectly impacted these two ECs, with an escalated use of triclosan in disinfectant products and experts suggesting increased caffeine consumption through certain beverages, thereby heightening the urgency of comprehending the removal mechanisms for both substances (Z. Chen et al., 2021).

As previously underscored, adsorption serves as a promising avenue. Nonetheless, batch adsorption processes face limitations dictated by the volume of treated wastewater. Thus, the exploration of continuous adsorption processes, particularly filtering systems, assumes significance. Filtering systems boast inherent merits such as cost-effectiveness, operational simplicity, and high efficiency. Furthermore, their integration with plants, earthworms, and/or microorganisms renders them adaptable to biofiltration technologies, surpassing conventional techniques, particularly for populations numbering $\leq 2,000$ inhabitants (Massoud et al., 2009).

While previous studies have indeed delved into the removal of ECs via both batch and continuous adsorption processes (filtration/biofiltration), several queries linger regarding the observed adsorption mechanisms between residues and composites (iron oxide nanoparticles + agro-industrial residues), composite stability, filter configurations, the amalgamation of photocatalytic processes with adsorption within filters, the efficiency of ECs removal in the presence of macro-contaminants, and other pertinent aspects. In an endeavor to shed light on these queries, the current study aims to investigate the removal of caffeine and triclosan utilizing rice husk, peanut shells, corn cob, coconut fiber, orange/banana peels, and iron oxide nanoparticles within batch/continuous adsorption processes, proposing an innovative wastewater treatment solution.

The ensuing sections of this manuscript encapsulate the outcomes of distinct research phases, with articles encompassing publication, review, and preparation for submission. This doctoral thesis unfurls across four meticulously curated chapters, designed to illuminate the relevance of the subjects under examination. Chapter one traverses the terrain of a comprehensive literature review, offering an in-depth analysis of conventional and non-conventional materials exploited in EC removal via batch adsorption processes and filtration technologies. This exploration encompasses their unique attributes, operational paradigms, efficiencies, advantages, disadvantages, and the intricacies of the removal mechanisms. With an appreciation of existing knowledge gaps, the subsequent chapters delineate both general and specific objectives.

Chapter two unfurls the results gleaned from batch adsorption processes involving residues and magnetic composites, focusing on their prowess in the removal of caffeine and triclosan. Building upon these findings, chapter three advances the discourse, delving into the optimization of operational parameters and configurations within continuous filtration processes tailored for caffeine and triclosan removal. The potential conversion of these continuous filtration mechanisms into biofiltration technologies is also meticulously examined. This exploration entails an evaluation of residue toxicity in *Eisenia foetida* (*Savigny*) and an assessment of biofiltration technologies on a mesocosm scale. The technologies surveyed encompass biofilters, vermifilters, constructed wetlands, and hybrid filters, all engineered for the elimination of contaminants from synthetic domestic wastewater. Their performance metrics are scrutinized through the lens of prospective utilization for EC removal from actual wastewater contexts.

Concluding this scholarly voyage, chapter four encapsulates the culmination of findings and extends a vista towards future prospects, beckoning forth avenues for further exploration and study.

1. Literature review

1.1. Emerging contaminants

ECs are unregulated “new” contaminants detected in wastewater in trace concentrations (ng/L to µg/L) nearly two decades ago (P. Rout et al., 2021). The ECs are classified as pharmaceuticals and personal care products (PPCPs), steroid hormones, pesticides, industrial/household chemicals, surfactants/industrial additives, and microplastics (J. Li et al., 2018; H. Tran et al., 2018). The ECs enter the environment through effluents from municipal treatment plants (the main route in developed countries), septic tanks, hospital effluents, livestock activities, subsurface storage of household and industrial wastes. Indirectly, ECs could enter through the groundwater-surface water exchange (P. Rout et al., 2021; Stuart & Lapworth, 2013). Furthermore, the massive consumption of different chemical substances has caused the EC to appear worldwide. For instance, several antibiotics (azithromycin, amoxicillin, ciprofloxacin, among others) have been found in wastewater influents from Asian, European, and North American countries at concentrations between 3 and 303,500 ng/L, 0.4 and 13,625 ng/L, and 6.1 and 246,100 ng/L, respectively (Stuart & Lapworth, 2013; H. Tran et al., 2018).

Some ECs upon reaching the environment, or even inside the water resource recovery facility (WRRF), should be degraded or biodegraded to by-products (metabolites or gases). The environmental degradation route of ECs is photochemical transformation, which can occur directly by solar radiation absorption and indirectly by photosensitized species reaction. For instance, diclofenac degrades to 1-(8-chlorocarbazolyl) acetic acid and carbazole. However, direct ultraviolet (UV) light degradation occurs inside the top 2 m of water (Wilkinson et al., 2017). On the other hand, EC's biodegradability depends on its bioavailability (the ability of EC to be absorbed and used by an organism) and complexity. Biodegradable ECs are characterized by having straight chains with short branches, unsaturated aliphatic compounds and substances with functional groups that donate electrons. Ibuprofen, natural estrogens, bisphenol A, triclosan, among others are examples of biodegradable ECs, which become other substances (e.g., triclosan to 2,8-dichloro dibenzo-p-dioxin under UV light), achieving degradation percentages greater than 50% (Luo et al., 2014). In some cases, ECs in the environment do not degrade but rather volatilize, reaching Henry's constant values between 10^{-2} and 10^{-3} mol/(m³ Pa). ECs such as dibutyl phthalate, di(2-ethylhexyl) phthalate, and nonylphenol are found at air concentrations between 0.031 and 0.055 ng/L (Luo et al., 2014; Wilkinson et al., 2017). Figure 1 shows which are the main routes of entry of EC into the environment, its behavior in it and the possible effects it could cause in different living beings.

Despite their low concentration, the ECs are substances with environmental and human risks due to their characteristics, such as a wide range of molecular weight (> 150 g/mol), polarity (pKa > 0.5), and bioavailability (log K_{ow} < 1 to > 4) (Luo et al., 2014; Matamoros et al., 2009). Commonly used non-steroidal anti-inflammatory drugs, such as diclofenac and ibuprofen, have increased the risk of gastrointestinal ulcers, kidney disease and gill abnormalities in rainbow trout (P. Rout et al., 2021). Other types of ECs also have negative effects on aquatic organisms; in fact, human health has also been compromised. Therefore, the ECs removal from wastewater is essential.

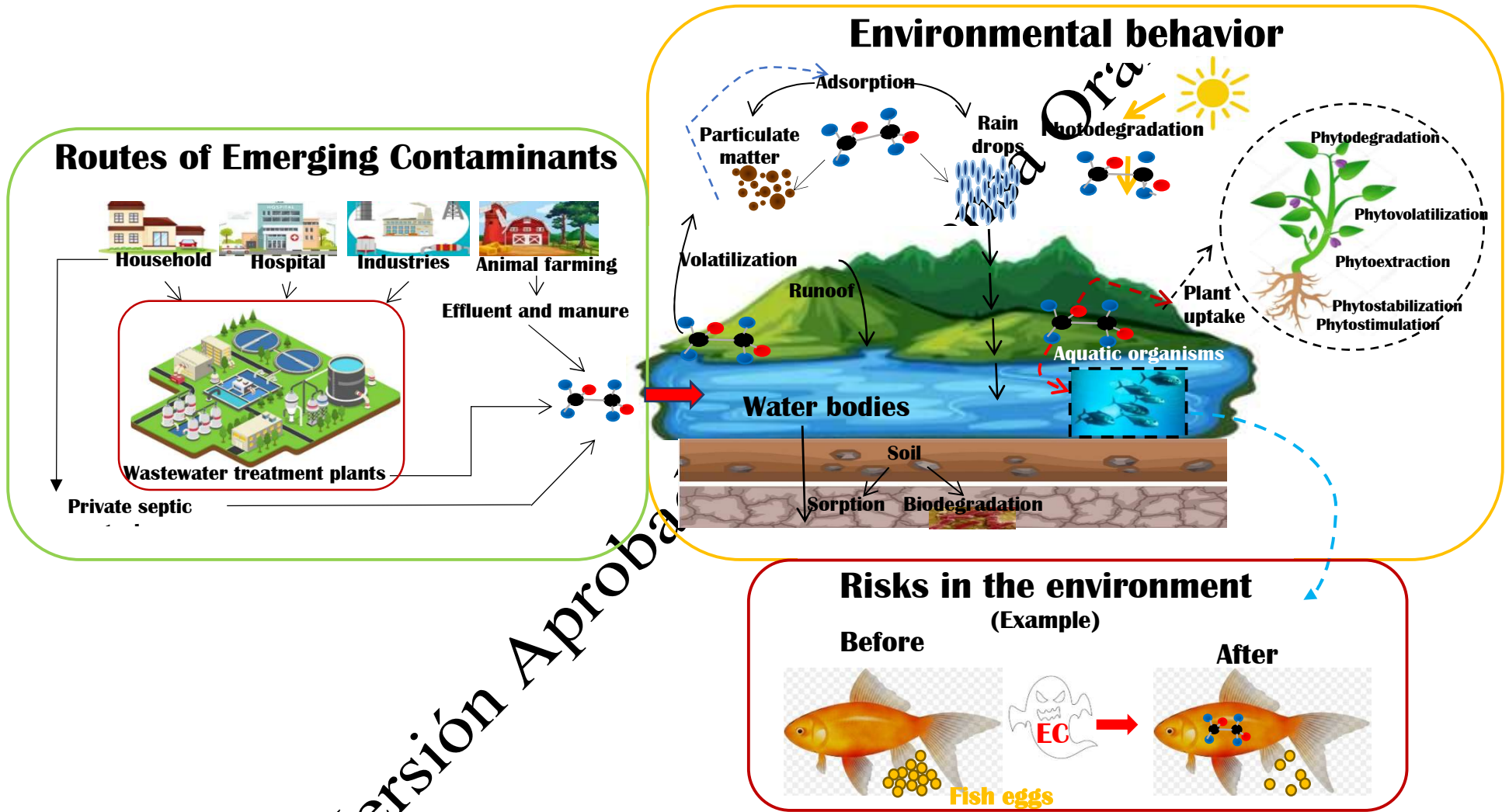


Figure 1. Routes of entry of ECs into the environment, its behavior and effects.

Among the main alternatives used for EC removal are membrane bioreactors, activated sludge systems, advanced oxidation processes, membrane processes, or hybrid systems (e.g., membrane bioreactors + membrane processes). However, some of these are carried out only on a lab scale. Besides, these technologies have high operational and maintenance costs, generate by-products and are difficult to operate. An efficient and low-cost alternative for EC removal is the adsorption process. The most widely used adsorbent is activated carbon due to its efficiency in the removal of ECs (e.g., 12 – 100% in pharmaceutical removal) (Mansour et al., 2018). However, its use is restricted due to its high cost (20 – 22 USD/kg) and complicated regeneration (De Andrade et al., 2018).

The purpose of the bibliographical review is to describe the classification of ECs, their characteristics, concentrations commonly found in different bodies of water, and the possible problems that they could generate for some species. In addition, it delves into the materials that have been used for their removal both in batch processes and in filtration technologies. The characteristics (physical/chemical) of the materials that influence the removal of ECs are presented. Likewise, the efficiency of the materials to remove several ECs (in different operating/functioning conditions) and the mechanisms exploited in the removal process are detailed. Finally, the characteristics of the filtration technologies and the function/characteristics/capacity and the removal mechanisms provided by the materials within them are described. Below is presented the EC classification:

1.1.1. Pharmaceuticals and Personal Care Products (PPCPs)

There are more than 3,000 substances (consume = 50 – 150 g/inhab) used as analgesics/anti-inflammatories, antibiotics, contraceptives, antidepressants, pressure regulators, among others (Quesada et al. 2019). Meanwhile, around 2,000 chemical compounds are used as Personal Care Products, which include fragrances, preservatives, disinfectants, sun protection agents, among others (Ebele et al. 2017). Indeed, PPCPs production has reached about 20 million tons/year (Wang and Wang 2016).

PPCPs have been found in surface water (up to 10,000 ng/L), groundwater (up to 100 mg/L), influents (75 – 73,730 ng/L), and effluents (24 – 4,800 ng/L) of WWTP, sludge, sediments and even in living beings (e.g., triclosan in fish at 2,100 ng/g) (Brausch and Rand 2011; Dhillon et al. 2015). In general, PPCPs can be made of several complex molecules with different structures and shapes, which vary widely according to their molecular weight (88.5 – > 900.0 g/mol) (H. Kaur et al. 2017; H. Tran et al. 2018). Moreover, they are polar molecules with ionizable groups (in the solid phase they have different adsorption mechanisms i.e., ion exchange), and most of them are hydrophilic (H. Tran et al. 2018). However, PPCPs have log K_{ow} values in a wide range (-2.4 – 13.1), from acid to basic substances under environmental conditions (pKa = 0.6 – 13.9) (Brausch and Rand 2011; H. Tran et al. 2018). PPCPs reach K_d values between 1.9 and 39,000, are partially/completely soluble in water ($0.02 – 3.12 \times 10^5$ mg/L, T = 20 °C) (H. Tran et al. 2018; Wang and Wang 2016), and dissipation times between < 3 and up to 300 days (Ebele et al. 2017).

The recurrent discharges of PPCPs could cause endocrine problems, genotoxicity, aquatic toxicity, and resistance in pathogenic microorganisms (Adeel et al. 2017). For instance, diclofenac at concentrations between 7 and 50 mg/L can increase plasma vitellogenin in fish (hormonal disorder). It has even caused effects on steppe eagles and vultures (Ebele et al. 2017; P. Rout et al. 2021). Meanwhile, ciprofloxacin, tetracycline, ampicillin, trimethoprim, erythromycin, and sulfamethoxazole can increase the antibiotic resistance of *E. coli* and *Xanthomonas maltophilia* (Ebele et al. 2017; Wang and Wang 2016). Personal care products, such as benzophenone-3 threaten coral reefs, and 4-methyl benzylidene camphor has been demonstrated to develop embryonic malformations in frogs. Meanwhile, triclosan produces adverse effects on the first stages of the frog's life (Dhillon et al. 2015; Kaur et al. 2019; Zepon-Tarpani and Azapagic 2018). PPCPs affect humans, as their presence has been detected in the breast milk, blood, and urine of children. Moreover, benzyl paraben and benzophenone-4 were found in the placenta, which could indicate a transfer from the mother to the fetus (Valle-Sistac et al., 2016).

1.1.2. Pesticides

Until 2020, around 3.5 million tons/year of pesticides were used, but only less than 0.1% is used by plants (Pietrzak et al. 2020). Some pesticides, such as glyphosate or its main metabolite (amino methylphosphonic acid) have been found in surface waters (0.02 – 6.0 g/L), soil (15.9 – 1,025.5 kg/kg), deep waters (0.1 µg/L) and sediments (0.1 – 100 mg/L).

Moreover, pesticides with high vapor pressure (1.51×10^{-7} – 1.29×10^{-1} Pa)/high volatility (e.g., pentachlorophenol) go into the air during their application (between 5 and 90% of them), moving long distances and even reaching pristine areas (Glinski et al. 2018; de Souza et al. 2020; Villamar-Ayala et al. 2019). This has been found in the rainfall, such as methyl parathion, which has been found near agricultural sites, where it was not used (~23 µg/L) (Glinski et al. 2018). According to their molecular structure, pesticides have different chemical properties, they have an acid character that goes from weak to strong (pKa= 9.1 – 0.7), medium to high solubility in water (2.0 – 1.2×10^6 mg/L, T= 20 – 35 °C), very low to very high bioaccumulation (log K_{ow}= -4.6 – 8.0) and high persistence (7 days – >5 years) (Glinski et al. 2018; Villamar-Ayala et al. 2019).

Pesticides mainly affect non-target organisms, e.g., atrazine (concentrations in water > 200 ng/L) (de Souza et al. 2020) causes sex change in male frogs and affected/altered the reproductive system and fertility of mice, fish, and humans (Glinski et al. 2018; Kaur et al. 2017; de Souza et al. 2020). Another widely used herbicide is glyphosate, which affects the entire food chain, delaying periphytic colonization and reducing the abundance of aquatic organisms, such as *Pseudokirchneriella subcapia* and *Lemma minor* (EC_{50-7d}=11.2 – 46.9 and EC_{50-4d}= 64.7 – 270.0 mg a.i./L, respectively) (Villamar-Ayala et al. 2019). Furthermore, its use in edible crops is related to antibiotic resistance in humans, even though it was classified as carcinogenic by the World Health Organization (Zavareh et al. 2018).

The by-products/metabolites of pesticides also cause negative effects (Glinski et al. 2018). For example, aminomethylphosphonic acid, at concentrations between 50 and 167 mg/L produced acute toxicity in *Vibrio fischeri* (Villamar-Ayala et al. 2019).

1.1.3. Steroid hormones

Steroid hormones (natural/synthetic) maintain hormonal balance, reproductive tissue health, tissue regeneration, stimulate the reproductive organs, germ cell maturation, etc. The most common hormones detected in wastewater/water bodies are estrogens. Natural estrogens are excreted by the adrenal cortex, testes, ovaries, and placenta of humans and animals (e.g., estrone/E1, 17β-estradiol/E2, estriol/E3). On the other hand, synthetic hormones are synthesized from cholesterol (e.g., 17α-ethinylestradiol/EE2). The human population generates about 30,000 and 700 kg/year of natural and synthetic estrogens, respectively. Synthetic estrogens come from oral contraceptives. However, the estrogen generated by cattle is much higher, in the US and the European Union alone it amounts to 83,000 kg/year (Adeel et al., 2018).

Steroid hormones are considered endocrine disruptors, they mainly come from the discharges of the human and animal population (Kestemont & Depiereux, 2013). Therefore, WRRF or feedlot effluents are the main pathways for hormones entering the soil, surface water, sediment, and groundwater. They have been found in WRRF influents (> 802 ng/L) and effluents (> 275 ng/L), surface waters (0.04 – 667 ng/L), groundwater (5 – >1000 ng/L), drinking water (up to 3,500 ng/L), drinking water (> 2.6 ng/L) and livestock waste (14 – 533 ng/g) (Stuart & Lapworth, 2013; H. Tran et al., 2018; Ying et al., 2002).

Steroid hormones are characterized by having a molecular weight between 242 and > 296 g/mol, being poorly soluble in water (8.8 – 441 mg/L, at 25 °C), with low to moderate hydrophobicity (log K_{ow} between 1.6 and 4.7), a pKa that border values between 10.3 and 18.9 (weak acid) and nonvolatile (vapor pressure between 9×10^{-13} and 3×10^{-8} Pa) (Adeel et al., 2017; Hamid & Eskicioglu, 2012; Ilyas & Hullebusch, 2020).

Despite their low persistence (half-life: 0.2 – 9.0 days water/sediments) compared with other ECs, they cause negative effects on ecosystems and humans by their disruptor endocrine character (Adeel et al.,

2017). Steroids alter the sexual and reproductive systems of living beings including humans (cancer and infertility) (H. Tran et al., 2018). Chronic exposure of fathead minnow to 17 α -ethinyl estradiol (5 – 6 ng/L) led to the feminization of male fish (development of the ovary cavity) and impaired oogenesis (alterations in oocyte formation in the female gonads) in females. E2 induced changes in vitellogenin production in male trout at concentrations of 1 ng/L, while between 1 and 10 ng/L it produced the feminization of some species of male fish. Levonorgestrel at 6.5 ng/L inhibited spermatogenesis, reduced fish egg production and reproduction, increased female weight and length and promoted female masculinization. Other species have also been affected by hormones, with EE2 at 10 ng/L affecting cardiac function in bullfrog tadpoles (Ilyas & Hullebusch, 2020).

1.1.4. Other emerging contaminants

A wide range of industrial and chemical substances are considered as ECs, among these are fire retardants, food additives, plasticizers, solvent stabilizers, surfactants/detergents, industrial additives (fluorinated organic compounds), and corrosion inhibitors (Stuart & Lapworth, 2013). The use/consumption of industrial and chemical substances is considerable worldwide. In the case of surfactants, it was estimated that the production for 2022 would be 24.2 million tons (Palmer & Hatley, 2018), plasticizers such as bisphenol A had a production of 2 million metric tons/year (Wilkinson et al., 2017). While 159,000 metric tons/year of synthetic non-nutritional sweeteners are consumed (Praveena et al., 2019). The physicochemical characteristics of this group are very varied due to the differences between them, this also makes their behavior in the environment different. For instance, artificial sweeteners present between medium and very high solubility (between 4 and 1,000 g/L at 20 °C), from low to the high acid character (pKa= 1.9 – 11.8) and very low bioaccumulation (log K_{ow}= -1.61 and 0.91) (J. Luo et al., 2019; Praveena et al., 2019). However, other substances such as bisphenol A (plasticizer), nonylphenol (surfactant), and Tris(2-Chloroethyl) phosphate (TCEP, fire retardant) present from low to high bioaccumulation with log K_{ow} values of 3.2, 4.4, and 6.8, respectively (Lapworth et al., 2012; Wilkinson et al., 2017). Besides, bisphenol-A and phthalates are semi-volatile, so they easily move into the environment. They have a short half-life (5 – 18 days) in the air because they could be photodegraded (Guerranti et al., 2019). On the other hand, fluorinated organic compounds with longer chains show persistence, from moderate solubility (e.g., perfluoro octane sulfonate= 1,080 mg/L) to high solubility (e.g., perfluorooctanoic acid >20 mg/L) in water, long-distance mobility, high to the very high potential of bioaccumulation (e.g., log K_{ow} of perfluoro octane sulfonate between 4.5 to 6.9), and toxic effects (Kumar, 2005; Wang et al., 2019).

The most investigated substances are plasticizers and fluorinated organic compounds. Plasticizers are used as material plasticity enhancers for plastic packaging, epoxy resins, coatings, construction materials, toys, medical instruments, plastic films, among others (Wilkinson et al., 2017; Wilkinson et al., 2018). Moreover, plasticizers are commonly found in surface water (< 1 – 12,000 ng/L), runoff (50 – 2,410 ng/L), and other water sources. They include bisphenol-A, bisphenol-S, bisphenol-F, and phthalates (Lapworth et al., 2012; Wilkinson et al., 2017; Wilkinson et al., 2018). Fluorinated organic compounds were detected in surface water (0.09–578,970 ng/L), groundwater (0.17 – 8.54 ng/L), influents (65 – 112 μ g/L) and effluents (43 – 78 μ g/L) of WRRFs, runoff (around 2 ng/L) and drinking water (around 54 ng/L) (Y. Wang et al., 2019; Wilkinson et al., 2017). Furthermore, traces of fluorides in concentrations between 0.023 to higher than 1,600 ng/g have been found in some species of fish, amphibians, crustaceans, seals, whales, and polar bears. There were affections on some organs such as the heart, kidneys, liver, and gonads (Y. Wang et al., 2019). Artificial sweeteners were found in drinking water (36 – 2,400 ng/L), surface water (0.03 – 9,600 ng/L), groundwater (non-detected – 33,600 μ g/L), seawater (200 – 393 ng/L) and lakes (non-detected – 780 ng/L) (J. Luo et al., 2019; Praveena et al., 2019).

Ethoxylated alcohol (surfactant) affects fish and invertebrates. In fathead minnows, it affects egg production and larval survival, with a no-observed effect concentration (NOEC) of 0.73 mg/L. In species such as Bluegills, it affects survival and growth at concentrations of 5.7 mg/L. Nonionic surfactants and nonylphenol ethoxylates exhibited acute toxic effects (EC₅₀=1.1 – 25.4 mg/L) on tadpoles of four Australian and two exotic frogs (Ivanković & Hrenović, 2010). On the other hand, artificial sweeteners such as aspartame caused cancer in rats and headache, nausea, and vomiting in humans at concentrations

between 2,000 and 50,000 mg/L, while 5% sucralose produced thymus shrinkage and migraine in rats and humans, respectively (Praveena et al., 2019).

Table 1 shows the physical and chemical properties of some ECs and their concentrations for different water sources. It is observed that there is a wide range of ECs found in different water bodies in their common concentrations (0.01 ng/L – > 6,010 mg/L). However, the health situation due to the COVID-19 pandemic could have caused a change in the concentration of ECs, as occurred with caffeine and triclosan, which are the contaminants studied in this research and will be discussed in later chapters. The consumption of the two substances has increased considerably. In the case of caffeine, although this use is not recommended for patients with COVID-19, this has been recommended in the diet of healthy people as a moisturizer in coffee and tea (Fuzimoto & Isidoro, 2020). According to Romeo-Arroyo et al., 2020, the consumption of coffee, tea, and other energizers has increased in confinement. In the case of triclosan, despite its use having been banned or limited in different parts of the world because it is considered an endocrine disruptor, several of the products used for washing or disinfecting hands and surfaces contain triclosan. It has even been used in mouthwashes (Ejtahed et al., 2020; Espejo et al., 2020; Singh et al., 2020). This will undoubtedly increase the concentration of both ECs in the wastewater.

Moreover, the very varied characteristics ($\log K_{ow} = -3.4 - 13.9$, water solubility = 0.49 – 21600 mg/L, molecular weight = 133.1 – 791.1), added to their behavior and toxicity of ECs make it essential to eliminate them from wastewater, so the following chapter describes some ways to eliminate them.

Versión Aprobada para Defensa Oral

Table 1. Physical and chemical characteristics of some ECs and their concentrations in water bodies.

EC type	EC Subtype	Contaminant	Water solubility [mg/L]	Log K _{ow}	Range of typical concentration [ng/L]	Type of water in which the EC can be found	Reference
	Stimulant	Caffeine	21,600	-0.07	753,500–1.0x10⁶	Surface water	
					20–23,970	Groundwater	[1-3]
					500–5,000	Drinking water	
	Anti-inflammatory	Ibuprofen	21	0.35	13.5–69,500	Effluent WWTP	[1,2,4,5]
	Anticonvulsant	Carbamazepine	112-236	13.90	500–3.5x10 ⁸	Influent WWTP	[4,6,7]
					1,200–6.6x10 ⁷	Effluent WWTP	
PPCPs	Lipid regulator	Clofibrac acid	214650	2.88	nd–420	Influent WWTP	[4,8]
	Antibiotic	Ciprofloxacin	650	0.28	2,200–14,000	Influent WWTP	[4,11,12]
					1,100–44,000	Hospital wastewater	
	Diagnostic Contrast Media	Iopromide	23.8	-2.1	780–11,4000	River water	[4,13]
					1,170–4,030	Urban effluents	
	Antidepressant	Diazepan	50	3.08	nd–100	Surface water	[4,17]
					nd–100	Influent WWTP	
	Beta-blocker	Atenolol	300	0.16	90–255	Influent WWTP	[4,18]
	Fragrance	Musk xylene	0.49–1.0	4.40	200,000–400,000	Drinking water	[4,14]
	Disinfectant	Triclosan	10,000	4.76	200–1,854	Influent WWTP	[1,2,15]
Pesticides	Herbicide	Glyphosate	15.70	-3.40	up to 6.01x10 ⁹	Surface water	[19,20]
		Acetamiprid	2,950	0.80	0.08–249	Surface water	[16,27]
	Insecticide	Clothianidin	304	0.70	1.0–740	Surface water	[16,21,22,25]
		Thiamethoxam	4,100	-0.13	1.0–914	Surface water	
Steroid hormones		E2	13	2.45	3.8–188.0	Influent WWTP	[4, 7, 9, 10]
	Natural	E1	13	3.43	12–196		
		17 α -estradiol	13.3	4.01	6.4–12.6	Effluent WWTP	[10]
	Synthetic	E2	4.8	3.67	0.59–5.6		
Other ECs	Anticorrosive	Methylbenzotriazole	366	2.72	nd–2,900	Effluent WWTP	[16]
	Plasticizer	BPA	120	2.2–3.4	0.01–8,800	Bottled water	[23,24]
					140–12,000	Surface water	

Information obtained from ¹Gavrilescu et al., 2015; ²H. Kaur et al., 2017; ³Almeida-Naranjo et al., 2021a; ⁴Wang & Wang, 2016; ⁵Ghauch et al., 2012; ⁶Deng et al., 2018; ⁷Jiang et al., 2020; ⁸Boudrahem et al., 2017; ⁹Honorio et al., 2018; ¹⁰Adeel et al., 2017; ¹¹Duan et al., 2018; ¹²Peng et al., 2019; ¹³Kim et al., 2014; ¹⁴Käfferlein et al., 1998; ¹⁵Zepon-Tarpani & Azapagic, 2018; ¹⁶de Souza et al., 2020; ¹⁷Akhtar et al. (2015); ¹⁸Lozano-Morales et al., 2018; ¹⁹Villamar-Ayala et al., 2019; ²⁰Meffe & Bustamante, 2014; ²¹Shoiful et al., 2016; ²²Man et al., 2018; ²³Akhbarzadeh et al., 2020; ²⁴Wilkinson et al., 2017; ²⁵Pietrzak et al., 2020. The information in blue color is from the contaminants studied in this research.

1.1. Alternatives to remove ECs

Conventional WRRFs (constituted by conventional technologies) are designed mainly to remove macro-contaminants efficiently (> 80%) (Chicaiza et al., 2020). However, conventional WRRF presents some disadvantages such as high operating costs (high energy consumption= 0.3 – 2.1 kW h/m³ of treated wastewater) (Panepinto et al., 2016), difficult operation, high sludge generation (e.g., 240 million wet tons/ year in Europe, USA and China combined), etc. (D. Wang et al., 2017). The WRRF consists of four stages: preliminary treatment (physical or mechanical methods), primary treatment (physical-chemical or chemical methods), secondary treatment (physical-chemical methods or biological treatment), and tertiary or advanced treatment (physical techniques or chemical methods). However, depending on the contaminants present in the wastewater, some of these could or could not be present (Crini & Lichtfouse, 2018).

It is difficult to define a universal method for wastewater treatment, different technologies/processes/methods or combinations of them are investigated and applied, and each of them have advantages and disadvantages. Therefore, to design/implement a WRRF, it is necessary to considerate the needs of a specific locality and find a way to take advantage of the available resources. In such a way that WRRFs be efficient, low-cost (implementation, maintenance, and operation), and generate the least possible adverse impact during their operation. Some characteristics of the different stages, the contaminants commonly removed in each stage and some examples of the technologies or processes used in a conventional WRRF are shown in Figure 2.

Conventional technologies are not efficient in the removal of ECs (e.g., PPCPs= 30 – 75% of anti-inflammatory and antibiotics) (Yang et al., 2017). Thus, in the last century, specialized literature has reported several methods for EC removal. The most attractive methods are membrane filtration and advanced oxidation processes. Nevertheless, they are expensive as they have high energy/chemical requirements and sludge/by-product generation (Varsha et al., 2022). On the other hand, the removal of ECs from aqueous media through adsorption processes has proven to be efficient (up to 100%) (Kaur et al., 2019) with minimal generation of secondary sludge (Sophia & Lima, 2018).

Versión Aprobada Para Defensa Oral

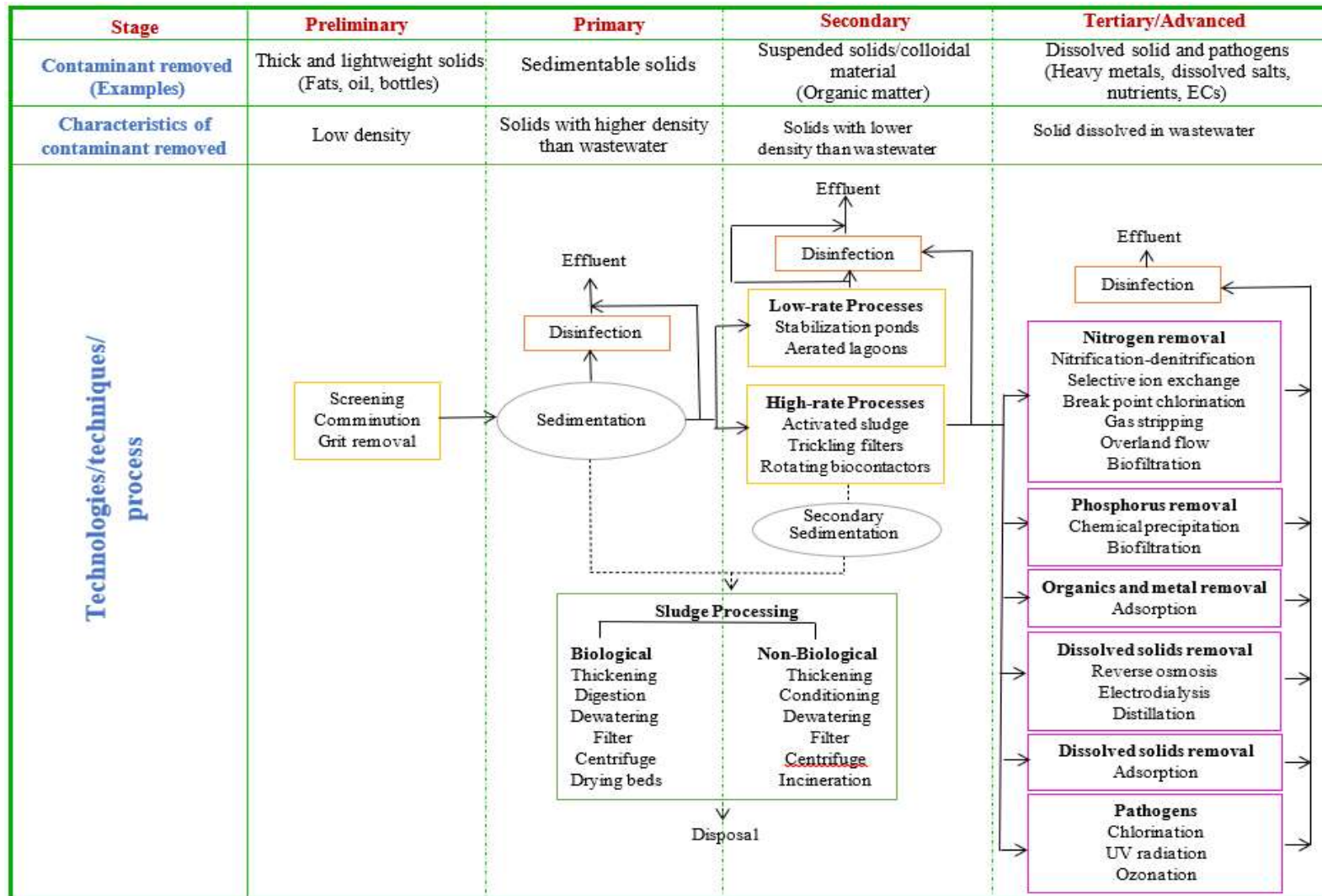


Figure 2. Stages/characteristics/technologies or processes used in conventional WRRF. Kestemont & Depiereux, (2013)

1.1.1. Adsorption process in the removal of ECs

The adsorption process is an efficient method to remove ECs. This advantages include simplicity, low costs (depending on the adsorbent used), and high adaptability compared to the other technologies used (Álvarez-Torrellas et al., 2018). Adsorption is a process in which a material (adsorbate) in a different state (solid, liquid, or gas) or size (atoms, molecules, ions) is retained on a surface (adsorbent) (Kammerer et al., 2019). In this case, in the adsorption process, the EC is deposited on the adsorbent surface through electrostatic/attraction forces (physical-sorption/physisorption) or chemical bonds (chemisorption). The equilibria (adsorption isotherms) and the adsorption kinetics allow the compression of the adsorption mechanisms, which are dependent on the type of adsorbent, adsorbate and adsorption conditions (pH, temperature, ionic strength, etc.) (Tran et al., 2017). The mechanism of the adsorption process is shown in Figure 3.

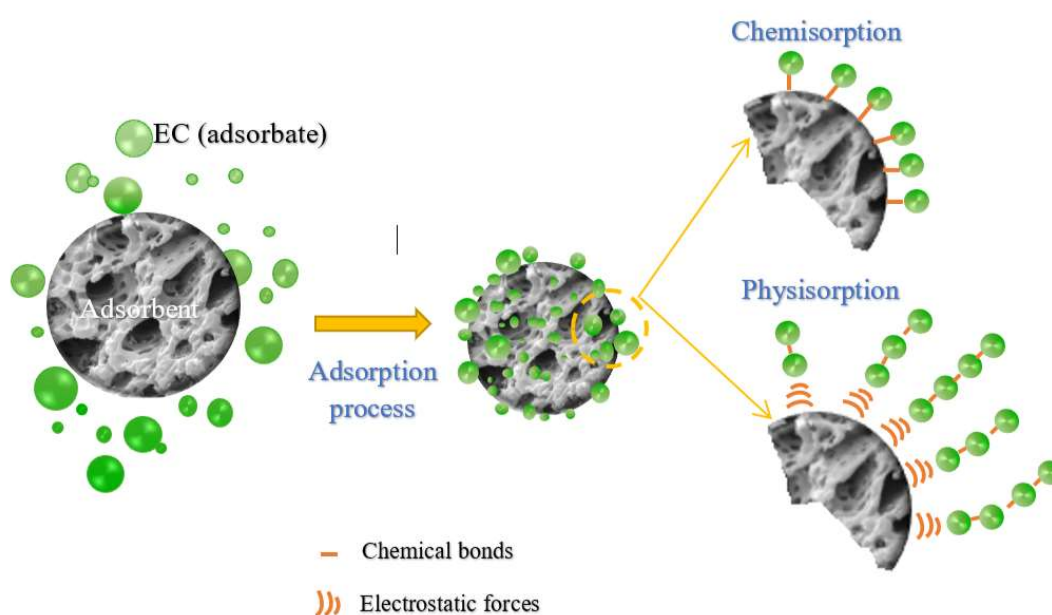


Figure 3. Adsorption mechanisms

The study of adsorption kinetics provides information on the adsorption rate, the performance of the adsorbent used, and the mass transfer mechanisms (Wang & Guo, 2020). While the adsorption isotherm describes the equilibrium performance of the adsorbents when the temperature is constant (Al-Ghouti & Da, 2020). Several models fit the kinetics (Pseudo-first-order, Pseudo-second-order, Elovich, Diffusion) and isotherms (e.g., Langmuir, Freundlich, Sips, etc.) of adsorption.

Due to the importance of determining the kinetics and equilibrium in an adsorption process, all studies involving the removal of ECs and other contaminants include adjustments to different models. By the way, many studies have been questioned since there are several errors in their application. Errors include the use of wrong formulas, the use of linear models, and misleading interpretations (Tran et al., 2017). In subsequent sections, the models applied in this study will be detailed.

1.2. Materials used to remove ECs from water in the batch adsorption process

The adsorbent type is very important in the adsorption process. The most used adsorbent in EC removal is activated carbon, due to this high efficiency (up to 100%), large specific surface area (300 – 2,500 m²/g), and hydrophobic interactions (Grassi et al. 2012a; Sophia and Lima 2018). Alumina, soil (e.g., sandy clay loam), zeolites, clays, composites (e.g., matrix: activated carbon and reinforcement: magnetite), metal-

organic frameworks, and nanoparticles (carbon nanotubes, magnetic nanoparticles, graphene, etc.) have reported be also used (Ahmad et al., 2019; P. Rout et al., 2021). However, the widespread use of activated carbon and other adsorbents is limited by their high costs (2 – 4 to 20 – 22 USD/kg) (Sophia & Lima, 2018). This has promoted the search for alternative materials that are less expensive, widely available, require little processing, and also are environmentally friendly. Even mineral, agricultural and other industrial by-products/residues have been used efficiently (Quesada et al., 2019).

This section describes the most common conventional/non-conventional materials used for EC removal. Information about the origin, availability, cost, physical characteristics (surface area, porosity)/chemical characteristics (composition, presence of functional groups), and efficiency/adsorption capacity for the removal of some ECs is detailed. Besides, the operating conditions/parameters of batch adsorption processes of some previous studies are presented. Even though batch processes are not very efficient concerning the amount of water treated, these processes are very useful because they permit determine the capacity of the adsorbent material that allows their efficient use in continuous adsorption processes. Figure 4, shows some alternatives to remove ECs, focusing mainly on adsorption and some adsorbents that have already been used efficiently.

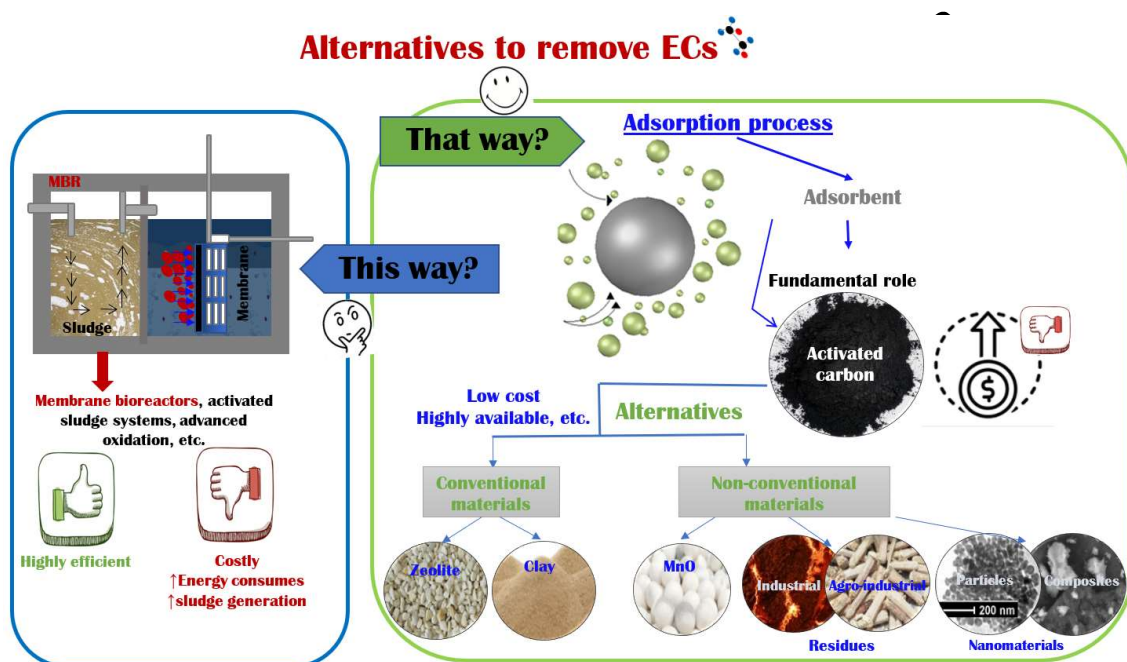


Figure 4. Alternatives to remove ECs

1.2.1. Conventional materials

1.2.1.1 Activated carbon

Activated carbon is the most used adsorbent material within WWTPs, reaching between 5.5 and 8.1% per year between 2008 and 2018, with 3,311 thousand metric tons in 2021 (Pallarés et al. 2018). Activated carbon has been recognized as the best adsorbent for the removal of diazinon, carbamazepine, diclofenac, ibuprofen, naproxen, ketoprofen, triclosan, p-Chloro-m-xylenol, (Grassi et al. 2012; Sophia and Lima, 2018), acetaminophen, androstenedione, E1, E2, E3, EE2, progesterone, testosterone (Grassi et al., 2012a), metronidazole (Forouzesh et al., 2019), paracetamol (García-Mateos et al., 2015). This absorption capacities are between 12 and up to 7,800 mg/g, with efficiencies from 20 to 100% (Grassi et al. 2012a; H. Kaur et al. 2017; Sophia and Lima 2018). Nevertheless, activated carbon is a costly adsorbent, which exhibits difficult and costly recovery, and the efficiency decreases after regeneration (< 40%) (Sophia & Lima, 2018).

1.2.1.2. Zeolites

Zeolites are natural (Si/Al ratio= 1 – 5) and low-cost adsorbents (0.03 – 0.12 USD/kg), which are available worldwide (Lin & Juang, 2009; Pačič & Valtchev, 2020). There are 200 zeolite framework types. Furthermore, they are synthesized at a lab scale even from residues such as fly ash to obtain higher Si/Al ratios (Khaleque et al., 2020; Lin & Juang, 2009). Zeolites with high silica content (Si/Al > 5) are more efficient in ECs removal because they show a high level of hydrophobicity (Jiang et al., 2020). High hydrophobicity prevents water absorption, this could allow more zeolite pores to be available for the diffusion/adsorption of ECs. However, zeolites with high silica content are used only at the laboratory scale (Jiang et al., 2018). Zeolites, such as Faujasite, Mordenite, Beta, and ZSM-5 are efficient in ECs removal, such as phenol, dichlorophenol (Lin & Juang, 2009), tetracycline, oxytetracycline (Lye et al., 2017), nitrobenzene, carbamazepine, nicotine, erythromycin, nitrosamines (Jiang et al., 2018), 2,4,6-trichlorophenol (Jiang et al., 2020). They also have reached adsorption capacities between 27 and 833 mg/g (Jiang et al. 2018, 2020; Rasamimanana et al. 2016; Sun et al. 2017) and removal efficiencies from 45 to 90% (Jiang et al. 2018; Lin and Juang 2009; Lye et al. 2017; Pukcothanung et al. 2018; De Sousa et al. 2018).

1.2.1.3. Clays

Clays are widely used in contaminant removal due to their worldwide abundance and low-cost (0.04 – 0.46 USD/kg), being at least 20 times cheaper than activated carbon. Clays were used in the EC removal, such as amitriptyline, atenolol, metformin, buspirone, ciprofloxacin, ranitidine, timolol (Thiebault 2019; Thiebault et al. 2015), amoxicillin (Grassi et al. 2012a; Thiebault 2019), diazepam, carbamazepine, clofibric acid, naproxen, salicylic acid, carbamazepine, diclofenac, ibuprofen, naproxen, phenol, atrazine, trimethoprim (Srinivasan, 2011), methomyl (León et al., 2021), sulfamethoxazole, diclofenac (Lozano-Morales et al., 2018). Indeed, clays have achieved adsorption capacities between 0.1 and 1900 mg/g (Bouras et al. 2007; Grassi et al. 2012a; 2012b; Nassar et al. 2012; Srinivasan 2011; Thiebault 2019). It is important to mention that clays have efficiencies similar to those of activated carbon (> 98%), but they require longer times to achieve them (Grassi et al., 2012a; Srinivasan, 2011). This occurs despite the surface area of clays, which is around 1/10 times lower than activated carbon (Sophia & Lima, 2018; Srinivasan, 2011; Thiebault, 2019; Zaghrouane-Boudiaf & Boutahala, 2011).

Some results of previous research about EC adsorption using conventional materials described before are shown in Table 2. Conventional materials are characterized to have a high surface area (10 – 2500 m²/g), porosity (0.1 – 16.9 cm³/g) (Reeve & Fallow, 2018; Sophia & Lima, 2018; Torrellas et al., 2015), and the presence of several functional groups (OH, COOH, CO, NH₂, SiO₂, cations, etc.) (Mubarik et al. 2012; Srinivasan 2011; Thiebault et al. 2015), which gives them high efficiency (up to 100%). In some studies, it can be established that the efficiencies of conventional materials used in EC removal are from 20 to 100% (Grassi et al., 2012a; Jiang et al., 2018; Lin & Juang, 2009; Lye et al., 2017). So, the adsorption parameters are very different, such as EC type, concentration, material dose, pH, and contact time, except the temperature that is maintained between 20 and 30 °C (Grassi et al. 2012a; Lozano-Morales et al. 2018; Rasamimanana et al. 2016; Yu et al. 2016). Some authors have made physical/chemical modifications (e.g., thermal/acid-basic treatments) to the material to increase the EC removal efficiency or decrease the adsorbent dose/contact time (Bouras et al. 2007; Reeve and Fallow 2018).

Table 2. Conventional materials used for ECs removal from synthetic water in the batch adsorption process.

Adsorbent characteristics			Adsorption behavior									
Adsorbent	Composition/ Functional Groups/ions	SA[m ² /g] P [cm ³ /g]	Adsorbent	EC removed	Adsorption conditions	Adsorption mechanism	Removal [%]	Adsorption capacity [mg/g]	Reference			
Activated carbon:	C, H, N, S and O ²	SA= 300– 2500 ⁴	Activated carbon from argan waste	Paracetamol Amoxicillin	CT=0.8–12, T = 25, pH=3-11, AD =0.1, [EC]= 100	Van der Waals forces, H- bonding, dipole- dipole interactions, ion exchange, covalent bonding, cation bridging, and water bridging ⁶⁻¹²	~95	512 319	[7]			
			Commercial activated carbon	Caffeine	CT= 4, T= 30±2, pH= 3–		44.1	71.7	[8]			
				Ibuprofen	8, AD= 0.1, [EC]=		52.7	72.3				
				Triclosan	1.125–1.252		60.8	70.0				
			Carbonized carbonaceous materials (S.O.) ¹	COOH, C=O, OH ⁻ , -NH ₂ , CHO, etc. ³	P=0.1–16.9 ⁵		Commercial GAC	Tetracycline	CT= 180, T = 30 pH= -, AD= 2.4 [EC]=100	-	845.9	[5]
							Commercial GAC	Ibuprofen	CT= 2, T = 20±1 pH= 3.9–10.2, AD= 5 [EC]= 99.27	69.0 – 80.0	-	[9]
Modified commercial activated carbon	Triclosan	CT= 4, T = 30±2 pH= 6, AD= 0.07 [EC]= 1.0				98.3	395.2	[10]				
			Activated carbon from biomass	Paracetamol	CT=240, T = 15-35, AD =0.1, [EC]=1–20	-	100	[11]				
Zeolites:	Si, Al, O and cations ²	SA= 300– 2300 ²	Natural zeolite	Tetracycline	CT= 2, pH= 6, AD= 6.0, [EC]= 44.4- 46.0	Van der Waals forces and acid- base forces, donor-acceptor interaction. ^{2,13}	90.0	-	[13]			
				Oxytetracycline	75.0		-					
			Modified zeolite	Mesosulfuron- methyl	CT= 72, T = 25, pH= 6, AD= 2.0, [EC]= 8		-	2.4-3.4	[14]			
				Zeolite + Hexadecyltrimethylammonium bromide or chloride	Diclofenac		CT= 24, Ta= 32, Tb= 42, Tc= 52, pH= 2–11, AD= 25 [EC]= 636.28	-	Up to 47.4	[15]		
			Crystalline microporous aluminosilicate (S.O. and N.O.) ²	K ⁺ , Na ⁺ , Ca ²⁺ , and Mg ²⁺ ¹²	P= 0.10– 0.35 ¹²		Zeolite Y (ZY)	2,4-dichlorphe- noxyacetic acid, paraquat	CT= 24, T= 28±2 pH= 3, AD= 1.0 [EC]= 20–250	-	82.6-175.4 71.4-92.6	[16]
							Cu ²⁺ zeolite 4A	Glyphosate	CT= 2, T= room, pH= 6– 8, AD= 2.0, [EC]= 100	-	112.7	[17]
							Powdered zeolites: FAU 1/FAU 2	Azithromycin, ofloxacin, sulfamethoxazole	CT= 6, pH= 6.5, [EC]= 0.1	≥ 80	7.0-8.5 25.3-31.2 -	[18]

Table 2. Conventional materials used for ECs removal from synthetic water in batch adsorption process (continuation)

Adsorbent characteristics			Adsorption behavior						
Adsorbent	Composition/ Functional Groups/ions	SA[m ² /g] P [cm ³ /g]	Adsorbent	EC removed	Adsorption conditions	Adsorption mechanism	Removal [%]	Adsorption capacity [mg/g]	Reference
Clays: Hydrous aluminosilicates (N.O.) ²⁰	SiO ₂ , CO ₃ ²⁻ , MO _x ^{19/} Ca ²⁺ , Mg ²⁺ , H ⁺ , K ⁺ , NH ₄ ⁺ , Na ⁺ , SO ₄ ²⁻ , Cl ⁻ , PO ₄ ³⁻ , NO ₃ ⁻ , and OH ⁻ ^{19,20}	SA: 10–426 ^{19,20} P: 0.1–0.5 ²¹	Natural clay	Methomyl	CT= 3, T= 25± 1 pH= 6.6, AD= 10 [EC]= 19.99–43.71	Ion exchange, coordination, dipole-dipole interactions, Van der Waals forces, H- bonding, hydrophobic bonding, acid- base forces. ²⁰	27.6–32.9	0.3–0.5	[22]
			Bentonite	Atenolol, sulfamethoxazole, diclofenac	CT= 24, T= 20 pH= 6.5–8.0, AD= 6 [EC]= 1–50		-	5.3–24.5 1.1–3.5 1.1–4.0	[23]
			Sodium smectite	Tramadol, doxepin	CT= 16, T= 20 pH= 6–7, AD= - [EC]= 10		-	210.7 279.4	[24]
			Bentonite + Surfactant	Diuron and their byproducts	CT= 24, T= 18–20 pH= 3, AD= 0.5 [EC]= 0.25		-	0.1–0.6	[25]
			Organo- montmorillonites,organo- pillared-montmorillon, organo-acid-activated montmorillonite	2,4,5- trichlorophenol	CT= 2, T= 20±1 pH= 4, AD= - [EC] = 10–200		-	374.9	[26]
			Natural/modified bentonite	Methomyl	CT= 2, T= 20, 30, 40 pH= 4, AD= 10 [EC] = 0.1		66–76	5	[27]

- meaning= this information is not presented in the bibliographical reference. Information obtained from ¹Grassi et al., (2012b),²Jiang et al., (2018), ³Mubarik et al., (2012), ⁴Sophia & Lima, (2018), ⁵Álvarez-Torrellas et al., (2016), ⁶Derylo-Marczewska et al. (2019), ⁷Benjedim et al. (2020), ⁸H. Kaur et al. (2017), ⁹Forouzesh et al. (2019), ¹⁰H. Kaur et al. (2019), ¹¹García-Mateos et al. (2015), ¹²Reeve et al., (2018), ¹³Lye et al. (2017), ¹⁴Rasamimanana et al. (2016), ¹⁵Sun et al. (2017), ¹⁶Pukcothanung et al. (2018), ¹⁷Zavareh, et al. (2018), ¹⁸De Sousa et al. (2018), ¹⁹Srinivasan et al. (2011), ²⁰Thiebault (2019), ²¹Kuila and Pasat (2013), ²²Nassar et al. (2012), ²³Lozano-Morales et al. (2018), ²⁴Thiebault et al. (2015), ²⁵Bouras et al. (2004), ²⁶Zaghouane-Boudiaf & Boutahala (2011), ²⁷León et al. (2021)

Versión Aprobada para Defensa Oral

1.2.2. Inorganic non-conventional materials

The use of inorganic non-conventional materials is most common in the removal of dyes and heavy metals. For EC removal, it is preferred to use inorganic materials with acid/basic modifications or impregnated (metal oxides or other functional groups) since these modifications increase their ability to remove them. The modifications can also reduce the contact time/dosage of the adsorbent, just like conventional materials (Akhtar et al., 2015; Islam et al., 2018). Among the most widely used non-conventional inorganic materials are alumina, manganese oxides, and silica.

Alumina is an amphoteric oxide ($\text{pH} < 7 = \text{charge}(+)$ and $\text{pH} > 7 = \text{charge}(-)$) so this adsorption capacity depends on pH (Kasprzyk-Hordern, 2004). Alumina is not commonly used in ECs removal. However, there are some studies in which tetracycline (Turku et al. 2007), atrazine, norfloxacin, ciprofloxacin (Nguyen et al., 2020), propazine, prometryne, propachlor, propanil, molinate, and phenols/chlorinated phenols (Aazza et al. 2017, 2018), acrylic acid (H. Khan et al., 2020) were removed. The efficiency/adsorption capacities have reached values from 15 to 95%/0.07 to 312.02 mg/g, respectively (Aazza et al. 2017, 2018; Bui and Choi 2009; Chen et al., 2015; H. Khan et al. 2020; Nguyen et al. 2020).

Meanwhile, manganese oxides (MnO_x) are considered efficient adsorbents due to their polymorphism, natural availability, easy synthesis at the industrial scale, low-cost (0.05 USD/kg), and non-toxicity (Islam et al., 2018). Some ECs, such as mercaptobenzothiazole, EE2, triclosan, tetracycline, endocrine disruptors, steroid estrogens, BPA, glyphosate, chlorophene, oxytetracycline (Islam et al., 2018), carbamazepine, niclosamide (Tran, 2018), clarithromycin and roxithromycin (Feitosa-Felizzola et al., 2009; Remucal & Ginder-Vogel, 2014), diclofenac (Liu et al. 2018; Remucal and Ginder-Vogel 2014), resorcinol (Zhao et al. 2012) have been removed using MnO_x , reaching removal efficiencies between 40 and > 90% (Islam et al. 2018; Remucal and Ginder-Vogel 2014; Zhang et al. 2008). Likewise, silica-based adsorbents are inexpensive and highly available (Turku et al., 2007). Silica has been used in the ECs removal, such as carbamazepine, clofibric acid, diclofenac, ibuprofen, ketoprofen, norfloxacin, ciprofloxacin, delta-9-tetrahydrocannabinol (Akhtar et al., 2015; Bui & Choi, 2009), naproxen, phenols, cloprop(2-(3-chlorophenoxy) propionic acid, dihydro carbamazepine (Bui & Choi, 2009); reaching removal efficiencies from 0 to > 90% with adsorption capacities from 2.1 to 429.0 mg/g (Akhtar et al., 2015; Bui & Choi, 2009; Diagboya & Dikio, 2018).

Table 3 summarizes previous studies using inorganic materials for the ECs removal. Inorganic materials are less used in the ECs removal, where fewer previous studies were found probably due to their lower adsorption capacity (0.16 – 52.00 mg/g). This could be associated with the lower surface area (12 – 1,000 m^2/g), porosity (0.53 – 1.03), and low variety of functional groups. Like adsorption with conventional materials, there are also very varied parameters, but the temperature has been kept in a range between 19 and 30 °C.

Versión Aprobada Para Defensa Oral

Table 3. Inorganic non-conventional materials in ECs removal using synthetic water in the batch adsorption process.

Adsorbent characteristics			Adsorption behavior						
Adsorbent	Composition/ Functional Groups/ions	SA[m ² /g] P [cm ³ /g]	Adsorbent	EC removed	Adsorption conditions	Adsorption mechanism	Removal [%]	Adsorption capacity [mg/g]	Reference
Manganese oxide: N.O. and S.O ¹	Mn(II), Mn(III), Mn(IV) or Mn(VII) ^{1,2/} Mn-O, OH ⁻³	SA: 12–236 ¹	Manganese oxide	Diclofenac	CT= 33, T= 30, pH= 7.0, AD =0.61 [EC]= 49946.41	Electrostatic, cation- exchange interactions and Van der Waals forces ⁴	Up to 90±0.7	-	[4]
			Manganese oxide	Phenol	CT= 1, T= 19, pH= 6.7±0.5, AD= 10.0 [EC]= 0.5		~40	-	[3]
			Manganese oxide	Clarithromycin Roxithromycin	CT= 24, T= 20, pH= 5.0, AD= 1.0 [EC]= 4.94–83.70		85–90	-	[5]
			Manganese oxide + Fe	Resorcinol	CT= 0.33–2.0, pH= 5.0, AD= 0.0157 [EC]= 35.0		~100	-	[6]
			Manganese oxide birnessite	Niclosamide	CT= 24, T= 22±2, pH= 5.0, AD= 0.015 [EC]= 0.042		-	-	[7]
			Alumina and surfactant modified alumina	Ortho-Nitro-Phenol	CT= 1, pH= 6.0, AD= 5.0 [EC]= 55.64		-	4.4–7.3	[8]
			α -Alumina nanoparticles and Modified α - Alumina nanoparticles	Ciprofloxacin	CT= 1.5, T= 25±2, pH= 6, AD= 5, [EC]= 10		33.6–97.8	34.5	[12]
Alumina: N.O. and S.O. <small>8.57u-64y*40-y7u9</small>	MO _x , FeO, SO ₄ ²⁻ , Al ₂ O ₃ (α , β , γ) ^{10/} O-Al-O, OH ⁻	SA: 50–300 _{9,10}	Raw alumina and Raw alumina modified with HCl	Acrylic acid	CT= 0.5–120, T= 20–50, pH= 4.5, AD= 66.7, [EC]= 0.08	Electrostatic interactions and hydrogen bonding ^{11,15}	32.1–36.2	0.29–0.31	[13]
			Alumina and HDTMA modified alumina	Metha-nitrophenol	CT= 1, T= 25–45, pH= 6.0, AD= 5.0 [EC]= 0.4		-	3.0–8.1	[14]
			MCM-41	Norfloxacin	CT= 1, T= 15, pH= 3.0–7.0, AD= 0.5 [EC]= 60.0		> 80	52	[19]

Vers

Table 3. Inorganic non-conventional materials used for ECs removal from synthetic water in batch adsorption process (continuation)

Adsorbent characteristics			Adsorption behavior						
Adsorbent	Composition/ Functional Groups/ions	SA[m ² /g] P [cm ³ /g]	Adsorbent	EC removed	Adsorption conditions	Adsorption mechanism	Removal [%]	Adsorption capacity [mg/g]	Reference
Silica: N.O. and S.O. _{16,17}	SiO ₂ ^{16/}	SA: 7.5–up to 1000 _{17,18}	Silica	Tetracycline	T= 23, pH= 6.0, AD= - [EC]= -	H bonds or cationic exchange _{17, 19}	-	-	[15]
			Mesoporous silica SBA-15	Carbamazepine	CT= 2, T= 25, pHa-d= 5, pHe=3, AD= 2.0 [EC]= 0.1				
	Diclofenac	0.34							
	Ibuprofen	0.41							
	Si-O-H, OH ⁻ ¹⁷	P: 0.53– 1.03 ¹⁹	Ketoprofen	0.28					
Clofibrac acid			0.07						

- meaning= this information is not presented in the bibliographical reference. Information obtained from ¹Remucal and Ginder-Vogel (2014); ²Islam et al. (2018); ³Zhang et al. (2008), ⁴Liu, et al. (2018), ⁵Feitosa-Felizzola et al. (2009), ⁶Zhao et al. (2012), ⁷Tran et al. (2018); ⁸Aazza et al. (2017); ⁹Gupta and Suhas (2009); ¹⁰Kasprzyk-Hordern (2004); ¹¹Dao et al. (2020); ¹²Nguyen et al. (2020); ¹³Khan et al. (2020); ¹⁴Aazza et al. (2018); ¹⁵Turku et al. (2007); ¹⁶Akhtar et al. (2015); ¹⁷Bui and Choi (2009); ¹⁸Diagboya and Dikio (2018); ¹⁹Chen et al. (2015); ²⁰Bui and Choi (2009).

Versión Aprobada para DC

1.2.3. Organic non-conventional materials

1.2.3.1. Biochar

Biochar is a product of the thermal/hydrothermal decomposition of biomass under anoxic/limited oxygen conditions (Ahmed et al. 2016a). Biochar presents some advantages concerning the common activated carbon as high availability, low-cost of renewable raw material (350 – 1,200 USD/ton), the high surface density of polar functional groups, and condensed structure (Thompson et al., 2016). In addition, raw/modified biochar has more environmental applications than activated carbon, such as soil amendment, carbon sequestration agent, in fuel cells and supercapacitors (Rangabhashiyam & Balasubramanian, 2019; Thompson et al., 2016).

Biochar is widely used in EC removal at the lab level, achieving similar efficiencies (~ 95%) as activated carbon (Rangabhashiyam & Balasubramanian, 2019). Among the ECs removed have been sulfamethoxazole, sulfathiazole, sulfamethazine, ibuprofen, triclosan, diclofenac, imidacloprid, atrazine, dibutyl phthalate, dimethyl phthalate (Bedia et al., 2018), tetracycline (Bedia et al., 2018; Ning et al., 2014), benzophene, benzotriazole (Kim et al., 2016), BPA, E2 (Bedia et al., 2018; Kim et al., 2016), carbamazepine, metolachlor, EE2, propranolol, phenols, pesticides (L. Li et al., 2018). In general, adsorption capacities from 1.5 to > 640 mg/g were reported (Bedia et al., 2018; Chen et al., 2020; L. Li et al., 2018; Rangabhashiyam & Balasubramanian, 2019).

1.2.3.2. Chitosan

Chitosan is a highly available and non-porous material from a deacetylated derivative of chitin, which is the second most abundant natural organic resource (J. Wang et al., 2018). In fact, more than 1,362 x 10⁶ and 1,818 tons/year are produced of chitin and chitosan, respectively. Chitosan is a relatively low-cost (2.2–4.4 USD/kg) adsorbent, non-toxic, biocompatible, biodegradable, and reactive, that has been easily modified through physical/chemical methods (Ali et al., 2012; Lessa et al., 2018; Zhou et al., 2014). Due to the low adsorption capacity, which is associated with its crystalline and swellable nature, low porosity, hydrophilicity, surface area, and stability in acid media, chitosan is used in composites within wastewater treatment (J. Wang et al., 2018).

Chitosan has been used in the removal of phenols (Tarasi et al., 2018; Zhou et al., 2014), pramipexole (Kyzas et al., 2013; Kyzas et al. 2017), alkyl benzene sulfonate, caffeine, sulpiride, bezafibrate (Zhou et al., 2014), sulfamethoxazole, BPA, A. Zhou et al., 2019), 2,4-dichlorophenol and 2,4,6-trichlorophenol, clofibrac acid, tannic acid, alkyl benzene sulfonate (Nie et al., 2014). This material has reached adsorption capacities from 27 to > 1,500 mg/g and adsorption efficiencies between 11 and 96% (Nie et al. 2014; A. Zhou et al. 2019; Zhou et al. 2014).

1.2.3.3. Peat moss

Peat is a complex product of the soil and organic matter decomposition and is available throughout the world from a few meters to tens of meters. Thus, it is a low-cost material (0.04 USD/kg) (Ali et al., 2012). Moreover, peat could compete industrially with adsorbents, such as activated carbon and zeolite due to their high cation exchange capacity. Peat has been used in the removal of sulfamethoxazole, sulfapyridine (Chen et al. 2017), metolachlor, phenol, p-chlorophenol (Ali et al., 2012), BPA (Zhou et al. 2012), p-nitrophenol, tri (n-butyl) phosphate, tris (2-butoxy ethyl) phosphate, and tris (2-chloroethyl) phosphate (Zheng et al., 2016). Thus, this material has achieved removal percentages higher than 70% and absorption capacities between 1.71 and 31.40 mg/g (Ali et al., 2012; Zheng et al., 2016; Zhou et al., 2011, 2012).

1.2.3.4. Agricultural/agro-industrial residues

Agricultural/agro-industrial residues, such as fruit peels and seeds, husks and shells of legumes and cereal are favorable for the ECs removal. These materials show a high availability, and chemical stability with the presence of lignin (20 – 30%), cellulose (35 – 50%), and hemicellulose (15 – 30%) (Almeida-Naranjo, et al. 2021a; Mo et al. 2018). They have a renewable nature, and low or no cost (e.g., rice husk between 1.6 and 2.7 USD/ton) (FAO, 2000; Mo et al., 2018). In addition, they are environmentally friendly, and

require little processing (washing, drying, grinding, and sieving), adding value to material that is generally not used to remove contaminants (Paredes-Laverde et al. 2018).

Agro-industrial residues have been reported removing acetaminophen, atenolol, caffeine, carbamazepine, diclofenac, ibuprofen, sulfamethoxazole, tetracycline, levofloxacin, ciprofloxacin, atrazine, clofibrac acid (Quesada et al., 2019), oxytetracycline, florfenicol (Ngigi and Thiele-Bruhn 2018), norfloxacin (Paredes-Laverde et al., 2018), phenolic compounds (Bhatnagar et al. 2015; Mallek et al. 2018; Mubarik et al. 2012; Ofomaja 2011). The removal efficiencies and adsorption capacities have achieved values between 60 and > 90% and from 0.37 to 689 mg/g, respectively (Bhatnagar et al., 2015; Larous & Meniai, 2012; Paredes-Laverde et al., 2018; Quesada et al., 2019).

1.2.3.5. Industrial residues

Fly ash (combustion residues), red mud (aluminum industry residues), slag (steel industry residues), slurry, and sewage are industrial residues (Lin & Juang, 2009). Municipal sewage sludge from EU27 (27 European Union) has estimated to reach around 13 million tons/year in 2020 (Devi & Saroha, 2016). Besides, the management of these residues could be costly. For instance, sludge treatment represents between 25 and 65% of the water treatment costs (Lin & Juang, 2009). Moreover, it is a problem for municipalities/industries due to the contaminant loading and huge production. A possible use of these residues is EC removal since they are considered good adsorbents due to their characteristics (Table 4) and low cost (0.020 – 0.1 USD/kg) (Lin & Juang, 2009; Tran et al., 2019).

Industrial residues have been used to remove tetracycline (Yang et al., 2019), sulfamethoxazole, trimethoprim (Nielsen & Bandosz, 2015, 2016), dichloro phenoxy acetic acid, phenols (Lin & Juang, 2009), carbamazepine (Nielsen & Bandosz, 2015), BPA, 17-beta-estradiol, 17-alpha-ethinylestradiol, sulfamethyldiazine, sulfamethazine, sulfathiazole, fluoxetine, ibuprofen, carbofuran (Devi and Saroha 2016; Gupta et al. 2006). The removal efficiencies have reached from 2 to > 90% and with adsorption capacities between 0.6 and 212 mg/g (Devi & Saroha 2016; Lin & Juang, 2009; Nielsen & Bandosz, 2015; Sharipova et al., 2016).

1.2.3.6. Polymeric adsorbents

Polymeric adsorbents are easily regenerated (soft washing) and their surface could be modified (polar or non-polar) to remove specific contaminants (Akhtar et al., 2015). Furthermore, polymeric adsorbents have lower costs than activated carbon (up to 4 times lower). They are produced sustainably and have higher adsorption (15 – 200 times faster) than activated carbon (Akhtar et al., 2015; Alsbaiee et al., 2016). ECs, such as cephalosporin C, penicillin V, delta-9-tetrahydrocannabinol, nalidixic acid (Akhtar et al., 2015), ibuprofen, cephalaxim, caffeine, phenols, cefadroxil, erythromycin, BPA, alachlor, trifluralin, prometryn, amitrole (Pan et al., 2009), diclofenac, BPA (Alsbaiee et al. 2016; X. Li et al. 2018a) have been removed using polymeric adsorbents. In their removal, polymers, such as β -cyclodextrin polymer (Alsbaiee et al., 2016), post-cross-linked polystyrene/poly (methyl acryloyl diethylenetriamine) (Li et al., 2016), polystyrene, polyacrylic ester, polyacrylamide, resins (Amberlite XAD-16, XAD-4, XAD-2, XAD-7), polymer-based inorganic hybrids (polymeric matrix+inorganic nanoparticles) have been used. They have achieved adsorption capacities between 22.2 and 1,401 mg/g and removals higher than 90% (Akhtar et al., 2015; Alsbaiee et al., 2016; Pan et al., 2009).

Table 4 resumes the performance of non-conventional organic materials used as adsorbents for ECs removal. Non-conventional organic materials have been widely used in ECs removal because some of them have a comparable efficiency with conventional materials (up to 100%). This is because they have comparable physical and chemical characteristics, except for their surface area concerning conventional materials. Moreover, non-conventional organic materials have other advantages, such as high availability, low/null cost, and even their use can avoid final disposal problems since some of these materials are residues (Almeida-Naranjo, et al., 2021a). Therefore, the use of materials such as these can be an alternative to wastewater treatment in developing countries (Tejedor et al., 2020).

Table 4. Organic non-conventional materials used for EC removal from synthetic water in the batch adsorption process.

Adsorbent characteristics			Adsorption behavior							
Adsorbent	Composition/ Functional Groups/ions	SA[m ² /g] P [cm ³ /g]	Adsorbent	EC removed	Adsorption conditions	Adsorption mechanism	Removal [%]	Adsorption capacity [mg/g]	Reference	
Biochar:	C, H, O, N ^{1/}	AS: 2.46–1500 ¹	Methanol-modified biochar from rice husk	Tetracycline	CT= 0.33, T= 30, pH= 2.0, AD= 1.0 [EC]= 100	Ion exchange, Electrostatic, hydrophobic, pore- filling, and bridging interactions ³	-	~80	[4]	
	S.O. ¹	P: 0.21– 0.95 ^{2,3}	Modified biochar + <i>Spirulina sp.</i>	Tetracycline	CT= 120, T= 20–40, pH= 3-9, AD= 0.1 [EC]= 100					-
Chitosan:	α-D-glucosamine ^{7/}	AS: 1.1–23.4 ^{8,9} P: 0.002–0.7 ^{8,9}	Modified chitosan with 2-hydroxy-1- naphthaldehyde	Phenol 2-chlorophenol 4-chlorophenol 2,4-dichlorophenol 2,4,6-trichlorophenol	CT= 3, T= 20, pH= 7.0, AD= 1.0 [EC]= 150	Electrostatic and hydrophobic interactions and hydrogen bonding ⁶	-	59.7 70.5 96.4 315.5 375.9	[8]	
			Chitosan grafted with sulfonic acid and cross- linked with glutaraldehyde	Pramipexole	CT= 24, T= 25, pH= 10, [EC]= 0– 500			181		[10]
	S.O. ⁶	OH ⁻ , -NH ₂ ⁶	Sulfonate-grafted chitosan	Pramipexole	CT= 0-24, T= 25, 45, 65, pH= 2-12, AD= 1.0 [EC]= 0–500			11–82	181–367	[11]
			Magnetic modified chitosan	Phenol BPA	CT= 0.67, T= 45, pH= 4.5, AD= 0.6 [EC]= 376–913			96 85.5	-	[12]
Peat:	Cellulose, lignin, humic acid, fulvic acid ^{9,6/}	AS: 0.9–>200 ¹³	Fibric peat modified	BPA	CT= 4, T= 25, pH= 6.9, AD= 0.05, [EC]= 45.0	Hydrophobic Interactions, hydrogen bonding ^{14,15}	-	31.4	[14]	
			Raw/modified peat	BPA	CT= 4, T= 25, pH= 7.0, AD= 1.0 [EC]= 2.0					80
	N.O.	Alcohols, aldehydes, ketones, carboxylic acids, and phenolic hydroxides ^{13,6}	P: 70–95% ¹³	Commercial peat soil	Sulfamethoxazole, sulfapyridine				CT= 168, T= 25±3, AD= 20.0, pH= 4.4– 9.5 [EC]= 0.15- 13.46	-
Agro- industrial residues:			Rice husk	Norfloxacin	CT= 1, T= 25, pH= 6.2, AD= 3.0 [EC]= 5		96.95	20.1	[17]	
			Coffee husk				99.66	33.6		

Table 4. Organic non-conventional materials used for ECs removal from synthetic water in batch adsorption process (continuation)


Adsorbent characteristics			Adsorption behavior							
Adsorbent	Composition/ Functional Groups/ions	SA[m ² /g] P [cm ³ /g]	Adsorbent	EC removed	Adsorption conditions	Adsorption mechanism	Removal [%]	Adsorption capacity [mg/g]	Reference	
Agro-industrial residues:	Cellulose (35–50%), lignin (20–30%), and hemicellulose (15– 30%), pectin, among others ^{6/}	SA: 0.034– 120 ^{6,18} P: 0.03–4.8 ^{18,19}	Rice husk	E1 +E2+ E3	CT= 4, T= 25, AD= 12, [EC]= 3.5–7		45–90	1.0–2.7	[22]	
			Granulated cork	<u>Phenols</u> Phenol, 2-chlorophenol, 2- nitrophenol, 2,4- dichlorophenol, Pentachlorophenol <u>PPCPs</u> Carbamazepine, naproxen, ketoprofen, diclofenac, triclosan, methyl paraben	CT= 0.5, T= 20±2, pH= 6.0, AD= 5–20 [EC](phenols)= 30.0, [EC](PPCPs)= 1.0		<u>Phenols</u> 20–100 <u>PPCPs</u> 50–100	<u>Phenols</u> 0.6–1.6 <u>PPCPs</u> 1.8–3.6	[23]	
			Pine cone + Pig manure (BCP)	Sulfamethazine, ciprofloxacin, oxytetracycline, florfenicol	CT= 48, T= 20, pH= 7.6 – 8.5, AD= 1.0 w/w%, [EC]= 1.2		-	-	[24]	
			Mansonia wood sawdust	4-nitrophenol	CT= 2.5, T= 26±4, pH= 4.0, AD= 1.5 [EC]= 120		π - π interactions, the formation of H-, - COOH and C = O bonds, and Electrostatic interactions ^{18,20,21}	22.5–55.5	7.4–18.0	[25]
			Charred sawdust of Sheesham	Phenol	CT= 1.5, T= 25±2, pH= 2-6, AD= 0.1– 10 [EC]=10–1000		-	> 95.0	300.6–337.5	[26]
			Sawdust from Finland wood	Phenol	CT= 3, T= 22, pH= 5.79, AD= 10 [EC]= 20		-	Up to 70.4	Up to 5.5	[27]
			Fertilizer and steel industry wastes	2,4-dichloro phenoxy acetic acid, carbofuran	CT= 1.67, T= 25, pH= 6.5–7.5, AD= 1.0 [EC]= 88.01–132.76		Polar interaction, hydrogen bonding, π - π	-	212 208	[32]
Industrial residues:	SiO ₂ , Fe ₂ O ₃ , Al ₂ O ₃ , CaO, MgO, organic compounds ^{29/}	Raw: 2– 34 Treated or activated: up to 1800 ^{21, 30,31} Treated or activated: 0.098-0.145 ^{21,31}	Sewage Sludge and fish waste	Carbamazepine+ sulfamethoxazole+ trimethoprim	CT= 5, T= 30, pH=9.39–11.82, AD= 5.0 [EC]= 100 (Of each one)	electron- donor- acceptor, acid-base interactions ²⁹⁻³¹	-	Up to 41.3 Up to 3.8 Up to 13.6	[31]	
			Sewage Sludge and fish waste	Trimethoprim, sulfamethoxazole	CT= 180, T= 30, pH= 4.53–7.64, AD= 5.0, [EC]=100	-	90.0 5.3	[29]		

Table 4. Organic non-conventional materials used for ECs removal from synthetic water in batch adsorption process (continuation)

Adsorbent characteristics			Adsorption behavior						
Adsorbent	Composition/ Functional Groups/ions	SA[m ² /g] P [cm ³ /g]	Adsorbent	EC removed	Adsorption conditions	Adsorption mechanism	Removal [%]	Adsorption capacity [mg/g]	Reference
Industrial residues:			Paper pulp-based adsorbents + H ₃ PO ₄	Carbamazepine, sulfamethoxazole	T= 25, pH= 7.5, [EC]= 5		-	92±19 13±0.6	[33]
			Phosphoric acid-activated corn straw porous carbon	Tetracycline	CT= 12, T= 30, pH= 4, AD= 0.2-1.0 [EC]= 50		8.03–97.0	227.3	[34]
			Activated carbon from gas mask	Triclosan	CT= 10, T= 24±1, pH= -, AD= 1x10 ⁻³ [EC]= 10–400		2-100	85	[35]
			Carbon slurry waste	2-bromophenol, 4-bromophenol, 2,4-dibromophenol	CT= 11, T= 25±2, pH= 5.8–6.8, AD= 1.0 [EC]= 69.2–100.76		-	40.7 170.4 190.2	[28]
			Hyper-crosslinked β-cyclodextrin	BPA	CT= 0.5-12, T= 25, AD= 0.25, [EC]= 40		94.45	278	[38]
Polymeric adsorbents:	Depending on the polymer ^{36,37/}		Post-cross-linked polystyrene/poly (methyl acryloyl diethylenetriamine)	Phenol, benzoic acid, P-hydroxybenzoic acid	CT= 2.0, T= 25, 35, 45, AD= 2.0 [EC]= 507.3	Hydrophobic interaction, π-π interaction, ionic attraction, hydrogen bonding; complex formation ^{36,37}	> 90	50 190 242.1	[39]
	Tertiary amino, Carboxyl, sulfonic acid, dicyandiamide, amido cyanogen, polyethylene glycol, 2-Carboxy-3/4-nitrobenzoyl, among others ³⁶	SA: 15–1000 ^{35,36} P: 0.16–1.22 ^{35,36}	Hyper-crosslinked β-cyclodextrin porous polymer	BPA	CT= 0.17, T= room, AD= 1 [EC]= 22.8		80–95	22.2	[40]
	S.O. ^{35,36}		Molecularly Imprinted Polymer	Diclofenac	CT= 1, T= room temperature, pH= 7, AD= 5 [EC]= 1-25		100	160	[41]

- meaning= this information is not presented in the bibliographical reference. Information obtained from ¹Rangabhashiyam and Balasubramanian (2019); ²Ahmed et al. (2016a); ³Kim et al. (2016); ⁴Jing et al. (2014); ⁵Choi et al. (2020); ⁶Mo et al. (2018); ⁷Zhai et al. (2019) ⁸Zhou et al. (2014); ⁹Nie et al. (2014); ¹⁰Kyzas et al. (2017); ¹¹Kyzas et al. (2013); ¹²Tarasi et al. (2018); ¹³Grassi et al. (2012b); ¹⁴Zhou et al. (2011); ¹⁵Zhou et al. (2012); ¹⁶Chen et al. (2017); ¹⁷Paredes-Laverde et al. (2018); ¹⁸Bhatnagar et al. (2015); ¹⁹Quesada et al. (2019); ²⁰Anastopoulos et al. (2020); ²¹Silva et al. (2017); ²²Honorio et al. (2018); ²³Mallek et al. (2018); ²⁴Ngigi et al. (2018); ²⁵Ofomaja (2011); ²⁶Mubarik et al. (2012); ²⁷Larous and Meniai (2012); ²⁸Bhatnagar (2007); ²⁹Nielsen and Bandosz (2016); ³⁰Devi and Saroha (2016); ³¹Nielsen and Bandosz (2015); ³²Gupta et al. (2006); ³³Oliveira et al. (2018); ³⁴Yang et al. (2019); ³⁵Sharipova et al. (2016); ³⁶Akhtar et al. (2015); ³⁷Pan et al. (2009); ³⁸X. Li et al. (2018) ³⁹H. Li et al. (2016); ⁴⁰X. Li et al. (2018); ⁴¹Abu et al. (2018)

Version 1

1.2.4. Nanomaterials

Nanomaterials have at least one size dimension between 1 and 100 nm. In recent years, nanomaterials (nanoparticles, nanotubes, nanofilms, and nanowires) have attracted a lot of interest in wastewater treatment applications, mainly in adsorption and photocatalysis at lab scale (Y. Zhang et al., 2016; Zhao et al., 2018). They are called new-generation adsorbents due to their high performance, high surface area (up to 3,200 m²/g), appropriate dispersibility, catalytic potential, large surface energy, abundant reactive sites, rapid dissolution, high reactivity and free surface energy (> surface reactivity) (Zhao et al., 2018). Nevertheless, the recovery of non-magnetic nanoparticles after the EC adsorption is still complicated and some of them are toxic (Y. Zhang et al. 2016). Therefore, adequate techniques must be used to separate the nanoparticles from the aqueous solution to take advantage of the benefits that these materials offer. In addition, the green synthesis of nanomaterials (e.g., Fe, Ag, Au, Zn, zero valent or magnetic nanoparticles) using biomolecules, biological waste products, cellular extracts of plants (e.g., Andean blackberry leaf) (Kumar et al., 2016), bacteria, fungi, and algae have been researched. Bio-reduction and bio-precipitation of polyphenols, peptides, amino acids, and other bioactive compounds obtained from living organisms (mainly plants) are the biogenic production mechanism of nanomaterials. Furthermore, these compounds prevent agglomeration because act as protective/stabilizing agents of the synthesized nanomaterials (Gautam et al., 2019).

The ECs removal efficiencies have achieved close to 100% using lower adsorbent doses than micro-adsorbents (Almeida-Naranjo et al., 2021b). Chemical modifications in nanoparticles to improve their adsorption capacities have been realized (Pham et al., 2020). Nevertheless, no study has used modified materials to explain if modifications are sustainable processes to improve EC removal. Thus, there is not enough information about the residues produced after the modification or if the higher efficiency obtained to use the raw material is costly representative (Almeida-Naranjo, et al., 2021a, b). Furthermore, all studies have been carried out at a lab scale, and none of them have analyzed the feasibility of full-scale synthesis of nanomaterials (Almeida-Naranjo, et al. 2021b). Among the most used nanomaterials in EC removal are carbon-based nanoparticles, metal oxides, metal nanoparticles, and nanocomposites. Some of these nanomaterials are described below.

1.2.4.1. Carbon-based nanomaterials

Carbon-based nanomaterials are the most used for the removal of contaminants from wastewater, due to their good adsorptive characteristics for the removal of organic/inorganic contaminants and microorganisms (Kim et al. 2014).

a. Carbon Nanotubes (CNTs)

CNTs are the most anisotropic materials available, which are formed by hollow and layered structures with a length from nanometers to millimeters (Yu et al. 2014). CNTs can be a single wall (SWCNT, cylindrical) or multiple walls (MWCNT, concentric cylinders), with diameters from 0.4 – 2.0 to 2.0 – 25.0 nm, respectively (Gupta et al., 2013; Yu et al., 2016). CNTs have chemically inert surfaces that promote physical adsorption. However, their surface could be modified by incorporating heteroatoms, this increasing their affinity with different ECs, the selectivity of adsorption through families of compounds, and improving their performance in the desorption process (Kim et al. 2014).

CNTs have been used to remove ECs, such as pharmaceuticals (tetracycline, oxytetracycline, sulfamethoxazole, sulfapyridine, sulfamethazine, ciprofloxacin, norfloxacin, ofloxacin, lincomycin, caffeine, etc.) (Kim et al., 2014; Yu et al., 2016; Zhao et al., 2018), and personal care products (triclosan) (Zhao et al., 2018), hormones (EE2), phenols, pesticides (atrazine, diuron, dichlobenil, isoproturon) (Joseph et al., 2011; Sophia & Lima, 2018), roxarsone (Hu et al., 2012). These materials have achieved removals between 67.5 and 99.8% and adsorption capacities between 8.6 and 554.0 mg/g (Hu & Cheng, 2015; Patiño et al., 2015; Sophia & Lima, 2018; Yu et al., 2016; Zhao et al., 2018).

b. Graphene

Graphene is a new material, considered the thinnest that exists (~ 0.03 nm). As a nano adsorbent, it includes three forms pristine graphene, graphene oxide (GO), and reduced graphene oxide (rGO) (Hiew et al., 2018). Graphene and these derivatives are characterized by having a large delocalized π -electron system and tunable chemical properties, characteristics that make them good adsorbents (Hiew et al., 2018; Yu et al., 2016). Besides, graphene has faster diffusion or surface reactions of antibiotics, which allows rapid and effective adsorption, and is cheaper at full-scale production than other adsorbents such as CNTs (M. Li et al., 2019). Nevertheless, the hydrophobicity and limited dispersibility of graphene decrease its potential for adsorbent purposes (Naseem & Waseem, 2021).

Graphene is considered a good adsorbent for ECs removal (19 – 3710 mg/g) (Catherine et al., 2018), reporting its use for the removal of EE2, E2 (Borthakur et al., 2018), diclofenac, levofloxacin, metformin, nimesulide, sulfamethoxazole, cefalexin, ofloxacin, amoxicillin, tetracycline, ciprofloxacin (Hiew et al., 2018), atenolol, clofibric acid, aminoglycoside, β -lactams, glycopeptide, macrolide, quinolone, sulphonamide (M. Li et al., 2019), acetaminophen (Moussavi et al., 2016), metformin (Balasubramani et al. 2020), nicotine (S. Liu et al. 2018). Moreover, graphene has achieved removals up to 100% (Baig et al., 2019; Hiew et al., 2018; X. Wang et al., 2019; Zhao et al., 2018)

1.2.4.2. Metal-based nano adsorbents

Metal-based nano adsorbents are characterized by their high efficiency for contaminant removal, relatively low-cost, and short distance of intraparticulate diffusion. Moreover, they are compressible without changes in their surface area, resistant to abrasion, magnetic, and photocatalytic (Y. Zhang et al., 2016). Additionally, metal oxide nanomaterials are environmentally friendly. Thus, these nanomaterials could be used combined with living beings in filter media, slurry reactors, powders, and pellets (Kundurur et al., 2017; Y. Zhang et al., 2016). Metal nano adsorbents include nanosized iron oxides, aluminum, manganese, titanium, magnesium, and cerium oxides. The characteristics that influence the ECs removal are described below.

Iron oxide nanoparticles are characterized by their relatively easy synthesis, magnetism, facilitates their recycling capability, low-cost (e.g., zero-valent iron: 1.66 USD/m³ of treated water), fast kinetics, and biocompatibility (Hamdy et al. 2018; Kumar et al. 2016). The iron nanoparticles most used in the adsorption processes for EC removal is zero-valent iron. However, magnetite (Fe₃O₄), maghemite (γ -Fe₂O₃), hematite (α -Fe₂O₃), and goethite (α -FeOOH) are also used but mainly as composites, and in degradation processes (Hamdy et al., 2018; H. Zhang et al., 2016).

Zero valent iron (ZVI) is characterized by having an iron oxide envelope and a Fe⁰ core, which exhibits a core-shell structure. ZVI shows a high reactivity, higher than conventional granular iron, dual properties of adsorption and reduction (-0.44 V), and easy dispersion (Crane & Scott, 2012). The removal of amoxicillin, norfloxacin, ampicillin, ciprofloxacin, chloramphenicol, dichloroacetamide, metronidazole, diazepam, tetracycline, oxytetracycline, cytostatic drugs, using ZVI has reported values between 50 and 100% (Zhou et al., 2019). Chloride (lindane, dichlorodiphenyltrichloroethane, atrazine) and organophosphates (tributyl phosphate) pesticides were removed by other mechanisms, such as oxidation, reduction, and coprecipitation (Crane & Scott, 2012; Zhou et al., 2019). To improve the capacity of zero-valent iron to remove ECs such as florfenicol, tetracycline, metronidazole, and enrofloxacin, chemical modifications were made, achieving removal efficiencies between more than 90 and 100% (Zhou et al., 2019).

ZVI has also been used in continuous adsorption processes for the removal of pharmaceuticals (carbamazepine, caffeine, sulfamethoxazole, 3,4-methylenedioxymphetamine, 3,4-methylenedioxymethamphetamine, ibuprofen, gemfibrozil, and naproxen) and sweeteners (acesulfame-K and sucralose) reaching efficiencies greater than 97 and 76%, respectively (Liu et al. 2019). However, ZVI presents some disadvantages associated with its very short life since it needs stabilization/surface modification and forms clumps due to the van der Waals and magnetic forces (Zhou et al., 2019).

Magnetite is commonly used in the adsorption of contaminants (mainly heavy metals) due to its low-cost, environmentally friendly nature and the possibility of treating large volumes of wastewater (Almeida-Naranjo, et al., 2021b). It is formed by octahedral layers, i.e. mixture of ferrous and ferric species and tetrahedral-octahedral structures (ferric species), interspersed with each other (Al-Jabari et al., 2019). Magnetite was used in the removal of ECs such as levofloxacin (Al-Jabari et al., 2019), caffeine (Almeida-Naranjo, et al., 2021b), nalidixic acid, salicylic acid, flumequine, benzotriazole (Minh et al., 2018), paracetamol, ciprofloxacin, oxytetracycline (Rakshit et al., 2013), reporting removals between 36.7 and 100.0% and adsorption capacities from 6.1 to 100.0 mg/g (Al-Jabari et al., 2019; Minh et al., 2018; Rakshit et al., 2013).

Maghemite is a low-cost material, and it is highly available. It has been used in the removal of diclofenac, achieving adsorption capacities between 120 and 261 mg/g (Leone et al., 2017). Magnetite and maghemite are characterized by their magnetism, which facilitates their separation after the adsorption process (Kunduru et al., 2017). However, these nanoparticles are very unstable because they can change to other phases, so before their use, they need to be stabilized. To avoid this problem these nanoparticles are used mainly in composites form (Zhao et al. 2017).

The other iron oxides used in EC removal are goethite and hematite. Goethite is not magnetic, so the separation from treated wastewater is more complicated, compared to magnetite and maghemite (Kunduru et al., 2017). Goethite is an abundant hydrated iron oxide from soils, that is used as a model adsorbent due to this thermodynamic stability at room temperature and its use in PPCPs adsorption in iron-rich soils (Qin et al., 2014). Thus, ECs such as levofloxacin (Qin et al. 2014), diclofenac, ibuprofen (R. Yin et al. 2018; Zhao et al. 2017), tetracycline, flumequine (Zhao et al., 2017), were removed using goethite, showing removal efficiency between 25 and 90% and adsorption capacities from 0.025 to 0.72 mg/g (Qin et al., 2014; R. Yin et al., 2018; Zhao et al., 2017). Hematite is the most stable phase of magnetic iron oxide (Kunduru et al., 2017), it was used in the removal of cephalexin (Nassar et al. 2018) and carbamazepine (Rajendran & Sen, 2018), and achieving removal efficiencies higher than 90% with adsorption capacities between 2.8 and 70.0 mg/g (Nassar et al., 2018; Rajendran & Sen, 2018).

There are other metal oxides, such as aluminum oxides, zinc oxides, magnesium oxides, and cerium oxides, which are used in the contaminant's removal. These oxides are characterized by their low-cost, thermal stability, easy synthesis, and regeneration, surface reactivity, versatility, among others (Dao et al., 2020; Fakhri & Behrouz, 2015). Nano-alumina (dichlorodiphenyltrichloroethane, polychlorinated biphenyls, ciprofloxacin) (Nguyen et al., 2020; Sivaselvam et al., 2020), nano-silica (ciprofloxacin) (Pham et al., 2020), zinc oxide (naphthalene) (Y. Kaur et al., 2017), magnesium oxide (linezolid) (Fakhri & Behrouz, 2015) are some nano-oxides used in the ECs removal, which have archived removal efficiencies between 55 and 100% (Fakhri & Behrouz, 2015; Y. Kaur et al., 2017; Pham et al., 2020; Sivaselvam et al., 2020).

1.2.4.3. Nanocomposites

A nanocomposite is a multiphase material where some materials are deposited on a support material. The most used support materials are polymers, graphene, zeolites, biochar, clay, CNT, activated carbon, silica, biopolymers (chitosan/cellulose/alginate), membranes, and magnetic substrates (Danalioğlu et al., 2017; Lompe et al., 2018; B. Wang et al., 2018). Nanocomposites are used in some environmental applications, including the removal of contaminants from wastewater (e.g., heavy metals, ECs, dyes) (B. Wang et al., 2018) since they exhibit better characteristics than many adsorbents, including activated carbon. Some properties that are improved when forming nanocomposites and make them better adsorbents are selectivity, stability (mechanical/chemical), porosity, separation of the aqueous medium (magnetism), reduction of adsorption time/adsorbent dose, cost, among others (Danalioğlu et al., 2017; Lompe et al., 2018).

Another advantage of nanocomposites is their photocatalytic properties. In the EC adsorption processes, these contaminants are only transferred from the aqueous medium to the adsorbent, but they are not degraded (Y. Zhang et al., 2016). Removing the ECs from the adsorbent to reuse it could be a difficult

and expensive process. Therefore, combining adsorption with photocatalysis may be efficient because the ECs will be degraded into less toxic substances (Zheng et al., 2016).

However, nanocomposites/nanoparticles can also have disadvantages, such as a complex synthesis that involves the use of substances that could be toxic (Boruah et al., 2016). Non-magnetic nanomaterials are difficult to separate from the aqueous medium. Even previous studies include nanomaterials within ECs (Sauvé & Desrosiers, 2014). Furthermore, the use of nanomaterials on a large scale is not possible yet.

Table 5 summarizes some research about the use of nanomaterials for EC removals, such as tetracycline, sulfachloropyradazine (Azhar et al., 2017), ametryn, prometryn, simazine, simeton, and atrazine (Boruah et al., 2016), metolachlor, BPA, tonalide, triclosan, ketoprofen, estriol (Alizadeh Fard & Barkdoll, 2018), linezolid (Fakhri & Behrouz, 2015), carbamazepine, ibuprofen, clofibrac acid (Deng et al., 2018; Wong et al., 2016), ciprofloxacin, erythromycin, amoxicillin (Danalioğlu et al., 2017; F. Wang et al., 2016), diclofenac (Hossein et al., 2017), sulfamethoxazole (Ma et al., 2020). They have achieved removal efficiencies between 25 and 100% with adsorption capacities between 0.9 and 3,070.0 mg/g (Alizadeh et al. 2018; Baghdadi et al. 2016; Lessa et al. 2018; M. Li et al. 2019; Peng et al. 2018; Reguval and Sarmah 2018; Wong et al. 2016; Y. Yin et al. 2018; Zaheer et al. 2018). The adsorption capacities of nanomaterials are comparable with conventional materials; however, the costs of nanomaterials are not discussed in the studies (Yu. Liu et al., 2014; Y. Liu et al., 2014).

Oral
Versión Aprobada para Defensa

Table 5. Nanoparticles used in ECs removal using synthetic water in the batch adsorption process.

Adsorbent characteristics			Adsorption behavior										
Adsorbent	Composition/ Functional Groups/ions	SA[m ² /g] P [cm ³ /g]	Adsorbent	EC removed	Adsorption conditions	Adsorption mechanism	Removal [%]	Adsorption capacity [mg/g]	Reference				
CNT: S.O. ¹	Graphene or graphite sheet with π conjugative structure and highly hydrophobic surface ^{1/} -OH, -C=O, - COOH, ²	SWCNT SA: 400–1020 ^{3,4} MWCNTs SA: 38.7–>500 ⁴ P= 0.59 ⁴	*SWCNT	17 α -ethynyl estradiol BPA	CT= 4, pH= 3.5-11, T= room, AD= 0.05 [EC]= 2.28-2.96	Hydrophobic effect, π - π interactions, hydrogen bonding, covalent bonding, and Electrostatic interactions ⁵	95–98 75–80	35.5–35.7 13.4–16.1	[6]				
			SWCNT MWCNT	Lincomycine, Sulfamethoxazole, iopromide	CT= 72, T= 20 \pm 1, pH= 6.0 \pm 0.2, AD=- [EC]= 12,000		-	-	[3]				
			MWCNT	Roxarsone	CT= -, T= 10, pH= 2–11.7, AD= 2 [EC]= 10		-	Up to 13.5	[7]				
			MWCNT MWCNT-COOH MWCNT-NH ₂ N-CNT	1,8dichlorooctane, nalidixic acid, 2-(4-ethylphenoxy) ethanol	CT= 72, T= 25, pH= 7.0 \pm 0.5, AD= 0.02–0.2 [EC]= 20–80		-	248–380 79–111	[8]				
			MWCNT modified with HNO ₃	Diclofenac	CT= 1, T= 25, pH= 7.0, AD= 5.4, [EC]= 50		Up to 95	Up to 8.6	[9]				
			Graphene: S.O. ¹⁰	2D single layer of sp ² hybridized carbon atom ^{10/} Epoxide, carbonyl, carboxyl, and hydroxyl groups ¹⁰	SA: 46.4–2630 (theoretical) ^{10,11} P: 0.065 ¹²		Graphene oxide	β -estradiol 17 α -ethynyl estradiol	CT= 0.83, T= 25, pH= 3.0, AD= 0.40 [EC]= 8.0	-	97.2 98.5	-	[13]
							Graphene oxide	Diclofenac	CT= 0.25, T= 60, pH= 6.0, AD= 0.16 [EC]= 400	Hydrophobic effect, π - π interactions, hydrogen bonding, covalent bonding, and Electrostatic interactions ^{5,10}	96.2	653.9	[14]
Graphene oxide	Metformin	CT= 1-3, T= 1545, pH= 4.5–8.5, AD= 0.05– 0.15 [EC]= 300–700				59–97.6	122.6	[15]					
Graphene oxide	Nicotine	CT= 0.5, T= 25–55 pH=3–10.5 AD= 0.1 [EC]= 5-150				-	96.5	[16]					
Double-oxidized graphene oxide	Acetaminophen	CT= 0.17, T= 25, pH= 8.0, AD= 0.02 [EC]= 10				83.7	704	[17]					
Graphene oxide nanoflakes	BPA, 4-nonylphenol, tetrabromineBPA	CT= 0.08–24, T= 25, pH= 4–9, AD= 1.25, [EC]=20	-	19-30	[18]								

Ver

Table 5. Nanoparticles used for ECs removal from synthetic water in batch adsorption process (continuation)

Adsorbent characteristics			Adsorption behavior						
Adsorbent	Composition/ Functional Groups/ions	SA[m ² /g] P [cm ³ /g]	Adsorbent	EC removed	Adsorption conditions	Adsorption mechanism	Removal [%]	Adsorption capacity [mg/g]	Reference
Nanocomposites: S.O. ³⁹⁻⁴¹	Depending on the components of the composite, for example, carbon atom, FeO _x , graphene, graphite sheet, among others/ Depending on the components of the composite, for example, OH-, COOH-, C=O, epoxy, amino, among others ⁴⁰⁻⁴²	SA: 3.18-around 1260 ³⁹ P: 0.15-0.72 ^{40,42}	MOFs UIO-66	Sulfachloropyridazine	CT= 2, T= 25, pH= 5.5, AD= 0.1, [EC]= 10-100	Depending on the components of the composite, are an example hydrogen bonding, π - π interaction, cation- π bonding, amidation reaction, Electrostatic interaction, hydrophobic interaction, ligand exchange, cation- π bonding, chemisorption, etc. ⁴⁰⁻⁴²	80	417	[43]
			Magnetic activated carbon	Triclosan Bisphenol-A Tonalide Metolachlor Ketoprofen E2	CT= 1, T= 25-45, pH= 7, AD= -, [EC]= 0.025-0.25		96 – 98	21.32 31.05 29.41 22.37 28.49 2020	[44]
			Magnetic activated carbon	Carbamazepine	CT= 0.5, T= 25, pH= 6.65, AD= 0.05, [EC]= 20.0		93	189.5	[45]
			Triethoxyphenylsilane (TECs)-functionalized magnetic palm-based powdered AC	BPA, carbamazepine, ibuprofen, clofibric acid	CT= 6, T= Room T, pH= 7, AD= 0.1, [EC]= 10		-	58.1-166.7	[46]
			Magnetic activated carbon/chitosan	Ciprofloxacin, erythromycin, amoxicillin	CT= 2, T= 25, pH= -, AD= 1.5, [EC]= -		54-82	90.1 178.6 526.3	[47]
			Magnetic cellulose ionomer/layered double hydroxide	Diclofenac	CT= 0.5, T= -, pH= 9, AD= 1.0, [EC]= 0.5		~100	268	[48]
			Magnetic chitosan grafted graphene oxide	Ciprofloxacin	CT= 8, T= -, pH= 5, AD= 0.33, [EC]= 20		-	282.9	[49]
			Fe ₃ O ₄ /graphene oxide reduced	Ametryn, atrazine prometryn, simazine, simeton	CT= 1.17, T= 25, pH= 5.0, AD= 0.5, [EC]= 10		93.6	54.8-63.7	[50]
			Fe ₃ O ₄ @SiO ₂ -Chitosan/GO	Tetracycline	CT= 8, T= 25, pH= 6, AD= 0.4, [EC]= 44.44		>90	-	
			Fe/Cu-GO	Tetracycline	CT= 0.25, T= 22, pH= 6.5, AD= 0.25, [EC]= 20-100		~100%	-	[41]
GO-BC	Sulfamethazine	CT= 12, T= 25, pH= 6, AD= 1, [EC]= 2031.8-20332	-	-					

Versi

Table 5. Nanoparticles used for ECs removal from synthetic water in batch adsorption process (continuation)

Adsorbent characteristics			Adsorption behavior						
Adsorbent	Composition/ Functional Groups/ions	SA[m ² /g] P [cm ³ /g]	Adsorbent	EC removed	Adsorption conditions	Adsorption mechanism	Removal [%]	Adsorption capacity [mg/g]	Reference
Nanocomposites: S.O. ³⁹⁻⁴¹	Depending on the components of the composite, an example carbon atom, FeO _x , graphene, graphite sheet, among others/ Depending on the components of the composite, an example OH ⁻ , COOH ⁻ , C=O, epoxy, amino, among others ^{40- 42}	SA: 3.18– ~260 ³⁹ P: 0.15– 0.72 ^{40,42}	Biochar+Chitosan	Ciprofloxacin	CT= 48, T= 20, pH= 3.0, AD= 5.0, [EC]= 160	Depending on the components of the composite, an example hydrogen bonding, π-π interaction, cation-π bonding, amidation reaction, Electrostatic interaction, hydrophobic interaction, ligand exchange, cation-π bonding, chemisorption, etc. ⁴⁰⁻⁴²	-	>76	[51]
			Sawdust + FeCl ₃	Tetracycline	CT= 2.0, T= 22±2, pH= 7.8, AD= 4.0, [EC]= 20		-	~5.4	[52]
			Magnetic bamboo- based activated carbon	Ciprofloxacin, norfloxacin	CT= 24, T= 25, pH= 6, AD= 2.0, [EC]= 300		-	245.6 293.2	[53]
			Magnetic pine sawdust biochar	Sulfamethoxazole	CT= 24, pH= 7±0.10, [EC]= 0.17–78		-	51.8–87.9	[54]
			Maize straw +manganese/iron oxides	Tylosin	CT= 0.25-24, T = 25, pH= 3–11, AD= 2, [EC]= 20		-	3070	[55]
			Palm-shell waste powdered AC + magnesium silicate	BPA	CT= 24, T= 24±1, pH= 4.5, AD= 0.1, [EC]= 10– 100		-	168.4	[56]
			Waste coffee grounds + Chitosan	Metamizole, acetylsalicylic acid, acetaminophen, caffeine	CT= 3, T= 25, pH= 6, AD= 0.2, [EC]= 0.5		52–95	0.9–6.3 1.2–9.9 0.9–7.5 1.1–8.2	[57]
			Carbon nanotube- supported sludge biochar	Sulfamethoxazole	CT= 0.08-2.0, T= 25, pH= 2-10, AD= 0.1-0.5, [EC]= 0.5		25.0–99.7	Up to 23.5	[58]
			Carbon dot-modified magnetic carbon nanotubes	Carbamazepine	CT= 3, T= 25±1, pH=7.0±0.2, AD= 0.2, [EC]= 3-30		80	65	[59]

*Synthetic Leachate. Information obtained from ¹Gupta et al. (2013); ²Sophia A. & Lima, (2018); ³Kim et al. (2014); ⁴Yu et al. (2016); ⁵Zhao et al. (2018); ⁶Joseph et al. (2011); ⁷Hu et al. (2012); ⁸Patiño et al. (2015); ⁹Hu and Cheng (2015); ¹⁰X. Wang et al. (2019); ¹¹Baig et al. (2019); ¹²Wang et al. (2018); ¹³Borthakur et al. (2018); ¹⁴Hiew et al. (2018); ¹⁵Balasubramani et al. (2020); ¹⁶S. Liu et al. (2018); ¹⁷Moussavi et al. (2016); ¹⁸Catherine et al. (2018); ¹⁹Leone et al. (2017); ²⁰Cao et al. (2017); ²¹Minh et al. (2018); ²²Qin et al. (2014); ²³R. Yin et al. (2018); ²⁴Y. Zhang et al. (2016); ²⁵Y. Zhou et al. (2019); ²⁶Rakshit et al. (2013); ²⁷Al-Jabari et al. (2019); ²⁸Zhao et al. (2017); ²⁹Nassar et al. (2018); ³⁰Al-Ahmari et al. (2018); ³¹Kasprzyk-Hordern (2004); ³²Taha and Mobasser (2015); ³³Turku et al. (2007); ³⁴Akhtar et al. (2015); ³⁵Pham et al. (2020); ³⁶Y. Kaur et al. (2017); ³⁷Sivaselvam et al. (2020); ³⁸Fakhri and Behrouz (2015); ³⁹Compe et al. (2018); ⁴⁰Naseem and Waseem (2021); ⁴¹M. Li et al. (2019); ⁴²Marcelo et al. (2020); ⁴³Azhar et al. (2017); ⁴⁴Alizadeh et al. (2018); ⁴⁵Baghdadi et al. (2016); ⁴⁶Wong et al. (2016); ⁴⁷Danalioğlu et al. (2017); ⁴⁸Hossein et al. (2017); ⁴⁹Wang et al. (2016); ⁵⁰Boruah et al. (2016); ⁵¹Zaheer et al. (2018); ⁵²Alidadi et al. (2018); ⁵³Peng et al. (2018); ⁵⁴Reguyal and Sarmah (2018); ⁵⁵Y. Yin et al. (2018); ⁵⁶Choong et al. (2018); ⁵⁷Lessa et al. (2018); ⁵⁸Ma et al. (2020); ⁵⁹Deng et al. (2018).

1.3. Technologies using materials to remove ECs from wastewater

Adsorption processes alone or in combination with other mechanisms are used and studied in different filtration and biofiltration technologies at different levels (lab/pilot/full). In biofiltration technologies, the materials used, in addition to adsorbing the contaminants, fulfill other fundamental functions. They act as a support medium for microorganisms (bacteria) and plants and retain nutrients, organic matter, solids, among others (Almeida-Naranjo, et al., 2021a; Tejedor et al., 2020). Therefore, the adsorbent materials must meet several requirements to achieve high efficiencies in contaminant removal and for the proper operation of the technologies. Material characteristics, cost, availability, hydraulic performance (clogging), feasibility, adsorption capacity, toxicity with living beings, chemical/mechanical stability, recoverability, and disposal ease are factors considered (X. Wang et al., 2019). Adequate adsorbent materials improve the operation and efficiency of filtration/biofiltration technologies. However, very little research has been done on the adsorbent material-technology relationship. Therefore, in this section, a review of the subject is carried out. Some of the alternative materials and mechanisms of EC removal are shown in Figure 5.

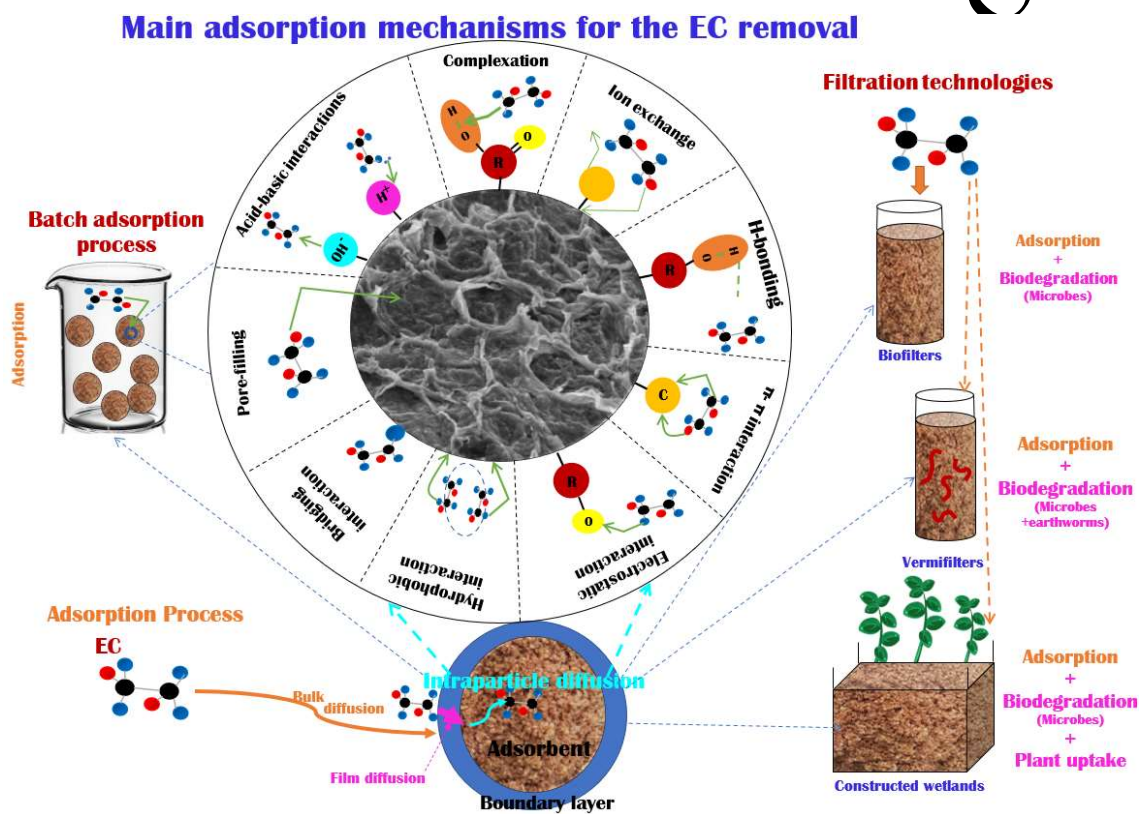


Figure 5. Mechanisms for the EC removal in the batch adsorption process

1.3.1 Filtration technologies

Fixed-bed columns or filtration technologies are low-cost and easy-to-operate technologies (lab/full-scale), low energy consumption, and easily scaled. Filtration technologies are used to treat secondary/tertiary effluents, achieving good efficiencies (up to 100%) for organic matter, and specific contaminants (Tejedor et al., 2020). The mechanisms for the contaminant removal are produced on the materials used as filter beds. These mechanisms depend on the contaminant nature, bed depth, quantity, packaging, size, and the feature of the material.

To improve the contaminant removal in fixed-bed columns, they are conditioned with microorganisms giving origin to biofilters. Biofilters are used more than filters in EC removal. Moreover, depending on the retention time (RT) or hydraulic load rate (HLR) used in filters/biofilters, there could be rapid or slow

filtration (Wang et al., 2021). Considering the feeding type, filters/biofilters could be continuous or intermittent. In the next paragraphs, the main characteristics of these processes are summarized.

1.3.1.1. Rapid filtration

Rapid filtration is widely used worldwide in water purification processes (Wang et al., 2021), they operate with a TOC loading of ~ 3.1 mg/L and organic loading = $3.7 - 36.7$ g/m³d (Zhang et al., 2019). Materials such as activated carbon, anthracite, garnet, and pumice have been used. However, sand (0.4 – 1.5 mm) is the most used material in them (Wang et al., 2021). Rapid filtration is considered a promising alternative to removing ECs with low consumption of energy and chemical products. Furthermore, rapid filters are already used in existing drinking water treatment plants; and despite not being designed to eliminate ECs, rapid filters have partially degraded (even > 50%) several contaminants of this type (Di Marcantonio et al., 2020).

The mechanisms observed in the EC removal are adsorption on sand, oxidation, and adsorption by metal oxides (FeO_x/MnO_x/bio-MnO_x), and biodegradation by autotrophic and heterotrophic bacteria. However, it was determined that biodegradation is more important than adsorption (only 10 – 15%) (Wang et al., 2021).

The hydraulic retention time (3.3 – 33.3 h) in rapid filters is essential in EC removal. Reducing the time by half decreased the removal efficiency (> 10%) of triclosan, galaxolide, nonalide, and celestolide (Hedegaard et al. 2019). Other ECs such as pentazocine (Hedegaard et al., 2019; Hedegaard & Albrechtsen, 2014), carbofuran, triclosan, gemfibrozil, ketoprofen, caffeine, erythromycin, naproxen, carbamyl, benzenesulfonamide, microcistin-LR, (Wang et al., 2021), dichlorprop (Hedegaard & Albrechtsen, 2017), atrazine, bentazon, carbamazepine (Brunner et al., 2018), present in surface and groundwater, were removed. The removal efficiencies in fast filters (microcosm, columns, field) have been reported being variable (0 – 99%) (Hedegaard et al., 2019; Hedegaard & Albrechtsen, 2014, 2017; Papadopoulou et al., 2018; Wang et al., 2021).

1.3.1.2 Slow filtration

Slow filtration uses a higher retention time than rapid filtration and does not require prior chemical coagulation (Pompei et al., 2017). Moreover, slow filtration is a technology with low operational cost due to the low energy consumption, and simplicity in operation and maintenance. The most common filter material is also sand (0.1 – 0.4 mm) however coarse sand and other materials (e.g., GAC, quartz/silica) have been used (Ji. Li et al., 2018).

Slow filtration is combined with microbiological action, so biosorption/biodegradation occurs, a phenomenon that predominates over adsorption. Adsorption, mechanical filtration, and degradation processes could occur after biodegradation. In this case, the material not only absorbs ECs but also fulfills other functions such as being a support for microorganisms and retaining their food until they consume it (Ji. Li et al., 2018).

Slow filtration has been used in the removal of ECs such as paracetamol, diclofenac, naproxen, ibuprofen, methylparaben, benzophenone-3, E1, E3, EE2 (Pompei et al., 2017), propranolol, iopromide, diclofenac, tebuconazole, propiconazole (Sharma & Garg, 2019), among others; achieving removals between < 15 and > 98% (Pompei et al., 2017).

1.3.2. Biofiltration

Biofiltration is a biological filtration. Initially, the adsorption in the filter bed material is an exclusive process. However, over time, the active sites of the material become saturated, and this mechanism diminishes so that other mechanisms begin to predominate. In the second stage, biological adsorption-degradation occurs due to the presence of aerobic, anaerobic, and facultative microorganisms, bacteria, fungi, algae, and protozoa (Almeida-Naranjo, et al., 2021a). At this stage, the function of the adsorbent is also to offer a specific area for the bacteria/plants/earthworm's growth. The adsorption decreases until in the third stage only biological degradation occurs. Therefore, the parameters that determine the biofilter efficiency are the surface characteristics of the material (pore size, specific surface area, functional

groups), the degree of compaction, the hydrophobicity of the bacteria, and the adsorbate characteristics (Boshir et al., 2017; Tejedor et al., 2020).

Biofiltration technologies for EC removal are generally used as secondary treatment (when there is a high load of organic matter) or tertiary treatment. Constructed wetlands (CWs), vermifilters, and biofilters are the types of biofiltration technology (Boshir et al., 2017).

1.3.2.1. Biofilters

In biofilters as water percolates through the filter bed material, microorganisms attach to the material surface (diffusion, convection, sedimentation, and active mobility of microbial cells), colonize it, and form biofilms. The upper part of the filter is initially populated with microorganisms and they advance over time. However, the maturation of biofilms (biomass formation) in the filter can take a long time because the filter has a continuous supply of organic matter and nutrients. Mature biofilms favor the functioning and efficiency of biofilters since they present higher biomass and metabolic activity. Indeed, they present greater resistance to toxic contaminants (Thuptimjang et al., 2020).

Materials such as clay, anthracite, activated carbon, and sand are used conventionally as adsorbents to remove ECs in biofilters. Activated carbon is more efficient in removing pesticides and pharmaceutical products, but not for personal care products and endocrine disruptors (due to their characteristics). Other materials such as biochar, rice husk (raw/biochar), peanut shells, fruit peels, sawdust, wood chips, or mixtures thereof are used (Boshir et al., 2017). These materials have proven to be efficient in removing some ECs (0 – 100%) (Boshir et al., 2017; Greenstein et al., 2018; S. Zhang et al., 2018; Zhang et al., 2017) such as 17 β -estradiol-17 α -acetate, pentachlorophenol, 4-tert-octylphenol, caffeine, gemfibrozil, BPA, benzophenone, atrazine, dicamba, triclosan, (Boshir et al., 2017), acetaminophen, erythromycin, sulfamethoxazole, cotinine, amino triazole, ibuprofen, atrazine, naproxen, among others (S. Zhang et al., 2018). The removal mechanisms of ECs in biofilters are adsorption and biodegradation, produced by the filter bed material/biofilm and microorganisms, respectively (Thuptimjang et al., 2020). Nevertheless, oxidation (in the material) could occur if other filter materials are used (e.g., manganese oxide) (Zhang et al., 2017).

1.3.2.2. Constructed wetlands

Constructed wetlands (generally used as secondary treatment) are systems formed by plants (macrophytes/ornamental), substrates (support materials), native microorganisms, and water, interacting with each other (Ávila et al., 2021). The substrate is fundamental in the efficiency of CWs since it fulfills physical, chemical, and biological functions to remove contaminants. Furthermore, the materials are the support medium (allow growth) of plants and microorganisms (Delgado et al., 2020). Other support material functions include physical sedimentation, filtration, and gas diffusion between the material particle gap (Gorito et al., 2017). The conventional materials used are soil, sand, and gravel (8 – 16 mm) even in the removal of ECs (Ahmed et al. 2016; Chen et al. 2019). Moreover, red soil, volcanic rock, stone, vesuvianite, zeolite, and brick were used. At the lab scale, materials such as rice husk, pine bark, and granulated cork were used for EC removal (Gorito et al., 2017).

Different types of CWs (surface free water, horizontal groundwater flow, vertical groundwater flow, and hybrid CWs) at full/mesocosm/microcosm/pilot/lab scale were used for the removal of several ECs (Ahmed et al. 2016b; Chen et al. 2019b; Gorito et al. 2017). The removal mechanisms of the ECs are produced by their sorption in the material support (e.g., hydrophobic partitioning, van der Waals interaction, electrostatic interaction, ion exchange, and surface complexation), plant uptake (phytostabilization, phytoaccumulation, phytodegradation) and/or biodegradation aerobic/anaerobic process. However, the main mechanisms in EC removal are biodegradation and sorption (Chen et al. 2019a, León et al., 2020). Among the ECs removed were phenols, diclofenac, naproxen, atrazine, endosulfan, erythromycin, clarithromycin, azithromycin, E1, E2, carbamazepine, gemfibrozil, sulfamethoxazole, sulfapyridine, ibuprofen, acetaminophen, triclosan, BPA, among others. The removal efficiencies achieved were between 0 and > 99% (Ahmed et al. 2016b; Gorito et al. 2017).

1.3.2.3. Vermifilters

Vermifilters are biofilters based on earthworms-microorganisms; they are one of the most studied biofiltration technologies since 1990. They are characterized by being an economical alternative for the treatment of point/diffuse sources of wastewater. Vermifilters are engineering systems made up of earthworms, microorganisms (biotic component), and filter material (abiotic component) that maintain symbiotic relationships. The main function of earthworms is to regulate microbial activity and biomass while microorganisms biodegrade waste materials/contaminants (Arora et al., 2021; Chicaiza et al., 2020). Vermifilters do not generate sludge and require less area compared to other processes/technologies (Shokouhi et al., 2019).

Earthworm species used in vermifilters include *Eisenia foetida*, *Lumbricus rubellus*, *Eudrilus eugeniae*, and *Eisenia andrei*. These are suspended on a filtration bed (active zone of earthworms) that can be soil, compost, and cow manure, here the degradation of contaminants occurs (Bhat, 2020). However, alternative materials (in toxicity tests and mesocosm scale) such as coconut fiber, corn cobs, peanut shells, and rice husks were used in the active zone of earthworms (Almeida-Naranjo et al., 2021; Tejedor et al., 2020). On the other hand, sand, gravel, cobblestone, and quartz sand are used as filter beds (Bhat, 2020). In vermifilters, the wastewater first passes through the active zone of earthworms and then through the filter bed. If the flow direction is considered, vermifiltration systems can be of three types: horizontal, vertical, and hybrid (horizontal + vertical flow) (Bhat, 2020). Currently, research is based on the use of vermifilters assisted by macrophytes, since it has been shown that the presence of plants improves the aerobic condition for the development of earthworms and microorganisms and therefore the degradation of organic contaminants (Bhat, 2020; Tejedor et al., 2020).

Vermifilters are used in the removal of ECs such as ciprofloxacin, ofloxacin, sulfamethoxazole, trimethoprim, tetracycline, metronidazole (Shokouhi et al., 2019), amoxicillin, ampicillin, ticarcillin, ceftazidime, cefotaxime, ceftriaxone, streptomycin, gentamicin, erythromycin, tetracycline, chloramphenicol, ciprofloxacin (Arora et al., 2021). Removal efficiencies between 40 and 98% were reached (Shokouhi et al., 2019). The mechanisms involved in the removal of ECs were absorption/degradation by earthworms, adsorption/degradation in the biofilm, biodegradation under the load of the microorganisms, and sorption in the bed filter material (Arora et al., 2021; Shokouhi et al., 2019).

Table 6 shows the operating conditions of different types of filters/biofilters that were used in the removal of some ECs. In addition, the material(s) used in the technologies and the mechanism by which the ECs are removed are indicated. It is observed that biofilters are more used than filters for the removal of ECs. Biofilters (fast and slow), that use sand as filter beds, are used to remove ECs present mainly in surface and groundwater. On the other hand, the presence of living organisms (microorganisms, plants, and earthworms) improves the efficiency of ECs removal. However, vermifilters are the least used biofilters (there is little previous research) in the removal of ECs compared to CWs and biofilters.

Table 6. Filtration/Biofiltration technologies using materials to remove ECs from wastewater.

Type of filtration (Scale)	Bed filter material (Size, mm)	Influent type	EC removed	Operational conditions	Removal mechanism	Removal [%]	Reference
Aerated rapid filtration (Microcosms)	Sand (3–5)	Anaerobic groundwater	Mecoprop, bentazone, glyphosate, p-nitrophenol	[EC]= 3×10^{-5} – 2.4×10^{-3} , RT=0.17	Biodegradation	1-85	[1]
Rapid filtration (Microcosms)	Sand (3–5)	Anaerobic groundwater	Dichlorprop	[EC]= 2×10^{-4} , RT=0.9	Biodegradation	>50	[2]
Rapid filtration (Microcosms)	Sand (3–5)	Anaerobic groundwater	Bentazone	[EC]= 5, RT=7	Biodegradation	92	[3]
Rapid filtration (Microcosms)	Filtralite clay (0.8–1.6)	Groundwater enriched with ECs	2,6-dichlorobenzamide, bromoxynil, chlorotoluron, diuron, ioxynil, isoproturon, linuron, 4-chloro-2-methyl phenoxy acetic acid	[EC]= 2.1×10^{-3} – 5.6×10^{-3} , RT=0.2–1, FR=21	Biodegradation	13–98	[4]
Rapid filtration (Lab scale)	Sand	Influent water from the RSF filters (WRK, Nieuwegein, The Netherlands) enriched with ECs	Atrazine, bentazon, metolachlor and clofibrac acid, carbamazepine	[EC]= 0.01, RT=8 and 96, FR=80	Biodegradation/Sorption	-	[5]
Rapid filtration: down-flow, up-flow, dual media downflow (Field)	Sand (0.7–2.5) Sand+hydroanthracite (1.4–2.5) Sand+anthracite (1.6–2.5)	Surface water from The Netherlands and Belgium	Caffeine, acesulfame-K, sucralose, metformin, phenazone, chloridazon, valsartan, sulfadiazine, sotalol, etc.	[EC]= $<1 \times 10^{-5}$ – 5.7×10^{-4} , RT=15–240	Biodegradation/Sorption (probably)	0–93	[6]
Slow filtration with rapid pulses of a carbon source (Lab scale)	Quartz sand (0.210–0.297)	WWTP effluent	Atenolol, metoprolol, ropromide, iomeprol, carbamazepine, diclofenac, sulfadiazine, sulfamethoxazole, etc.	RT=150, FR=0.15	Biodegradation	-	[7]
GAC sandwich slow filtration (Lab scale)	Coarse sand (0.6) GAC (0.4–1.7) Coarse sand+ GAC	Synthetic wastewater	Mix of D, E1, paracetamol, caffeine and triclosan	[EC]=0.025, HLR= 5, 10, 20	Adsorption (GAC) + Biodegradation	18.8–100	[8]
Slow filtration (Pilot-scale)	Silica sand (0.15–0.30) Support: pea gravel Sand	Stream water/ Stream water+ 1% of primary effluent added, both enriched with ECs	Caffeine, carbamazepine, 17- β estradiol, E1, gemfibrozil, phenazone	[EC]=0.05, HLR=5	Sorption and/or biodegradation	<10–100	[9]
Household slow filtration with intermittent and continuous flows (Pilot-scale)	(0.09–0.5) Support: coarse sand (1–3)+ fine gravel (3–6)+coarse gravel (10–12) Top: non-woven polyester	Synthetic wastewater	BPA	[EC]=2.35 Continuous flow HLR=1.58 Intermittent flow HLR=0-875	Biodegradation	Continuous flow 14±6 Intermittent flow 3±8	[10]

Table 6. Technologies using materials to remove ECs from water (continuation)

Type of filtration (Scale)	Bed filter material (Size, mm)	Influent type	EC removed	Operational conditions	Removal mechanism	Removal [%]	Reference
Biofilters (Bench-scale)	GAC (1.0-1.2) and anthracite (0.8-2.0)/sand (0.55-0.65) dual media	Municipal waste streams	Acetaminophen, ibuprofen, erythromycin, sulfamethoxazole, trimethoprim, carbamazepine, atenolol, gemfibrozil, tri(2-chloroethyl) phosphate, DEET, cotinine, amino triazole, atrazine, caffeine, E2, iopromide	[EC]= 2.27x10 ⁻⁴ -6.44x10 ⁻³ , RT=0.17 and 0.29	Biodegradation	>75	[11]
Biofilters (Pilot-scale)	Anthracite/sand (1.07/0.52)	Superficial water of Grand River enriched with ECs	DEET, atrazine, naproxen, ibuprofen, nonylphenol, carbamazepine	[EC]=5x10 ⁻⁴ -5x10 ⁻³ , RT=0.08 and 0.23, HLR=500	Adsorption (non-biodegradable ECs) and biodegradation (biodegradable ECs)	<20-100	[12]
Biofilters (Pilot-scale)	GAC/sand and anthracite/sand	Water from the full-scale re-carbonation chambers enriched with ECs	Atenolol, atrazine, carbamazepine, fluoxetine, gemfibrozil, metolachlor, sulfamethoxazole, tris(2-chloroethyl) phosphate	[EC]= 1x10 ⁻⁴ -2x10 ⁻⁴ , 1x10 ⁻³ -3x10 ⁻³ , RT=8.4 and 4.2, HLR=488 and 976	Adsorption and biodegradation	GAC/sand: 49.1-94.4 anthracite/sand: 0-66.1	[13]
Biofilters (Pilot-scale)	Natural manganese oxides (3-5)	Secondary effluent of WWTP	1-hydroxy benzotriazol, 4'-hydroxy diclofenac, 10.11-dihydroxy-10.11-dihydroxy carbamazepine, cyclovir, benzotriazole, diclofenac, carbamazepine, carbonyl cyclovir, diatrizoic acid, erythromycin, gabapentin, temazepam, tolyl triazole, sulfamethoxazole, tramadol,	RT=5 and 10, FR=8000, HLR=400,	Adsorption, biodegradation, oxidation	70-98	[14]
Biofilters (Pilot-scale)	Anthracite-sand and previously used biological activated carbon (BAC)-sand dual media BAC=(0.9)	Raw surface water (Colorado River) enriched with ECs	sulfamethoxazole, caffeine, gemfibrozil, naproxen, DEET, trimethoprim, acetaminophen, ibuprofen, sucralose, meprobamate	[EC]= 1x10 ⁻⁴ -1x10 ⁻³ , RT=0.17, HLR=904.56	Biodegradation and BAC sorption	<50->99	[11]
Horizontal/vertical subsurface flow and hybrid CWs, aerated/un-aerated (mesocosm-scale)	Zeolite (20-30)	Domestic sewage enriched with ECs	Sulfamonomethoxine, sulfamethazine, sulfameter, trimethoprim, norfloxacin, ofloxacin, enrofloxacin, erythromycin-H ₂ O, roxithromycin, oxytetracycline, lincomycin	[EC]= 5x10 ⁻³ , HLR=1.67, PT= <i>Iris tectorum</i>	Sorption and biological processes	87.4-99.1	[15]
Combination of partially saturated and unsaturated vertical subsurface flow CWs (experimental-scale)	Top: sand layer (1-2) Underneath: gravel (3-8)	Urban waste water (surrounding residential area) from primary treatment	Ciprofloxacin, ofloxacin, pipemidic acid, azithromycin	[EC]= 5x10 ⁻⁴ , HLR=0.55, PT= <i>Phragmites australis</i>	Sorption and biodegradation	<-200->90	[16]

Table 6. Technologies using materials to remove ECs from water (continuation)

Type of filtration (Scale)	Bed filter material (Size, mm)	Influent type	EC removed	Operational conditions	Removal mechanism	Removal [%]	Reference
Line 1: Partially vertical flow Line 2: unsaturated vertical flow+ horizontal subsurface flow + free water surface CWs (experimental-scale) Four CWs of subsurface horizontal flow (pilot-scale)	-	Urban wastewater from primary treatment	Caffeine, trimethoprim; sulfamethoxazole, DEET, sucralose	HLR=0.55, FR=38.89	Biodegradation	<10~100	[17]
Vertical flow CW	Gravel (12.7–19.05) Top: gravel (4.8–9.5) Filter media: sand (0.27) Bottom: medium gravel (4.8–9.5)+coarse gravel (25–32)	Wastewater	Carbamazepine, sildenafil, methylparaben	[EC]= 0.2, FR=15, RT=72, PT= <i>Heliconia Zingiberales and Cyperus Haspan</i>	Biodegradation, adsorption, plant absorption	<10–97	[18]
Integrated CW	Chaff and soil	Domestic + livestock wastewater	Ibuprofen and caffeine	[EC]= <0.1, HLR=16, RT=168, PT= <i>Heliconia rostrata</i>	Biodegradation, adsorption, plant absorption	90–97	[19]
Vermifiltration (Pilot-scale)	Soil Sand (0.1–0.8) Detritus (3–10) Support: cobblestone (10–50)	Hospital effluent from the sedimentation tanks	Androsta-1,4-diene-3,17-dione, 17 α -trenbolone, 17 α -boldenone, 17 β -boldenone, testosterone, stanozolol, progesterone, ethynyl testosterone, 19-norethindrone, norgestrel, medroxyprogesterone, cortisol, cortisone, prednisone, miconazole, fluconazole, itraconazole, etc.	[EC]= 6.3x10 ⁻⁷ -1.05x10 ⁻⁴ , RT=36, PT= <i>Myriophyllum verticillatum L.</i> and <i>Pontederia cordata</i>	Biodegradation, adsorption, plant absorption	<10–97.6	[20]
Vermifiltration (Pilot-scale)	Top: vermigratings (0.118) and cow-dung (0.05–5), Small gravel (2–4), Medium gravel (6–8) Support: coarse gravel (12–14)	Clinical laboratory wastewater	Ciprofloxacin, ofloxacin, sulfamethoxazole, trimethoprim, tetracycline, metronidazole	HLR= 4.17, ET= <i>Eisenia foetida</i> , ED=10000	Adsorption, earthworm absorption (mineralization/transformation), biodegradation	40–98	[21]
			Amoxicillin, ampicillin, ticarcillin, ceftazidime, cefotaxime, ceftriaxone, streptomycin, gentamicin, erythromycin, tetracycline, chloramphenicol, ciprofloxacin	HLR= 4.17, RT=7-8, ET= <i>Eisenia foetida</i> , ED=10000	Earthworms/microorganisms degradation, biofilm adsorption, filter media sorption	-	[22]

¹Hedegaard and Albrechtsen (2014); ²Hedegaard and Albrechtsen (2017); ³Hedegaard et al. (2019); ⁴Papadopoulou et al. (2018); ⁵Brunner et al. (2018); ⁶Di Marcantonio et al. (2020); ⁷Zhang et al. (2019); ⁸Ji. Li et al. (2018); ⁹Alessio et al. (2015); ¹⁰Sabogal-Paz et al. (2020); ¹¹Greenstein et al. (2018); ¹²Zhang et al. (2018); ¹³Ma et al. (2018); ¹⁴Zhang et al. (2017); ¹⁵Chen et al. (2019a); ¹⁶Ávila et al. (2021); ¹⁷Sgroi et al. (2018); ¹⁸Delgado et al. (2020); ¹⁹Oliveira et al. (2019); ²⁰Chen et al. (2019b); ²¹Shokouhi et al. (2019); ²²Arora et al. (2021).

In the finished chapter, the extensive research performed worldwide on the removal of ECs using batch and continuous adsorption processes has been briefly discussed. Concluding that they are highly efficient under controlled parameters (at the laboratory level).

Although there are thousands of studies focused on batch adsorption as a process to remove different contaminants from wastewater (mainly dyes and heavy metals), this use in the removal of ECs is still limited. This is probably associated with the great diversity of ECs present in the wastewater. Likewise, a wide variety of materials have been used to remove this type of contaminants. The selection of the material in most cases is related to the abundance of the same in the place of study. Among these materials, there is a high tendency to use agro-industrial residues, which is associated with their low-cost and high availability. The agro-industrial residues used in a lot of cases are modified (physically, chemically, residues + nanoparticles) to improve their adsorptive properties, achieving good results. In the studies carried out with modified materials, it is not analyzed whether the modification is efficient in terms of economic, environmental (generation of by-products, consumption of chemicals, etc.), or large-scale production. While the information on raw residues is scarce and this is due to the low efficiency of some residues.

Furthermore, despite a large number of works carried out, there are very few that scale up batch adsorption to continuous adsorption processes (fixed bed columns); and much fewer studies in which the material is used in filtration/biofiltration technologies. In this way, the application of these studies is only analyzed on a laboratory scale, this leaving their application on a real scale in time. In other words, there is still a very large knowledge gap in this field. Therefore, to solve some of the unknowns found and thinking about the theories of the circular economy, the objectives of sustainable development, and that in Ecuador the treatment of wastewater and the recovery of agro-industrial residues are limited, it has been proposed this research. Proposing the following hypothesis and objectives:

2. Hypotheses and Objectives

2.1. Hypotheses

Agro-industrial residues with a high content of lignocellulosic material and lower toxicity present higher efficiencies in the removal of caffeine and triclosan in batch adsorption and filtration/biofiltration processes, and efficiency improves by impregnating them with iron oxide nanoparticles.

2.2. General Objective

To study the removal of caffeine/triclosan separately using agro-industrial residues and iron oxide nanoparticles first in batch adsorption processes and subsequently in continuous.

2.3. Specific objectives

- a. To determine the best adsorbent among six agro-industrial residues, in terms of particle size, physicochemical characteristics, efficiency, and toxicity, which allow the greatest removal of caffeine and triclosan in discontinuous adsorption processes.
- b. To determine the optimal number of nanoparticles that can be impregnated in the best adsorbent (objective a), to increase the removal of caffeine and triclosan in batch adsorption processes.
- c. To determine the hydraulic behavior and the efficiency of the materials (objectives a and b) in continuous adsorption processes in the removal of caffeine and triclosan, to establish the saturation time of the materials.
- d. To evaluate the operational performance of the materials in the filtration/biofiltration process, using different hydraulic loads and filter bed configurations, to remove caffeine, triclosan, and organic matter, to establish their possible application on a real scale.

2.4. Research challenges

The research challenge starts from understanding the adsorption mechanisms between the different agro-industrial residues and caffeine/triclosan. To improve the performance of the systems/technologies that involve these mechanisms (e.g., filters and biofilters), in such a way that they can be applied efficiently on a real scale.

In the case of iron oxide nanoparticles (IO) and composites (agro-industrial residues + iron oxide nanoparticles), it is essential to define the optimal operating conditions that favor the removal of caffeine/triclosan in both batch and continuous processes (amount of impregnated nanoparticles, contact time, dose, bed height, hydraulic head, etc.). In addition, it will be necessary to determine the advantages and disadvantages of the synthesis of these materials on a large scale, to be used for example in biofiltration technologies. Finally, considering the importance of the filter bed material in biofiltration technologies, it will be essential to evaluate the biocompatibility of the adsorbents with the biota that can be used in them.

To overcome each proposed challenge, the following experimental model was proposed (Figure 6): Six agro-industrial residues (rice husk, peanut shells, coconut fiber, corn cob, and orange/banana peels) were selected. For this selection, it was considered that these raw/modified residues were used in previous studies for the removal of different contaminants. Furthermore, they are highly produced residues in Ecuador, so they are highly available.

In the first stage, rice husk (RH), peanut shells (PS), coconut fiber (CF), and corn cob (CC) were used as adsorbents; because they present a similar composition of lignocellulosic residues. The parameters to be analyzed were particle size (levels: 3), type of EC (2 levels: caffeine and triclosan), optimal dose (levels: 4), and contact time (levels: 4). The data obtained were adjusted to the commonly used kinetic and isotherm models. In this stage, the most efficient particle size and the EC with the lowest removal efficiency will be selected, and under these conditions orange and banana peels will be used. This is to determine the influence of the adsorbent composition in the contaminant removal. In the batch adsorption tests using orange/banana peels, the parameters, optimal dose (levels: 4) and contact time (levels: 4) were analyzed. Since the most difficult-to-remove EC will be used in this stage, the orange/banana peels will be impregnated with IO nanoparticles (level: 1), to determine if there is an increase in removal efficiency, as it happens in previous studies. As with RH, PS, CF, and CC, the data obtained were adjusted to the commonly used kinetic and isotherm models. As the idea is to use agro-industrial residues in biofiltration technologies, they will be tested for toxicity. With the results of efficiency and toxicity, the residue(s) with the best adsorptive characteristics will be selected and used in the next stages.

In the second stage, the residue(s) selected will be impregnated with IO nanoparticles (levels: 3), and batch adsorption tests will be performed to determine the most efficient composite. The data obtained will be adjusted to the most efficient kinetic and isotherm models. The most efficient residue(s) and composite in the batch adsorption processes will be used in continuous adsorption processes (small columns). The influence of the flow rate (levels: 3), particle size (levels: 3, the same as the batch tests), and filter bed height (levels: 3), on the removal of caffeine and triclosan, will be analyzed.

In the next stage, the residue(s) will be used in the biofiltration processes, the hydraulic load (levels: 3) and the particle size (levels: 4) that allow maximum removal of EC (the most difficult to remove in batch processes, stage 1) will be evaluated. With optimal conditions, the other EC will be removed. In the final stage, preliminary tests will be carried out in mesocosms of biofiltration technologies using synthetic wastewater, to determine the possibility of using them in subsequent studies in the ECs removal.

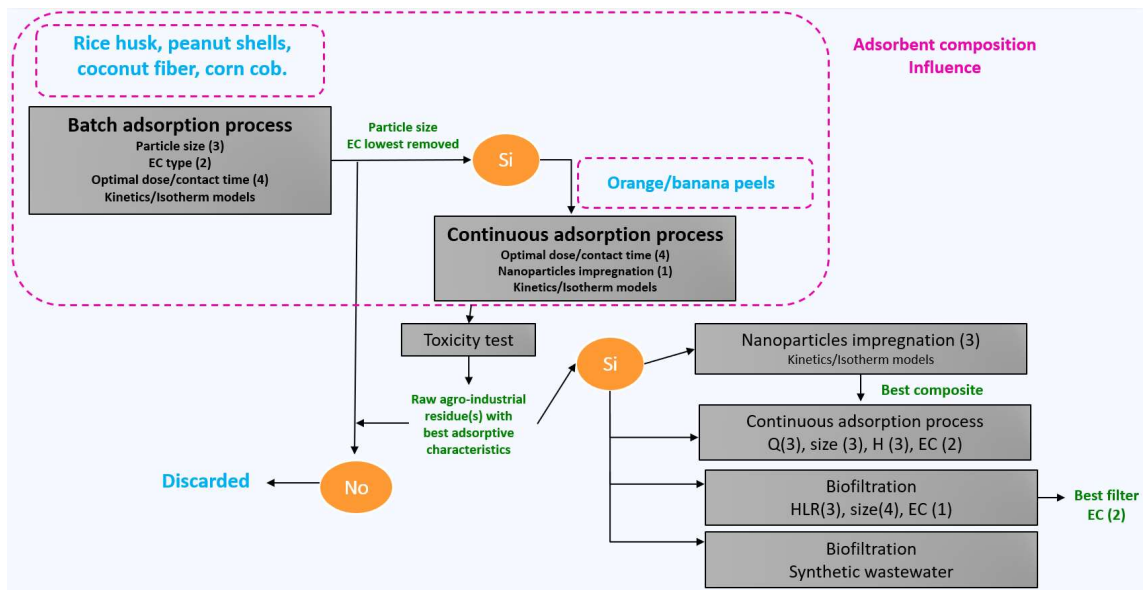


Figure 6. Experimental model

To meet the first and second specific objectives of the research, the following chapter presents the results obtained in the removal of caffeine and triclosan in the batch adsorption process, using different adsorbent materials.

Versión Aprobada para Defensa

3. Optimization of variables to remove caffeine and triclosan in batch adsorption processes using residues and composites

The evaluation of different agro-industrial residues aimed to identify the residue(s) exhibiting higher efficiency in the removal of caffeine and triclosan. This selection serves the purpose of utilizing the most effective residue in subsequent stages of the research. As previously mentioned, the decision to focus on caffeine and triclosan for removal assessment stems from their distinct chemical properties, leading to varied removal mechanisms and parameter application in batch adsorption processes. Additionally, these compounds were chosen due to their status as anthropogenic markers, heightened consumption/use during the SARS-CoV-2 pandemic, and their prevalence in water bodies, among other factors elucidated in later sections.

Hence, this chapter presents the outcomes of caffeine and triclosan removal using diverse materials, including rice husks, peanut shells, corn cob, coconut fiber, fruit peels (banana and orange), iron oxide nanoparticles, and magnetic composites (fruit peels + iron oxide nanoparticles and corn cob + iron oxide nanoparticles). Concurrently, the experimental data were subjected to kinetics/isotherms models for fitting to determine the adsorption mechanism and its correspondence.

2.1. Batch adsorption processes using agro-industrial residues

The use of bio-adsorbents could be an alternative for EC removal, since their benefits include high availability (e.g., rice husk: 16 million tons/year, peanut shells: 11 million tons/year) because they do not have defined reuse, simple conditioning and lower costs (20, 36 and 28% in operating, treatment, and total costs, respectively) than conventional wastewater treatments (Barka et al., 2013; FAO, 2018; Shamsollahi & Partovinia, 2019). Moreover, they contain minerals, lipids, lignin (20 – 30%), cellulose (35 000 50%), and hemicellulose (15 – 30%). The presence of active surface functional groups (OH, COOH-, C₆H₆O, CH₃O⁻) in the biopolymers (Figure 7) and their good chemical/mechanical stability, make them good alternatives to remove caffeine and triclosan (Mo et al., 2018; Pode, 2016).

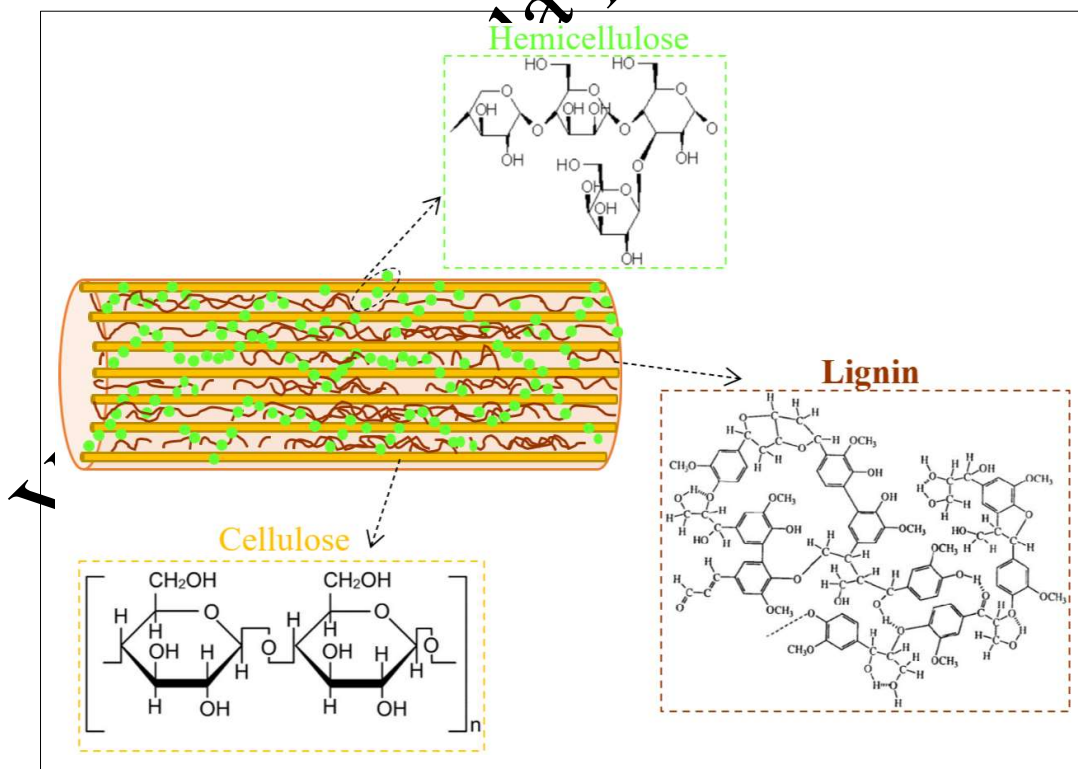
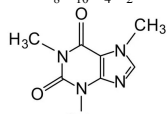
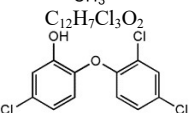


Figure 7. Structure of natural fibers

Indeed, previous studies that use raw or treated agro-industrial residues have achieved values greater than 75% (grape stalk) and 80% (activated carbon from coconut pulp), in the removal of caffeine and triclosan, respectively (Mohd-Khori et al., 2018; Portinho et al., 2017). The mechanisms associated with the removal of these contaminants are associated with the porosity of the residues and the attractions between adsorbents and adsorbates. Therefore, characteristics/properties of caffeine and triclosan also play an important role in their removal. Some of the physicochemical characteristics and structure of caffeine and triclosan are presented in Table 7.

Table 7. Characteristics of caffeine and triclosan

Contaminant	Formula	Formula weight (g/mol)	Molecular size (nm)
Caffeine	<chem>C8H10N4O2</chem> 	194.19	0.98 x 0.87 x 0.56
Triclosan	<chem>C12H7Cl3O2</chem> 	289.54	1.42 x 0.69 x 0.75

Likewise, rice husk (RH) and peanut shells (PS) were demonstrated to be efficient in the removal of other ECs such as antibiotics (e.g., sulfathiazole and sulfamerazine, adsorption capacities= 18.2 µg/g and 11.7 µg/g, respectively) (R. Li et al., 2018) and compounds with similar effects to those of caffeine and triclosan in the environment (Balarak et al., 2019). Moreover, RH and PS are highly available in Ecuador and several other countries around the world (16 and 11 million tons/year, respectively) (Barka et al., 2013; FAO, 2018; Shamsollahi & Partovinia, 2019). However, their use in batch tests for the removal of caffeine/triclosan and other ECs is limited. Studies have been carried out mainly with ash/activated carbon/modified RH/PS or with the derivatives of RH (silica), but no information on the costs that the RH/PS modification processes imply and if this is convenient concerning the removal achieved (Mohd-Khori et al., 2018; Shamsollahi & Partovinia, 2019). Furthermore, the ECs studied previously present similar characteristics to each other, which is also a limitation since it is not explained whether the adsorbent used is efficient or not in the ECs removal with different characteristics (water solubility/ K_{ow}). Therefore, in this section, the results obtained for the removal of caffeine and triclosan from synthetic solutions using RH/PS in batch tests are presented. RH/PS were characterized to determine how their constituents/characteristics influence the adsorption process. Batch tests were performed to determine the optimal adsorbent dose, contact time and particle size to remove caffeine and triclosan. The kinetics and equilibrium of the adsorption process were determined by fitting the experimental data to different models available in the literature. The results of both studies are presented in Articles 1 and 2.

Versión Aprobada para Defensa Oral

Article 1. Caffeine/triclosan removal from synthetic solutions using rice husk in batch and fixed bed columns

ABSTRACT

Abundant, easily accessible, and low-cost agro-industrial residues represent attractive alternatives for removing emerging contaminants from water. In this work, the aqueous adsorption of caffeine/triclosan onto rice husk (RH) was studied in batch and continuous processes. For this purpose, adsorbents with three particle sizes (120 – 150, 300 – 600, 800 – 2,000 μm) were prepared and evaluated. The composition, structure, surface morphology, functionality, and specific surface area of the RH biosorbents were determined. This characterization showed that RH is mainly composed (80.1%) of lignin, cellulose, and hemicellulose. RH also exhibited an irregular surface, with several functional groups (OH, C=O, CH, C=C, C-OH), and a relatively small specific surface area (1.18 m^2/g). Batch tests were carried out using different RH doses (1 – 50 g/L) and contact times (5 – 300 min). Triclosan removal was greater (2.5 – 25.5%) than that of caffeine with all three particle sizes, requiring less adsorbent (2.5 – 5.0 times), and shorter times (3 times). The experimental data fitted better the Sips isotherm and Elovich kinetics models. The small (120 – 150 μm) particles achieved the highest caffeine/triclosan batch adsorption capacities (6.3/28.6 mg/g). Continuous tests were performed on fixed-bed using columns of 1 cm in diameter, packed with 4, 5, and 8 cm of RH, operated with hydraulic loading rates between 2 and 4 $\text{m}^3/\text{m}^2\text{day}$. Small particles also reached the highest adsorption capacity in the removal of caffeine/triclosan (352.7/3797.2 mg/L), and the experimental data were well-fitted to the Bohart-Adams model. According to these results, RH represents a promising option in water treatment technologies based on adsorption.

1. Introduction

Events such as the COVID-19 pandemic increased the consumption of chemical substances worldwide, mainly antibiotics and disinfectants. In fact, in March 2020, more than 2,000 tons of disinfectants were used in Wuhan (Chen et al., 2021). The residues of these substances are considered emerging contaminants (ECs) (Gil et al., 2018). ECs are pseudo-persistent organic substances found in low concentrations in the environment (ng/L - $\mu\text{g}/\text{L}$) (Portinho et al., 2017). Their low concentrations, wide variety (100,000 different chemical substances) (Flynn et al., 2021), and different physical-chemical characteristics (solubility, volatility, bioaccumulation capacity, etc.), make conventional wastewater treatments inefficient in the EC elimination (e.g. Ibuprofen= 32.8%, diclofenac= 0.0% using activated sludge at lab scale) (Peng et al., 2019). This opens the possibility for ECs to reach water bodies and enter the food chain (Brack et al., 2015).

Caffeine (Trimethylated xanthine, CAS 58-08-2) is an EC of great interest, it is part of the daily diet (consume ~ 70 mg/person) (Rigueto et al., 2020) because it is found in highly consumed beverages such as coffee, tea, soft drinks and in some medications (Korekar et al., 2019). Caffeine is soluble in water (21.6 g/L, at 25°C) and hydrophilic (log K_{ow} = 0.5). About 5% of ingested caffeine is not metabolized and is excreted in the urine (Rigueto et al., 2020), which is why it has been frequently found in different water bodies (surface water= 3 – 1,500 ng/L, groundwater= 10 – 80 ng/L), wastewater (20 – 300 $\mu\text{g}/\text{L}$) and in effluents from wastewater treatment plants (0.1 – 20 $\mu\text{g}/\text{L}$) (Álvarez-Torrellas et al., 2016). Moreover, caffeine and its metabolites are not volatile substances, which makes them persistent (3-6 weeks to be naturally mineralized) in water bodies, generating toxic effects in biota and affecting the environment as a whole (Pereira et al., 2017; Rodríguez-Gil et al., 2018). Caffeine (0.6 mg/L) combined with other ECs, such as paracetamol (1.0 mg/L), can increase the reproductive activity of tadpoles of the *pipiens* species, altering the trophic chain since it increases the predator's number (Dafouz et al., 2018).

Triclosan (5-cloro-2-(2,4-diclorofenoxi) phenol, CAS 3380-34-5) is another highly consumed EC (1,500 tons/year). It is a synthetic and lipid-soluble antimicrobial agent, found in health care (e.g., antiseptic, disinfectant), veterinary products, and personal care products (e.g., hand soaps, shampoos, deodorants, cosmetics) in concentrations between 0.1 – 2.0% (Yanxia Li et al., 2019; Triwiswara et al., 2020a). Triclosan has low solubility in water (10 mg/L, at 25 °C) and high bioaccumulation/hydrophobicity (log K_{ow} = 4.30), so this anionic compound is compatible with many materials (Kaur et al., 2018). In aquatic habitats, triclosan is accumulated in sediments/sludge that could be deposited in agricultural areas. Triclosan has been found in surface waters (1.4 – 40,000 ng/L), municipal wastewater (0.07 – 14,000 $\mu\text{g}/\text{L}$), wastewater treatment plant effluents (23 – 5,370 ng/L), seawater (< 0.001 – 150 ng/L) and in sediments (lake/river/other surface waters, < 100 – 53,000 $\mu\text{g}/\text{kg}$ in dry weight) (Z. Luo et al., 2019; Montaseri & Forbes, 2016). The presence of triclosan in the environment could produce bioaccumulation

(algae and snails), inhibit algae growth, endocrine disrupting effects, formation of toxic by-products, and even the development of microbial resistance (Yanxia Li et al., 2019).

Treatment technologies, such as ozonation, advanced oxidation, reverse osmosis, or activated sludge, can substantially reduce the EC effluent concentrations (up to 80%) (Chaukura et al., 2016). Nevertheless, the implementation, operation, and maintenance costs of using these types of treatments are relatively high (e.g., reverse osmosis ~ 0.52 USD/m³). Additionally, their difficult operation, high energy consumption (e.g., reverse osmosis: 35% of the total cost), among others, make them not accessible to developing countries (Abejón et al., 2015; Chaukura et al., 2016; Parida et al., 2021). Adsorption is a low-cost alternative, does not generate potentially toxic products, and can reach superior performance than other wastewater treatments (N. Khan et al., 2020).

On the other hand, the use of husks, seeds, fibers, and other agro-industrial residues constitutes a sustainable alternative to remove ECs. Using bio-adsorbents derived from these materials could also be profitable since their benefits include high availability (e.g., rice husk: 16 million tons/year), simple conditioning, and about 20, 36 and 28% lower operating, treatment, and total costs compared to conventional wastewater treatments (Barka et al., 2013; Shamsollahi & Partovinia, 2019). Moreover, their composition (minerals, lipids, polyphenols, and lignocellulosic compounds) allows them to have variety of functional groups (hydroxyl, carbonyl, carboxyl, methylene, etc.) that could act as binding agents with ECs (Portinho et al., 2017). The removal of caffeine and triclosan using raw or treated agro-industrial residues have achieved values around 40-80% (using moringa seeds, grape stalk, and activated carbon from coconut pulp) (Mohd-Khori et al., 2018; Portinho et al., 2017). In particular, rice husk (RH) residues have been used to remove ECs such as bisphenol A (69.2%) (Balarak et al., 2019), phenol (37.5 – 59.9%), 2,4-dichlorophenol (98%) (Shamsollahi & Partovinia, 2019), aspirin (47.0 mg/g) (N'diaye & Kankou, 2020) and triclosan (5.9 mg/g) (Triwiswara et al., 2020b). In fixed-bed columns, RH was used for the removal of 2,4-dichloro phenoxy acetic acid (24.6 mg/g) (Bahrami et al., 2018). However, the use of raw RH in batch tests or fixed-bed columns for the removal of caffeine/triclosan and other ECs is limited.

In this work, the removal of caffeine and triclosan from synthetic solutions using RH in batch tests and fixed-bed columns was studied. RH was characterized to determine how their constituents/characteristics influence the adsorption process. Batch tests were performed to determine the optimal conditions to remove both contaminants. The kinetics was determined by fitting the experimental data to pseudo-first-order, pseudo-second-order, Elovich, and Thomas models. Meanwhile, Langmuir, Freundlich, and Sips models were used to model the equilibrium experimental data. Moreover, to determine if RH could be used on a real scale (treating a greater amount of water), tests were carried out in fixed-bed columns. The data obtained were adjusted to the Bohart-Adams model.

2. Materials and methods

2.1. Rice husk conditioning

RH was obtained from a rice processing plant in Ecuador (location: S 2°11'46.2" W 79°53.173'). Caffeine and triclosan standards with purity greater than 99.0 and 97.0%, respectively, were purchased from Sigma-Aldrich.

RH was washed with drinking water to remove impurities from the surface, such as dust and rice residues. The last washing cycle was carried out with distilled water. Subsequently, a Venticell stove was used to dry the material at 60 °C for 24 h. Dry RH was crushed using a Thomas knife mill and sieved in three different particle size ranges: 120 - 150 µm (small), 300 - 600 µm (medium), and 800 - 2,000 µm (large).

2.2. Experimental model

2.2.1. Batch adsorption tests

In the batch adsorption tests, synthetic solutions of 30 mg/L of caffeine/triclosan were used. The solutions (V= 20 mL) were placed in beakers and mixed in a CIMAREC multipoint magnetic stirrer at 150 rpm. Optimal RH doses were determined using 8 different doses to remove caffeine (1.0 – 60.0 g/L) and triclosan (0.1 – 12.0 g/L), for 180 min. The optimal contact time and adsorption kinetics were determined using the optimal RH dose for each particle size. Different adsorption times (8 – 10) were tested for

caffeine (0 – 360 min) and triclosan (0 – 180 min). Adsorption isotherms were obtained using optimal conditions (dose and contact time) with caffeine/triclosan solutions with 7 concentrations (5 – 60 mg/L). All batch adsorption tests were performed in triplicate for the three particle sizes, keeping pH = 6.5 (\pm 0.2) and temperature constant (room temperature= 22.7 (\pm 1.1) °C). The efficiency in the caffeine/triclosan removal was the variable analyzed in batch adsorption tests.

2.2.2. Fixed-bed columns

Fixed-bed column tests were carried out for the three particle sizes by duplicate. Columns 10 cm high and 1 cm diameter were used, being packed with 4, 5, and 8 cm of material. RH was washed with distilled water until the wash water was colorless. The columns were operated using the caffeine/triclosan solutions (30 mg/L) with hydraulic loading rates between 2 and 4 m³/m²day, which are in the range of hydraulic loads used in previous studies at lab scale with commercial adsorbents such as granular activated carbon (Sandoval et al., 2011).

2.3. Analytical/Instrumental methods

2.3.1. Material characterization

The point of zero charge (pHpzc) of RH was determined using 50 mL of distilled water, it was placed in Erlenmeyers and the pH was adjusted between 2 and 11 using 0.01 M NaOH and HCl solutions. RH (mass= 0.5 g) was added, samples were shaken at 150 rpm for 48 h. The test was carried out for the three particle sizes in duplicate.

The RH physical-chemical characterization was performed according to ASTM standards and considering thermogravimetric analysis (TGA), aiming to understand how the adsorbent composition and structure influence its capacity. Moisture (ASTM D 4442-20), extractives in organic and aqueous solvent (ASTM D 1107-21/ASTM D 1110-21), lignin (ASTM D 1106-21), hemicellulose and cellulose (ASTM D 1109-21), ash (ASTM D 1102-21) and volatile material (ASTM D 872-19) were determined. TGA was performed using a SHIMADZU thermo-balance model 50, between 20 and 600 °C, with a heating rate of 10°C/min and a nitrogen flow of 50 mL/min.

The functional groups present on the RH surface (before/after adsorption) were identified using a Perkin Elmer FTIR-6800 spectrometer equipped with a diamond crystal ATR. Nine scans were performed in the range from 400 to 4000 cm⁻¹ with a resolution of 4 cm⁻¹. The analysis of the RH surface was performed by using an ASPEX PSEM express scanning electron microscope with a working distance of 20.4 mm and 15 kV of acceleration. The pore size (Barret-Joyner-Halenda, BJH) and the specific surface area (Brunauer-Emmett-Teller, BET) of the small RH were determined by nitrogen adsorption in a micrometric NOVA touch 1LX equipment. More than 6 multi-points were considered to determine the surface characteristics of the material, which was conditioned by drying it at 105 °C under a vacuum.

2.3.2. Caffeine/Triclosan quantification before/after adsorption tests

Caffeine and triclosan solutions were prepared using distilled water and an acetone solution (5 v/v%) as solvents, respectively. The wavelength of greatest absorbance (caffeine= 287 nm, triclosan= 295 nm) was determined by scanning between 200 and 800 nm using 10 mg/L solutions (Gil et al., 2018). Subsequently, the calibration curves of caffeine ($y= 0.0153x + 0.0185$, $R^2= 0.996$) and triclosan ($y= 0.0008x + 0.0126$, $R^2= 0.995$) were obtained using solutions with concentrations between 1 and 70 mg/L (Pereira et al., 2017). The quantification of the concentration of both contaminants before/after the adsorption processes was carried out in a Specord® 210 Plus UV-VIS spectrophotometer.

2.4. Data analysis

2.4.1. Isotherm and kinetic models

The data obtained in the kinetics test were fit to the non-linear pseudo-first-order (1), pseudo-second-order (2) and Elovich (3) models:

$$q_t = q_e(1 - e^{-k_1 t}) \quad (1)$$

$$\frac{t}{q_t} = \frac{1}{k_2 * q_e^2} + \frac{t}{q_e} \quad (2)$$

$$q_t = \frac{1}{\beta} \ln(1 + \alpha\beta t) \quad (3)$$

Furthermore, the intraparticle diffusion model (4) was used to obtain information about the adsorption process.

$$q_t = k_p \sqrt{t} + C \quad (4)$$

where q_t (mg/g) is the amount of caffeine/triclosan adsorbed at time t , q_e (mg/g) is the amount of caffeine/triclosan adsorbed at equilibrium, k_1 (min^{-1}) is the pseudo-first-order rate constant, k_2 ($\text{g}/(\text{mg} \cdot \text{min})$) is the pseudo-second-order rate constant, α ($\text{mg}/\text{g} \cdot \text{min}$) is the initial rate constant, β (mg/g) is the desorption constant, k_p ($\text{mg}/\text{g} \cdot \text{min}^{1/2}$) is the rate constant of the intra-particle diffusion model, and C (mg/g) is a constant associated with the thickness of the boundary layer.

The data obtained in the isotherm tests were fitted to the non-linear models of Langmuir, Freundlich and Sips isotherms, which are shown in equations 5 to 7, respectively:

$$q_e = \frac{q_m * K_L * C_e}{1 + K_L * C_e} \quad (5)$$

$$q_e = K_F * C_e^{1/n} \quad (6)$$

$$q_e = \frac{q_m (K_L * C_e)^{1/n}}{1 + (K_L * C_e)^{1/n}} \quad (7)$$

where q_e (mg/g) is the amount of caffeine/triclosan adsorbed per unit mass of RH at equilibrium, q_m (mg/g) is the maximum adsorption capacity of RH, C_e (mg/L) is the liquid phase concentration of caffeine/triclosan in equilibrium, K_F (mg/g) is the Freundlich capacity constant, K_L (L/mg) is Langmuir constant and n is Freundlich intensity parameter (Jiang et al., 2017). The selected models are classic models that have shown a good fit to the kinetics and equilibrium models ($R^2 \sim 1$) described by agro-industrial residues in the removal of several contaminants (Anastopoulos et al., 2015).

The adsorption tests were performed in triplicate and the control was placed with distilled water/acetone solution (5.0 v/v%) for caffeine/triclosan. Moreover, the adsorption tests were carried out in the dark to avoid photodegradation.

2.4.2. Breakthrough curve

Effluent-time concentration curves were used to evaluate the adsorption of caffeine/triclosan in continuous adsorption processes. The amount of caffeine/triclosan adsorbed at the breakthrough time (q_b) and saturation time (q_s) (mg/g) was calculated using equations 8 and 9:

$$q_s = \frac{C_o * Q}{1000 * m} \int_0^{t_s} 1 - \frac{C_s}{C_o} \quad (8)$$

$$q_b = \frac{C_o * Q}{1000 * m} \int_0^{t_b} 1 - \frac{C_b}{C_o} \quad (9)$$

where C_o (mg/L) is the initial concentration of caffeine/triclosan, C_b and C_s (mg/L) are the effluent concentration (caffeine/triclosan) at the breakthrough time and the saturation time, respectively, Q (mL/min) is the volumetric flow, m (mg) is the RH mass and t_b and t_s (min) are the breakthrough and saturation times when C/C_o is 0.1 and 0.9, respectively. The data obtained were fit to the non-linear Bohart-Adams model (Eq. 10), since this model provides an easy and rapid evaluation of adsorption performance. Moreover, it has shown a good fit when ECs are adsorbed by agro-industrial residues such as cane bagasse (Peñafiel et al., 2021).

$$\frac{C_t}{C_o} = \frac{1}{1 + e^{\left(\frac{K_{BA} * N_o * h}{u} - K_{BA} * C_o * t\right)}} \quad (10)$$

where k is the rate constant of the Bohart-Adams model, N_0 (mg/L) is the maximum adsorptive capacity, h (cm) is the bed height, t (min) is the service time of the column, u (cm/min) is the linear flow velocity, and C_t (mg/L) is the concentration at time t .

In addition, useful parameters for column design were calculated, such as the empty bed contact time (EBCT), the percentage of fractional bed utilization (%FBU), and the height of the mass transfer zone (h_{MTZ}) (cm) using equations 11 to 13, respectively (Peñafiel et al., 2021; Sotelo et al., 2012):

$$EBCT = \frac{V_c}{Q} * 100 \quad (11)$$

$$\%FBU = \frac{q_b}{q_s} * 10 \quad (12)$$

$$h_{MTZ} = \left(1 - \frac{q_b}{q_s}\right) * h \quad (13)$$

where V_c is the fixed-bed volume (L); Q is the flow rate (L/d) and V_b is the volume treated at breakthrough (L).

2.5. Statistical Analysis

The optimal RH dose in the different particle sizes was determined using the significant differences between the doses used in the adsorption of caffeine/triclosan and the performance achieved (removal efficiency, %) in batch tests. Analyses of variance (ANOVA) with a single factor analyzed by Tukey's test, with a significance level of 0.05, were applied. Data normality was determined using normality (Shapiro-Wilks) and homogeneity (Levene) tests. Minitab 18 version 1.0 was the software used in statistical analysis. The same statistical analysis was performed to determine the optimal bed height in the adsorption of caffeine/triclosan in fixed-bed columns.

The statistical analysis of data from kinetics (pseudo-first-order, pseudo-second-order, and Elovich), isotherm (Langmuir, Freundlich, and Sips), and Bohart-Adams non-linear models, considered the calculation of means, standard deviation, error, and linear regressions using Microsoft Excel Solver version 2016. For this purpose, in batch and continuous tests, the coefficient of determination (R^2), the chi-square (χ^2), and the sum of squared errors (SSE) were calculated (equations 14-16) to determine the models that best fit the caffeine and triclosan adsorption data:

$$R^2 = 1 - \frac{\sum (V_{e,exp} - V_{e,cal})^2}{\sum (V_{e,exp} - V_{e,mean})^2} \quad (14)$$

$$\chi^2 = \sum \frac{(V_{e,exp} - V_{e,cal})^2}{V_{e,cal}} \quad (15)$$

$$SSE = \sum (V_{e,exp} - V_{e,cal})^2 \quad (16)$$

where $V_{e,exp}$ are the experimental value of parameters (q , C_f/C_0 for batch tests and fixed-bed columns, respectively), $V_{e,cal}$ are the calculated parameters using the Solver tool, $V_{e,mean}$ is the mean of $V_{e,exp}$ values (Nguyen et al., 2021).

3. Results and Discussion

3.1. Point of zero charge

The pHzpc of RH in the three-particle size was around 7.6 (Figure 8). This means that at pHs lower than pHpzc RH will adsorb contaminants with a negative charge, and at higher pHs contaminants with a positive charge. Caffeine and triclosan have a pKa of 8.3 and 7.9, suggesting that they could be more efficiently removed at pHs lower than pHpzc (Fiol & Villaescusa, 2009).

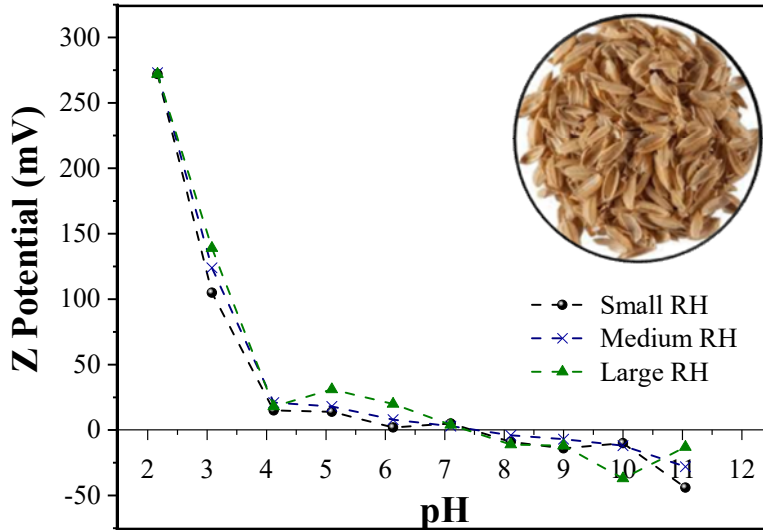


Figure 8. Point of zero charge for the small, medium, and large RH particles.

3.2. Physical-chemical characterization and TGA analysis

Figure 9 (inset) shows the RH physical-chemical characterization. RH shows a high content of lignin (20.2%), hemicellulose (24.7%), and cellulose (35.2%), polysaccharides that have functional groups such as phenols, carboxyl, and methyl. They provide positive and negative charges to RH, which will be able to retain caffeine/triclosan molecules (Chakraborty et al., 2014; Değermenci et al., 2019). Meanwhile, TGA shows that there is a weight loss in the clean RH after continuous heating (below 100 °C). The initial weight loss (8.6%) is mainly due to water vaporization/moisture removal (Kaur et al., 2020). The weight loss (20.6%) between 280 and 340 °C is attributed to the degradation of hemicellulose. Meanwhile, the weight loss between 340 and 400 °C (29.8%) and the carbonization of RH (temperature > 450°C= 7.8%) are attributed to cellulose and lignin degradation, respectively (Gajera et al., 2020).

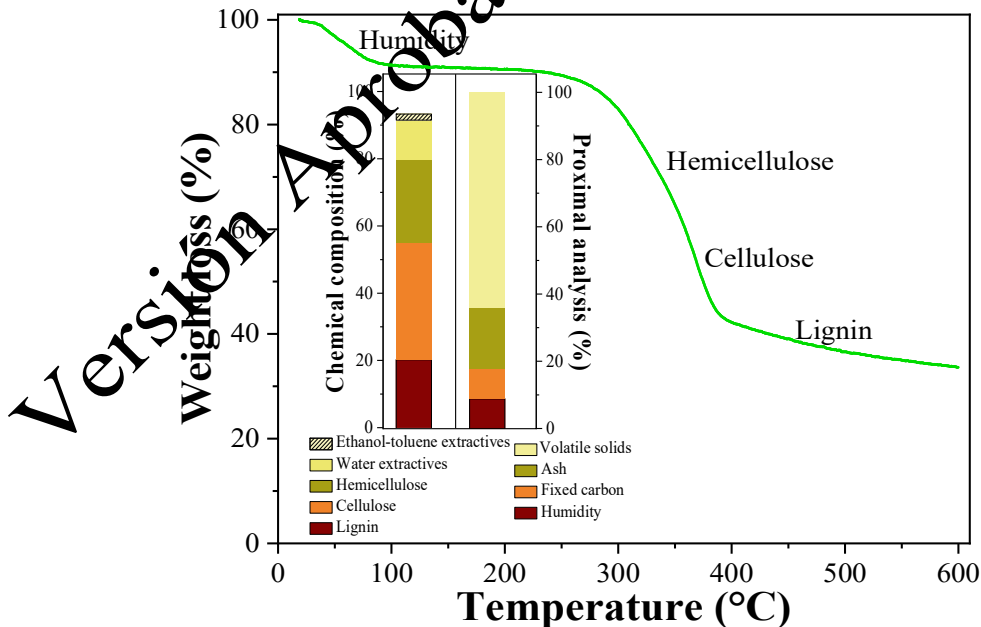


Figure 9. TGA curve of rice husk adsorbent. Inset: physical-chemical characterization and proximal analysis.

3.3. SEM and BET analyses

SEM and BET results are presented in Figure 10. RH evidences an irregular surface with cavities and grooves where caffeine/triclosan could be retained. On the other hand, the surface area of small RH (1.18

m²/g) is similar to that found in other studies, where values between 0.14 and 7.14 m²/g were reported. The range for the specific surface area of RH is relatively wide since it depends on the rice species and its particle size (Daffalla et al., 2020; Kolar & Jin, 2019). However, the surface area determined is lower than the values presented by RH with thermal and chemical modifications (25.06 m²/g) (Nizamuddin et al., 2018).

The average pore radius was 4.99 nm, which according to the IUPAC corresponds to a mesopore material (Wei et al., 2019). This is verified with the nitrogen adsorption-desorption isotherms of RH (Fig. 2), which is a combination of type II and V isotherms, that characterize macro and mesoporous adsorbents. The shape of the RH hysteresis slope is of the H1 type, with a sharp inflection in the range of 0.7 – 1.0 P/Po. The hysteresis presents two parallel and practically vertical bands that indicate the presence of cylindrical pores (Álvarez-Torrellas et al., 2016; Daffalla et al., 2020). Therefore, the morphological characteristics (irregular surface and presence of pores) of RH could favor the adsorption process between it and caffeine/triclosan

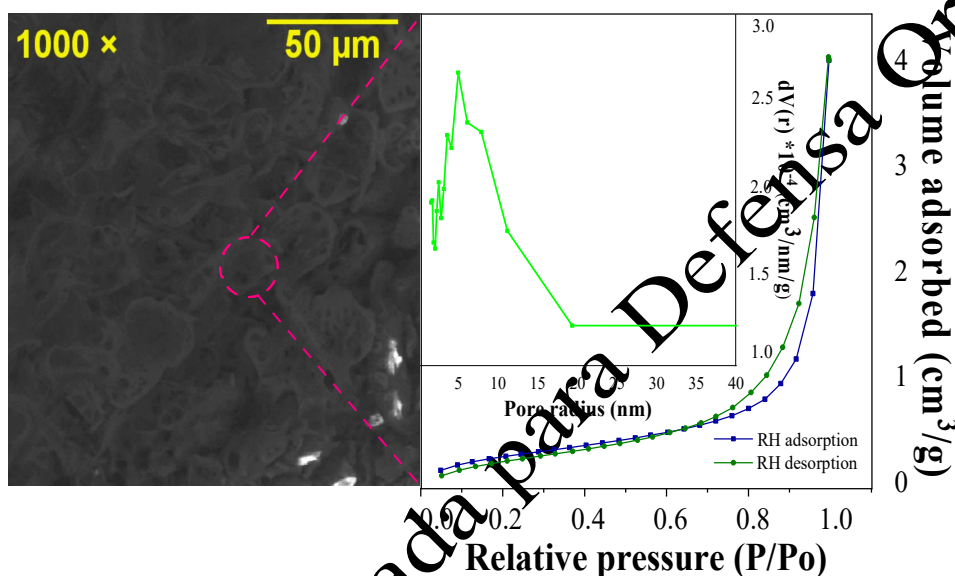


Figure 10. SEM analysis, nitrogen adsorption/desorption isotherms of RH, and pore radius distribution.

3.4. FTIR spectroscopy analysis

Figure 11 shows the FTIR spectra of RH before/after the adsorption process. The region between 3300 – 2500 cm⁻¹ denotes the presence of OH- and CH- bonds. The bands around 1639 – 1723 cm⁻¹ correspond to the C=O stretch; while the band around 1375 cm⁻¹ corresponds to the CH bending. Both groups can be attributed to the aromatic groups of hemicellulose and lignin (Rwiza et al., 2018; Shen et al., 2017). Meanwhile, the bands around 1039 – 1370 cm⁻¹ correspond to the vibration of the C=O group in lactones.

After caffeine/triclosan adsorption with the same conditions for all RH sizes, the spectra of three RH sizes showed changes. Modifications in the intensity of bands around 2924 – 3500 and 1100 – 1490 cm⁻¹, which are related to lignin, cellulose, and hemicellulose were evidenced. The intensity of the band around 1598 cm⁻¹ assigned to the carbonyl group changed after adsorption. The changes in band intensity after caffeine/triclosan adsorption suggest chemical reactions/attraction forces between caffeine/triclosan molecules and the functional groups of the RH surface (Mohd-Khori et al., 2018).

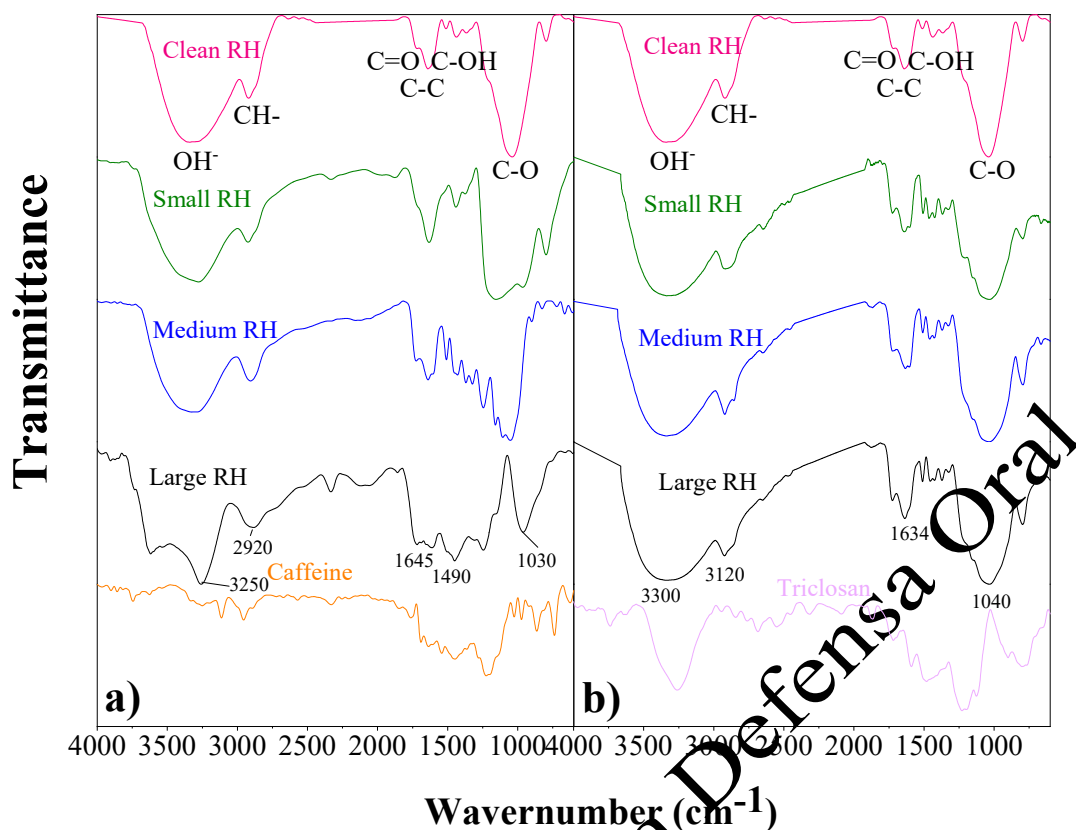


Figure 11. FTIR spectra for a) caffeine, and b) triclosan, before and after the caffeine/triclosan adsorption. RH small= 120 – 150 μm , RH medium= 300 – 600 μm , RH large= 800 – 2,000 μm .

3.5. Optimal dose and contact time

Figure 12 shows the influence of the RH dose and contact time in the removal of caffeine and triclosan for each particle size. For the removal of caffeine (Figure 12a), the optimal doses for small particles (120 – 150 μm) and medium particles (300 – 600 μm) were 4.0 and 8.5 g/L, achieving removals of 72.5 (\pm 1.6) and 71.1 (\pm 0.6)%, respectively. Initially, as the RH dose increases, the caffeine removal is also increased. However, after reaching the maximum adsorption with small and medium particles, an increase in the RH dose reduced the caffeine removal (20 - 30%). This suggests that RH agglutinates when the adsorbent dose was increased (Noreen et al., 2013). This is due to the interaction between the adsorbent particles, which reduced the surface area and negatively influences the caffeine adsorption process (Ata et al., 2012). For the large particles (800 – 2,000 μm), the optimal RH dose increased considerably, reaching 50.0 g/L with a maximum adsorption percentage of 96.5 (\pm 1.7)%. In this case, the caffeine removal increases while increasing the RH dose, due to the higher availability of superficial area (Noreen et al., 2013). Figure 12c shows the optimal doses for triclosan removal. The optimal doses for the small, medium and large particle sizes were 1.5, 2.5, and 10.0 g/L, respectively. These doses achieved removals of 97.2 (\pm 1.0), 96.9 (\pm 0.1), and 98.7 (\pm 0.4)%, respectively.

On the other hand, figures 12b and 12d show the optimal contact time for the removal of caffeine and triclosan, respectively. The optimal contact time for the caffeine removal using the small, medium, and large particle sizes was 180 min. At that time, the highest removal percentage was achieved, reaching between 71.4 (\pm 0.8) and 96.2 (\pm 1.7)%. For triclosan, the optimal contact time for the three particle sizes was 60 min, achieving removals between 96.9 (\pm 0.1) and 98.7 (\pm 0.4)%. The removal of caffeine and triclosan was greater than 80% and 70% in the first 60 and 10 minutes, respectively. The increase in the removal of both at the beginning of the process is because there are abundant empty adsorbent sites on the RH surface. As the contact time increases, the availability of empty spaces on the RH surface was reduced, and the adsorption efficiency of caffeine/triclosan decreased (Gil et al., 2018).

Therefore, it was verified that particle size influences the adsorption process. An adsorbent with a smaller particle size requires a lower dose because the surface area and the available sites to retain the

caffeine/triclosan are higher (H. Kaur et al., 2018). Likewise, the characteristics of the contaminants will facilitate or not their removal from the aqueous medium. In this case, triclosan has a lower solubility in water (4.8×10^{-4} times) compared to caffeine, which allows it to be adsorbed more quickly (3 times) with a lower RH dose (2.7 – 5.0 times). Moreover, the high K_{ow} of triclosan results in a greater affinity with organic matter so it easily adheres to the RH surface (Montaseri & Forbes, 2016). Another factor that hinders caffeine removal is its dipole moment (3.64 D) since it could affect the separation processes from the solution. This is due to the strength of the bonds that exist between the caffeine molecules and water (Rigueto et al., 2020).

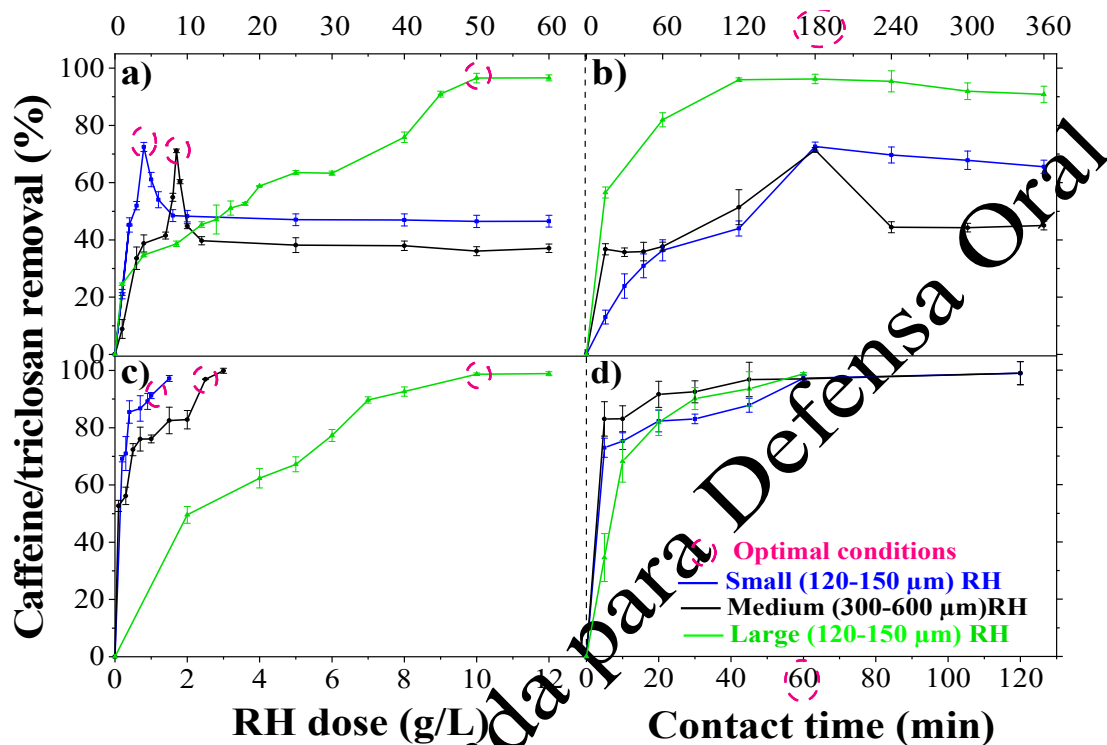


Figure 12. Optimal dose/contact time: a)/b) caffeine removal and c)/d) triclosan removal.

3.6. Adsorption isotherm and kinetics

The kinetics adsorption performance of caffeine and triclosan on RH was analyzed at different times to study the rate of adsorption and the adsorption mechanism. The fitting to the different models is presented in Figure 13. The caffeine adsorption on large and small RH and triclosan adsorption on large RH particles were better fitted to the pseudo-second order model ($R^2 = 0.971-0.987$). Meanwhile, the adsorption using medium size particles better fitted the Elovich model ($R^2 = 0.996-0.999$) for both contaminants. The χ^2 and SSE values show lower values (closest to zero) for the models that best fit the data obtained (higher R^2 , closest to 1).

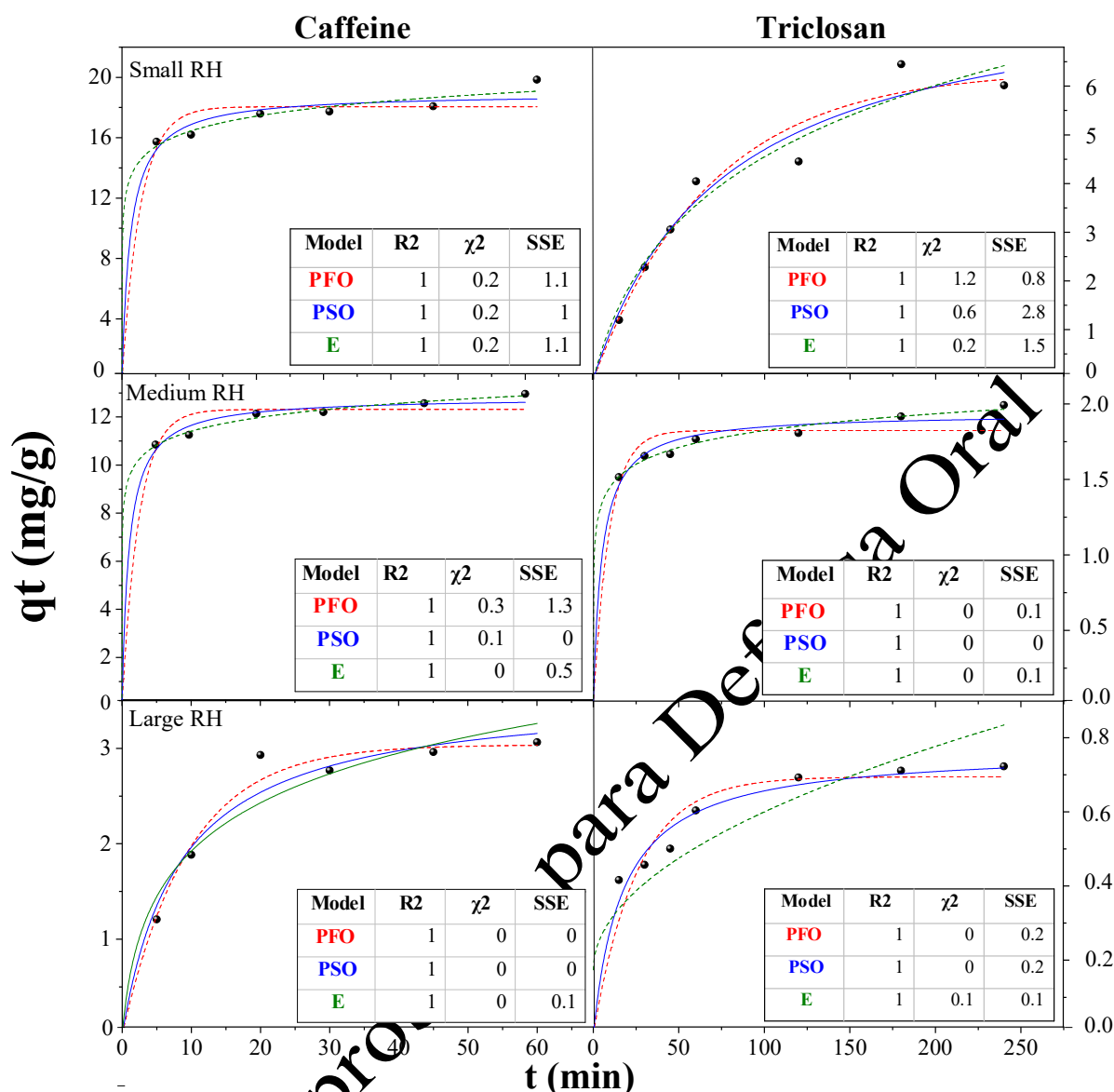


Figure 13. Kinetic models for caffeine and triclosan adsorption in three particle sizes. Black points= experimental data, red line= pseudo-first-order model, blue line= pseudo-second-order model, green line= Elovich model.

The pseudo-second-order model assumes that the contaminant concentration is constant over time and that the total number of active sites depends on the amount of contaminant adsorbed at equilibrium (Yokoyama et al., 2019). Caffeine and triclosan adsorption also followed a pseudo-second-order model when cotton-derived carbon microtubes were used. The q_e values achieved were higher (caffeine= 19.8 – 212.9 times, triclosan= 39.8 times) than those of this study, probably due to the thermal modification of cotton and its greater surface area (380 – 540 m^2/g) (Shirvanimoghaddam & Trojanowska, 2020). Although using modified residues such as oxidized biochar from pine needles and RH nano-silica, lower q_e values were obtained (caffeine: 2.0 – 40.2 times, triclosan: 17.5 times) compared to those of this study (Anastopoulos et al., 2020a; Tejedor et al., 2022).

On the other hand, the Elovich model assumes that the adsorbent surface is energetically heterogeneous and that adsorption kinetics is not substantially affected by either desorption or interactions between adsorbed species (Keerthanam et al., 2020b; Yokoyama et al., 2019). Furthermore, α (associated with adsorption rate) and β (associated with desorption rate) indicate the interaction between RH and caffeine/triclosan. High values of α (13.6 – 110.1 $mg/(g \text{ min})$) and low values of β (0.62 – 0.68 mg/g) suggest the appearance of stable interactions (Yokoyama et al., 2019). In previous studies in which

caffeine (adsorbent: tea-waste biochar and *Gliricidia sepium* biochar) and triclosan (adsorbent: PVC and activated carbon from Stevia residues) were removed, the experimental data obtained were also fitted to the Elovich model (Keerthanan et al., 2020a; 2020b; Ma et al., 2019; Yokoyama et al., 2019). Some authors suggest that if the experimental data fit the Elovich model, chemisorption occurs (Keerthanan et al., 2020; 2020b). Meanwhile, other authors indicate that the fit to the pseudo-second-order models does not reveal the adsorption mechanisms. Since to determine the adsorption mechanisms (physics, chemistry) it is necessary to use several analytical techniques (FTIR, SEM, BET, Raman, Z potential, etc.) together with enthalpy and entropy changes (adsorption thermodynamics) and activation energies and adsorption (Tran et al., 2017). The parameters for both models are shown in Table 8 and Figure 13.

Table 7 also shows the parameters for the intraparticle diffusion model. According to Tran et al., 2017, the intraparticle diffusion model can be useful to identify the reaction pathways, the adsorption mechanisms and also predict the adsorption rate control step. In the process of removing a contaminant present in an aqueous medium using an adsorbent (solid-liquid sorption), contaminant transfer is generally characterized by film diffusion or external diffusion, surface diffusion and pore diffusion, or combined surface and pore diffusion. In summary, if the q_t vs. $t^{1/2}$ curve passes through the origin, then the adsorption process is limited only by intraparticle diffusion. However, Figure 14 shows the presence of two linear zones, whereby the adsorption process is controlled by a two-step mechanism. In the first stage caffeine/triclosan are transported from the liquid phase to the external surface of the RH through the hydrodynamic boundary layer (film diffusion). In the second stage, there is a slow diffusion (intraparticle diffusion) of the caffeine/triclosan molecules from the outside of the RH to its pores. In the final stage, the caffeine/triclosan are rapidly adsorbed in the pores (Tran et al., 2017).

Table 8. Kinetics model parameters for caffeine and triclosan adsorption.

Kinetic model	Parameter	Caffeine			Triclosan		
		RH: 120 – 150 μm	RH: 300 – 600 μm	RH: 800 – 2,000 μm	RH: 120 – 150 μm	RH: 300 – 600 μm	RH: 800 – 2,000 μm
Pseudo-first-order	q_e experimental [mg/g]	5.242	1.787	0.648	18.311	12.466	2.865
	q_e [mg/g]	6.329	1.824	0.695	18.057	12.314	3.038
	k_1 [min^{-1}]	0.015	0.107	0.039	0.375	0.397	0.105
	R^2	0.951	0.745	0.803	0.458	0.605	0.964
	SSE	1.084	0.073	0.019	5.802	1.251	0.102
Pseudo-second-order	q_e [mg/g]	8.271	2.938	0.770	18.951	12.826	3.591
	k_2 [$\text{g}/(\text{mg min})$]	0.002	0.106	0.075	0.043	0.075	0.034
	R^2	0.952	0.857	0.919	0.991	0.891	0.942
	SSE	1.037	0.002	0.008	2.812	0.001	0.161
	α [$\text{mg}/(\text{g min})$]	0.137	13.613	0.189	110.139	66.888	0.844
Elovich	β [mg/g]	0.420	0.622	7.891	0.682	1.194	1.285
	R^2	0.967	0.998	0.987	0.996	0.999	0.955
	SSE	1.108	0.055	0.087	1.547	0.519	0.116
	K_{p1} [$\text{mg}/(\text{g min}^{1/2})$]	0.721	0.060	0.046	0.840	0.581	0.773
	C_1 [mg/g]	-1.643	1.295	0.223	13.743	9.502	-0.535
Intraparticle diffusion	R^2	0.996	0.934	0.895	0.967	0.988	0.999
	SSE	0.033	0.002	0.002	0.062	0.010	8.436×10^{-4}
	K_{p2} [$\text{mg}/(\text{g min}^{1/2})$]	0.358	0.041	0.007	0.915	0.330	0.131
	C_2 [mg/g]	0.878	1.363	0.621	12.473	10.383	2.063
	R^2	0.601	0.996	0.996	0.835	0.996	0.984
	SSE	0.880	6.500×10^{-5}	1.760×10^{-6}	0.426	0.001	6.944×10^{-4}

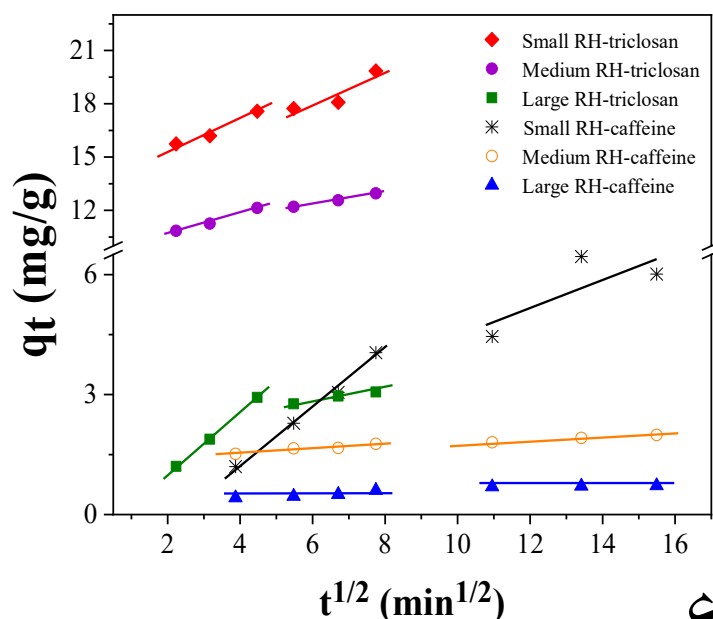


Figure 14. Intraparticle diffusion kinetics for adsorption of caffeine and triclosan.

On the other hand, the parameter values and the fittings to the Langmuir, Freundlich, and Sips isotherm models are shown in Table 9 and Figure 15, respectively. The adsorption of caffeine and triclosan fits well with the three isotherm models used. Nevertheless, the adsorption in the small (caffeine, triclosan), medium (caffeine, triclosan), and large (triclosan) RH particles show a better fitting to the Langmuir and Sips models ($R^2 > 0.91$).

Langmuir's model supposes that caffeine/triclosan adsorption occurs in a monolayer without interaction or steric hindrance between adsorbate molecules because the active sites have the same energy (same affinity for adsorbate molecules) (Yokoyama et al., 2019). Meanwhile, the Sips model is a combination of Langmuir and Freundlich models, which indicates that caffeine/triclosan can occupy more than one RH adsorption site (heterogeneous surface). The q_m values calculated with the Langmuir (caffeine) and Sips (triclosan) models are very close to those obtained experimentally, which suggests that a monolayer and heterogeneous adsorption occurs, respectively (Nguyen et al., 2021). The results obtained coincide with studies in which it is observed that the adsorption of caffeine in adsorbents such as tea leaves, orange, and banana peels, activated carbon from grape stem, water hyacinth biochar, activated carbon from coconut residues, etc. fit better the Langmuir model (Almeida-Naranjo et al., 2021b; Castillo et al., 2020). Likewise, triclosan adsorption using nano silica from RH and activated carbon from civilian gas masks fit better with the Sips model (Shirvanimoghaddam & Trojanowska, 2020; Tejedor et al., 2022).

In the other hand, the adsorption using the large RH particles fit better to the Freundlich model ($R^2 = 0.96$) in the caffeine removal. The same happened with adsorbents such as biochar from tea waste and *Gliricidia sepium* (Kerthan et al., 2020a; 2020b). The Freundlich model supposes multilayer adsorption because the energy is not equal on the surface. Likewise, the χ^2 (0.001–0.257) and SSE (0.008–1.693) values are lower (close to zero) in the models that better fit the data obtained.

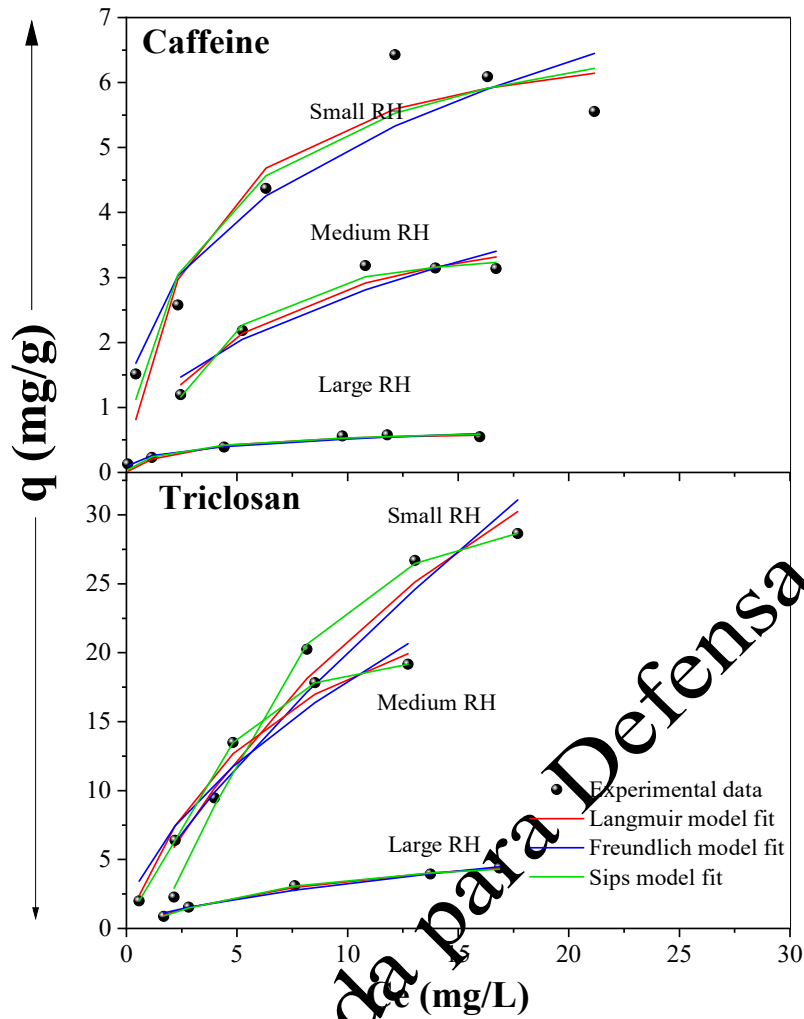


Figure 15. Isotherm models for caffeine and triclosan adsorption in three particle sizes.

Furthermore, the K_L and n values in the Langmuir and Freundlich models are lower than 1.0, which indicates that the caffeine/triclosan adsorption in RH is favorable. In the triclosan adsorption, the K_L value is even lower than 0.1 (low surface energy), which indicates a greater intensity in the bonds between triclosan and RH (Almeida-Naranjo et al., 2021b; N'diaye & Ahmed-Kankou, 2020).

Table 9. Adsorption isotherm model parameters for caffeine and triclosan adsorption

Isotherm model	Parameter	Caffeine			Triclosan		
		RH: 120 – 150 μm	RH: 300 – 600 μm	RH: 800 – 2,000 μm	RH: 120 – 150 μm	RH: 300 – 600 μm	RH: 800 – 2,000 μm
	q_e [mg/g]	6.425	3.182	0.578	28.635	19.164	4.378
Langmuir	q_m [mg/g]	7.084	4.433	0.668	70.772	30.613	7.012
	K_L [L/mg]	0.309	0.178	0.382	0.042	0.147	0.097
	R^2	0.909	0.958	0.899	0.955	0.985	0.996
	χ^2	0.069	0.010	0.007	0.257	0.054	0.003
	SSE	1.816	0.129	0.018	22.995	3.216	0.036
Freundlich	K_F [(mg/g) $^{1-1/n}$]	2.264	0.991	0.249	3.419	4.723	0.819
	$1/n$	0.343	0.438	0.316	0.768	0.580	0.601
	R^2	0.885	0.902	0.956	0.932	0.952	0.980
	χ^2	0.086	0.023	0.003	0.394	0.177	0.013
	SSE	2.283	0.300	0.008	35.027	10.545	0.180
Sips	q_m [mg/g]	8.147	3.450	0.810	31.400	22.579	5.747
	K_L [L/mg]	0.218	0.276	0.248	0.165	0.264	0.148
	$1/n$	0.766	1.760	0.707	2.196	1.513	1.202
	R^2	0.915	0.984	0.927	0.998	0.995	0.998
	SSE	0.064	0.004	0.013	0.011	0.018	0.001
		1.693	0.048	0.005	0.943	1.062	0.019

These results show that the RH adsorption capacity is a function of the particle size and the characteristics of the contaminant (solubility, K_{ow}). The small RH particles have a higher adsorption capacity for caffeine/triclosan (8.1/31.4 mg/g) than the medium (3.4/22.6 mg/g) and the large RH particles (0.8/5.7 mg/g), respectively. The adsorption capacity achieved by RH in caffeine removal is comparable to that achieved with other raw low-cost adsorbents, such as groundnut shell (100 μm , 4.21 mg/g), grape stalk (700 μm , 0.938 mg/g), *Balanites aegyptiaca* seeds (< 100 μm , 4.28 mg/g) and treated adsorbents (pine needles oxidized biochar < 300 μm , 5.35 mg/g) (Anastopoulos et al., 2020a; N'diaye & Ahmed-Kankou, 2020; Portinho et al., 2017). The caffeine adsorption by RH is even higher than adsorbents such as grape stalk (~ 1 mg/g), which has a greater surface area (6.23 m^2/g) and pore volume (0.003 cm^3/g) comparable to RH (0.006 cm^3/g). Something similar happened in the removal of triclosan with activated carbon from coconut pulp residues of 595 μm (2.02 – 31.57 mg/g) (Mohd-Khori et al., 2018), microplastic polystyrene with a specific surface between 0.58 and 2.53 m^2/g (0.29 – 0.43 mg/g) (Yandan Li et al., 2019) and nano silica from RH with a specific surface between 208 – 223 m^2/g (2.74 mg/g) (Tejedor et al., 2020). However, there are other adsorbents with higher adsorption capacity than RH to remove caffeine, triclosan, and other ECs. The latter received chemical or thermal treatments, but the costs or the environmental impact that could be generated are not indicated.

3.7. Fixed-bed columns

The main results obtained in fixed-bed columns are summarized in Table 10. The tests in the fixed-bed columns were carried out to determine the influence of the bed height and the hydraulic load on the three particle sizes of RH to remove caffeine/triclosan. The efficiencies achieved in the removal of caffeine and triclosan using the three sizes of RH at bed heights of 4, 5, and 8 cm did not show significant differences ($p > 0.05$). On the other hand, the hydraulic load (4 $\text{m}^3/\text{m}^2\text{-day}$) produced clogging in the columns that used the small RH at 30 min of operation (spillage of the caffeine/triclosan solution was observed at the top of the column), so it was not possible to construct the breakthrough curve for this hydraulic load and establish its influence on the three particle sizes. The experimental breakthrough curves for the three RH particle sizes using a bed of 4 cm high and with a hydraulic loading rate of 2 $\text{m}^3/\text{m}^2\text{-day}$ are presented in Figure 16.

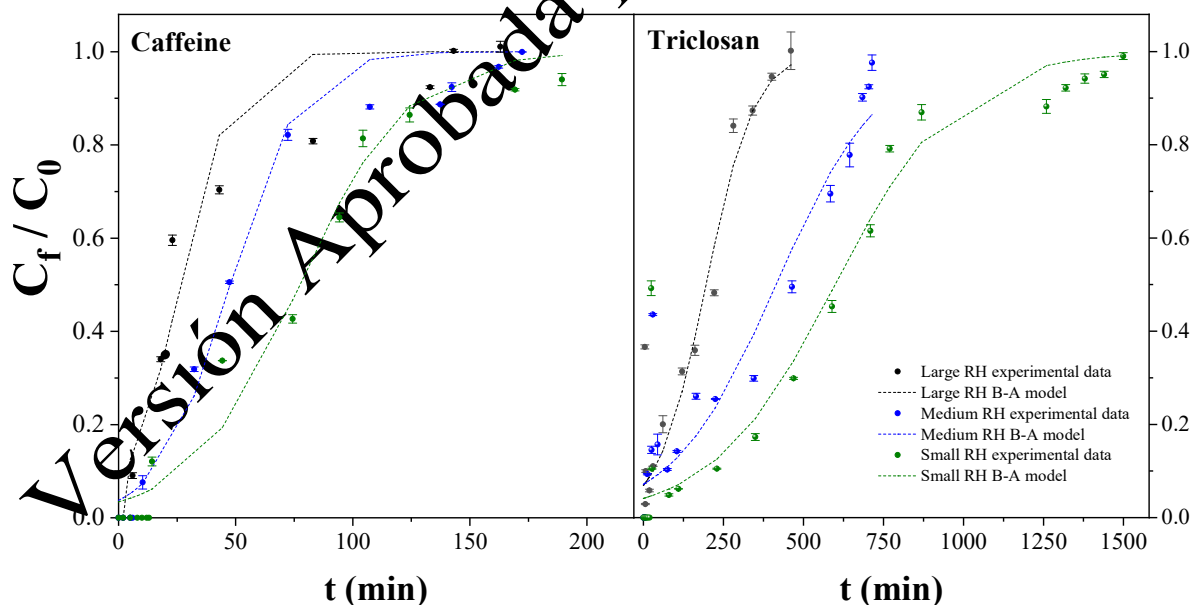


Figure 16. Effect of particle size and contaminant type on breakthrough curve

The size of the adsorbent particles is a very important parameter in the operation of fixed-bed columns since it defines the available surface area and the void fraction, and the available path for the movement of caffeine/triclosan solutions (Sivarajasekar et al., 2018). An increase in particle size decreased the adsorption capacity at breakthrough time (q_b decrease: caffeine= 16.7 – 33.3% and triclosan= 43.3 – 60%) and saturation time (q_s decrease: caffeine= 7.7 – 23.1% and triclosan= 19.8 – 33.3%). The smaller RH

particles allow a shorter diffusion path for the caffeine/triclosan molecules. Therefore, the molecules of both contaminants will easily penetrate the pores of the RH, resulting in a higher adsorption rate (Gupta & Garg, 2019; Sivarajasekar et al., 2018). The effect of particle size on adsorption capacity in both breakthrough time and saturation time is lower for caffeine, probably due to its physicochemical characteristics (e.g., high water solubility) (Álvarez-Torrellas et al., 2016; Rigueto et al., 2020). Something similar happens with the values of the breakthrough/saturation time. Therefore, an increase in RH particle size results in faster bed depletion and lower volume (V_b) of treated water (Jaria et al., 2019; Peñafiel et al., 2021).

The smaller RH particles also had lower h_{MTZ} than the medium (1.3/1.1) and large (2.6/1.1) particles for both contaminants (caffeine/triclosan). A smaller particle size allows a higher mass transfer rate and thus a smaller mass transfer zone (Gupta & Garg, 2019). This shows that the small RH has better performance. A similar behavior was observed in cadmium adsorption when using date palm trunk fiber with size ranges of 250 – 355 and 560 – 630 μm (Al-Shawabkeh et al., 2021). A smaller mass transfer zone with a higher slope can also be identified on the C_f/C_o vs. t plot (Figure 16). Increasing h_{MTZ} in the larger RH reduced fractional bed utilization (FBU) by 2.97 – 14.21% for caffeine and between 7.68 – 9.40% for triclosan. The larger particles leave larger spaces between each other (the fraction of voids in the bed increases), so the contact time between the caffeine/triclosan and the RH particles decreases and this reduces the fraction of bed which is being effectively used (Sivarajasekar et al., 2018).

Table 10. Adsorption isotherm model parameters for caffeine and triclosan adsorption

Contaminant	Particle size (μm)	Mass (g)	V_c (L)	EBTC (d)	FBU (%)	h_{MTZ} (cm)	$C/C_o = 0.1$		$C/C_o = 0.9$		
							t_b (min)	V_b (mL)	q_b (mg/g)	t_s (min)	q_s (mg/g)
Caffeine	120 – 150	1.741	0.003	0.436	91.04	0.36	4	7.15	0.12	169	0.13
	300 – 600	1.689			88.07	0.47	10	5.15	0.10	142	0.12
	800 – 2,000	1.545			76.83	0.92	6	3.00	0.08	133	0.10
Triclosan	120 – 150	1.741	0.003	0.436	24.00	3.6	26	13.15	0.30	1259	1.26
	300 – 600	1.489			16.62	2.34	12	6.15	0.17	684	1.01
	800 – 2,000	1.145			14.60	1.42	7	3.50	0.12	341	0.84

EBTC= empty bed contact time, %FBU= percentage of fractional bed utilization, h_{MTZ} = height of the mass transfer zone

Table 11 shows the results of the fitting of the experimental data obtained in the absorption of fixed-bed columns to the Bohart-Adams model. The Bohart-Adams model correlates C/C_o with contact time in a continuous adsorption system. The model considers only the first region of the breakdown curve where $C/C_o < 0.5$ and assumes negligible mass transfer. Therefore, the adsorption rate will depend on the residual capacity of the adsorbent and the concentration of the contaminants (Ahmed & Hameed, 2018). Both caffeine and triclosan adsorption show a relatively good fit to the model, presenting R^2 values between 0.91 and 0.99 and very low values of SSE (2.706×10^{-3} – 0.245) and χ^2 (6.151×10^{-3} and 0.032). A good fit of the experimental data with the Bohart-Adams model indicates that surface diffusion is the rate-limiting step in the adsorption process (de Franco et al., 2017). The values of adsorption capacity (N_o) for triclosan are higher and the Bohart-Adams constant (K_{BA}) are lower, compared to those for caffeine. This is associated with the lower solubility/higher hydrophobicity of triclosan. A similar behavior was observed in the removal of sulfapyridine (less soluble in water) and sulfamethoxazole (more soluble in water), in which sulfapyridine reached a higher removal (20.72 mg/L) (Ahmed & Hameed, 2018). Furthermore, the smallest particles presented the greatest adsorption capacities, which is related to their largest surface area (Sivarajasekar et al., 2018).

Table 11. Adsorption isotherm model parameters for caffeine and triclosan adsorption

Contaminant	Particle size (μm)	K_{AB} [L/(min mg)]	N_o (mg/L)	R^2	χ^2	SSE
Caffeine	120 – 150	1.340×10^{-3}	352.706	0.993	2.685×10^{-3}	2.706×10^{-3}
	300 – 600	2.114×10^{-3}	216.708	0.981	6.151×10^{-3}	0.042
	800 – 2,000	2.828×10^{-3}	119.931	0.943	0.017	0.101
Triclosan	120 – 150	1.172×10^{-4}	3797.217	0.929	0.028	0.245
	300 – 600	1.379×10^{-4}	2628.774	0.910	0.032	0.210
	800 – 2,000	2.962×10^{-4}	1240.89	0.937	0.024	0.133

N_o = adsorption capacity, K_{BA} = Bohart-Adams constant

4. Conclusions

The use of rice husk represents a promising alternative for the removal of emerging contaminants such as caffeine and triclosan, as is evident from the batch/continuous tests carried out in this work. The size of the RH and the characteristics of caffeine/triclosan (solubility, K_{ow}) notably influenced their adsorption in batch and fixed-bed columns. The optimal dose of the small RH was lower than the other two sizes (caffeine= 2.1 – 12.5 times, triclosan= 2.0 – 6.7 times), reaching efficiencies of 72.5 and 97.2% for caffeine and triclosan, respectively. The optimal contact time for caffeine removal was 3.0 times greater than triclosan. The adsorption of both contaminants for most particle sizes was better fitted to the Elovich and Sips/Langmuir models, and the removal of both contaminants was dominated by film and intraparticle diffusion. Besides, the operation of the fixed-bed columns fit the Bohart-Adams model quite well, being also the small RH particles the most efficient in the removal of both contaminants (caffeine: $q_b= 0.12$ mg/g, $q_s= 0.13$ mg/g and triclosan: $q_b= 0.30$ mg/g, $q_s= 1.26$ mg/g). The relatively high adsorptive capacity of RH and its affinity with the contaminants studied, open the possibility of exploring its use in water treatment technologies that could benefit from its availability, ease of processing, and relatively low cost.

Versión Aprobada para Defensa Oral

Article 2. Peanut shells: characterization and performance in adsorption of caffeine and triclosan

ABSTRACT

Several materials and technologies are being studied to remove the variety of contaminants currently found in wastewater, aiming to avoid their negative impacts on ecosystems and human health. Low-cost and environmentally-friendly alternatives are of particular interest. For this reason, the adsorption performance of peanut shells in the removal of caffeine and triclosan was studied in this work. The chemical composition, morphology, and functional groups of peanut shells were determined using ASTM standards and thermogravimetric analysis (TGA), scanning electron microscopy, and Fourier Transforms Infrared Spectroscopy (FTIR), respectively. Batch adsorption tests were carried out using 30 mg/L caffeine and triclosan solutions, and considering as variables the peanut shell particle granulometry (120 – 150, 300 – 600 and 800 – 2,000 μm), adsorbent dose (0.02 – 60 g/L) and contact time (up to 180 min). Once the optimal adsorption conditions were found, the adsorption kinetics and isotherm models were determined. Peanut shells were composed mainly of polysaccharides (lignin, cellulose, and hemicellulose $\approx 70\%$), and showed an irregular surface with an area of 1.7 m^2/g and a pore volume of 0.005 cm^3/g . The highest removal of caffeine and triclosan (85.6 ± 1.4 and $89.3 \pm 1.5\%$) was achieved using 10.0 and 0.1 g/L of the smallest particles, at 180 and 45 min, respectively. Triclosan was easier to remove than caffeine due to its lower water solubility and higher hydrophobicity. The pseudo-second-order kinetics model showed the best fit to the experimental data, indicating that the adsorption occurs between caffeine/triclosan and the adsorbent. The adsorption equilibrium was fit to the Sips model with maximum adsorption capacities of 3.3 mg/g and 289.3 mg/g for caffeine and triclosan, respectively.

1. Introduction

The massive consumption/use of chemical products such as pesticides, hormones, pharmaceuticals, and personal care products oscillates around 2.0 million tons/year (Wang & Wang, 2018). The residues of these substances have caused widespread contamination of water bodies, despite their low concentrations (ng/L to $\mu\text{g}/\text{L}$) (Almeida-Naranjo et al., 2021b). These residues are called emerging contaminants (ECs) and come from several sources such as industrial wastewater, domestic discharges, and agricultural effluents (Anastopoulos et al., 2020a). ECs present different behaviors in the environment since they have different physicochemical properties, some of them are toxic (K_{ow} chlorobenzene = 2.98), persistent (lifetime benzophenone = 1-10 days), non-biodegradable (soil persistence dieldrin = 100 days), endocrine disrupting (bisphenol A), and recalcitrant (dichlorodiphenyltrichloroethane).

Other ECs such as caffeine and triclosan are considered anthropogenic markers because they have been found in different water resources (Rodríguez-Narvaez et al., 2017). Caffeine and triclosan were found in wastewater (20 – 300 and 0.5 – 300000 $\mu\text{g}/\text{L}$), in the effluents of wastewater treatment plants (0.1 – 20.0 and 0.1-0.6 $\mu\text{g}/\text{L}$), and in surface water sources (10 – 80 and 50 – 2300 ng/L), respectively (Álvarez-Torrellas et al., 2016; Dann & Hontela, 2011).

Caffeine is widely used in beverages (coffee, tea, energy drinks), food, and some medicines (Anastopoulos, et al., 2020a). Meanwhile, triclosan has disinfecting properties so it is included in personal care products such as detergents, cosmetics, and soaps (Triwiswara et al., 2020a).

Caffeine and triclosan have different physicochemical properties. Caffeine is very soluble in water (21.6 mg/L at 25 °C) and has low bioaccumulation (K_{ow} = 0.85) (León et al., 2020). Caffeine was found in fishes and frogs, as well as in certain fruits and vegetables (Dafouz-Ramírez & Valcárcel-Rivera, 2017). In zebrafish species, it produced a decrease in the growth rate of fish embryos (Anastopoulos et al., 2020a). On the other hand, triclosan is poorly soluble in water (10 mg/L at 20 °C) and shows high hydrophobicity or bioaccumulation (K_{ow} = 4.76), inhibiting plant growth and soil respiration. In addition, it has toxic effects on aquatic organisms, such as microbial resistance, dermal irritation, alteration of the endocrine, and metabolic system (Dhillon et al., 2015). In *Mytilus californianus*, *Ruditapes philippinarum*, and *Carcinusmaenas*, caffeine produces cellular stress (Anastopoulos et al., 2020b). On the other hand, in terrestrial organisms, such as *Eisenia foetida*, it leads to the mortality of about 50% population when using 58 μg CAF/ cm^2 (Mckelvie et al., 2011).

On the other hand, triclosan (5-chloro-2-(2,4-dichloro phenoxy)phenol) is another EC found in water bodies, which is a synthetic and lipid-soluble antimicrobial agent that has been used as an antiseptic, disinfectant, and constituent of personal care products, such as hand soaps, shampoos and detergents (Ejtahed et al., 2020; H. Kaur et al., 2018). In these days of the coronavirus pandemic, just like caffeine, the use of detergents with triclosan has increased exponentially (Ejtahed et al., 2020). Triclosan has low solubility in water (10 mg/L) and high bioaccumulation ($\log K_{ow} = 4.30$) (H. Kaur et al., 2018). This anionic compound is compatible with many raw materials, photo-unstable, and continues to decompose after being released in the aquatic environment. In aquatic habitats, triclosan is accumulated in sediments or sludge that can be deposited in agricultural areas. Exposure to triclosan decreases the rate of population increase in zooplankton (H. Zhang et al., 2016). Even triclosan exposure has a profound impact on the human gut microbiome, inducing disturbances at both the compositional and functional levels. Indeed, it may be related to adverse effects, such as endocrine alteration, resistance to antibiotics, inflammation of the colon, and tumorigenesis (Ejtahed et al., 2020). These characteristics/toxicities make it essential to remove caffeine and triclosan from wastewater.

Natural attenuation and conventional treatment processes are not capable of efficiently removing all types of ECs from wastewater. Meanwhile, adsorption using agricultural residues has been recognized as a promising alternative for wastewater treatment, due to their low-cost compared to other treatments (i.e., activated sludge system) (Couto et al., 2015) and their high efficiency in the removal of ECs (up to 100%) (Mallek et al., 2018; Paredes-Laverde et al., 2018) and other contaminants (i.e., heavy metals, organic matter) (Castro et al., 2021; Tejedor et al., 2020). Among the agricultural residues studied as adsorbents of ECs are bagasse, straw, vegetable peels, fruit peels (i.e., banana, orange, coconut, coffee, etc.), seeds (peach stone, moringa, etc.), rice husk, peanut shells, among others (Almeida-Naranjo et al., 2021b; León et al., 2020; Mo et al., 2018).

Moreover, agricultural residues generally do not have a defined use and are produced in large quantities: sugarcane residues $\sim 3.21 \times 10^8$ tons/year, wheat straws $\sim 1.12 \times 10^9$ tons in 2016 (Bundhoo, 2019), which often complicate its integrated management. Likewise, more than 11 million tons of peanut shells in 2018 were produced (FAO, 2018). The high availability of peanut shells added to characteristics such as relatively high surface area (2.01 m²/g), presence of lignin (27.0 – 33.0%), cellulose (34.7 – 45.0%), and hemicellulose (around 9.0%) suggest that they could be an alternative adsorbent (Messina et al., 2015; R. Li et al., 2018; Taşar et al., 2014). Peanut shells have been mainly used in the removal of metals (adsorption capacity $_{cadmium} = 6$ mg/g) and dyes (adsorption capacity $_{reactive\ black\ 5} = 50$ mg/g). Nevertheless, there are few studies using peanut shells in the removal of ECs. Antibiotics such as sulfathiazole and sulfamerazine have been removed achieving adsorption capacities of 18.2 µg/g and 11.7 µg/g, respectively (R. Li et al., 2018; Liu et al., 2010; Tanyildizi, 2011). Considering the very limited use of raw peanut shells in the removal of ECs with different physicochemical characteristics, their high availability, and their good adsorption characteristics, this study aimed to evaluate their adsorption capacity during the removal of caffeine and triclosan from synthetic solutions through batch and continuous adsorption tests. The data obtained were adjusted to models of kinetic (pseudo-first-order, pseudo-second-order, Elovich and diffusion), equilibrium (Langmuir, Freundlich, and Sips), and breakthrough curve (Bohart-Adams).

2. Materials and methods

2.1. Materials

Peanut shells were obtained from a peeling plant located in the city of Loja (southern Ecuador, -3.99313 and -79.20422). Caffeine and triclosan used for the synthetic solution preparation were ReagentPlus®, Sigma-Aldrich brand, 99.0%, and $\geq 97.0\%$, respectively.

2.2. Peanut shell conditioning

Peanut shells were washed with drinking and distilled water to remove impurities. Clean shells were dried at 80 °C for 24 h and crushed in a Thomas knife mill model 3379 - K05 (Taşar et al., 2014). Finally, shells were sieved and separated into three size groups: small particles (125 – 150 µm), medium particles (300 – 600 µm) and large particles (850 – 2,000 µm).

2.3. Peanut shell characterization

Moisture (ASTM D4442-20), extractives (ASTM D1110-21, ASTM D1107-21), lignin (ASTM D1106-21), cellulose and hemicellulose (ASTM D1109-21), ash (ASTM D1102-21) and volatile material (ASTM E872-19) of peanut shells were determined according to the ASTM standards given. To supplement the physicochemical characterization, a thermogravimetric analysis was carried out using a thermo-balance SHIMADZU, model 50 from 20 to 600 °C with a heating rate of 10°C/min under nitrogen atmosphere (50 mL/min). The functional groups of caffeine, triclosan, and peanut shells (before/after the adsorption tests) were determined using a Perkin Elmer FTIR-6800 spectrometer equipped with a diamond crystal ATR. The morphology of the peanut shells, in the three particle size ranges, was observed using an ASPEX PSEM eXpress scanning electron microscope (SEM) with a 20.4 mm working distance and a 15 keV acceleration voltage. The surface area, pore volume, and pore radius of peanut shells were determined by physical nitrogen adsorption at a bath temperature of 77.35 K, using the standard Brunauer, Emmett, and Teller (BET) procedure. Peanut shells were heated up to 100 °C at 10 °C/min, and held for 1440 min under vacuum.

2.4. Batch adsorption tests

Initially, calibration curves were built, using solution concentrations between 1 and 10 mg/L of caffeine (solvent: distilled water), and triclosan (solvent: 5 v/v.% acetone solution) (Oliviera et al., 2009). The batch adsorption tests were performed in dark conditions (to avoid the degradation process) and in triplicate using a control system. The control system for caffeine was distilled water and for triclosan was a 5 v/v.% acetone solution.

The optimal dose of peanut shells was determined using 20 mL of caffeine/triclosan solutions with a 30 mg/L concentration, stirring at 150 rpm for 180 and 45 min, respectively. The doses of peanut shells for the removal of caffeine/triclosan were 5 – 60/0.1 – 35 g/L, 3 – 40/0.1 – 1.5 g/L and 1 – 20/0.02 – 1.0 g/L for large, medium and small particles, respectively. The optimal contact time was determined using the optimal dose for each particle size. Peanut shells were placed in contact with the caffeine/triclosan solutions for 300/120 min, respectively. The peanut shells were separated from the aqueous solution using cellulose filters with a 0.2 µm pore size (R. Li et al., 2018).

Caffeine and triclosan concentrations were determined using an Analytik Jena Sperscord 210 Plus UV-VIS spectrophotometer at a wavelength of 287 and 295 nm, respectively. The removal of caffeine/triclosan (%) was calculated using Equation 1.

$$\text{Removal (\%)} = \frac{(C_o - C_f)}{C_o} * 100 \quad (1)$$

where C_o and C_f are the initial and final concentrations of caffeine/triclosan (mg/L), respectively.

2.5. Adsorption kinetics and isotherm study

Adsorption kinetics describes the adsorption rate of caffeine/triclosan and provides information about reaction pathways (Al-Qodah et al., 2017). Adsorption kinetics of caffeine and triclosan were calculated using data obtained to determine the optimal contact time. The amount of caffeine/triclosan adsorbed per gram of peanut shells was calculated using Equation 2.

$$q = \frac{(C_o - C_f)V}{W} \quad (2)$$

where q (mg/g) is the concentration of caffeine/triclosan per gram of peanut shells, W (g) is the mass of peanut shells used, and V (L) is the caffeine/triclosan solution volume.

The data obtained were fitted to non-linear pseudo-first and pseudo-second-order models. Equations 3 and 4 were used, respectively (Al-Qodah et al., 2017)

$$q_t = q_e(1 - e^{-k_1 t}) \quad (3)$$

$$\frac{t}{q_t} = \frac{1}{K_2 q_e^2} + \frac{t}{q_e} \quad (4)$$

The development of an isotherm model is essential for designing and optimizing adsorption processes. The adsorption isotherms were obtained with the optimal adsorption conditions corresponding to each particle size. Caffeine/triclosan solutions of 10, 20, 30, 40, and 50 mg/L were used. The data obtained were fitted to non-linear Langmuir, Freundlich, and Sips models. The equation models are presented in equations 6, 7 and 8, respectively (Al-Qodah et al., 2017):

$$q_e = \frac{q_m * K_L * C_e}{1 + K_L * C_e} \quad (6)$$

$$q_e = K_F * C_e^{1/n} \quad (7)$$

$$q_e = \frac{q_m (K_S * C_e)^{1/n}}{1 + (K_S * C_e)^{1/n}} \quad (8)$$

where q_e (mg/g) is the amount of caffeine/triclosan per unit mass of peanut shells in equilibrium, C_e (mg/L) is the liquid phase concentration of caffeine/triclosan in equilibrium, q_m (mg/g) is the maximum adsorption capacity of peanut shells, K_L (L/mg) is the Langmuir constant related to adsorption energy, K_F ((mg/g)/(mg/L)ⁿ) is the Freundlich capacity constant, $1/n$ is the Freundlich intensity parameter, and K_S (L/mg) is the Sips constant related to micropores energy (Nguyen et al., 2021).

The kinetics and isotherm models used were selected because they have typically presented good fits (R^2 close to 1) when agricultural residues are used in the removal of several contaminants (dyes, heavy metals, ECs) (Anastopoulos et al., 2015).

2.6. Statistical analysis

The optimal dose and contact time were determined using an analysis of variance (ANOVA) with a single factor analyzed by Tukey's test (significance level of 95.0%). The statistical analysis was performed using the Minitab 18 software 1.0 version. To calculate the parameters of non-linear: isotherms (Langmuir, Freundlich and Sips), and kinetics (pseudo-first and pseudo-second-order), the Solver add-in of Microsoft Excel (version 2016) was used. To determine the model that best fitted to data obtained, equations 9, 10 and 11 were used to calculate squared errors (SSE), chi-square (χ^2), and coefficient of determination (R^2), respectively.

$$R^2 = 1 - \frac{\sum (P_{e,exp} - P_{e,cal})^2}{\sum (P_{e,exp} - P_{e,mean})^2} \quad (9)$$

$$\chi^2 = \sum \frac{(P_{e,exp} - P_{e,cal})^2}{q_{e,cal}} \quad (10)$$

$$SSE = \sum (P_{e,exp} - P_{e,cal})^2 \quad (11)$$

where $P_{e,exp}$ is the experimental parameters: q (batch) and C_f/C_o (fixed-bed columns), $P_{e,cal}$ is the calculated parameter using the solver tool, and $P_{e,mean}$ is the mean of $P_{e,exp}$ values (mg/g) (Nguyen et al., 2021).

3. Results and Discussion

3.1. Peanut shell characterization

Table 12 shows the physicochemical composition of the peanut shells used in this study and the results from previous characterization. Lignin is the component with the highest concentration concerning cellulose and hemicellulose (16.8 and 10.1% less than lignin, respectively). Lignin acts as a fiber binder, filling the spaces between cellulose and hemicellulose which confer mechanical resistance to the cell wall and, consequently, to the entire structure (Ramírez & Enríquez, 2015). Furthermore, lignin has functional groups (hydroxyl, methoxyl, carbonyl, carboxyl, and sulfonates) which allow the adsorption process (Khezami., 2005; Ramírez & Enríquez, 2015). Likewise, cellulose is considered a substance capable of

removing contaminants, due to the presence of hydroxyl groups, which are linked to hemicellulose. These groups promote interaction with cations, favoring contaminant adsorption (El-bisi, 2014). Together cellulose, hemicellulose and lignin form the cell wall of peanut shells, giving porosity and allowing caffeine and triclosan solutions to interact with different components of the cell wall (Al-Qodah et al., 2017).

The extractives are in lower concentration (between 4.2 and 21.0%) than polysaccharides; they give color, smell and flavor to the shell. The presence of extractives can decrease the availability of pores and could interfere with the adsorption of caffeine/triclosan (Pholosi et al., 2013). According to León et al., 2020, a higher extractives content suggests a reduction in the adsorption of caffeine and triclosan.

Comparison of the peanut shell characterization with previous studies indicates that the amount of cellulose is between 1.7 and 2.8 times lower, while the amount of lignin and hemicellulose are higher (1.1-1.3 and up to 2.9 times, respectively) (R. Li et al., 2018; Messina et al., 2015; Taşar et al., 2014). The differences could be attributed to the growing conditions of the peanut (different weather conditions), the maturity of the product before being consumed, the processing conditions, among others (Mo et al., 2018).

Table 12. Chemical composition of peanut shells.

Chemical Composition	Previous studies [%]		Current study [%]
	(Messina et al., 2015)	(Taşar et al., 2014)	
Humidity	6.5	-	8.9 ± 0.1
Lignin	30.9	31.6	36.2 ± 4.4
Cellulose	54.6	34.7	19.4 ± 5.9
Hemicellulose	14.5	9.0	26.1 ± 1.7
Extractives	-	13.8	15.2 ± 0.4
Volatile material	68.8	76.0	74.1 ± 0.4
Ash	5.5	5.5	3.1 ± 0.1
Fixed carbon	19.20	-	13.8 ± 0.4

Figure 17 shows the TGA curve for peanut shells. Three very marked weight loss regions are identified. The first (10.8%) goes from 20 to 122.6 °C and it is attributed to the loss of water (humidity) from the peanut shell. The second important loss (52.1%) occurred between 122.6 and 409.5 °C. The final stage (410.3 – 600 °C) produced a weight loss of 9.2%. These losses are attributed to the degradation of polysaccharides (hemicellulose, cellulose and lignin) and the carbonaceous material in the peanut shell (S. Wang et al., 2020).

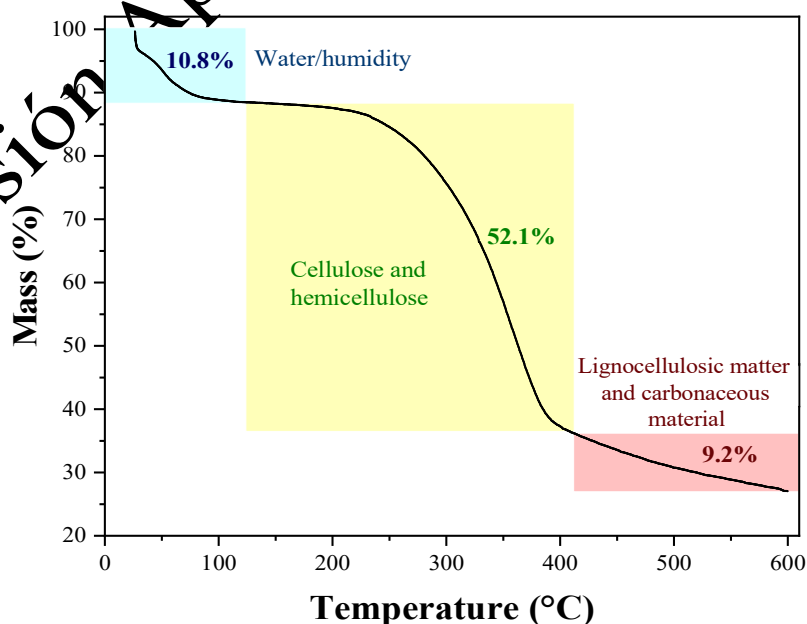


Figure 17. Thermogravimetric analysis of peanut shell.

Figure 18 shows the peanut shell FTIR spectra before/after the adsorption of contaminants. For peanut shells before adsorption, the first band (3350 cm^{-1}) is attributed to the OH- groups present in lignin, cellulose and hemicellulose. At 2920 cm^{-1} appear the band related to the C=O stretch and the bands around 1700 and 1369 cm^{-1} are assigned to the carboxyl and hydroxyl groups, respectively. The presence of C-O bonds from cellulose appears at 1259 cm^{-1} , and the presence of lignin and the vibration of its aromatic rings are associated with the bands at 1620 , 1509 and 1422 cm^{-1} . Meanwhile, the 1024 cm^{-1} band is related to the C-H₂ group in cellulose and the band at 1369 cm^{-1} corresponds to C-H bonds present in cellulose and hemicellulose (R. Li et al., 2018; Zhu et al., 2009).

The FTIR spectra of peanut shells in their different particle sizes after caffeine adsorption does not present a great difference between them. However, the transmittance decreased between 1530 and 1183 cm^{-1} concerning the FTIR spectra of peanut shells before adsorption. A decrease in the bands at 1369 cm^{-1} (belonging to cellulose), 1509 cm^{-1} (belonging to hemicellulose) and 1620 , 1509 , and 1422 cm^{-1} (belonging to lignin) are shown because these groups have an affinity with caffeine. The band at 1620 cm^{-1} is a little wider probably due to the caffeine showing a band at 1642 cm^{-1} ; something similar occurs with the 1024 cm^{-1} band widening (R. Li et al., 2018; Zhu et al., 2009). Nevertheless, caffeine bands located between 1024 and 1548 cm^{-1} can be more intense in the small particles, probably because the amount of caffeine adsorbed by the peanut shells is higher in this particle size.

As with caffeine, the FTIR spectra of peanut shells in their different particle sizes after triclosan adsorption are very similar to each other. The biggest difference between the spectra before and after adsorption is a slight decrease in transmittance. Changes in the bands at 3350 and 2920 cm^{-1} are shown probably because they join the triclosan molecule. Something similar occurs in the bands between 1024 and 1700 cm^{-1} , these suggest that an adsorption process occurs. Moreover, they coincide with the bands of functional groups that correspond to cellulose, hemicellulose and lignin, groups that are involved in the adsorption process (Almeida-Naranjo et al., 2021b).

Versión Aprobada para Defensa Oral

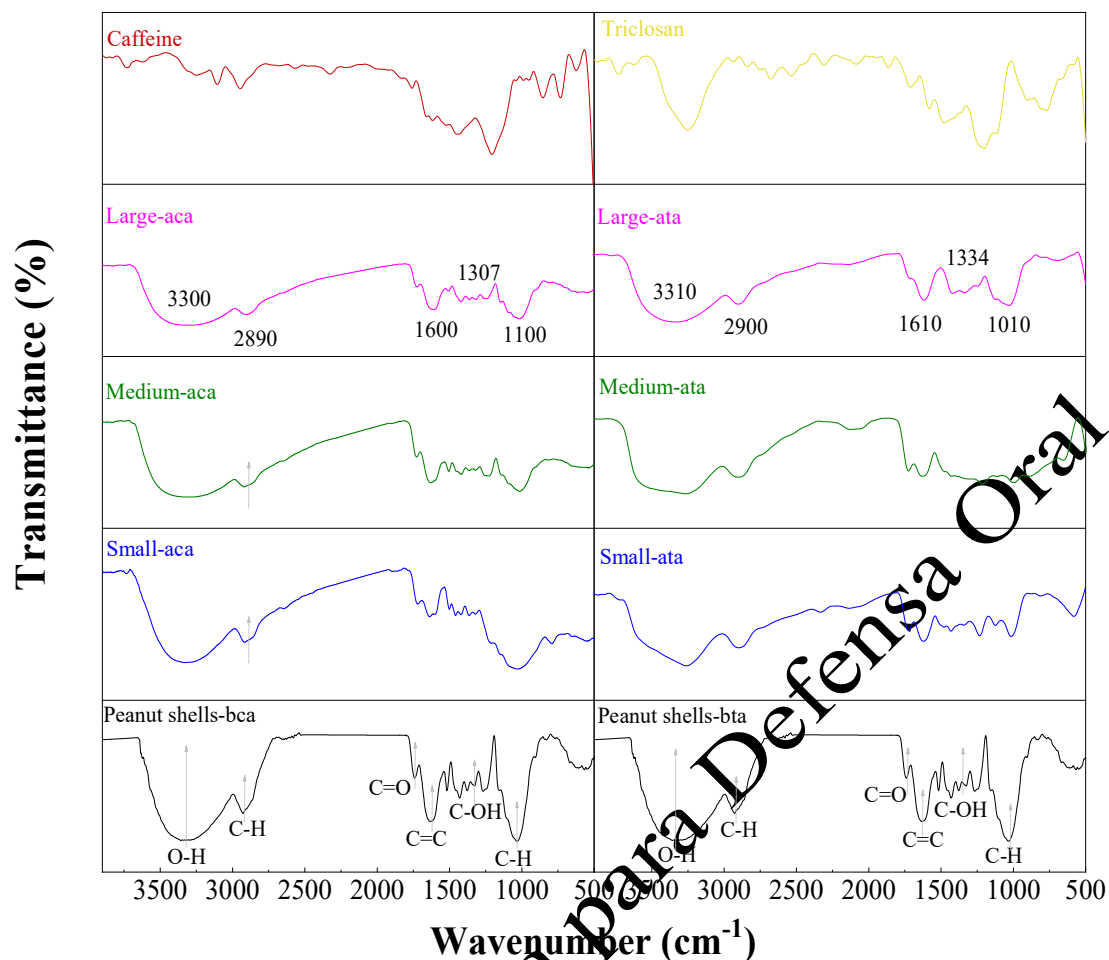


Figure 18. FTIR spectra of peanut shells before and after adsorption of caffeine and triclosan. bca= before caffeine adsorption, aca= after caffeine adsorption, bta= before triclosan adsorption, ata= after triclosan adsorption.

Figure 19 corresponds to SEM images of small, medium, and large particles. An irregular morphology and the presence of pores are observed, which coincides with the results of R. Li et al. (2018). The morphological characteristics observed in peanut shells suppose good adsorption properties that will favor the removal of caffeine and triclosan.

The surface area of the peanut shells, obtained with a BET multipoint test, was $1.7 \text{ m}^2/\text{g}$. It is lower than the surface area found in previous studies (2.4 and $5.0 \text{ m}^2/\text{g}$). This is probably due to the differences between peanut species and their particle size ($177 - 250 \text{ }\mu\text{m}$ and $250 - 500 \text{ }\mu\text{m}$) (Lochananon & Chatsiriwech, 2009). The pore volume and pore diameter determined by the Barrett-Joyner-Halenda (BJH) method were $0.005 \text{ cm}^3/\text{g}$ and 3.14 nm , respectively. According to the IUPAC standard, a pore diameter between 2 and 50 nm is characteristic of mesoporous materials (Wei et al., 2019). Figure 19 also shows the nitrogen adsorption-desorption isotherm for the peanut shells studied. This is a type III isotherm, according to the Brunauer, Deming, Deming and Teller (BDDT) classification, and corresponds to a macroporous or non-porous material with the little affinity between the adsorbate and the adsorbent. So once the molecule is adsorbed, it acts as if it is free to adsorb another molecule; thus some parts act as monolayers and some others as multilayers (Sultan et al., 2018).

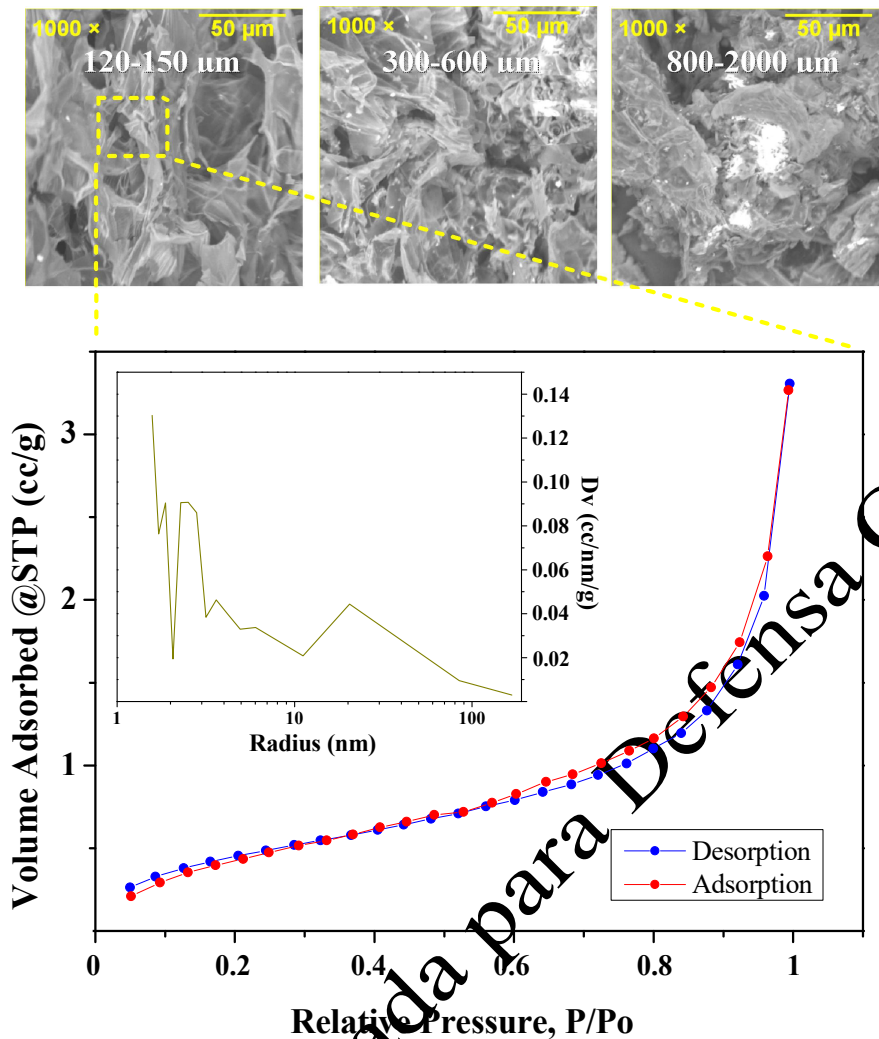


Figure 19. SEM images of small, medium, and large particles, nitrogen adsorption-desorption isotherm and pore radius distribution of small particles

3.2. Adsorption Tests

Figures 20a and 20b show the removal of caffeine/triclosan using different doses of small (120 – 150 μm), medium (300 – 600 μm) and large (800 – 2,000 μm) particles of PS, and different contact times. The optimal doses of PS in the removal of caffeine (Figure 20a) for small, medium, and large particles were 10.0, 17.0 and 35.0 g/L, achieving removals of 85.6 (\pm 1.4), 84.1 (\pm 0.1) and 87.8 (\pm 2.7)%, respectively. Figure 20b shows that the optimal doses of peanut shells in the triclosan removal for small, medium and large particles were 0.1, 1.0 and 10.0 g/L, achieving removals of 89.3 \pm 1.5, 90.8 \pm 0.3 and 90.9 \pm 4.6%, respectively.

A higher dose of PS is required to remove caffeine/triclosan when the peanut shell size increases. This is because the smaller particle size has a higher surface area available to adsorb caffeine/triclosan (Taşar et al., 2014). Therefore, small particles were the best to remove caffeine and triclosan. Nevertheless, when a higher dose of peanut shells is used, the color of the solution turns dark (color released by the peanut shell) (Pholosi et al., 2013). This problem creates competitive adsorption between water, the compounds released from the peanut shells and caffeine/triclosan (Couto et al., 2015).

Figures 20c and 20d show the removal of caffeine and triclosan for the three different PS granulometry studied, using the optimal doses at different contact times. The optimum contact time for caffeine with the three particle sizes of peanut shells was 180 min. Removal percentages after this time were 85.0 \pm 1.4, 89.7 \pm 0.3 and 88.8 \pm 1.2% for the small, medium, and large particles, respectively. Meanwhile, the optimum contact time using the three particle sizes of peanut shells for triclosan adsorption was 45 min.

The removal percentages for small, medium and large particle sizes were 90.1 ± 2.1 , 89.2 ± 2.7 and $94.9 \pm 1.4\%$, respectively.

The highest adsorption of caffeine/triclosan occurs in the first 30/15 minutes. This is because the active sites at the beginning of the process are empty, and adsorption happens quickly on the external surface of PS. This is followed by slow adsorption that happens inside the pores until the equilibrium is reached (Santacufemia et al., 2019).

Furthermore, a higher affinity between triclosan and peanut shells was observed, since triclosan has a higher hydrophobicity ($\log K_{ow} = 4.76$). High hydrophobicity makes triclosan only a little soluble in water with a bioaccumulation potential in peanut shells (Dhillon et al., 2015). This explains why the doses of PS and the contact times used to remove triclosan are lower than the ones used to remove the same concentration of caffeine ($\log K_{ow} = -0.7$).

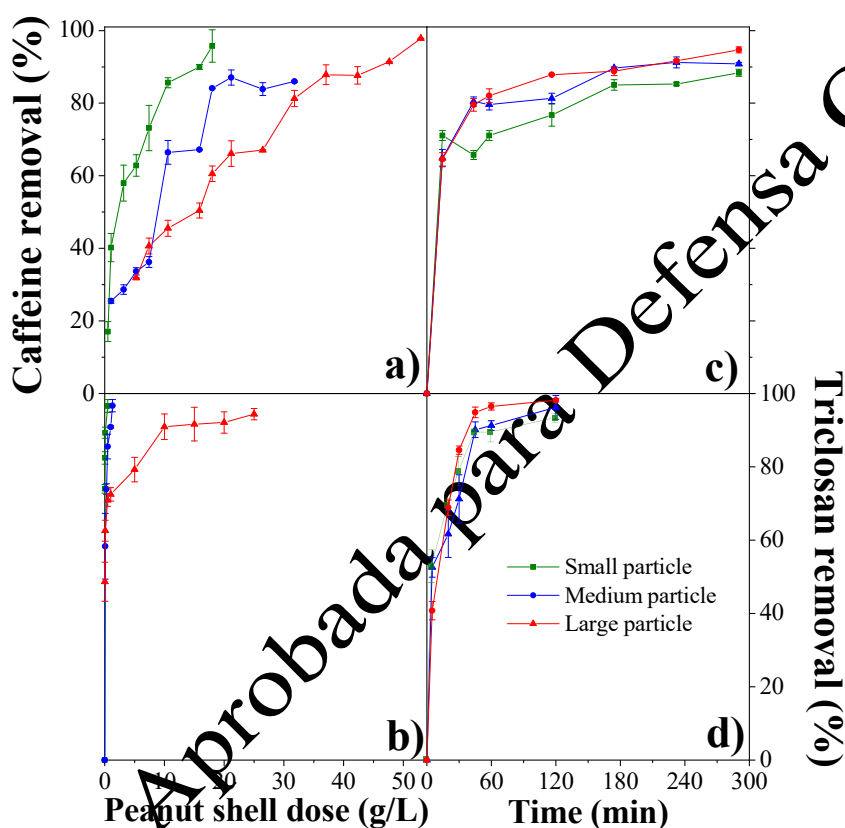


Figure 20. Optimal dose of peanut shells and contact time for the removal of a), c) caffeine and b), d) triclosan. Green line: small particles, blue line: medium particles and red line: medium particles. Caffeine/triclosan concentration= 30 mg/L, stirring rate= 150 rpm.

3.3. Adsorption kinetics and isotherm models

Table 13 and Figures 19a and 19b show data for the non-linear pseudo-first and pseudo-second-order kinetics models for caffeine and triclosan adsorption. According to the values of R^2 , χ^2 , and SSE for the three particle sizes, the model that best fits the removal of both contaminants is the pseudo-second-order model. The maximum adsorption capacity in the adsorption kinetics tests for caffeine and triclosan was obtained with the small particles, reaching values of 3.2 and 289.3 mg/g, respectively. The fitting to the pseudo-second-order kinetic model complemented with the several functional groups presented in peanut shells suggest chemical adsorption, which indicates that speed control is given by reactions between peanut shells and caffeine/triclosan, rather than by a mass transfer. This involves the exchange of electrons between the OH- or ligand groups and the contaminants (Al-Qodah et al., 2017).

Likewise, in previous studies, in which peanut shells were used to remove sulfonamides (R. Li et al., 2018), PB5 dye (Tanyildizi, 2011), and some metals such as Cu (II), Cd²⁺, Hg²⁺, Pb (II) (Taşar et al., 2014; Zhu et al., 2009), the kinetic models were also fitted to pseudo-second-order kinetics. The same

adjustment was obtained, using adsorbents such as thermally modified verde-lodo bentonite (Oliveira et al., 2019), oxidized biochar from pine needles (Anastopoulos et al., 2020a), rice husk, coconut fiber, corn cob (Almeida-Naranjo et al., 2021a) in the removal of caffeine and kenaf-derived biochar (Cho et al., 2021), activated carbon from coconut pulp waste (Khorriha et al., 2018) and char from palm kernel shells (Triwiswara et al., 2020b) in the removal of triclosan. The authors conclude that the adsorption of both contaminants occurs by chemisorption (Almeida-Naranjo, et al., 2021a; Anastopoulos et al., 2020a; Khorriha et al., 2018; Triwiswara et al., 2020b).

Table 13. Parameters for non-linear adsorption kinetic models for caffeine and triclosan removal.

	Particle size (μm)	Pseudo-first-order model					Pseudo-second-order model				
		Q_e [mg/g]	K_1 [1/min]	R^2	SSE	χ^2	Q_e [mg/g]	K_2 [g/mg ² min]	R^2	SSE	χ^2
Triclosan	120 – 150	255.350	0.154	0.509	6724.559	4.805	289.324	0.001	0.766	3199.143	2.280
	300 – 600	25.863	0.174	0.737	27.087	0.189	28.573	0.008	0.918	8.455	0.059
	800 – 2,000	2.907	0.081	0.927	0.159	0.011	3.270	0.036	0.969	0.067	0.005
Caffeine	120 – 150	2.993	0.031	0.868	0.067	0.004	3.267	0.016	0.964	0.011	0.001
	300 – 600	1.782	0.086	0.757	0.059	0.005	1.892	0.077	0.929	0.017	0.001
	800 – 2,000	0.901	0.092	0.772	0.011	0.002	0.951	1.134	0.961	0.011	0.002

Table 14, and Figures 21c and 21d show the data calculated for the Langmuir, Freundlich and Sips non-linear isothermal fittings. Triclosan adsorption best fitted the Sips model for small (120 – 150 μm), medium (300 – 600 μm), and large (800 – 2,000 μm) particles with an R^2 equal to 0.997, 0.973, and 0.989, and a q_m of 238.98, 29.45, and 7.38 mg/g, respectively. This is corroborated by the SSE and χ^2 values, which are the lowest values among the three isothermal models applied. The Sips model combines the Freundlich and Langmuir models, considering the heterogeneity of peanut shells as in the Freundlich model and the monolayer formation of the Langmuir model. In addition, at the beginning of the adsorption, the model will resemble Freundlich, with no apparent limit on the adsorption capacity of triclosan. As the adsorption continues, the model with the best fit is that of Langmuir. It was observed that the experimental triclosan adsorption data also fit the Sips model when using activated carbon from coconut shells (raw and modified) (Bernal et al., 2020) and gas masks (Sharipova et al., 2016), and empty palm cluster biochar (Choudhary & Philip, 2022).

For the caffeine adsorption, R^2 values close to 1 (0.84 – 0.995) were obtained for the three isotherm models used. Small (120 – 150 μm) and large (800 – 2,000 μm), particles have a better fit to the Freundlich model while medium particles fit the Langmuir and Sips models. However, considering the value of $1/n$ calculated with the Freundlich model (< 1) and the adjustment of the experimental data (experimental q_e) when using more concentrated caffeine solutions (closer to the Langmuir model), it was determined that the correct fit is to the Sips model. Values of $1/n$ greater than 1 indicate cooperative adsorption and those smaller than 1 correspond to monolayer adsorption (Khezami et al., 2005). These results would indicate a combination of the Freundlich (low concentrations of caffeine) and Langmuir (high concentrations of caffeine) models. Lower values of SSE and χ^2 for the Sips model confirm that this is possible. Similar results were obtained when using the grape stalks, grape stalk chemically modified, and activated carbon from the grape stalks in the caffeine removal (Portinho et al., 2017).

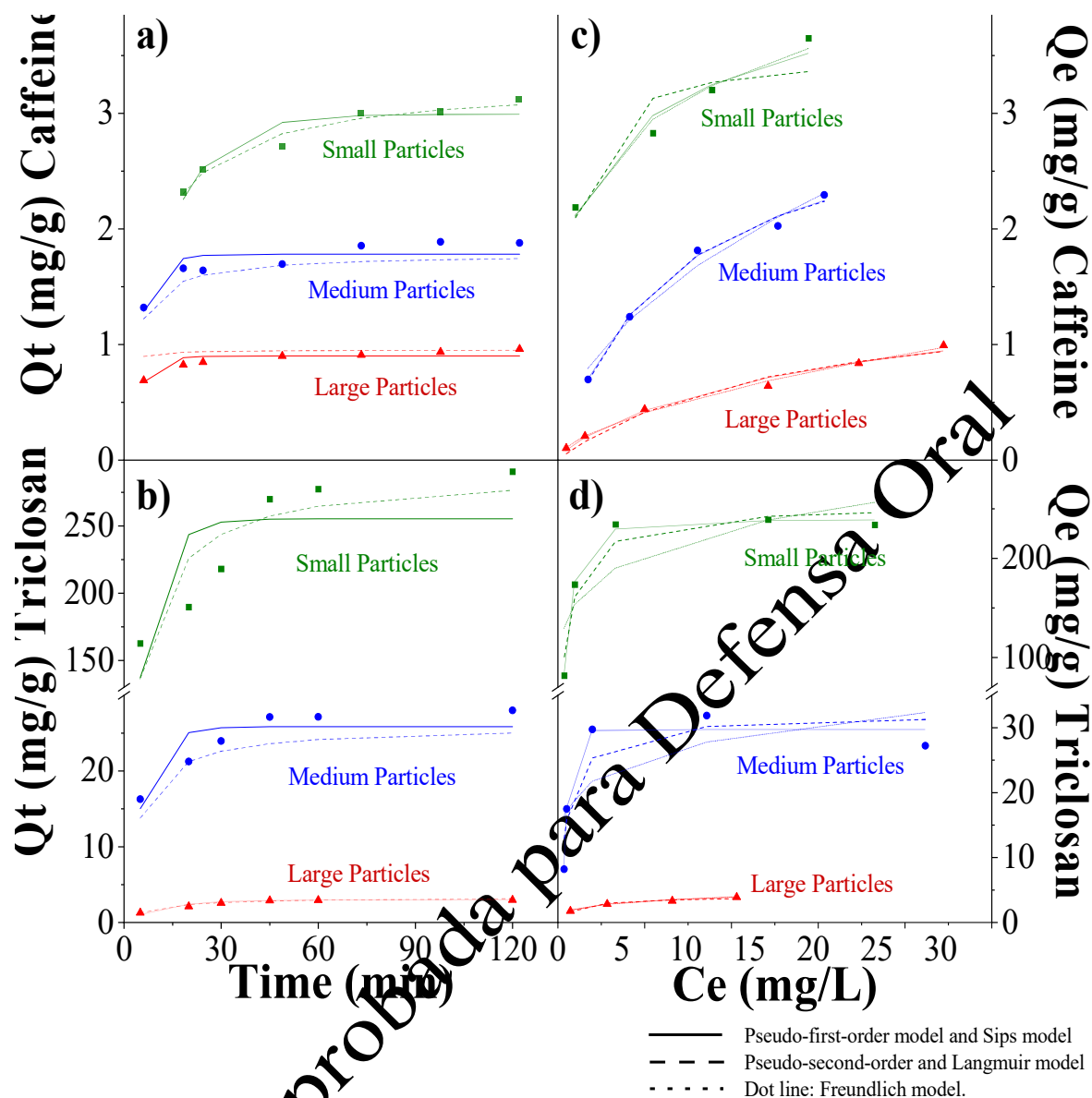


Figure 21. Adsorption kinetics (a, b) and isotherm models (c, d) for caffeine and triclosan.

Most of the research previously performed using peanut shells was carried out to remove heavy metals and dyes. As mentioned before, there are only a few studies performed to remove ECs. R. Li et al. (2018), achieved removals between 32.8 and 72.8% and adsorption capacities between 8.2 and 18.2 $\mu\text{g/g}$ in the removal of sulfamerazine, sulfamethazine, sulfathiazole and sulfamethoxazole using 500 – 600 μm size peanut shell particles. The adsorption of the four contaminants was fitted to the Freundlich and the pseudo-second-order model. Meanwhile, Tomul et al., 2020, used particles with a 150 – 250 μm size and achieved adsorption capacities of 56.1 and 24.5 mg/g for the removal of diclofenac and bisphenol, respectively (Tomul et al, 2020).

Even though caffeine/triclosan removal using peanut shells has not been sufficiently studied, we can mention that the adsorption capacities of peanut shells obtained are comparable to or even higher than those reached with other agricultural residues. Triclosan removal using activated carbon from coconut pulp (595 μm) was fitted to a pseudo-second-order kinetics model and the Langmuir isotherm ($q_m = 38.91 \text{ mg/g}$) (Mohd-Khori et al., 2018). These results are similar to those obtained with the medium size peanut shell particles even though raw (untreated) peanut shells are used. Likewise, in the study carried out by Triwiswara et al., 2020, the triclosan removal using rice husk treated at 300 $^{\circ}\text{C}$ (150 – 500 μm) was fitted to the pseudo-first-order kinetics and to Langmuir model ($q_m = 72.7 \text{ mg/g}$) (Triwiswara et al., 2020). This adsorption capacity is lower compared to that obtained with small peanut shell particles. In the case of caffeine, the adsorption capacity of hydro chars from pistachio shells (500 – 1000 μm) obtained with the

Langmuir model was slightly higher (5.5 mg/g) than the capacity obtained with large particles of peanut shells (Román et al., 2018). Meanwhile, using grape stalks with a mean particle size of 700 μm , the adsorption data best fitted the Sips model with a $q_m = 89.2$ mg/g, which was much higher than the value obtained in this work (Portinho et al., 2017).

Table 14. Parameters for the non-linear Langmuir, Freundlich and Sips adsorption models for caffeine and triclosan removal

	Particle size (μm)	Non-linear Langmuir model					Non-linear Freundlich model					Non-linear Sips model					
		q_m [mg/g]	K_L [L/mg]	R^2	SSE	χ^2	K_F [(mg/g)/(mg/L) n]	1/n	R^2	SSE	χ^2	q_m [mg/g]	K_s [L/mg]	1/n	R^2	SSE	χ^2
Triclosan	120 – 150	253.559	1.317	0.947	962.730	0.995	145.638	0.176	0.719	5109.194	5.288	238.975	1.359	1.737	0.997	53.348	0.055
	300 – 600	32.049	1.396	0.838	63.380	0.548	18.328	0.168	0.561	171.613	1.490	29.647	1.585	3.645	0.973	10.721	0.094
	800 – 2,000	4.041	0.707	0.959	0.100	0.008	1.846	0.280	0.985	0.036	0.003	7.376	0.083	0.450	0.989	0.028	0.002
Caffeine	120 – 150	3.522	2.619	0.838	0.186	0.016	2.370	0.196	0.976	0.028	0.002	6.899	0.141	0.355	0.958	0.049	0.004
	300 – 600	3.147	0.289	0.993	0.012	0.001	0.804	0.492	0.980	0.033	0.004	3.273	0.264	0.959	0.993	0.012	0.001
	800 – 2,000	1.490	0.139	0.977	0.014	0.005	0.225	0.582	0.995	0.003	0.001	1.978	0.072	0.802	0.987	0.008	0.003

3. Conclusions

The adsorption of caffeine and triclosan is favorably influenced by the composition of the peanut shells and their particle size, being the small particles (120 – 150 μm) the ones that achieved the highest removal efficiency with the lowest dose. Moreover, the lower solubility (10 mg/L) and the higher hydrophobicity ($\log K_{ow} = 4.30$) of triclosan favor its removal. The optimal contact time/peanut shell dose were 4/3.5-100 times lower than those found for the caffeine removal. The adsorption kinetics shows that the processes fit the pseudo-second-order model, which means that a chemisorption occurs for both contaminants. Regarding the adsorption isotherms, the model that best fits the data for three particle sizes was Sips (R^2 between 0.958 and 0.997). The results obtained contribute to the valorization of peanut shells and may become the basis for formulating an alternative to remove ECs with different water solubilities and hydrophobicity.

Discussion about Articles 1 and 2

According to the results obtained in Articles 1 and 2, it was observed that the type of adsorbent, its size and the characteristics of the contaminant influence the adsorption process. PS and RH showed differences in their adsorption capacity, being PS the one with the highest capacity for triclosan (between 1.3 and 7.6 times), this difference is attributed to the composition of the residues. The PS has a higher content of lignin (10.7%), which is the biopolymer that favors the removal of contaminants (Mo et al., 2018; Pode, 2016), while the RH has a higher content of ash (around 14.9% more), related to silica presence. Silica influences negatively in the adsorption process (Chowdhury et al., 2011).

In the case of caffeine, the adsorption capacity of PS and RH are very similar and much lower than in triclosan (up to 29.5 times). This is due to the high solubility of caffeine in water (21.6 g/L) and low bioaccumulation/hydrophobicity ($\log K_{ow} = 0.07$) (Álvarez-Torrellas et al., 2016). In addition, the influence of adsorbent particle size was very important for both PS and RH, reaching the maximum removal efficiencies for caffeine/triclosan using the smallest particle size (120 – 150 μm). This happens because smaller particles have more active sites (H. Kaur et al., 2018).

The results obtained are a very important premise, because to choose an adsorbent it is necessary to know its adsorption capacity, especially if it will be used in continuous adsorption processes. In this case, in terms of adsorption capacity, PS is a better option than RH. However, from the cost/benefit point of view, the fact that PS must be ground and the grinding process involves energy consumption should also be analyzed, while RH can be used without being ground. Or in turn, the influence of using PS on their size of origin can be analyzed.

3.4. Batch adsorption processes using residues and their magnetic composites

After establishing that PS (presumably referring to polystyrene) is more efficient than RH (likely referring to rice husks), further analysis of additional agro-industrial residues becomes imperative. Among the abundantly available residues in Ecuador and worldwide, fruit peels stand out (e.g., banana: 35.4 – 47.2 million tons/year, orange: 12 – 20.8 tons/year) (Martínez-Ruano et al., 2018; Portinho et al., 2017), along with coconut fiber (50 million tons/year) (Lin & Cramon-Taubadel, 2019), and corn cobs. These residues have demonstrated efficacy in removing certain ECs, achieving efficiencies surpassing 70%, which are comparable to other adsorbents. Consequently, leveraging the adsorptive capacity for wastewater treatment presents a viable option for valorizing fruit peels, corn cobs, and coconut fibers.

Despite the promising outcomes with magnetic adsorbents, scant research has addressed EC removal. Thus, the objective of this section was to assess the potential enhancement in caffeine/triclosan removal from synthetic solutions using magnetic composites derived from high-production agro-industrial residues in Ecuador. The investigation encompassed the analysis of various parameters in batch adsorption, such as adsorbent dosage, contact time, and quantity of impregnated nanoparticles. The acquired data underwent fitting to diverse isotherm and kinetic models. Furthermore, the capacity of magnetic particles to facilitate adsorbent separation from the aqueous solution was evaluated.

All these endeavors are geared towards augmenting the adsorption efficacy of agro-industrial residues in EC removal. Moreover, attempts will be made to stimulate EC removal through composite engineering and nanostructuring. This aims to ascertain whether these composites/nanostructures can be employed in continuous adsorption processes to handle larger volumes of wastewater while exhibiting advantages over raw agro-industrial residues in EC removal.

Versión Aprobada para Defensa Oral

Article 3. Caffeine removal from synthetic wastewater using magnetic fruit peel composites: material characterization, isotherm and kinetic studies

Almeida-Naranjo, C. E., Aldás, M. B., Cabrera, G., & Guerrero, V. H. (2021). Caffeine removal from synthetic wastewater using magnetic fruit peel composites: Material characterization, isotherm and kinetic studies. *Environmental Challenges*, 5, 100343.

ABSTRACT

This work investigated the adsorption capacity of banana and orange peels, magnetite and their corresponding magnetic composites in the removal of caffeine from synthetic wastewater. The characteristics of the adsorbents were studied using proximal analysis, Fourier transform infrared spectroscopy (FT-IR), Raman spectroscopy, scanning electron microscopy (SEM), energy dispersive spectroscopy (EDS), Brunauer, Emmett and Teller (BET) analysis and X-ray diffraction. Batch adsorption tests were conducted to determine the influence of the adsorbent dose (0.5 and 10.0 g/L), contact time (5 – 180 min) and initial caffeine concentration (10 – 50 mg/L) in the caffeine removal. The fittings of the experimental data to the pseudo-first-order, pseudo-second-order, Elovich, and diffusion kinetic models, as well as to the Langmuir, Freundlich and Sips isotherm models were also studied. The use of magnetic peels improved around 1.7 times the adsorption capacity of peels. The effective doses were 3.5 g/L of orange peel, 9.5 g/L of banana peel, 2.5 g/L of orange peel composite, 0.5 g/L of banana peel composite, and 5 g/L of magnetite, achieving caffeine removal efficiencies of $95.5 \pm 0.3\%$, $90.5 \pm 0.5\%$, $93.6 \pm 0.2\%$, $89.2 \pm 0.01\%$ and $54.8 \pm 0.8\%$, respectively. The adsorption using the peels, magnetite, and their magnetic composites better fitted the pseudo-first-order kinetic model and the Langmuir and Sips isotherm models.

1. Introduction

The availability of clean water is not only essential for life, but also of crucial importance for social and economic development. Paradoxically, this same development and the growth of the population demand the consumption of larger amounts of water (4600 km³/year) and are related to the contamination and subsequent impacts (Boretti & Rosa, 2019). During the last few decades, the potential environmental impacts of a series of new anthropogenic contaminants have attracted the attention of the scientific community and the public in general. These so-called “emerging contaminants” (ECs) include pharmaceuticals, personal care products, endocrine disrupting compounds, illegal drugs, among others. These substances have been found in water bodies and wastewater in concentrations between ng/L and µg/L (e.g., pharmaceuticals between 0.02 ng/L to 50.00 µg/L). Several studies determine that ECs are both potentially toxic and very persistent, and they can directly or indirectly affect several organisms due to bioaccumulation and biomagnification (Quesada et al., 2019). Besides this, their removal is not effectively performed in conventional wastewater treatment plants (WWTPs). Conventional mechanical-biological WWTPs were used achieving an efficiency around 60% (Kot-Wasik et al., 2016). Therefore, it is desirable and necessary to improve the traditionally used treatment technologies and to develop non-conventional technologies. The efforts in this sense must consider not only the performance that needs to be achieved but also the capital and technology requirements (Ishaq et al., 2020).

Caffeine is a stimulant of the central nervous system, present in drinks such as coffee, tea, soft drinks, and energy drinks; becoming one of the most widely consumed pharmaceuticals (177.7 mg/person/day) (Korekar et al., 2019). Caffeine has been found in the WWTP influents and effluents (0.1 to 20 µg/L), in groundwater (10 to 80 ng/L), and in rivers, lakes and sea water (3 to 1500 ng/L) (Álvarez-Torrellas et al., 2016). The presence of caffeine in aquatic ecosystems represents a risk for biota (e.g., zebra fish, *Mytilus californianus*, *Ruditapes philippinarum*, *Carcinus maenas*, etc.) due to this physicochemical properties and the chronic toxicity (Korekar et al., 2019). Therefore, the search for alternatives to remove caffeine from wastewater is important. Treatments such as biochemical degradation, photolysis, reverse osmosis, ozonation, advanced oxidation and adsorption process are used in the caffeine removal (Sotelo et al., 2014).

Adsorption is an economical, easy-to-implement, highly efficient and environmentally friendly process to remove various types of contaminants. One of the most widely used and marketed adsorbent materials is activated carbon; but this cost (20 – 22 USD/kg) could limit the use at large scale (Portinho et al., 2017; Sotelo et al., 2014). Several non-conventional adsorbents have been used in the removal of emerging

contaminants, including heavy metals, from aqueous environments (Zamora-Ledezma et al., 2021). For instance, fungal strains biomass for Pb(II) ion removal and inactive bacterial strains biomass for Cd(II) ion removal were used, achieving high efficiencies (Long et al., 2019; Zamora-Ledezma et al., 2021). Other adsorbent materials used for the caffeine removal from solutions and real wastewater were polymeric resins, nanomaterials, carbon nanotubes, biochar, modified graphite sheets, zeolites, aluminosilicates, among others. Furthermore, organic, lignocellulosic or agro-industrial residues (husk, shells, peels, leaves or fruit seeds, stalks) and new-generation adsorbents (nanoparticles and composites) are also presented as an alternative (Bachmann et al., 2021). In any case, the adsorbent material used should exhibit desirable characteristics such as selectivity, high surface area, high adsorption capacity, low cost, long service life, and recyclability (Rigueto et al., 2020). Agro-industrial residues are available at low or no cost and have a porous surface with the presence of functional groups that improves the adsorption process (Portinho et al., 2017). In particular, around 12.0 to 20.8 tons of orange peels and 35.4 to 47.2 million tons of banana peels are produced annually worldwide, and do not have a defined use (Martínez-Ruano et al., 2018; Portinho et al., 2017). Moreover, they have already been used for the removal of some ECs, reaching efficiencies higher than 70%, which are comparable to other adsorbents. Banana peels have been used in the removal of atrazine (> 90%), ametrine (> 90%), sulfamethoxazole (70%), 17-ethinylestradiol (> 80%) and estrone (> 80%) (De Sousa et al., 2019). Therefore, the adsorptive removal of contaminants from wastewater could be an alternative of fruit peel valorization.

However, some peels have low adsorption capacity and separability from aqueous media. The adsorption capacity of peels will be enhanced with the impregnation of nanoparticles (iron oxides, titanium dioxide, zinc oxide, carbon nanotubes, among others), since nanoparticles have a greater specific surface. The difficulties of separation between the adsorbent and the aqueous medium could be solved with the preparation of magnetically modified adsorbents. Magnetic separation is a fast, efficient and cost-effective method that can be used in both small-scale and large-scale wastewater treatment. Thus, magnetic composites with an agro-industrial residue matrix could be an alternative for the contaminant removal (Ahmed et al., 2020). Magnetite (Fe_3O_4) is an iron oxide commonly used in the adsorption of contaminants due to the magnetic character, low-cost, environmentally friendly nature and the possibility of treating large volumes of wastewater. Magnetite has highly active surface sites and high surface area (between 30 and greater than 200 m^2/g), achieving adsorption capacities around 100 mg/g in the removal of ECs (Zheng et al., 2018, Ahmed et al., 2020). Magnetic composites (agro-industrial residues + magnetite) have been used in several studies with heavy metals and dyes (i.e. brilliant black, methylene blue), obtaining efficiencies between 50 and 99% (Çatlıoğlu et al., 2020; Zheng et al., 2018). Zheng et al. (2018), reported that diclofenac was removed using a magnetic composite (MOF-100(Fe)) obtaining a removal efficiency of 80%.

Despite the efficiency obtained with magnetic adsorbents, only a few studies have been carried out to remove ECs. Therefore, the objective of this work was to evaluate if the caffeine removal from synthetic solutions improves when magnetic composites (fruits of high production in several countries around the world, and particularly in Ecuador) are used. For the study, the influence of the adsorbent dose, contact time and initial concentration of caffeine were evaluated, the data obtained were adjusted to different isotherm and kinetic models. Likewise, it was determined whether the presence of the magnetic particles facilitates the separation of the adsorbent from aqueous solutions.

2. Materials and methods

2.1. Material conditioning and composites synthesis

The orange peels were collected at the southern zone of Quito city (-0.266667; -78.5333), while the banana peels were donated by one of the companies that processes the fruit in Ecuador. The iron salts used were $\text{FeCl}_3 \cdot 6\text{H}_2\text{O}$ and $\text{FeSO}_4 \cdot 7\text{H}_2\text{O}$ from Sigma Aldrich. Sodium hydroxide and all the other reagents used were at least 98.0% w/w pure. Peels were cut and washed with drinking and distilled water to remove impurities. Then the peels were dried at 60 °C for 24 h, grinded in a knife mill (Thomas Wiley, model 3379-K05, Thomas Scientific) and sieved. The material between 125 and 149 μm was used in adsorption tests (Castro et al., 2021).

The co-precipitation method was used for the synthesis of magnetite. For this purpose, $\text{FeCl}_3 \cdot 6\text{H}_2\text{O}$ and $\text{FeSO}_4 \cdot 7\text{H}_2\text{O}$ were used, in a 3:2 M ratio. The mixture was heated to 70 °C with constant bubbling of

argon and stirring at 1250 rpm. An 8.0 M NaOH solution was added to reach a pH= 11. Then, the materials were separated from the aqueous solution by using a magnet. Magnetite was washed with distilled water to achieve pH=7.0 and dried at 80 °C for 12 h. The synthesis of magnetic composites began with the procedure used for the synthesis of magnetite. Immediately after reaction with NaOH, 5.00 g of the previously conditioned peels were added to the magnetite solution. The mixture was kept under constant stirring at 70 °C for 30 minutes. The composite was magnetically separated, washed until pH= 7.0 and dried at 80 °C for 12 hours (Castro et al., 2021; Kapur & Mondal, 2016).

2.2. Material characterization

The materials were characterized using ASTM standards to evaluate their physical chemical characteristics. Lignin, hemicellulose and cellulose (ASTM D1106-21); (ASTM D1109-21), extractives (ASTM D1107-21; ASTM D1110-21), moisture content (ASTM D 4442-20), ash (ASTM D 1102-21), volatile matter (ASTM E 872-19) and pH (D 4972-19) were determined.

The main functional groups of the synthesized adsorbents were identified by Raman and Fourier transform infrared spectroscopy (FT-IR). The Raman analysis were made using a Horiba Scientific equipment, LabRam Evolution model, with a wavelength laser of 532 nm, power of 50 mW at 5.0% of fraction, hole size of 180 and rate of 2.4. The FT-IR analysis were made using a Perkin Elmer Spectrum 200 spectrometer within the 4000 – 500 cm^{-1} range.

The morphology of the adsorbents was studied using a Tescan Mira 3 equipped with a Schottky field emission gun at 20 kV. EDS was performed in a SEM chamber, using a detector Bruker X-Flash 6|30 with a 123 eV resolution. X-ray diffraction patterns were recorded in a Panalytical diffractometer model AERIS RESEARCH, using a copper X-ray tube ($K\alpha$, $\lambda = 1.54056 \text{ \AA}$) at 40 kV and 15 mA. The diffractogram analysis was performed on the average of four measurements between 5° and 85° (θ -2 θ , Bragg-Brentano geometry) using the HighScore Plus software. The surface characteristics of the adsorbents (surface area, pore size and pore volume) were determined with BET analysis, using a 1LX micrometer NOVA touch. The adsorbents were conditioned under vacuum up to 100 °C with a heating rate of 10 °C/min, then they held for 1440 min.

2.3. Batch adsorption tests

The batch adsorption tests were carried out to determine the dose of adsorbents and contact time that achieve the highest caffeine removal. Moreover, the influence of the initial concentration of caffeine was analyzed. The caffeine removal was evaluated using a 30 mg/L caffeine solution. In previous studies caffeine solutions between 5 and 5000 ppm using crude (grape stalk) and modified/advanced/non-conventional adsorbents (activated carbons, nanoparticles and nanocomposites) were applied (Anastopoulos et al., 2020; Panneerselvam et al., 2011; Rigueto et al., 2020).

The process was carried out at room temperature ($22.7 \pm 1.0 \text{ }^\circ\text{C}$), pH = 6.9 ± 0.24 and stirring at 150 rpm. The adsorbent material dose used were between 0.5 and 10.0 g/L. Eight tests were carried out for each adsorbent material with reaction times between 5 and 180 minutes. Finally, to determine the influence of initial caffeine concentration in the adsorption process, solutions between 10 and 50 mg/L were used. The batch tests were carried out in triplicate, using distilled water as control. After each experiment the adsorbent was removed from the aqueous phase using magnetic separation and a 0.20 μm pore size filter membrane. Measurements of caffeine concentrations were performed in an Analytik Jena Specord 210 Plus UV – VIS spectrophotometer, at 287 nm.

2.3.1. Kinetic and isotherm study tests

Kinetic and isotherm studies were conducted at room temperature ($22.7 \pm 1.0 \text{ }^\circ\text{C}$), pH = 6.9 ± 0.24 and stirring at 150 rpm using the optimal dose and contact time, respectively. In the adsorption kinetic tests, caffeine solutions of 30 mg/L and in the isothermal ones, caffeine concentrations between 10 and 90 mg/L were used. The kinetic, isotherm and their respective statistical analysis were carried out using the same models and equations used in Article 1.

3. Results and Discussion

3.1. Physical-chemical characterization

Table 15 summarizes the physicochemical properties of the peels. The moisture is higher (21.2%) in the banana peel. Both peels have high volatile material contents (between 69.8 and 77.1%) due to their organic nature (lignin, cellulose, hemicellulose, lipid, protein and carbohydrate presence) (Kamsonlian et al., 2011). The total extractives content is higher in the orange peel (around 10%) than in the banana peel. This value represents the content of oils, fats and proteins, components that form bonds between the contaminant and the adsorbent and allow the efficient contaminant removal (Orozco et al., 2014).

Fruit peels have a low ash content, between 6.4 and 8.2%. Ash content of 5.0% and 4.0% have been reported for banana and orange peels. Ash represents the inorganic matter that is formed by minerals (e.g., silica) and micronutrients. In high concentrations, the adsorption process could be affected due to ash low adsorption capacity (Pathak et al., 2017). The lignin (23.1 – 16.6%), cellulose (33.3 – 50.0%) and hemicellulose (15.4 – 15.9%) contents are higher in orange and banana peels compared to the other components, respectively. This is because agro-industrial residues are abundant in polysaccharides (cellulose and hemicelluloses) and lignin, which are part of the structure of the cell wall. Lignin, cellulose and hemicellulose indicate the presence of carboxyl, hydroxyl and other functional groups capable of interacting with contaminants. The high content of lignin, cellulose and hemicellulose suggests that orange and banana peels could be effective bio-adsorbents for the removal of organic contaminants (Almeida-Naranjo, et al., 2021a).

Table 15. Chemical composition of peanut shells.

Parameter	Orange peel (mean ± SD)	Banana peel (mean ± SD)
pH	5.2 ± 0.0	6.3 ± 0.0
Moisture (%)	65.0 ± 0.4	69.2 ± 0.3
Volatile material (%)	77.1 ± 0.1	69.8 ± 0.1
Ash (%)	8.2 ± 0.1	6.4 ± 0.3
Extractives (ethanol-toluene) (%)	18.4 ± 2.6	8.8 ± 1.7
Extractives (water) (%)	5.9 ± 0.8	4.7 ± 0.6
Total extractives (%)	24.5 ± 3.2	13.5 ± 2.3
Lignin (%)	23.1 ± 0.5	16.6 ± 1.1
Hemicellulose (%)	15.4 ± 0.3	15.9 ± 0.1
Cellulose (%)	33.3 ± 3.0	50.0 ± 1.0

3.2. Instrumental Characterization

Figure 22a shows Raman spectra for magnetic composites. They show the presence of magnetite bands (319.20, 535.98 and 668.33 cm^{-1} on magnetite, 638.13 cm^{-1} on the orange peel composite and 619.40 cm^{-1} on the banana peel composite). Additionally, there are other bands belonging to maghemite, formed from the oxidation of magnetite (around 350, 500 and 700 cm^{-1}). Therefore, the magnetic composites and magnetite are a mixture of magnetite and maghemite particles. The additional peaks in the composites are attributed to the nature of peels (Shebanova & Lazor, 2003).

Figure 22b shows the infrared spectra for orange and banana peels. They present intense peaks at 3281.3 and 3321.8 cm^{-1} for orange and banana peels respectively, the bands are characteristic of hydroxyl groups (O-H). The peaks at 2917.8 cm^{-1} (orange peel), 2918.7 and 2851.2 cm^{-1} (banana peel) correspond to the C-H vibrations of the stretch methyl (CH_3), methylene (CH_2) and methoxy groups (O-CH_3), main components of lignin and pectin. The peaks around 1730 cm^{-1} are characteristic of the carbonyl group ($\text{C}=\text{O}$) stretch, they represent the presence of aldehydes, ketones and the carbonyl ester group. The peaks around 1600.0 cm^{-1} represent the $\text{C}=\text{C}$ bond stretch and could show the presence of benzene, aromatic rings, or amino acids. At 1422.2 cm^{-1} and 1442.5 cm^{-1} (orange and banana peel, respectively) the presence of aliphatic, aromatic groups, vibrations of methyl, methylene and methoxy groups resulting from the vibration of the aromatic ring of lignin (Feng et al., 2009). The bands around 1000.0 cm^{-1} represent the C-O group from alcohols, phenols and carboxylic acids and represents the band of hemicellulose, cellulose and lignin. Finally, the band in the region of 500.0 cm^{-1} was attributed to the presence of amino groups (Alaa El-Din et al., 2018; Dahiru et al., 2018). In the magnetite, there were bands around 3371.9 cm^{-1} , typical of hydroxyl groups. The vibration of the carboxylate and amide groups is presented in the band around 1624.7 cm^{-1} . At 1110.80 cm^{-1} the stretching vibration of C-OH and C-O was presented. The intense peak at 547.69 cm^{-1} is related to the stretching vibration of Fe-O (iron oxides) evidencing the magnetic particle presence (Gupta & Nayak, 2012).

The FTIR spectra for the composites show that the peaks of the functional groups from peels are maintained. However, the hydroxyl and C-H groups have reduced their intensity due to the reactions generated in the magnetite impregnation process. The peak of the carbonyl group decreases in the spectral images. The peaks at 611.32 and 552.51 cm^{-1} , for orange peel composite and banana peel composite, respectively; evidence the presence of Fe-O iron oxides in the materials (Dahiru et al., 2018; Kapur & Mondal, 2016). The presence of the functional groups presents in lignin, cellulose, hemicellulose and in the iron oxides indicate that materials could be good adsorbents.

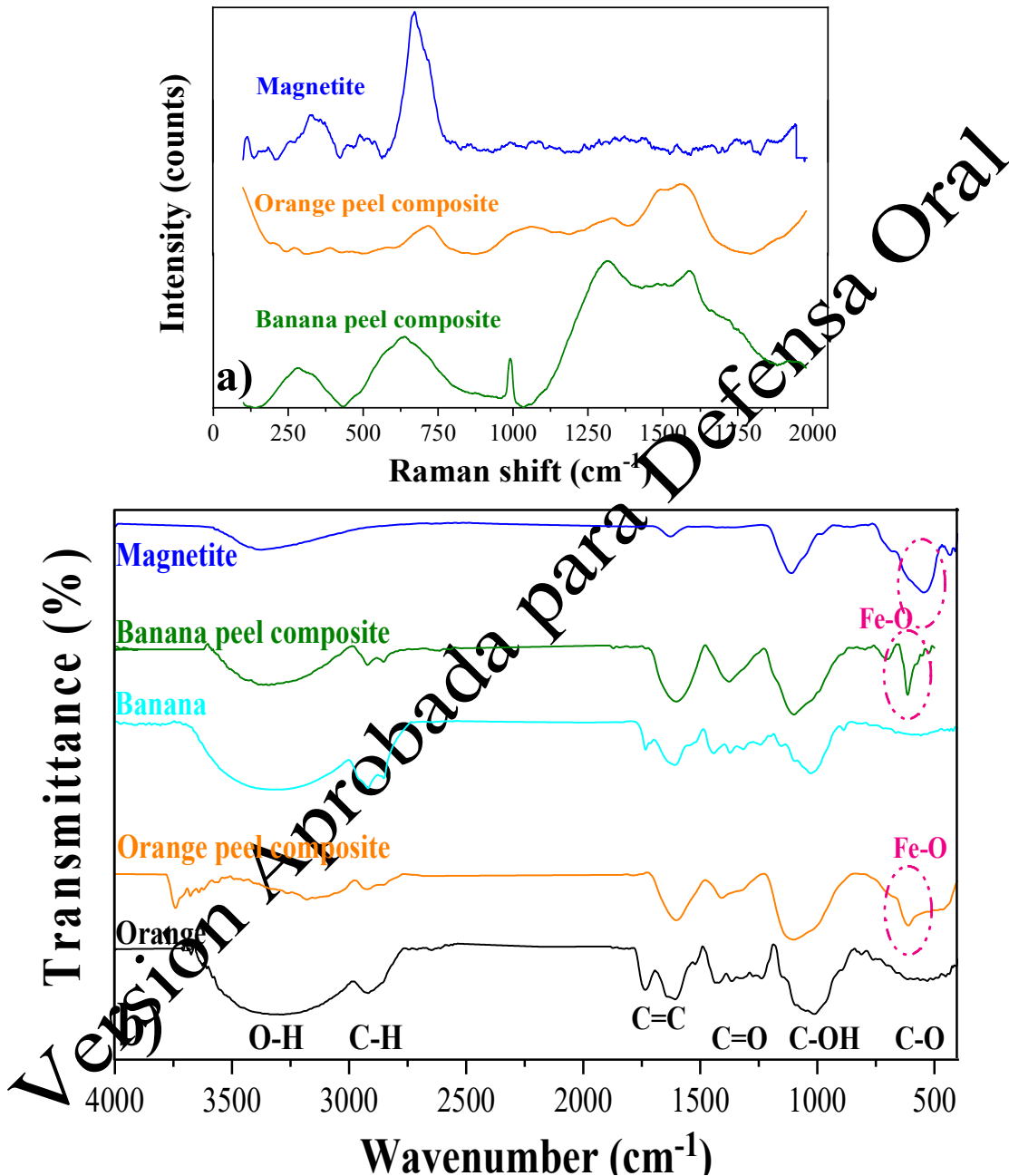


Figure 22. a) Raman spectra and b) FT-IR spectra of adsorbent materials.

The XRD pattern of magnetite and composites is shown in Figure 23. Magnetite (peaks at $2\theta=31.8, 35.6$ and 62.9°) and maghemite (peaks at $2\theta=35.6, 43.4$ and 57.1°) were identified. In composites the most important bands of magnetite (peaks at $2\theta=35.6$ and 62.9°) were found (Yuchen Liu et al., 2014).

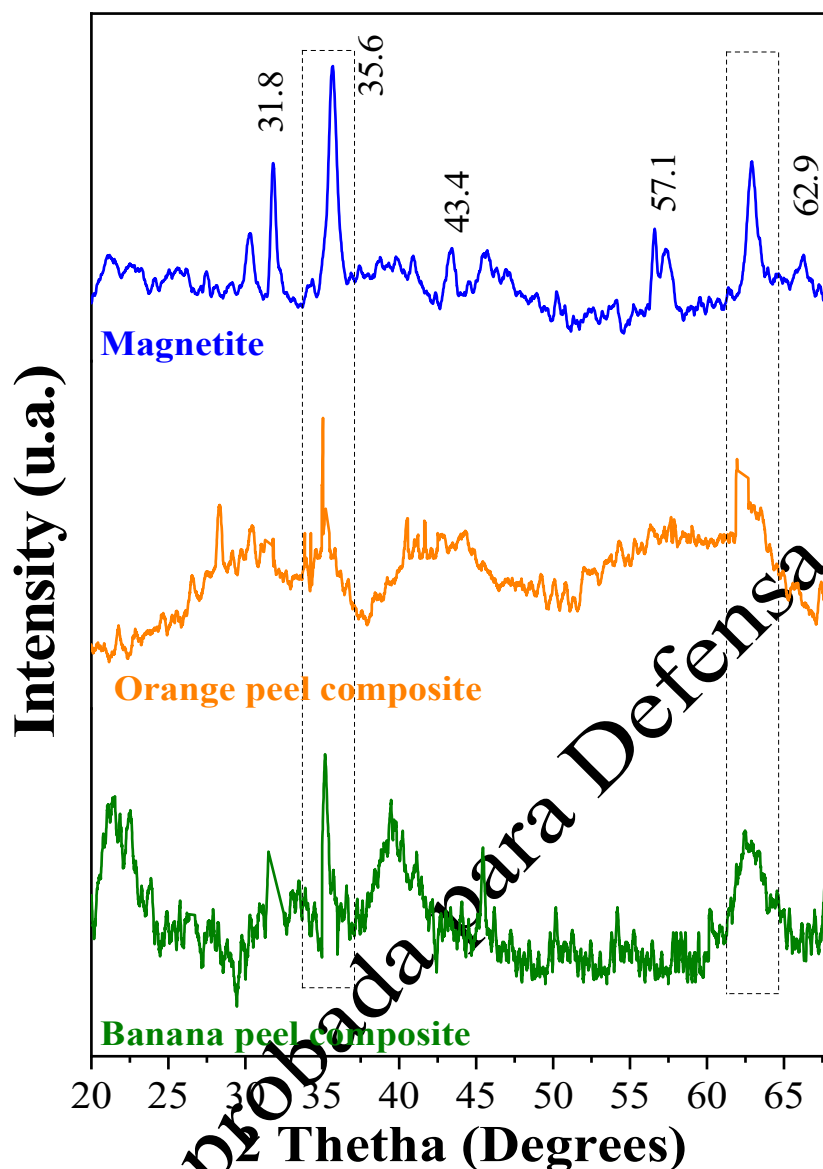


Figure 23. XRD analysis of adsorbent materials.

Table 16 shows the parameters of BET analysis for adsorbents. The surface area of orange and banana peels is low (0.8 and 0.08, respectively). The results obtained coincide with those reported by previous studies (orange: 0.83 m²/g and banana: < 0.1 m²/g) (Feng & Guo, 2012; Yuchen Liu et al., 2014; Stavrinou et al., 2018). The low values of surface area and pore volume are attributed to the presence of pectin, lignin, and viscous compounds that the fruit peels present. This is verified by what is observed in Figure 24. Despite the heterogeneous surface, it is observed that the particles are compact mainly in banana (Figure 24b), leaving very little spaces (pores) between them. Heterogeneous surfaces favor the adsorption process (Oyekanmi et al., 2019).

According to Figure 24, the surface of the composites showed the presence of smaller particles of different sizes distributed randomly on the fruit peels, due to the inclusion of magnetite nanoparticles (57.3 m²/g). As a result, composites increased their surface area and pore volume as suggested by Ahmed et al., (2020) and Çatlıoğlu et al., (2021). Panneerselvam et al., (2011), also show an increase in the surface area of tea waste when impregnating them with magnetite nanoparticles. The presence of Fe in both composites were confirmed with EDS graph with the peak at 6.4 keV (Figs. 24d and 24f). On the other hand, the N₂ adsorption-desorption isotherms of materials are type II according IUPAC classification. This is characteristic of non-porous or microporous materials (Çatlıoğlu et al., 2021).

Table 16. Surface area, pore volume and pore diameter of adsorbents

Adsorbents	Surface area (m ² /g)	Pore volume*10 ⁻³ (cm ³ /g)	Pore diameter (nm)	N ₂ adsorption/desorption isotherm Volume adsorbed/desorbed (cm ³ /g STP) vs Relative pressure (P/P ₀) Black line: Adsorption isotherm Orange line: Desorption isotherm
Orange peel	0.801	2.560	3.9906	
Banana peel	0.079	0.452	7.078	
Magnetite	57.258	592.206	12.102	
Orange peel composite	14.282	23.14	13.255	
Banana peel composite	8.140	32.420	3.440	

Versión Aprobada para Defensa Oral

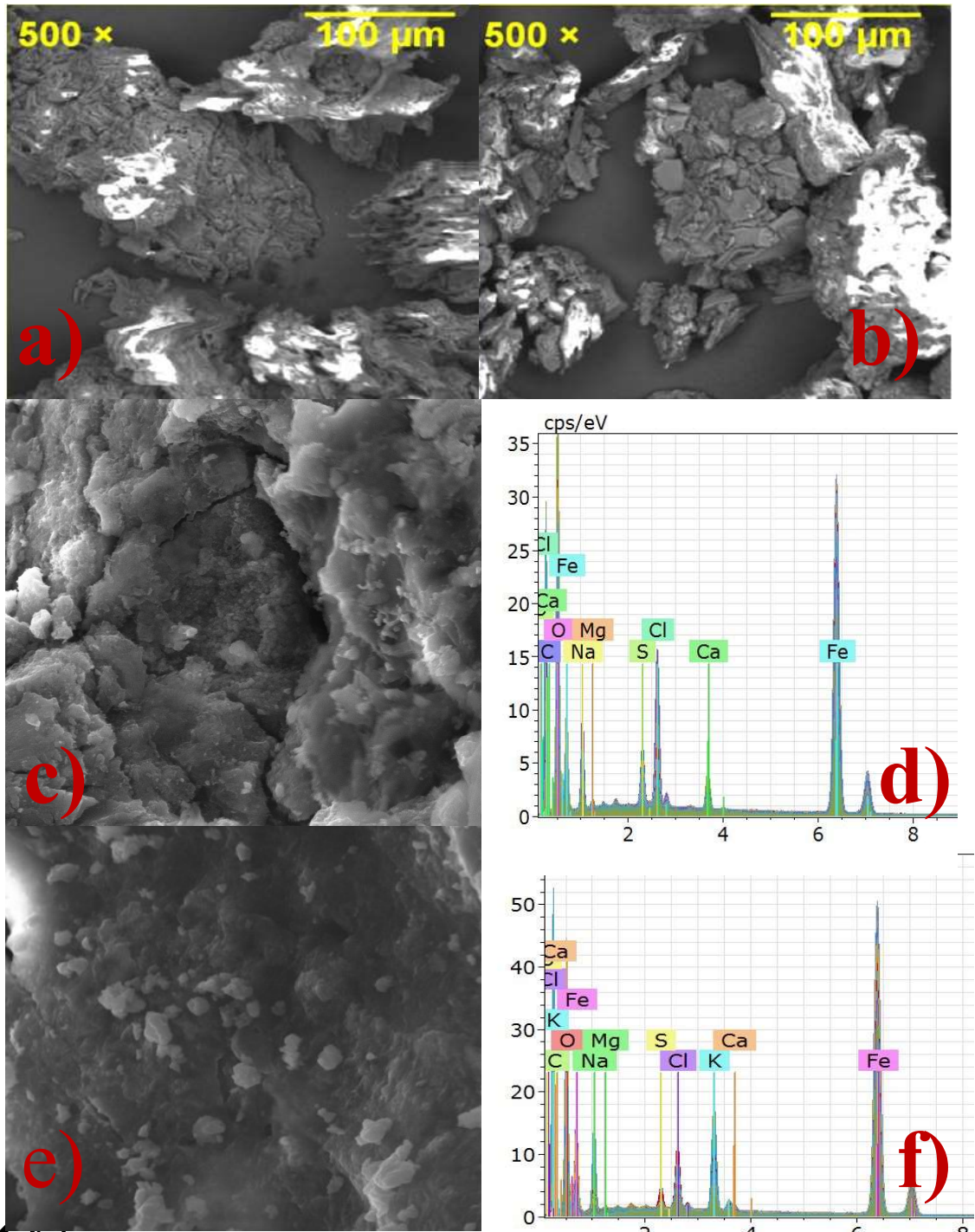


Figure 24. SEM images and EDS of materials. a) Orange peel, b) banana peel, c) orange peel composite, e) banana peel composite. d) and f) EDS of orange peel composite and banana peel composite, respectively.

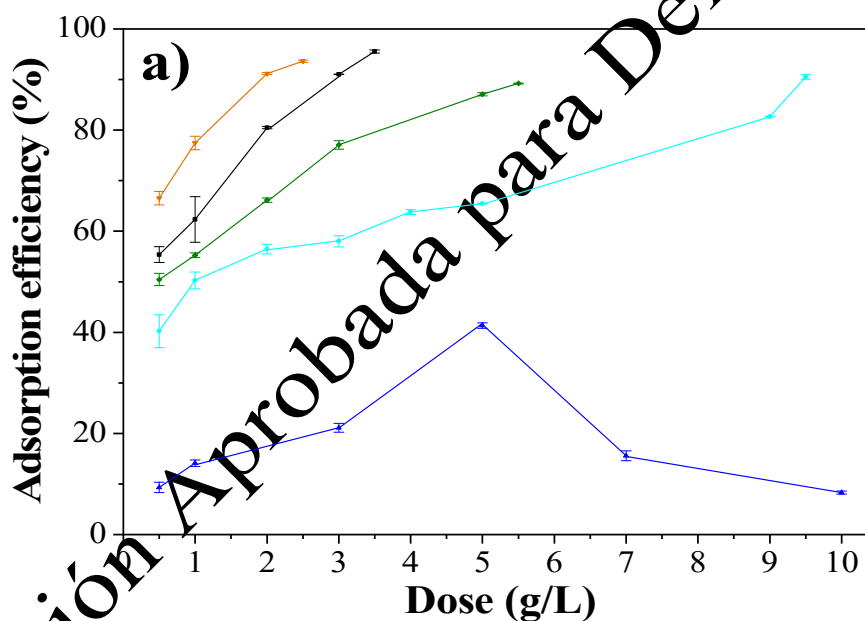
2.3. Adsorption process

The material dose used for the caffeine removal is shown in Figure 25a. An increase in the dose of fruit peels and composites produces a higher efficiency, due to the greater surface area and functional groups present (Ahmed et al., 2020). The highest caffeine removal efficiencies (mean \pm SD) achieved with orange and banana peels were $95.5 \pm 0.3\%$ and $90.5 \pm 0.5\%$, using 3.5 g/L and 9.5 g/L, respectively. The higher dose of banana peels required could be due to their lower lignin contents in their composition (around 7.0% less) compared with orange peels. A higher lignin content in the orange peel suggests the

formation of bonds between the hydroxyl and carboxyl functional groups and caffeine, process by which caffeine was efficiently removed (Almeida-Naranjo, et al., 2021a).

The carbonyl group, C=C group and C-O group present in the orange peel have a higher intensity than those of the banana peel. In addition, the SEM images for the peels show amorphous morphologies, the orange peels are the ones that present higher porosity. This is characteristic of agro-industrial residues, and favors the retention of caffeine (J. Liu et al., 2016).

Figure 25b shows that magnetite (using a dose of 5 g/L) reached a maximum caffeine removal of $41.3 \pm 0.5\%$, after 3h of contact time. In the caffeine removal, electrostatic interaction occurs by H-bond interaction (hydrogen bridges) and the π - π interaction. In some carbonaceous materials, the carbon surface has polar groups with hydrophilic behavior, such as -NH, -OH, -O and -COO. Consequently, caffeine adsorption could occur by dipole-dipole interactions (Rigueto et al., 2020). However, the agglomerates and non-homogeneous size distribution formed during magnetite synthesis (showed in SEM images) produce a reduction of active sites in the surface (Zheng et al., 2018). The composites improved the caffeine removal (9.0% for orange peels and 23.0% for banana peels). In this case, 2.5 g/L of magnetic orange peel and 5.5 g/L of magnetic banana peel removed $93.6 \pm 0.2\%$ and $89.2 \pm 0.01\%$, respectively; after 3h of contact time. An improvement in the removal percentage using composites has been also reported by Edathil et al., (2018) when coffee waste was used as a matrix to synthesize a magnetic coffee waste by dispersing Fe_3O_4 nanoparticles on its surface via a single pot precipitation method in order to remove Pb^{+2} from aqueous solutions (18% compared with waste without modification).



Versión Aprobada para Defensa Oral

Versión Aprobada para Defensa Oral

Figure 25. Optimal conditions for caffeine removal: a) optimal dose, b) optimal contact time. Black line: orange peel, cyan line: banana peel, blue line: magnetite, orange line: orange peel composite, green line: banana peel composite.

The use of the 8.0 M NaOH solution generated the degradation of the peel's components due to the demethylation of the methyl ester present in lignin, cellulose and hemicellulose. In the FT-IRs (Figure 22b) the demethylation process is observed in the changes that the composites present compared with the fruit peels, showing a decrease in the intensity of the bands around 1750 cm^{-1} and an increase in the intensity of the bands around 1000 and 1640 cm^{-1} . The amount of the carboxylate ion increases on the peel surface in this process (Kapur & Mondal, 2016; Savrinou et al., 2018). According to Feng et al., (2010), the carboxyl groups are responsible for the binding between adsorbent and the adsorbate, increasing the adsorption capacity of caffeine. Furthermore, the presence of NaOH causes the swelling of lignocellulosic compounds, which increases the surface area and reduces both the degree of polymerization and the crystallinity of the fruit peels, thus it favor the adsorption capacity of them (Sharma et al., 2018). Therefore, the higher caffeine removal using composites appears to be influenced by the change that the fruit peels have undergone in the magnetite co-precipitation process than by the magnetite (caffeine removal around 50%) itself. However, separating the composites from the aqueous solution after the adsorption process was easier than removing the fruit peels (Figure 26).



Figure 26. Photographs of the magnetic separation of the composites from the aqueous phase after caffeine adsorption.

Figure 25b shows the removal as a function of contact time using the optimal dose of each material. The fruit peels and their composites showed rapid adsorption during the first 10 min, then the adsorption gradually slows down until equilibrium is reached. Banana peel, magnetite and composites reached concentrations close to the equilibrium (optimum contact time) at 60 minutes, while the orange peel achieved the equilibrium in 45 min. The maximum removals were 93.7 ± 0.06 , 89.3 ± 0.1 , 91.9 ± 0.1 and $85.9 \pm 0.4\%$ for orange peel, banana peel, orange peel composite and banana peel composite, respectively.

Adsorption on magnetite is slower, the maximum caffeine removal was $54.8 \pm 0.8\%$ with a dose of 5 g/L in 60 min. Once the maximum electrostatic interaction is reached, the process efficiency decreases. Probably, this occurs due to the low magnetic intensity of the magnetite particles due to the agglomerate formation, so agglomerates of magnetite are not in the nanometric order. Some researchers have found that often the relative adsorption efficiency decreases because of particle aggregation/agglomeration that leads to a specific surface reduction. Agglomeration/aggregation could become an obstacle between the caffeine molecules and the empty sites of the adsorbents (De Sousa et al., 2019; Panneerselvam et al., 2011).

On the other hand, it was determined that an increase in the initial caffeine concentration (from 10 to 50 mg/L) reduced their removal efficiency. This reduction was 6.1, 5.8, 13.7, 6.5 and 9.1% for orange peel, banana peel, magnetite, orange peel composite and banana peel composite, respectively. The decrease in the caffeine adsorption is produced by the presence of a greater quantity of caffeine molecules that are competing for the active sites available in the adsorbents (Bachmann et al., 2021).

2.1.1. Kinetic model

The adsorption kinetics determines the residence time required to complete the adsorption process. The pseudo-first-order, pseudo-second-order and Elovich models performed well (SSE= 0.046 – 12.006 and $\chi^2= 0.005 – 0.868$) with R^2 values ranging from 0.887 to 0.994 for fruit peels, from 0.974 to 0.997 for magnetite, and from 0.936 to 0.998 for composites. The parameters of kinetic adsorption model are shown in Table 17 and Figure 27.

Peels, magnetite and orange composite were best adjusted to the pseudo-first-order model and banana composite was best adjusted to the pseudo-second-order kinetic model. However, the q_e value obtained using the pseudo-first-order model is closer to the experimental q_e value, as with the other 4 adsorbents. Although the pseudo-first-order model adequately describes the adsorption kinetics of the experimental data for all adsorbents, this model does not reveal the adsorption mechanisms.

Table 17. Kinetic parameters calculated from pseudo-first-order, pseudo-second-order and Elovich models for the adsorption of caffeine.

Kinetic model	Parameter	Unit	Adsorbents				
			Orange peel	Banana peel	Magnetite	Orange peel composite	Banana peel composite
Experimental data	q_e	mg/g	8.889	3.088	3.091	12.174	5.269
	q_e	mg/g	8.977	3.072	3.118	11.972	5.056
Pseudo-first order	K_1	1/min	0.095	0.074	0.034	0.089	0.112
	R^2	-	0.985	0.994	0.997	0.991	0.981
	χ^2	-	0.179	0.009	0.005	0.192	0.062
	SSE	-	1.249	0.046	1.571	10.474	12.006
	q_e	mg/g	9.918	3.445	3.695	13.328	5.518
Pseudo-second order	K_2	g/(mg min)	0.013	0.028	0.010	0.009	0.030
	R^2	-	0.956	0.987	0.991	0.984	0.998
	χ^2	-	0.539	0.017	0.017	0.333	0.005
	SSE	-	3.279	0.093	1.567	8.078	10.346
	α	mg/(g min)	5.437	1.416	0.227	5.696	6.483
Elovich	β	mg/g	0.635	1.788	1.158	0.452	1.286
	R^2	-	0.887	0.952	0.974	0.936	0.976

χ^2	-	0.868	0.015	0.048	0.625	0.008
SSE	-	7.926	0.485	1.566	11.529	10.345

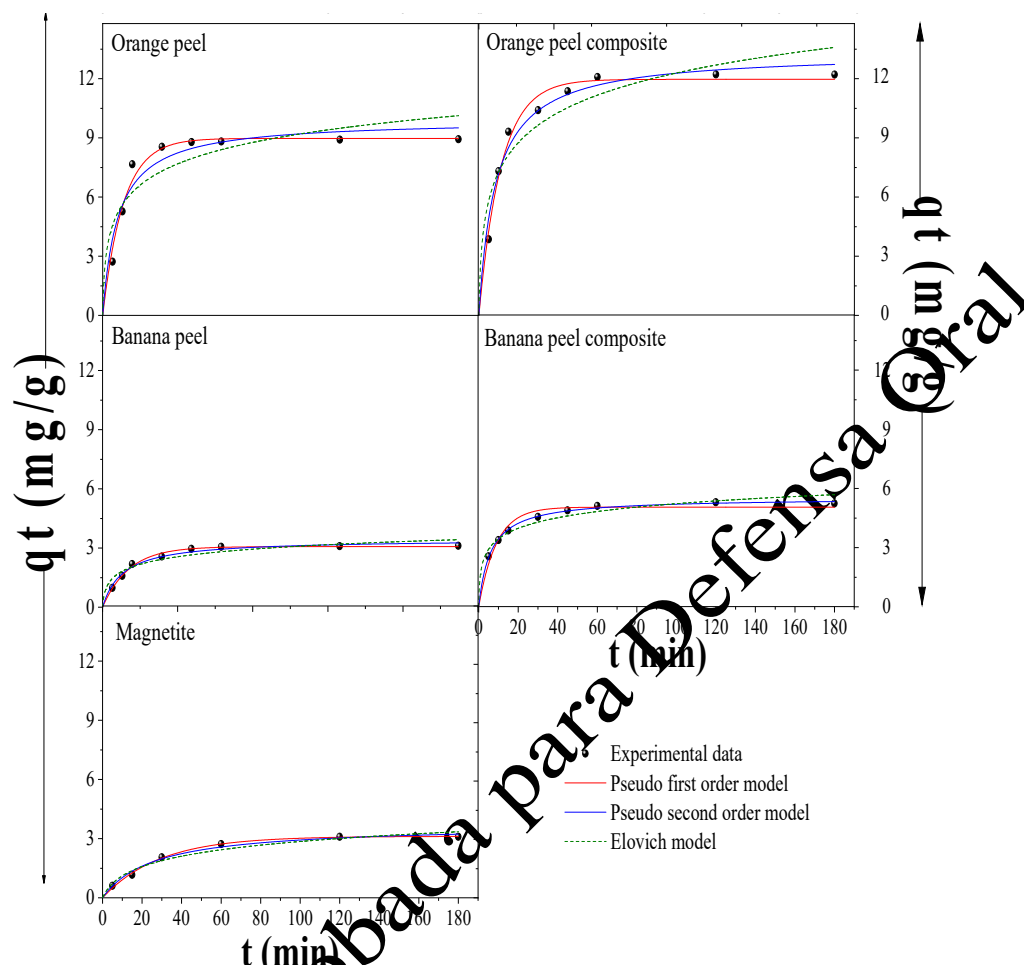


Figure 27. Pseudo-first-order, pseudo-second-order and Elovich kinetic models for adsorption of caffeine.

Generally, a solid-liquid adsorption process is characterized by a diffusion process, so it will be necessary to analyze this model (Fran et al., 2017). If the intraparticle diffusion curve passes through the origin, then intraparticle diffusion is the only one that limits the adsorption rate. However, Table 18 and Figure 28 show the presence of two linear regions, so the adsorption process is controlled by a multi-step mechanism. At first, there were a rapid diffusion of caffeine on the external surface of the adsorbents and later an intraparticle diffusion occurs. In the latter, the caffeine molecules migrate from the outside of the adsorbents into their pores, where the adsorption took place (Yuchen Liu et al., 2014).

Table 18. Kinetic parameters calculated from intraparticle diffusion model for caffeine adsorption.

Parameter	Unit	Adsorbents				
		Orange peel	Banana peel	Magnetite	Orange peel composite	Banana peel composite
K_{p1}	mg/(g min ^{1/2})	1.782	0.424	0.443	1.526	0.504
C_1	mg/g	-0.515	0.234	-0.436	1.904	1.689
R^2	-	0.869	0.940	0.980	0.849	0.949
K_{p2}	mg/(g min ^{1/2})	0.023	0.009	0.068	0.024	0.023
C_2	mg/g	8.641	2.996	2.243	11.914	4.970
R^2	-	0.947	0.993	0.810	0.772	0.482

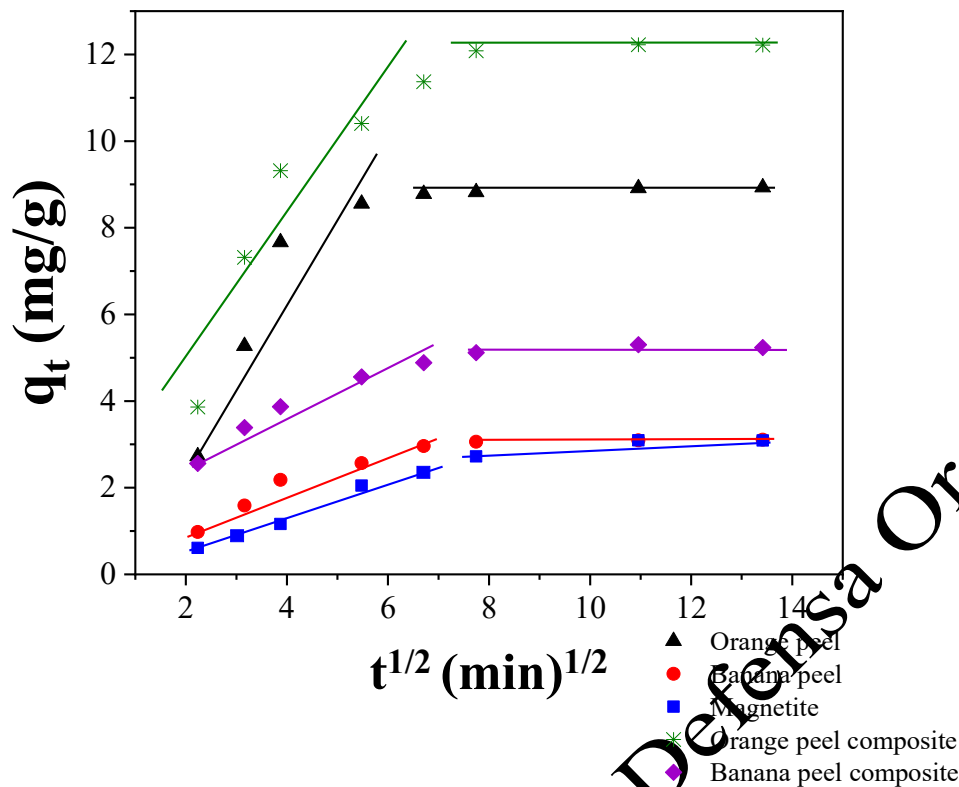


Figure 28. Intraparticle diffusion kinetics for adsorption of caffeine

2.1.2. Adsorption Isotherms

The contaminant distribution between the liquid phase and the adsorbent at equilibrium is determined by the adsorption isotherms. The Langmuir, Freundlich, and Sips models were used to determine the caffeine distribution in the adsorbents, the data are presented in Table 19 and Figure 29. Langmuir's model assumes that the adsorbent has active sites with the same energy (homogeneous surface) and caffeine adsorption occurs in a monolayer without lateral interaction. Freundlich's model assumes that active sites have different energy (heterogeneous surface) and that adsorption occurs in multilayers. Meanwhile, the Sips model is a combination between the Langmuir and Freundlich models (Sahoo & Prelot, 2020).

The studied materials have a higher correlation factor with the Langmuir and Sips isothermal model with values of correlation coefficient (R^2) between 0.927 and 0.999. A similar result was obtained by N'diaye & Ahmed Kankou using *Ziziphus Mauritiana* seeds in the caffeine removal (N'diaye & Ahmed Kankou, 2019). K_L (Langmuir) and $1/n$ (Freundlich) values are < 1 , so the caffeine adsorption is favorable in the adsorbents (Nguyen et al., 2021). Furthermore, lower values of SSE (0.079 – 1.76) and χ^2 (0.001 – 0.040) were achieved for three models, being slightly higher for the Freundlich model. Likewise, the adsorption capacity values obtained from the Langmuir and Sips models are close to the values of the experimental adsorption capacity. Therefore, the results suggest that the caffeine adsorption take place onto a homogeneous surface (Medina et al., 2010; Panneerselvam et al., 2011; Sharma et al., 2018).

Besharati & Alizade (2018) demonstrated strong positive evidence that the adsorption of malachite green dye onto lignocellulosic adsorbents impregnated with magnetite nanoparticles (tea waste, peanut husk, Azolla and Fig leaves) follows the Langmuir isotherm, as well as the caffeine adsorption onto magnetite impregnated used black tea (Mahmood et al., 2018). In addition, the crystal violet dye adsorption on magnetized orange peels also exhibits a reasonable fit to the Langmuir model (Ahmed et al., 2020). Stavrinou et al. (2018) demonstrated that the Langmuir isotherm was found to describe satisfactorily the biosorption of methylene blue and orange G onto banana peels. Besides, the adsorption of rhodamine B using acid modified banana peels showed the same behavior. Beltrame et al. (2018), showed that the adsorption of caffeine onto the surface of the prepared activated carbon fibers from pineapple plant leaves was fitted to the Langmuir isotherm model. The material with the highest adsorption capacity was the orange peel-magnetite composite ($q_m = 25.6 \text{ mg/g}$), while the material with the lowest adsorption capacity was magnetite ($q_m = 3.26 \text{ mg/g}$).

Table 19. Isotherm parameters calculated from Langmuir, Freundlich, and Sips models.

Isotherm model	Parameter	Unit	Adsorbents				
			Orange peel	Banana peel	Magnetite	Orange peel composite	Banana peel composite
Langmuir	q_m	mg/g	15.188	6.761	4.905	25.604	11.668
	K_L	L/mg	0.978	0.310	0.049	0.412	0.238
	R^2	-	0.978	0.981	0.927	0.999	0.993
	χ^2	-	0.028	0.008	0.016	0.002	0.005
	SSE	-	1.154	0.126	0.183	0.091	0.121
	K_F	(mg/g) ^{1-1/n}	7.152	1.679	0.465	7.636	2.569
Freundlich	1/n	-	0.394	0.558	0.539	0.522	0.541
	R^2	-	0.966	0.970	0.876	0.987	0.972
	χ^2	-	0.042	0.013	0.027	0.022	0.020
	SSE	-	1.760	0.1971	0.309	1.332	0.519
	q_m	mg/g	16.085	6.590	3.259	2.992	8.500
Sips	K_L	L/mg	0.896	0.326	0.095	0.366	0.400
	n	-	1.211	0.979	0.509	1.052	0.650
	R^2	-	0.980	0.981	0.968	0.999	0.973
	χ^2	-	0.025	0.009	0.007	0.001	0.020
	SSE	-	1.036	0.126	0.079	0.072	0.502

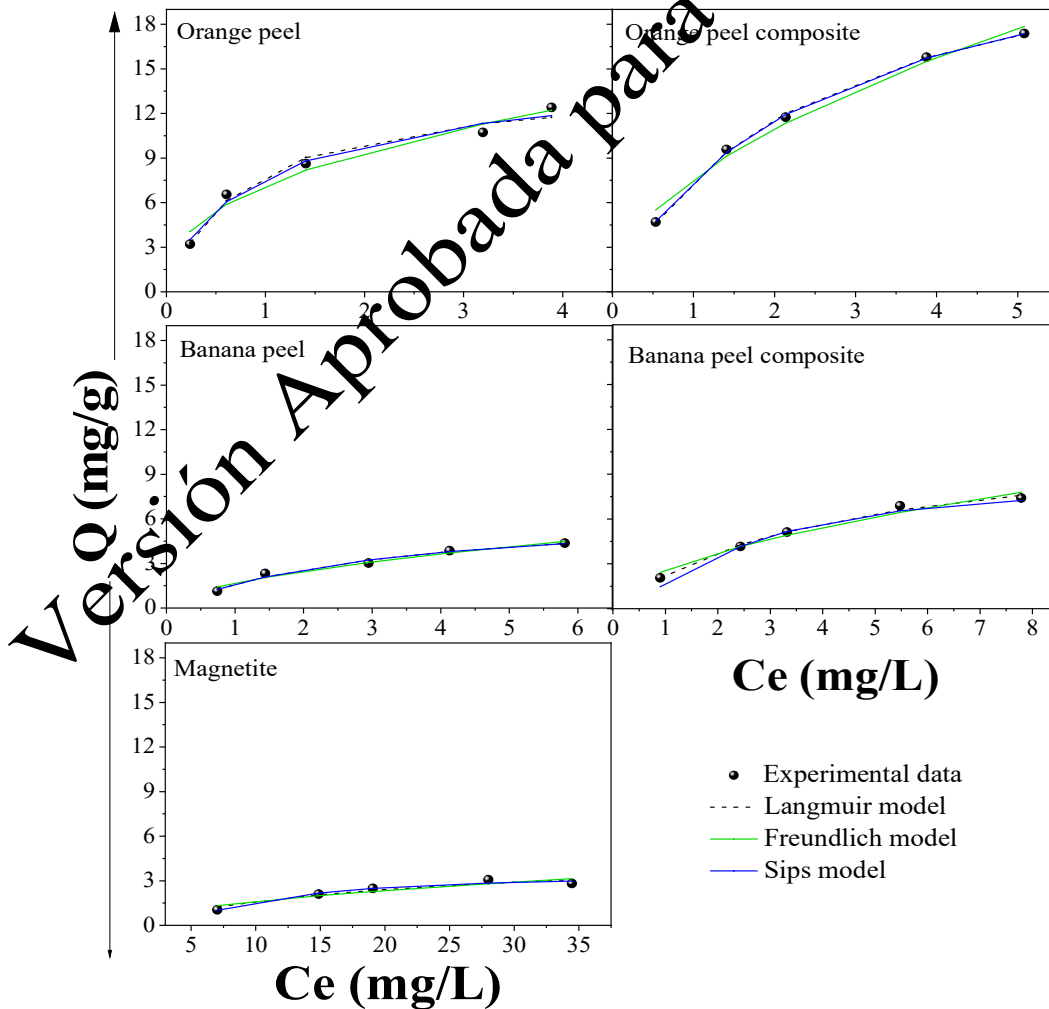


Figure 29. Langmuir, Freundlich and Sips isotherm models for adsorption of caffeine

Table 20 lists some results of adsorption for caffeine removal from aqueous solutions with different adsorbents. Values of specific area, dose, pH, q_m and isotherm model are shown. Several of the adsorbents used in caffeine removal have a higher adsorption capacity than fruit peels and composites. This is linked to the high surface area of these adsorbents. However, most of these adsorbents are activated carbons, whose cost is higher than that of fruit peels and even composites. This cost is not analyzed in any of the studies. On the other hand, there are materials with adsorption capacities that are comparable to those of the materials studied. Despite the high surface area of graphene and the complex synthesis, the adsorption capacity is comparable to that of the orange peel composite. While the composite coffee residues + chitosan, charcoal from rice husk and charcoal from rice husk + corn cob present adsorption capacities similar to those obtained with fruit peels, magnetite and banana peel composite (Beltrame et al., 2018a; 2018b; Besharati & Alizadeh, 2018; Couto et al., 2015; Danish et al., 2020).

Table 20. Results of caffeine removal onto different adsorbents.

Material	Specific area [m ² /g]	Dose [mg/L]	pH	q_m [mg/g]	Isotherm model	Reference
Commercial PAC	882.6	3000	6.2	51.8	Freundlich	
Composite from coffee residues and chitosan	-	200	6.0	8.66	Freundlich	Rigueto et al., 2020
Charcoal from rice husk	63	1000	5.0	2.09	Langmuir	
Charcoal from rice husk blended with corn cob	144	1000	5.0	8.04	Langmuir	
Graphene	570.2	50	7.5	22.77	Langmuir	
<i>Acacia mangium</i> wood (activated carbon)	-	3000	7.7	30.3	-	Danish et al., 2020
Pineapple plan leaves (activated carbon)	1031	25	7	145.5	Langmuir	Beltrame et al., 2018
Babassu coco (activated carbon)	980	10	3	86.9	Langmuir	Couto et al., 2015
Tea leaves	-	-	-	435	Langmuir, Freundlich	Seedher and Sidhu 2007
Raw grape stalk	-	-	-	89.194	Sips	Portinho et al., 2017
Grape stalk modified by phosphoric	-	-	-	129.568	Sips	
Activated carbon from grape stalk	1099.86	-	4	-	Sips	
				916.7		
Coconut waste (activated carbon)	-	-	-	171.23	Langmuir	De Souza et al, 2017
Peach stones (helium, activated carbon)	1064	120	4.8	260	Sips	Torrellas et al., 2015
Peaches stones (activated carbon)	1216	120	6.3	260	Sips	
Peaches stones modified by oxidation (activated carbon)	959	120	6.3	270	Sips	

3. Conclusions

The performance in the adsorption process improved with the use of the composites due to the chemical modification with sodium hydroxide (demethylation) and higher magnetite surface area. The demethylation increases the number of carboxylate ligands on the composite surfaces allowing the caffeine removal from synthetic wastewater. Using 2.5 g/L of orange peel composite and 5.5 g/L of banana peel composite an 8.6% and 21.2% higher efficiency in the caffeine removal was achieved compared with non-modified orange and banana peel. The adsorbents fitted well to the Langmuir and Sips isotherm models achieving adsorption capacities between 4.9 and 25.6 mg/g. While the fruit peels, magnetite and composites were adjusted to the pseudo-first-order kinetic and the adsorption process is controlled by a multi-step mechanism. The challenge for future work is to synthesize nanoparticulate magnetite and achieve a homogeneous distribution on fruit peels or other types of residues, with the aim that the nanoparticle presence favors the removal of contaminants such as caffeine.

Article 4. Triclosan/Caffeine removal using coconut fiber, corn cob, and magnetic corn cob in batch process and filter bed columns

The findings presented in Article 3 offer intriguing insights, particularly regarding the enhanced adsorption capacity facilitated by the presence of nanoparticles within the two utilized fruit peels. Nevertheless, a pivotal investigation awaits: the examination of whether this observed improvement translates to the realm of continuous adsorption processes, spanning a spectrum of agro-industrial residues featuring diverse attributes such as larger size and composition, all of which are more readily available within the country.

In pursuit of this crucial objective, the research detailed in this article embarks upon an exploration that encompasses coconut fibers and corn cobs as the initial subjects of scrutiny. This comprehensive evaluation seeks to identify the residue endowed with the most favorable adsorptive traits. Furthermore, an indispensable facet to ascertain is the optimal dosage of iron oxide nanoparticles to be infused within this chosen residue. It is imperative to emphasize that the determination of this latter variable holds significant weight, as an excessive presence of nanoparticles within the composite matrix could potentially lead to a diminution in its overall adsorption capacity.

ABSTRACT

The efficiency of corn cobs (CC), coconut fiber (CF), magnetite and magnetic composites of corn cobs in removing caffeine and triclosan was investigated in batch adsorption tests and fixed bed columns. The adsorbents were characterized by analytical methods (ASTM standards) and instrumental methods (microscopy, spectroscopy, BET.). Batch adsorption tests were performed to determine the influence of adsorbent particle size (small=120 – 150, medium= 300 – 600 and large= 800 – 1200 μm), residue dose (0.001 – 50 g/L), contact time (2.5 – 60 min) and the percentage of nanoparticle impregnation (1:1, 1:2, 1:4) in the removal of caffeine and triclosan (30 mg/L). The results of the batch tests were fitted to the pseudo-first-order and pseudo-second-order kinetic models, as well as the Langmuir, Freundlich and Sips isotherm models. In the continuous adsorption tests, the adsorbents that presented higher efficiencies in the batch tests were tested. Both the corn cob (cellulose= 45.5 w/w.%) and the coconut fibers (lignin= 40.5 w/w%) have high contents of lignocellulosic material, low surface area (0.4 – 1.8 m^2/g) and a surface irregular with the presence of different functional groups (OH, C=O, C-O-H). Nanoparticles (size ~ 15 nm) present a relatively high surface area (66.3 m^2/g) but do not considerably increase the surface area of composites (1.4 – 2.2 m^2/g). The optimal doses for CC (0.3, 1.0 and 2.0 g/L) were lower than those for CF (1.0, 2.0, 4.0 g/L) for small, medium, and large particles, respectively; achieving triclosan removals between 85.3 and 92.6% for CC and between 47.1 and 81.0% for CF for, respectively. While the optimal dose of nanoparticles and composites was between 3.75 and 25 times lower than that determined for the CC. The optimal contact time was 20 min for the small CC particles and 30 min for the CC (medium, large), magnetite and composites. For CF it was 40 min (small) and 60 min (medium and large). The experimental data of CC, small and medium CF, magnetite and composites were adjusted to the pseudo-second-order model ($R^2= 0.89 - 0.99$) while the isotherm data for adsorbents, were fitted better to the Langmuir and Sips isothermal models ($R^2= 0.97 - 0.99$). In fixed bed columns, small particles show clogging, being the medium particles those that had better hydraulic behavior and a saturation time of 1400 and 70 min for triclosan and caffeine, respectively. The composite, as in the batch tests, presented better adsorption capacity than the raw CC (1.5 times for both contaminants). The experimental data of fixed bed columns were well-fitted to the Bohart-Adams model.

1. Introduction

In today's world, people produce, consume, and use widely pharmaceutical and personal care products. The residues/by-products of these chemical substances are part of the so-called emerging contaminants (ECs). ECs enter the environment in small quantities (ng/L – $\mu\text{g}/\text{L}$) continuously through the WRRF, since these facilities cannot eliminate them. Upon reaching the aquatic environment, ECs present a great potential for environmental risk (chronic toxicity, endocrine disruption and bioaccumulation) (Patiño et al., 2015) and even adverse effects on public health have been recorded (Gavrilescu et al., 2015).

Among the EC commonly found in different water resources are caffeine and triclosan. Caffeine is considered the most consumed psychoactive substance in the world because it has stimulating characteristics (Porthino et al., 2017). It is found naturally in about 60 plant species, of which the best known are coffee, cocoa, and tea leaves. Moreover, it is found in soft drinks, energy drinks and some drugs (Almeida-Naranjo et al., 2021a). The global average consumption of this substance is approximately 70 mg/person-day (Viviano et al., 2017), but it varies depending on the country. For example, in the US, its consumption is between 140 and 210 mg/person-day (Rodriguez del Rey et al., 2012). Between 0.5 and 10.0% of caffeine is not metabolized and it is excreted in the urine and feces, reaching the WRRF (Viviano et al., 2017). However, other sources of caffeine in wastewater are leftover beverages that are poured down the drain, along with utensil rinsing, which causes the caffeine concentration in wastewater to be approximately 20 to 300 µg/L (Sauvé et al., 2012). In treated effluents, it varies based on the level of treatment achieved between the processes (from primary to tertiary) which reach from 0.1 to 20 µg/L. Regarding surface water bodies (rivers, lakes and seas), the concentrations decrease, reaching concentrations between 0.003 to 1.5 µg/L (Busse & Nagoda, 2015; Dafouz & Valcárcel, 2017). The presence of caffeine in bodies of water has adverse effects, due to continuous exposure. This substance can alter different organisms, causing growth problems, bioaccumulation and behavioral alteration, triggering problems at the highest trophic levels (Rosi-Marshall et al., 2013; Dafouz & Valcárcel, 2017).

On the other hand, triclosan (a synthetic antimicrobial) is used in some personal care products such as deodorants, toothpaste, shampoo, lotions, body washes, and other products such as detergents and washing substances for dish/children's toys (Luo et al., 2019). Just as caffeine was found in WRRF effluents (European countries = 2 – 47,800 ng/L). Meanwhile in the USA, China and Japan it was found in surface waters (up to 2,300 ng/L, 500 ng/L and 365 ng/L, respectively) (Zhang et al., 2016). Triclosan has also produced toxic effects in different aquatic organisms, blocking the enzyme that transports proteins to aquatic organisms in algae (Zhang et al., 2021). In addition, during wastewater treatment processes, triclosan acts as a potential precursor for dioxins and halo chlorine disinfection byproducts (Zhang et al., 2016; Zhang et al., 2021).

Due to the potential risks of triclosan and caffeine to humans and the environment, their disposal from wastewater is critical. Different processes and technologies have been studied to reduce the concentration of both ECs in wastewater. In the removal of ECs, tertiary and advanced treatments are often used efficiently. However, these advanced technologies are rarely applied in WRRFs, due to the high implementation/operation/maintenance costs involved (Tejedor et al., 2020). The removal of caffeine and triclosan occurs through biological and physical-chemical processes. Within the latter, is the adsorption process (Wang et al., 2016).

Adsorption can be defined as a process in which different materials are used, where the contaminant is retained by molecular interactions, occupying the spaces of the adsorbent material and removing it from wastewater. The most commonly used material in the removal of ECs is activated carbon. However, its main disadvantage is its excessive cost of regeneration and disposal after its use (Thompson et al., 2016). Therefore, it has been necessary to search for alternative materials such as agro-industrial residues. These materials are found in abundance (1,549.42 x 10⁹ tons/year on a global scale) and have little or no commercial value (Almeida et al., 2021a). Among these are corn cob and coconut fiber, which have been tested to remove different contaminants from wastewater (e.g., dyes: acid red 40 ~ 95%, heavy metals: Cd ~ 81% and Cr VI > 95%, etc.) (Tokay & Akpınar, 2021). Both residues are characterized by their high content of hemicellulose (18 – 34%), cellulose (34 – 45%), and lignin (4 – 45%), biopolymers associated with the removal of ECs (Almeida-Naranjo et al., 2021a).

However, some agro-industrial residues have low adsorption capacity and separability from aqueous media. Both deficiencies will be enhanced with the impregnation of nanoparticles such as iron oxides since these nanoparticles have a greater specific surface area and magnetic character. Magnetic separation can be used in both small and large-scale wastewater treatment as it is a fast, efficient, and cost-effective method. Thus, magnetic compounds from an agro-industrial residue matrix could be an alternative for the removal of ECs (Ahmed et al., 2020). Magnetite (Fe₃O₄) is an iron oxide that is used in the adsorption of various types of contaminants (e.g., ECs=100 mg/g) due to its high surface area (between 30 and more than 200 m²/g), magnetic character, low-cost, non-toxic and the possibility of treating large volumes of wastewater (Zheng et al., 2018, Ahmed et al., 2020). On the other hand, magnetic compounds (agro-industrial residue + magnetite) have been used to remove heavy metals, dyes and some ECs, obtaining high efficiencies (e.g., brilliant black= 99%, methylene blue= 99%, diclofenac=80%) (Çatlıoğlu et al., 2020; Zheng et al., 2018).

Information on the use of corn cobs, coconut coir, magnetite nanoparticles, or their compounds in the removal of caffeine and triclosan is limited. Therefore, the objective of this work was to determine the adsorption capacity of these materials to remove caffeine and triclosan. Moreover, the kinetic and isothermal models in batch adsorption processes and the breakthrough curves in continuous adsorption were studied.

2. Materials and methods

2.1. Residue conditioning

Corn cob comes from a micro-enterprise that is dedicated to the preparation of humitas in Sangolqui city. However, corn comes from Loja city (location S 3° 59' 35.3", W 79° 12' 15.2"). Coconut fiber (CF) was obtained from Lomas de Sargentillo city (location S 1° 53' 00", W 80° 05' 00"). The residues were conditioned with the same methods used in Articles 1 and 2, obtaining three different sizes (120 – 150, 300 – 600, 800 – 2,000 μm).

2.2. Iron oxide nanoparticles and composites synthesis

Iron oxide nanoparticles were synthesized following the same procedure described in Article 3. After determining the best adsorbent between CC and CF, it was impregnated with iron nanoparticles (to form composites) in three residue/iron oxide weight ratios: 1residue:1IO, 2residue:1IO and 4residue:1IO. Composites were synthesized using the coprecipitation method just like in the case of banana/orange peel composites (Almeida-Naranjo, et al., 2021b).

2.3. Adsorption tests

2.3.1. Batch adsorption tests

The adsorption batch tests were performed using 100 mL Erlenmeyer flasks at room temperature (24 ± 0.35 °C), in dark conditions, to avoid the caffeine/triclosan photodegradation. A volume of 20 mL of aqueous solutions of 30 mg/L of caffeine (solvent: water) and triclosan (solvent: 0.01 M NaOH solution) were prepared. The caffeine/triclosan solution (30 mg/L) was stirred at 300 rpm for 20 seconds, to ensure uniform wettability of the adsorbent. To improve the dispersion of iron oxide nanoparticles, they were sonicated for 1 min at 70% of amplitude, using a Misonix sonicator S-4000 model. After this, the adsorption process was carried out at 150 rpm using different doses of each adsorbent (between 0.001 and 50 g/L). Each test was performed in triplicate and distilled water was used as a control system.

The optimal adsorption dose was determined for the adsorbents, using a contact time of 60 min. The optimal contact time was determined using the optimal dose of each adsorbent in times between 2.5 and 60 minutes. At the end of the test, to remove the adsorbent (CC, CF and composite), the samples were filtered using a 0.45 μm pore fiberglass filter. The iron oxide nanoparticles were magnetically separated from the aqueous medium.

2.3.2. Isotherm and kinetic study test

The data obtained from the adsorption kinetics and adsorption equilibrium isotherms were fit to the same models used in Articles 1 and 3, using equations from 1 to 7.

2.3.3. Fixed-bed columns

The fixed bed column tests were carried out using the residue (in its three particle sizes: 120 – 150, 300 – 600 and 800 – 2,000 μm) and the composite with the best adsorbent characteristics. Columns of high= 6 cm and diameter= 1 cm were used, they were packed with 4 and 5 cm of material. The residue/composite was washed with distilled water until the wash water was colorless. Columns were operated using the caffeine/triclosan solutions (30 mg/L) with hydraulic loads of 2 and 4 $\text{m}^3/\text{m}^2\text{-day}$, which are in the range of hydraulic loads used with commercial adsorbents such as granular activated carbon (Sandoval et al., 2011). The fixed-bed column tests were performed in duplicate.

Effluent-time concentration curves were used to evaluate the adsorption of caffeine/triclosan in a continuous adsorption process. The amount of caffeine/triclosan adsorbed at the breakthrough time (q_b) and saturation time (q_s) (mg/g) was calculated using (11) and (12) equations:

$$q_s = \frac{C_o * Q}{1000 * m} \int_0^{t_s} 1 - \frac{C_s}{C_o} \quad (11)$$

$$q_b = \frac{C_o * Q}{1000 * m} \int_0^{t_b} 1 - \frac{C_b}{C_o} \quad (12)$$

where C_o is the initial concentration of caffeine/triclosan (mg/L), C_b and C_s are the effluent concentration (caffeine/triclosan) at the breakthrough time and the saturation time, respectively (mg/L), Q is the volumetric flow (mL/min), m is the RH mass and t_b and t_s are the breakthrough and saturation time when C/C_o is respectively 0.1 and 0.9. The data obtained were fit to the non-linear Bohart-Adams model (13), due to its ease and rapid evaluation of adsorption performance (Peñafiel et al., 2021).

$$\frac{C_t}{C_o} = \frac{1}{1 + e^{\left(\frac{K_{BA} * N_o * h}{u} - K_{BA} * C_o * t\right)}} \quad (13)$$

where K_{BA} is the rate constant of the Bohart-Adams model (L/(min*mg)), N_o is the maximum adsorptive capacity (mg/L), h is the bed height (cm), t is the service time of the column (min), u is the linear flow velocity (cm/min), and C_t is the concentration at time t .

Also, the empty bed contact time (EBCT), the percentage of fractional bed utilization (%FBU), and the height of the mass transfer zone (h_{MTZ}) (cm) were calculated according to Peñafiel et al., 2021, using equations from 14 to 16, respectively:

$$EBTC = \frac{V_c}{Q} * 100 \quad (14)$$

$$\%FBU = \frac{q_b}{q_s} * 100 \quad (15)$$

$$h_{MTZ} = \left(1 - \frac{q_b}{q_s}\right) * h \quad (16)$$

Where V_c is the fixed-bed volume (L); Q is the flow rate (L/d) and V_b is the volume treated at breakthrough (L).

2.4. Analytical and instrumental methods

Physical-chemical characterization and instrumental analysis of CC and CF was carried out with the same ASTM standards and equipment described in the previous articles. An FTIR, Raman, BET and SEM characterization was performed on the composite, using the same equipment as that used for the characterization of magnetic fruit composites. Meanwhile, iron oxide nanoparticles were characterized using FTIR, Raman, BET, SEM, and transmission electron microscopy (TEM) with selected area electron diffraction (SAED). TEM analysis was performed to determine the shape and size of nanoparticles.

2.5. Statistical analysis

As in Articles 1-3, the optimal dose for each material particle size was determined by performing an ANOVA statistical analysis with a single factor analyzed by Tukey's test, with a significance level of 95.0%, using the Minitab 18 software version 1.0. The statistical analysis of data from kinetics (pseudo-first-order, pseudo-second-order, and Elovich), isotherm (Langmuir, Freundlich, and Sips), and Bohart-Adams non-linear models considered the calculation of means, standard deviation, error, and linear regressions using Microsoft Excel Solver version 2016. The coefficient of determination (R^2), the chi-square (χ^2), and the sum of squared errors (SSE) were calculated (equations 8-10 and 16-18) to determine the models that best fit the caffeine and triclosan adsorption data:

$$R^2 = 1 - \frac{\sum(V_{e,exp} - V_{e,cal})^2}{\sum(V_{e,exp} - V_{e,mean})^2} \quad (16)$$

$$\chi^2 = \sum \frac{(V_{e,exp} - V_{e,cal})^2}{V_{e,cal}} \quad (17)$$

$$SSE = \sum (V_{e,exp} - V_{e,cal})^2 \quad (18)$$

where $V_{e,exp}$ are the experimental value of parameters (q , C_t/C_0 for batch tests and fixed-bed columns, respectively), $V_{e,cal}$ are the calculated parameters using the Solver tool, $V_{e,mean}$ is the mean of $V_{e,exp}$ values (Nguyen et al., 2021).

3. Results and Discussion

3.1. Material characterization

3.1.1. Physical-chemical characterization of residues

Table 21 shows the physical-chemical characterization of CC and CF. Results evidenced that CF had the highest lignin ($40.5 \pm 0.5\%$ w/w) and the lowest hemicellulose ($19.8 \pm 0.3\%$ w/w) content, meanwhile CC reported the highest cellulose ($45.5 \pm 1.0\%$ w/w) and hemicellulose ($33.3 \pm 0.8\%$ w/w) content. According to Mo et al. (2018) and Pode (2016) lignocellulosic compounds, from agro-industrial residues generate a fibrous and porous structure with the presence of several functional groups (e.g., methoxy, methyl, hydroxyl, phenolic, ether and carboxyl), that provide to agro-industrial residues good adsorbent characteristics. However, a higher lignin content favors the contaminant removal process through adsorption processes. Therefore, CF can be expected to have a higher caffeine/triclosan adsorption capacity than CC, due to its higher lignin concentration. However, the CF adsorption capacity could be affected by the presence of extractives. Extractives could reduce the active sites of CF (Chowdhury et al., 2011).

Table 21. Physical-chemical characteristics of residues.

Parameter	Unit	Adsorbent	
		CC	CF
Lignin		15.4±0.2	40.5±0.5
Cellulose		45.5±1	28.3±0.6
Hemicellulose	% w/w.	33.3±0.8	19.8±0.3
Water extractives		1.6±0.1	4.4±0.1
Ethanol-toluene extractives		1.1±0.1	4.3±0.2

3.1.2. Instrumental characterization of materials

3.1.2.1. SEM, TEM and BET analyses

The results of the BET analysis are shown in Table 22. The values of the surface area and pore volume are relatively low in both CC and CF, which is characteristic of agro-industrial residues. This is due to the presence of polysaccharides and other substances (Almeida-Naranjo et al., 2021). The surface area of the CF is comparable with previous studies that report a surface area <2 m²/g, such as that of Brito Pires et al. (2020), in which the CF presented an area of 1.54 m²/g. Likewise, the CC surface area is inside the range obtained by other authors (0.4 – 0.78 m²/g) (Hoang et al., 2019; Pezhhanfar et al., 2021).

Figure 30 shows the SEM images of CF and CC. The SEM image of CF shows a large number of globular protuberances that are embedded in the surface of the fiber, the same ones that are known as "tylides" (Rout et al., 2001). The surface of the CC also presents heterogeneous pores and cavities (Pezhhanfar et al., 2021). The irregular and porous surface of CF and CC could favor the removal of triclosan.

Iron oxide nanoparticles have a relative high surface area, this is associated with their small size (around 15 nm); this size was determined by TEM analysis (Figure 31c). Iron nanoparticles have a cubic shape and their size is comparable to that of nanoparticles synthesized by Braga et al., (2121). Despite this, probably the specific surface area and pore volume of these nanoparticles could be higher but they present clumping, this can be noted in Figure 31b and the SEM analysis (better quality) of the 4CC:1IO composite (Figure 31a). This is a problem of magnetic nanoparticles; therefore, it is important to improve their dispersion in the composite synthesis.

On the other hand, CC composites present a higher surface area and pore volume than CC. According to Ahmed et al., (2020); Çatlıoğlu et al., (2021); Çatlıoğlu et al., (2020); Panneerselvam et al., (2011), this is due to the presence of the iron oxide nanoparticles (around 66 m²/g). The surface area of CC is similar to the surface area of magnetic moringa (2.14 m²/g), but magnetic CC has a lower pore diameter and pore volume than magnetic moringa. This difference could be because the moringa was chemically/thermally treated before the impregnation of the iron oxide nanoparticles (Cusioli et al., 2021).

In the SEM images of the composites, the presence of nanoparticles (small white dots) is observed, this suggests a good formation of the composites (Cusioli et al., 2021). Similar images (presence of small particles on the surface of the matrix) can be seen in the studies carried out by Almeida-Naranjo et al. (2021b) and Hoang et al. (2019) in which they used fruit peels and biochar from CC, respectively.

In the composite 2CC:1IO it is observed (Figure 30) that the distribution of the nanoparticles is not homogeneous, even the presence of agglomerations can be seen. This reduces the surface area and pore volume relative to the 1CC:1IO composite. In the case of the 4CC:1IO composite, there is a slight increase in the surface area compared to the 1CC:1IO composite. This increase may be because there are more nanoparticles in the 1:1 composite, and there is a greater probability that they will agglomerate, and the agglutinated nanoparticles (being larger particles) in addition to having a smaller area (than without agglutination) can clog the pores of the CC. Hoang et al. (2019) report a 1.9-fold increase in the surface area of biochar from CC when impregnating 20 w/w.% magnetic nanoparticles, this increase is similar in this study. These results suggest that the 1CC:1IO composite would be the most efficient in contaminant removal due to its larger specific surface area.

Table 22. BET analysis of materials

Parameter	Units	Adsorbent						
		CF (120 – 150 µm)	CC (120 – 150 µm)	CC (800 -2,000 µm)	1CC:1IO	2CC:1IO	4CC:1IO	IO NPs
Specific surface area	m ² /g	1.8	1.1	0.4	2.0	1.4	2.2	66.3
Pore volume (x10 ⁻³)	cm ³ /g	4.1	4.1	1.1	7.8	5.3	7.9	276.2
Pore diameter	nm	3.4	4.2	3.4	9.3	3.4	3.4	11.9

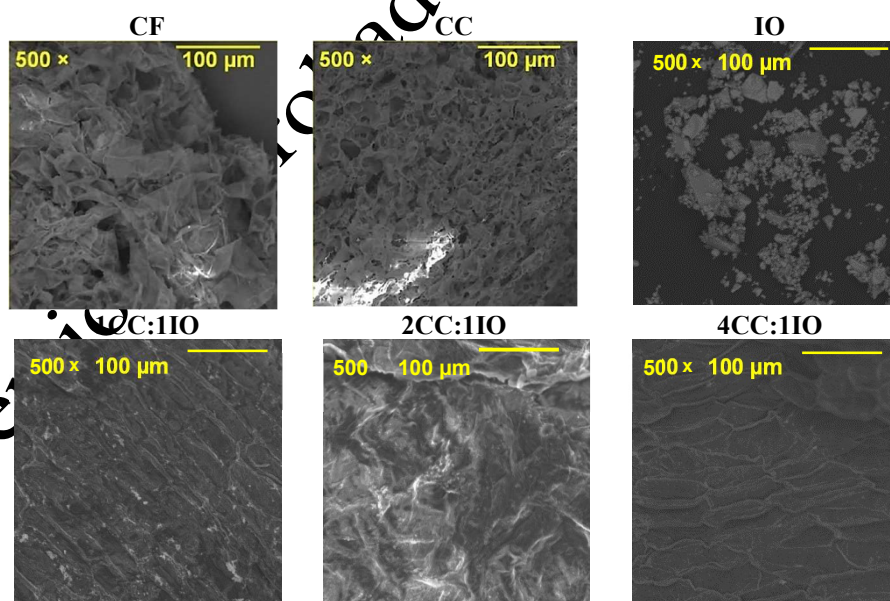


Figure 30. SEM images of residues, iron oxide nanoparticles and CC composites

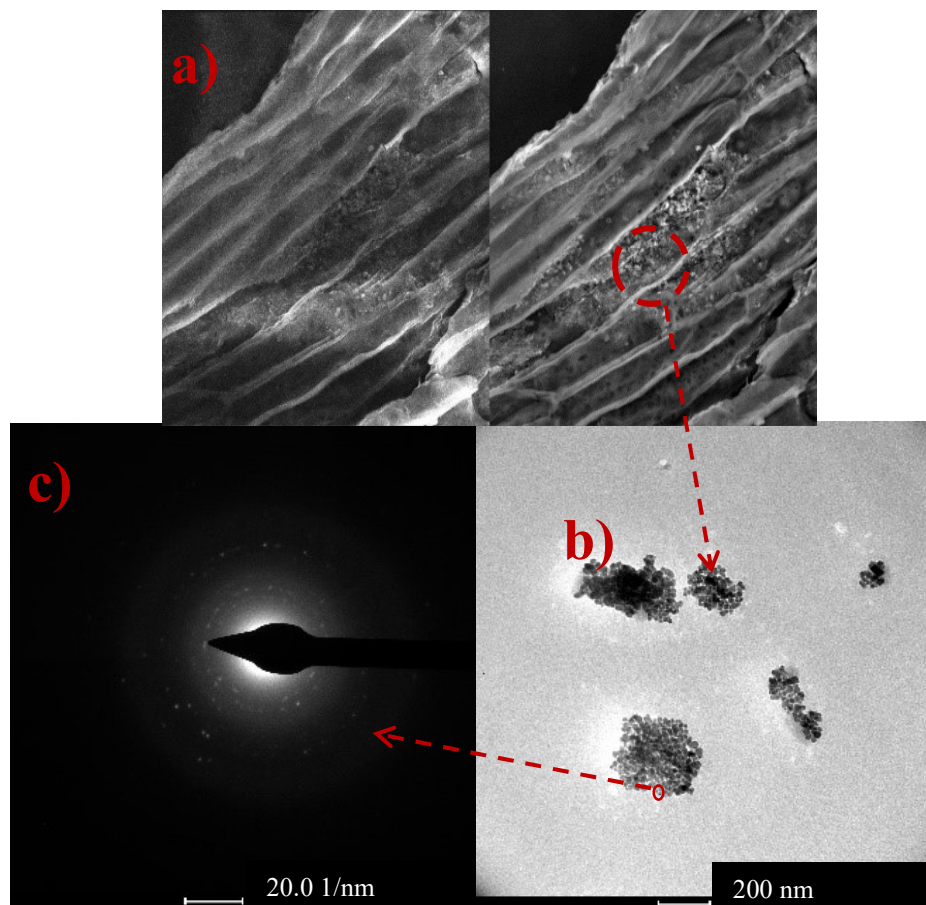


Figure 31. a) SEM composite 4CC:1IO, b) TEM iron oxide nanoparticles and c) SAED of iron oxide nanoparticles.

3.1.2.2. FTIR and Raman analyses

Figure 32a shows the FTIR spectra for residues, iron oxide nanoparticles and CC composites. CF and CC present intense bands around 3250 cm^{-1} . They are characteristic of hydroxyl groups (OH^{\cdot}). The bands around 2900 cm^{-1} correspond to the C-H vibrations of the stretch methyl (CH_3), methylene (CH_2), and methoxy groups (O-CH_3), main components of lignin. The bands around 1700 cm^{-1} are characteristic of the carbonyl group ($\text{C}=\text{O}$ bond stretch), they represent the presence of aldehydes, ketones and the carbonyl ester group. The bands around 1600 cm^{-1} ($\text{C}=\text{C}$ bond stretch) show the presence of benzene, aromatic rings, or amino acids. Around 1400 cm^{-1} there is the band of the vibration of the aromatic ring of lignin (Almeida-Naranjo et al., 2021a). The bands around 1000 cm^{-1} represent the C-O group from alcohols, phenols and carboxylic acids that belong to hemicellulose, cellulose and lignin (Alaa El-Din et al., 2018; Dahid et al., 2018).

In iron oxide nanoparticles, there were a small band around 3500 cm^{-1} , typical of hydroxyl groups. The bands around 1600 and 1100 cm^{-1} are attributed to the vibration of the carboxylate/amide groups and the stretching vibration of C-OH and C-O, respectively. Meanwhile, the band around 550 cm^{-1} is related to the stretching vibration of iron oxides (Fe-O bonds) evidencing the presence of the magnetic particles (Almeida-Naranjo et al., 2021b).

On the other hand, the FTIR spectra for the composites show that the bands of CC are maintained. However, the intensity of bands of OH- and C-H groups were reduced due to the reactions produced in the nanoparticle impregnation process. Something similar (a decrease) occurs with the band of the $\text{C}=\text{O}$ group. The bands around 500 cm^{-1} , for composites, showed the presence of Fe-O iron oxides (Gupta & Nayak, 2012; Panneerselvam et al., 2011). The presence of the functional group's characteristics of lignocellulosic compounds and in the iron oxides suggest that the materials could be good adsorbents.

Figure 32b shows the Raman spectra for the iron oxide nanoparticles and CC composites. They show the presence of magnetite bands: around 193 (weak), 306 (weak), 538 (weak) and 668 (strong) cm^{-1} , similar

bands were found in the three composites. However, in nanoparticles and composites there are other bands belonging to maghemite, formed from the oxidation of magnetite (around 350, 500 and 700 cm^{-1}) (Slavov et al., 2010). Therefore, the iron oxide nanoparticles (alone and in composites) are composed of a mixture of magnetite and maghemite particles. The other bands in the composites are attributed to the CC (residue presence) (Almeida-Naranjo et al., 2021b).

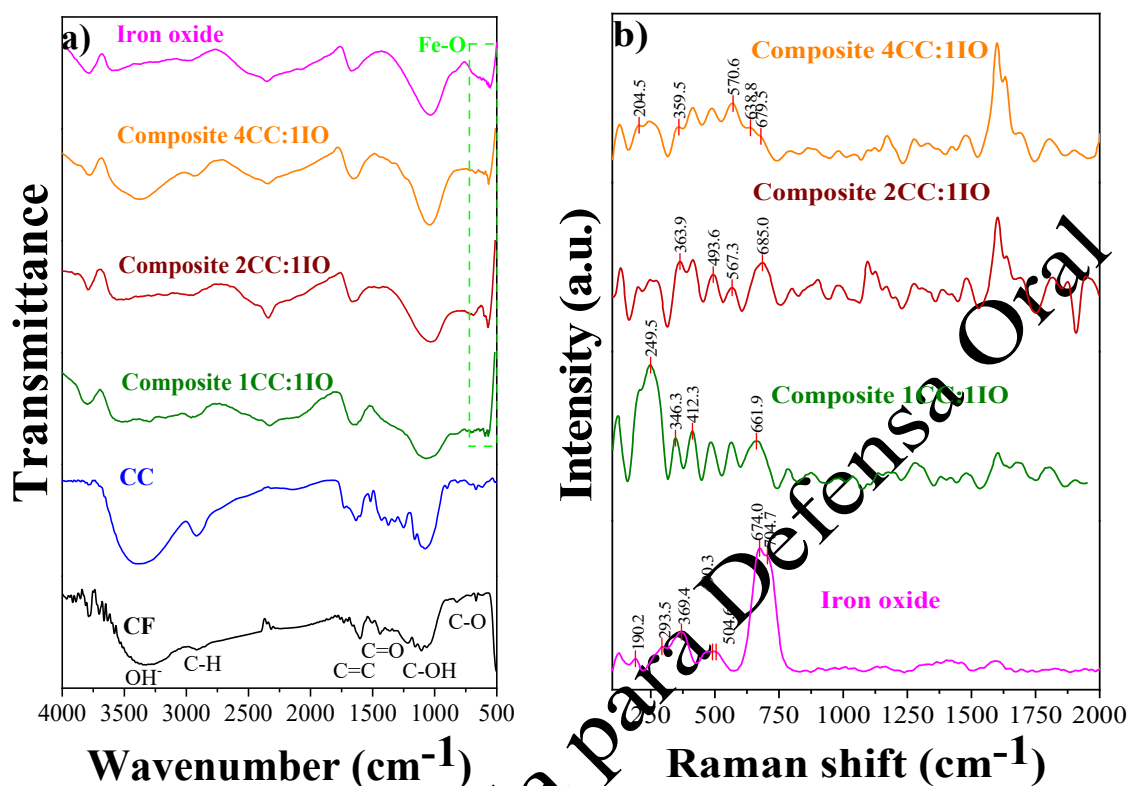


Figure 32. a) FT-IR and b) Raman spectra of the materials studied.

3.2. Optimal batch adsorption conditions using CC and CF for triclosan removal

Figure 33a presents the relationship between the increase in the adsorbent dose and the contact time with respect to the triclosan removal. The optimal doses of CC (0.3, 1.0 and 2.0 g/L) were lower than those of CF (1.0, 2.0, 4.0 g/L) for small (120 – 150 μm), medium (300 – 600 μm) and large particles (800 – 2,000 μm), respectively. Initially until reaching the optimal dose, an increase in the dose of the adsorbents (for the three particle sizes) favored the triclosan removal, reaching efficiencies between 85.3 and 92.6% for CC and between 47.1 and 81.0% for CF. By increasing the amount of the adsorbents, their amount of active sites and their surface area increase (Yanxia Li et al., 2019). However, doses higher than the optimal decrease the triclosan removal between 8.5 and 21.0, and between 3.9 and 66.5% for CC and CF, respectively. An excess of CC or CF could cause interaction between their particles generating agglutination and therefore the decrease of the surface (overlapping of the adsorption sites) that will be in contact with triclosan (Mohd-Khori et al., 2018; Żóltowska-Aksamitowska et al., 2018).

On the other hand, the optimal contact time (Figure 33b) for the triclosan removal was 20 min for the small CC particles, and 30 min for the medium and large particles of CC. Meanwhile the optimal contact time using CF was higher, specifically 40, 60, and 60 min for the small (120 – 150 μm), medium (300 – 600 μm) and large particles (800 – 2,000 μm), respectively. Therefore, CC is more efficient than CF, which is attributed to the higher (3.2 times) extractives concentration of CF, as mentioned before (Almeida-Naranjo, et al., 2021a).

The effectiveness in the triclosan removal by the small CC particles could be attributed to the larger pore size compared to the small CF particles. An adsorbent with a larger pore size will allow the triclosan (molecule size = 1.42 x 0.69 x 0.75 nm) to have greater access to the inner pores (Triwiswara et al., 2020a).

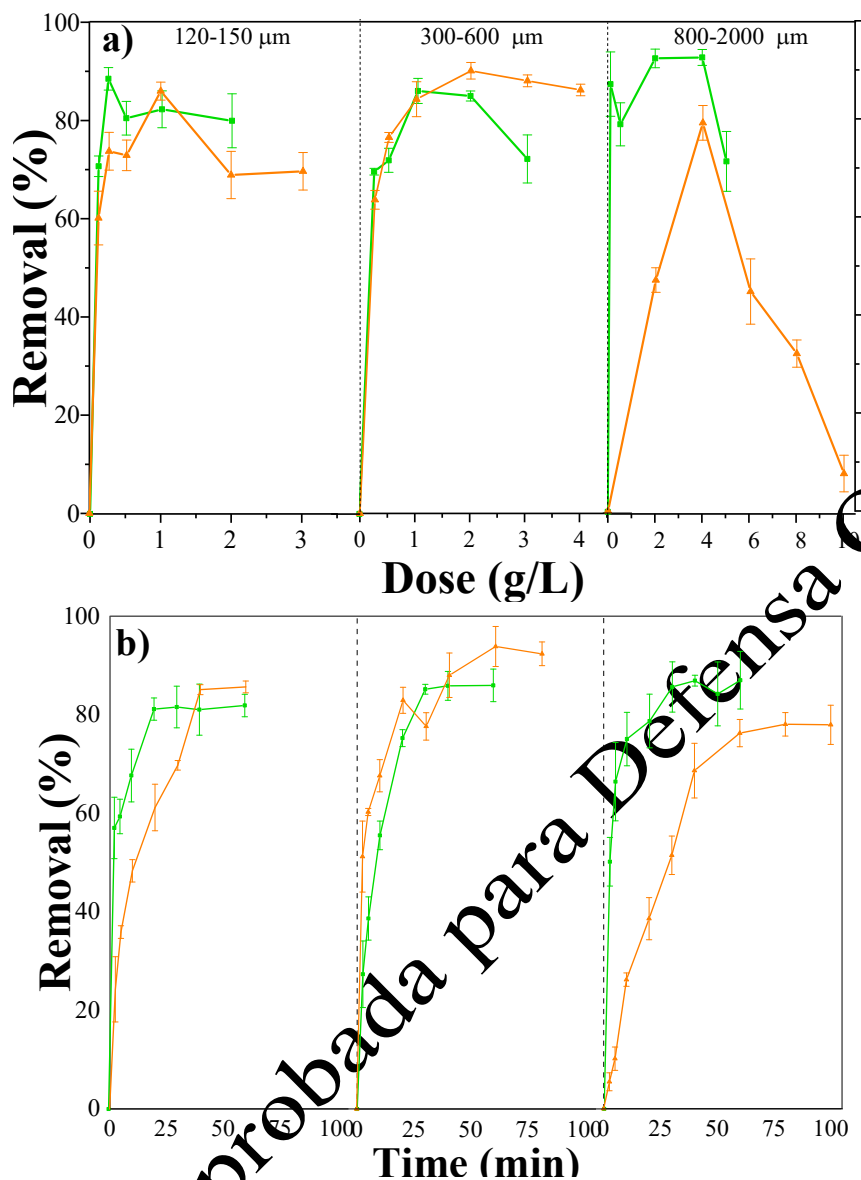


Figure 33. Optimal adsorption conditions for triclosan adsorption. a) Optimal dose, b) Optimal contact time. Green line: CC adsorption, orange line: CF adsorption.

3.3. Batch adsorption tests

3.3.1. Kinetics using CC and CF for triclosan removal

Table 27 shows the fittings for pseudo-first and pseudo-second-order non-linear models used to describe the experimental adsorption kinetics data. The kinetics data for small (120 – 150 μm) and large (800 – 2,000 μm) particles of CC were better fitted to the pseudo-second-order model ($R^2 = 0.985, 0.988$, respectively). Indeed, the experimental value of Q_e is near to the Q_e of the pseudo-second-order model. In the case of CF, the small (120 – 150 μm) and medium (300 – 600 μm) particles were better fitted also to the pseudo-second-order model ($R^2 = 0.889-0.988$). In spite of, the experimental Q_e value of small CF is near to the Q_e of pseudo-first-order model, so small CF fitted to pseudo-first-order model. The triclosan adsorption in the CC and CF that fit to pseudo-second-order model is controlled by an electron sharing/exchange between CC/CF functional groups and triclosan molecules (chemisorption processes) (Beltrame et al., 2018). Other studies proved that triclosan kinetics adsorption data were fitted to the pseudo-second-order model, the adsorbents used were graphene and multi-walled carbon nanotubes (F. Wang et al., 2017; Zhou et al., 2013). Meanwhile, medium CC (300 – 600 μm) and large CF (800 – 2,000 μm) adsorption data were fitted to pseudo-first-order model ($R^2 = 0.995$ and 0.985 , respectively). Additionally, the experimental Q_e value of both residues is near to the Q_e of pseudo-first-order model, this

suggest that the adsorption of triclosan is produced by a physisorption process. Other adsorbents, such as rice husk modified thermally and activated carbon used in the removal of triclosan also fitted data to pseudo-first-order kinetics model (Triwiswara et al., 2020a; F. Wang et al., 2017).

Table 23. Parameters for the kinetics models fitted for the data obtained for triclosan removal using to the CC and CF.

Models	Adsorbent	CC			CF		
	Size (μm)	120 – 150	300 – 600	800 – 2,000	120 – 150	300 – 600	800 – 2,000
	Q_e exp. (mg/g)	81.307	26.561	13.005	23.742	13.431	5.191
Pseudo-first-order	Q_e (mg/g)	78.464	26.975	12.223	24.408	13.007	6.394
	K_1 (min^{-1})	0.408	0.112	0.422	0.089	0.273	0.033
	R^2	0.675	0.995	0.657	0.929	0.750	0.985
	χ^2	0.444	0.013	0.076	0.180	0.106	0.018
	SSE	226.006	1.799	6.067	21.426	9.841	0.605
Non-linear pseudo-second-order	Q_e (mg/g)	83.450	31.970	13.190	29.389	14.058	8.559
	K_2 (g min mg^{-1})	0.008	0.004	0.050	0.003	0.029	0.008
	R^2	0.889	0.988	0.955	0.969	0.906	0.955
	χ^2	0.151	0.033	0.009	0.077	0.039	0.031
	SSE	77.066	4.633	0.111	9.342	3.690	1.017

Q_e exp.= Q_e experimental value

3.3.2. Adsorption isotherms using CC and CF for triclosan removal

The Langmuir, Freundlich and Sips non-linear models were used to study the adsorption of triclosan on the CC and CF particles; the isotherm data are presented in Table 24. Langmuir's model assumes that the adsorbent has active sites with the same energy (homogeneous surface) and the triclosan adsorption would occur in a monolayer without lateral interaction. Freundlich's model considers that active sites have different energy (heterogeneous surface) and that adsorption occurs in multilayers. Meanwhile, the Sips model is a combination between the Langmuir and Freundlich models (Sahoo & Prelot, 2020).

The isotherm data for CC and CF, in their three particle sizes, have a higher correlation factor with the Langmuir and Sips isothermal models with values of correlation coefficients (R^2) between 0.971 and 0.999. The values of K_L (Langmuir) and $1/n$ (Freundlich) are lower than 1, so the triclosan adsorption is favorable in the three particles size of both residues (Nguyen et al., 2021). Furthermore, lower values of SSE (0.12–8.12) and χ^2 (0.005–0.031) were achieved for both models, while higher values were achieved for the Freundlich model SSE (1.61–20.15) and χ^2 (0.045–0.297). Likewise, the adsorption capacity values obtained from the Langmuir and Sips models are close to the values of the experimental adsorption capacity. Therefore, the results suggest that the triclosan adsorption takes place onto a homogeneous surface. Other residues such as thermally modified rice husk at 300°C and sewage sludge biochar also fit the Langmuir model when used in triclosan removal (Czech et al., 2021; Triwiswara et al., 2020a).

Table 24. Isotherm model using CC and CF in the triclosan removal

Isotherm model	Parameter	Unit	Adsorbents					
			CC size (μm)			CF size (μm)		
			120 – 150	300 – 600	800 – 2,000	120 – 150	300 – 600	800 – 2,000
Langmuir	q_m	[mg/g]	285.556	92.081	16.383	96.929	20.930	7.854
	K_L	[L/mg]	0.1153	0.122	0.958	0.078	0.895	0.307
	R^2	-	0.999	0.999	0.989	0.999	0.980	0.971
	χ^2	-	0.006	0.009	0.014	0.004	0.031	0.017
	SSE	-	4.013	1.709	0.856	0.670	2.776	0.4344
Freundlich	K_F	$[(\text{mg/g})^{1-1/n}]$	40.243	11.786	8.495	8.689	10.414	2.652
	$1/n$	-	0.565	0.647	0.220	0.685	0.229	0.315
	R^2	-	0.986	0.994	0.850	0.997	0.889	0.891
	χ^2	-	0.297	0.045	0.188	0.024	0.173	0.064
	SSE	-	20.148	8.432	11.263	4.132	15.478	1.612
Sips	q_m	[mg/g]	293.076	117.278	16.499	96.890	20.084	7.627
	K_L	[L/mg]	0.109	0.072	0.946	0.075	0.959	0.326
	$1/n$	-	0.971	0.919	0.973	0.966	0.809	1.081
	R^2	-	0.999	0.994	0.989	0.999	0.984	0.972
	SSE	-	3.557	8.121	0.844	1.346	2.223	0.422

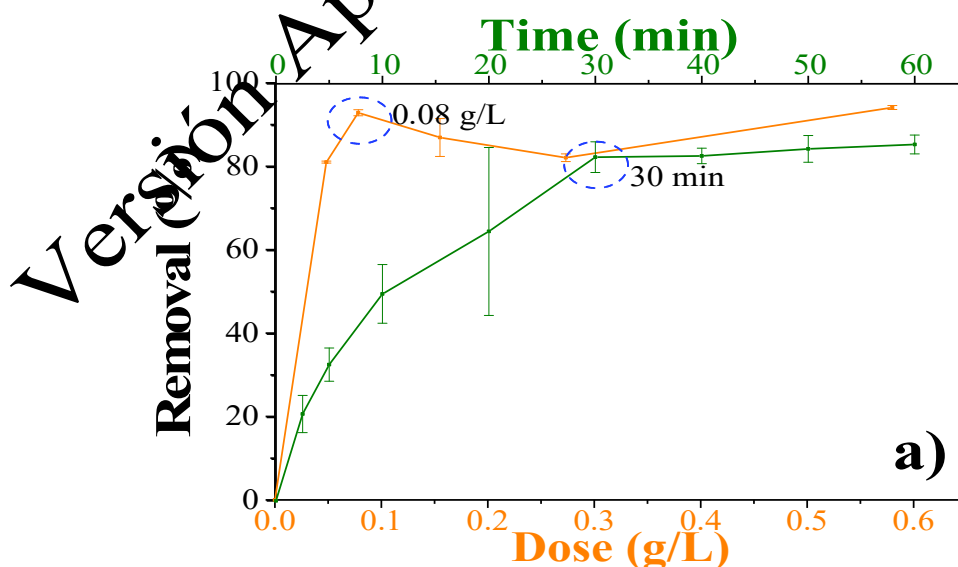
Before presenting the results obtained, it is important to indicate which is the residue that will be used in the composites, despite its characterization was already presented in the previous point. Corn is a very important crop in Ecuador (dry corn production is greater than 1 million tons) (Martillo-Aseffe et al., 2020) since it is produced in the 4 regions of the country, mainly in the Coast (hard corn= 300,000 hectares planted) and Sierra (soft corn=67,000 ha planted) (Nopsa-Hernández, 2019). Corn harvest residues (leaves and stems) are used as feed for livestock, while gophers are left in the field or burned in the open. Few documented studies are related to its energy use (Martillo-Aseffe et al., 2020).

On the other hand, coconut is grown only in the coastal region, mainly in the provinces of Esmeraldas and Manabí. Considering also that CC had better adsorbent characteristics, it was decided to use CC as the matrix of the composites. In addition, the largest CC (800 – 2,000 μm) was used because it presented lower efficiency than the other two particle sizes and therefore the impregnation would increase its adsorption capacity. Furthermore, the use of this particle size in continuous adsorption processes can also avoid clogging problems inside the column. Small particles could cause a hydraulic malfunction of the fixed bed columns because they produce poor hydraulic conductivity and thus higher head losses and a decrease in the efficiency of contaminant removal (Le et al., 2020).

3.3.3. Optimal dose and adsorption time for triclosan removal with iron oxides and CC composites

Figure 34 shows the optimal dose/contact time for the triclosan removal using iron oxides and CC composites. The optimal dose of nanoparticles and composites is lower (between 3.75 and 25 times) than that determined for the CC. This is because nanoparticles and composites have higher specific surface area and different functional groups (Table 22). An increase in the specific surface area favors the adsorption capacity, due to the presence of more active sites (Noreen et al., 2013). The optimal dose of the composites is almost twice that of the nanoparticles; however, it is also less than that of the CC alone. In other words, the presence of nanoparticles favors the removal of caffeine/triclosan. Despite this, the 1CC:1IO composite requires a higher dose of material, a greater number of nanoparticles implies that they could be occupying the active sites of the matrix (CC) or, in turn, a greater number of particles generate a greater attraction of them and therefore an agglutination process. On the other hand, the other composites need the same quantity, the efficiencies achieved (2CC=87.84 \pm 1.80 and 4CC=86.28 \pm 1.40) don't show statistical differences (p value<0.05). The optimal contact time was 30 min for all materials.

Braga et al. (2011), obtained removal efficiencies (89.7-96.5%) slightly higher than those obtained using doses between 0.01 and 0.05 g/L and triclosan solutions of 10 mg/L. While using 0.8 g/L of core-shell structured magnetic covalent organic framework nanocomposites, efficiencies greater than 90% were achieved. Triclosan solutions had a concentration of 1 mg/L (Yanxia Li et al., 2019).



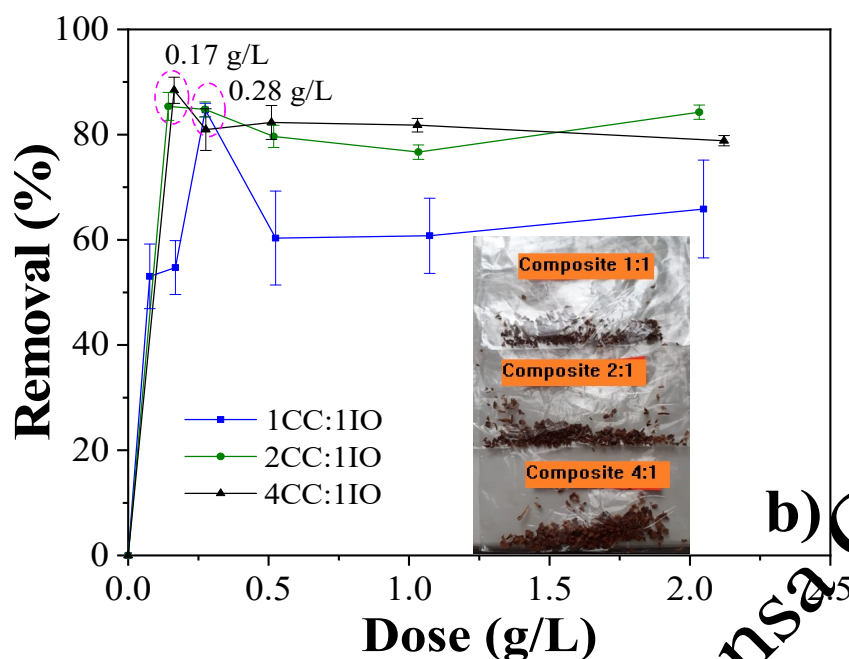


Figure 34. a) Optimal contact time and optimal dose using iron oxide nanoparticles, b) Optimal dose using CC composites; for the triclosan removal

3.3.4. Kinetics and isotherm model for triclosan removal with iron oxide and CC composites

Figures 35 and 36 present the fittings to the kinetics and isothermal models that followed the experimental data obtained in the removal of triclosan using iron oxide nanoparticles and composites, respectively. The adsorption of triclosan with magnetite (Figure 35a) fitted better to the pseudo-second-order model ($R^2=0.951$). Similarly, the three CC composites fitted better to the pseudo-second-order model, presenting the highest R^2 (between 0.921 and 0.977) (Figure 36a).

The pseudo-second-order model that fits the triclosan adsorption onto iron oxide nanoparticles and composites suggest a chemisorption and more than one-step may be involved in sorption, as explained by Almeida-Naranjo et al. (2021b). Moreover, χ^2 and SSE were lower in the pseudo-second-order model. The adsorption of triclosan on the adsorbents is rapid over the first 10 min of contact time; then it remains constant as the contact time increases. This could indicate that the adsorption process is carried out by strong chemisorption or strong surface complexation (M. Liu et al., 2011). This is because triclosan is gathered on the adsorbent surface as the time progresses, as explained by Sharif et al. (2018). A rapid adsorption of triclosan onto adsorbents within 10 min is due to the availability of a large number of vacant sites on them (Castro et al., 2021). Other magnetic materials used in triclosan removal also fit a pseudo-second-order kinetic model. Using the core-shell structured magnetic covalent organic framework nanocomposites, the authors associate the pseudo-second-order model with an adsorption process that can be divided into two steps. The first was dominated by a diffusion process through Van der Waals forces that occurred in the first 10 minutes, while the second step was dominated by special intermolecular interactions of the π - π stacking of the benzene ring between triclosan and the magnetic composite, and a space embedding effect of triclosan on the mesoporous surface (Yanxia Li et al., 2019).

Meanwhile, regarding the isotherm models: triclosan adsorption fits better to Sips model (Figure 35b) using iron oxide nanoparticles ($R^2= 0.996$), composites 2CC:1IO and 4CC:1IO fit better to Langmuir and Sips models ($R^2= 0.989-0.998$), and composite 1CC:1IO was fit to Langmuir and Freundlich ($R^2= 0.999$) models (Figure 36b). In composites 2CC:1IO and 4CC:1IO the R^2 values for Langmuir and Sips models are very close, but the χ^2 values were lower for the fittings to the Sips models. As a result, the isotherms for these composites were considered better fitted to the Sips model. Sips model, which follows a combination of Freundlich and Langmuir isotherm models. Low triclosan concentrations correspond to the Freundlich isotherm, meanwhile high concentrations predicts a monolayer adsorption capacity (Langmuir model) (Rajput et al., 2016). In the case of composite 1CC:1IO, present the same values for R^2 and χ^2 , This means that there is a fit to both models, initially a monolayer adsorption occurs and over time a multilayer is formed (Almeida-Naranjo et al., 2021b). Moreover, K_L values in the Langmuir model and

1/n (Table 25) in the Freundlich model, show a value less than 1, which indicates that the adsorption was favorable both in the composites and in the iron oxide nanoparticles (Nguyen et al., 2021).

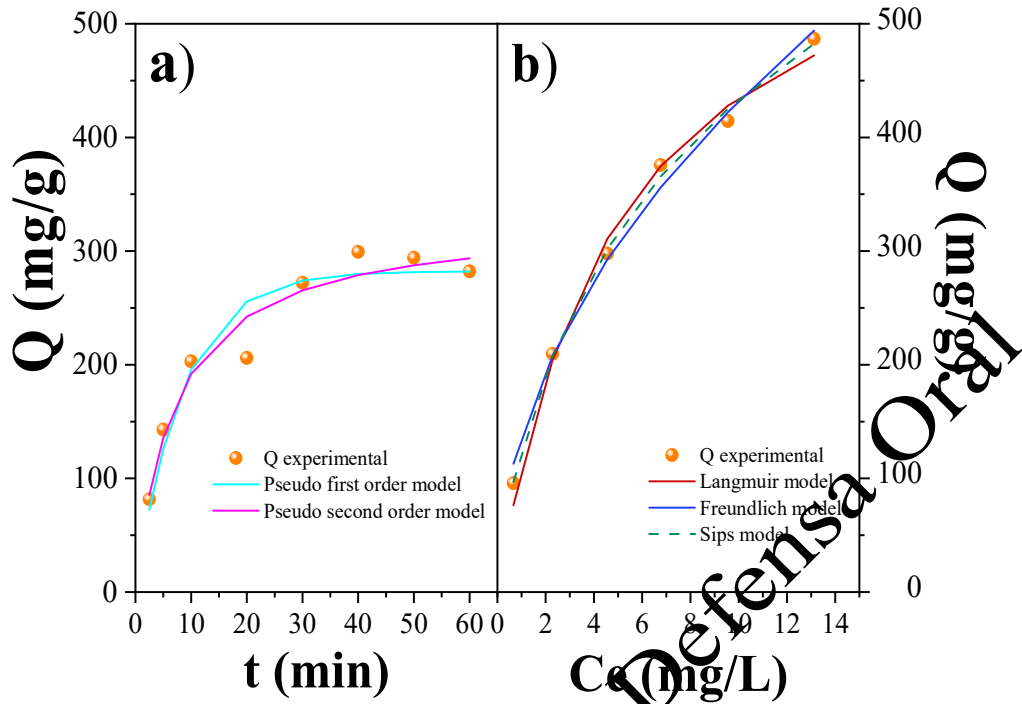
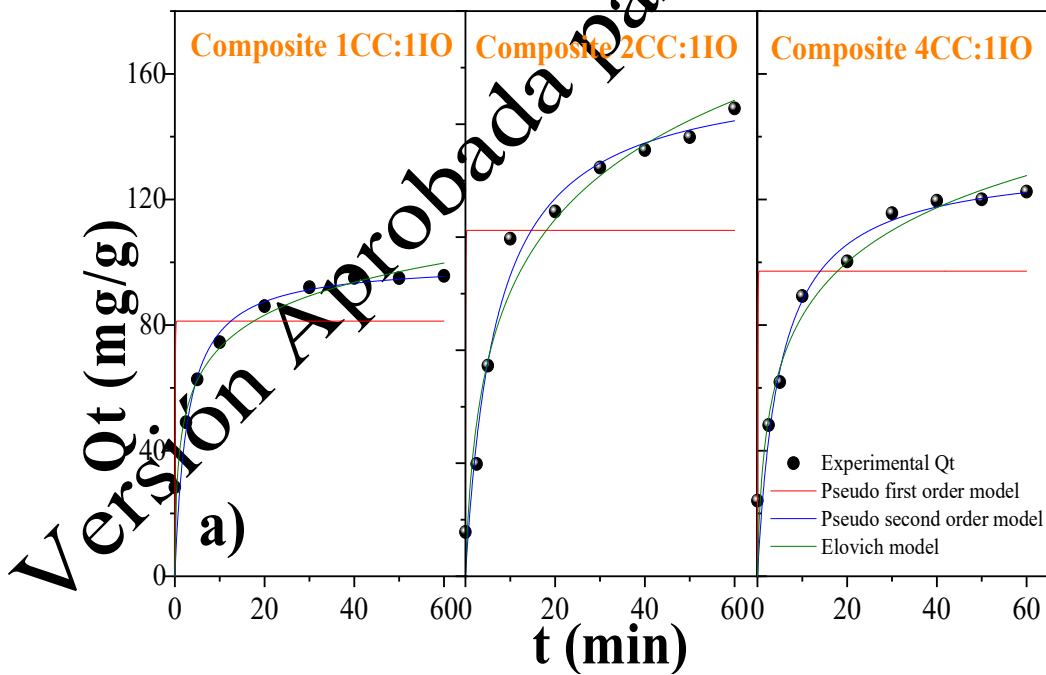


Figure 35. a) Kinetics model fitting, b) isotherm model fitting for triclosan removal using iron oxide nanoparticles.



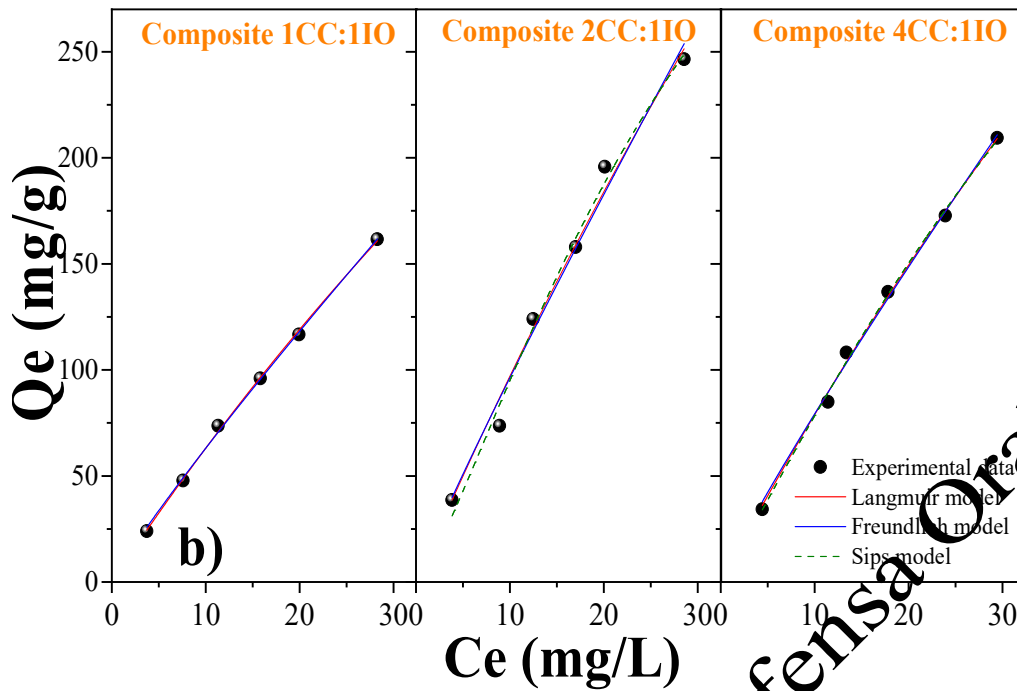


Figure 36. Fittings to the (a) kinetics, and (b) isotherm models for triclosan removal using CC composites.

Table 25. Parameter values for the kinetics and isotherm models fitted to the data about triclosan removal using iron oxide and composites.

Material			IO	1CC:1IO	2CC:1IO	4CC:1IO		
Models	Parameter	Units						
Kinetics models	Pseudo-first-order	Q_e	[mg/g]	282.268	81.261	110.162	97.165	
		K_1	[min ⁻¹]	0.118	15.948	21.024	18.833	
		R^2	-	0.921	0.362	0.419	0.398	
	Pseudo-second-order	K_2	[g*min/g]	1.951	422.458	1582.442	901.198	
		K_2	[mg/g]	328.400	100.064	161.693	132.632	
		K_2	[g*min/g]	4.284×10^{-4}	0.003	8.992×10^{-4}	0.001	
Isotherm models	Langmuir	R^2	-	0.951	0.921	0.977	0.937	
		χ^2	-	1.204	118.574	62.147	93.662	
		q_m	[mg/g]	652.141	1057.970	1765.48	1373.244	
		K_L	[L/mg]	0.200	0.006	0.006	0.006	
		R^2	-	0.990	0.999	0.989	0.997	
		χ^2	-	0.522	3.311	85.121	634.617	
	Freundlich	K_F	[(mg/g) ^{1-1/n}]	138.207	7.839	11.489	9.841	
		$1/n$	-	0.495	0.876	0.923	0.906	
		R^2	-	0.992	0.999	0.983	0.999	
		χ^2	-	0.432	3.311	100.470	0.672	
		Sips	q_m	[mg/g]	1007.53	86.677	561.118	765.451
			K_L	[L/mg]	0.068	0.941	0.029	0.014
$1/n$	-		0.723	78.125	1.300	1.100		
R^2	-		0.997	-3.659×10^{-10}	0.992	0.998		
χ^2	-		0.138	4069.357	83.690	15.700		

In addition to the pseudo-first and pseudo-second-order models, a diffusion analysis was performed. This is because several ECs have been shown to adjust to this process when adsorbed on agro-industrial residues (Tran et al., 2017). For which the data obtained in the experiments were adjusted to this model (equation 19).

$$q_t = k_p \sqrt{t} + C \quad (19)$$

Table 26 shows the parameters for the intraparticle diffusion model. As mentioned in Article 1, if the curve q_t versus $t^{1/2}$ passes through the origin, then the adsorption process is limited only by intraparticle diffusion. However, Figure 37 shows two linear zones, indicating that the adsorption process is controlled by a two-step mechanism. In the first stage, triclosan is transported from the aqueous medium to the external surface of the adsorbents (CC, IO, and their composites) through the hydrodynamic boundary layer, that is, film diffusion occurs. In the second stage, a slow diffusion (intraparticle diffusion) of the triclosan molecules occurs from the outside of the adsorbent towards its pores. In the final stage, triclosan is rapidly adsorbed into the pores of the adsorbent (Tran et al., 2017). Moreover, in the first linear zone, it is observed that the highest intercept value (C) is presented by the IO nanoparticles and decreases as the CC content increase. This indicates that the contribution of surface adsorption is greater when IO is presents.

Table 26. Parameter values for intraparticle diffusion model fitted to the data about triclosan removal using CC, iron oxide and composites.

Parameters		CC	IO	1CC:1IO	2CC:1IO	4CC:1IO
Intraparticle diffusion	K_{p1} [mg/(g min ^{1/2})]	1.027	38.159	12.418	19.298	18.580
	C_1 [mg/g]	7.320	42.005	32.540	27.841	21.698
	D_i [cm ² /s]	2.000x10 ⁻⁶	5.627x10 ⁻¹⁷	2.000x10 ⁻⁶	8.333x10 ⁻⁷	1.000x10 ⁻⁶
	R_i	0.443	0.851	0.666	0.813	0.823
	C/Q_{ref}	0.557	0.149	0.340	0.187	0.177
	R^2	0.931	0.801	0.584	0.874	0.938
	SSE	0.368	20.705	2.731	5.245	10.737
	K_{p2} [mg/(g min ^{1/2})]	0.040	3.903	2.669	7.951	2.791
	C_2 [mg/g]	12.726	260.950	23.148	85.774	100.864
	R^2	0.713	0.720	0.781	0.958	0.929
	SSE	0.210	49.153	1.703	7.879	1.702
Bangham diffusion	α	-	0.467	0.352	0.446	0.362
	k_0 [dm ³ /g]	-	0.099	0.211	0.099	0.114
	R^2	-	0.901	0.971	0.956	0.960
Film diffusion	D_1 [cm ² /s]	7.596x10 ⁻⁸	1.730x10 ⁻¹⁷	1.460x10 ⁻⁷	4.390x10 ⁻⁷	3.026x10 ⁻⁷
	R^2	0.967	0.935	0.941	0.878	0.985
Pore Diffusion	D_2 [cm ² /s]	1.615x10 ⁻⁶	4.703x10 ⁻¹⁷	1.675x10 ⁻⁶	1.745 x10 ⁻⁶	1.346x10 ⁻⁶
	R^2	0.947	0.729	0.995	0.889	0.947
Chemisorption diffusion	q_c [mg/g]	5.718	88.834	30.861	43.960	38.000
	K_{CD} [mg/(g min ^{1/2})]	3.453	88.834	30.861	43.960	38.000
	R^2	-4.326	0.740	-0.484	0.735	0.522

Versión Aprobada para Defensa Oral

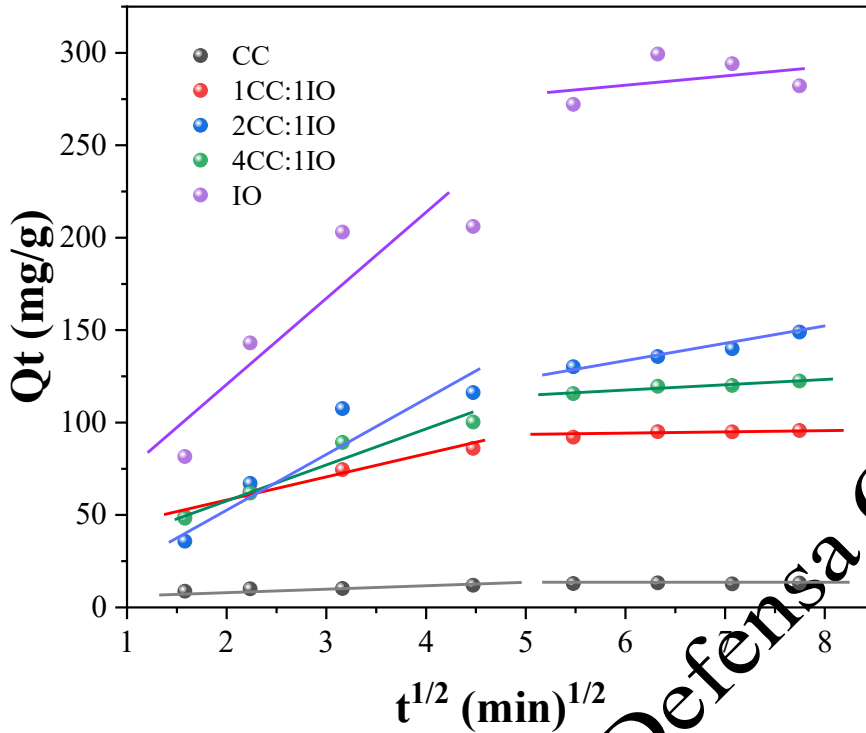


Figure 37. Intraparticle diffusion kinetics for adsorption of triclosan.

The diffusion coefficient of intraparticle diffusion, D_i , for triclosan adsorption on adsorbents can be calculated using the equation 20:

$$D_i = \frac{0.08 * r^2}{t_{0.5}^{0.5}} \quad (20)$$

where D_i is the intraparticle diffusion coefficient (cm^2/s), $t_{0.5}$ is the time to complete half the adsorption (min) and r is the radius of the adsorbent particle (cm).

Intraparticle diffusion plays a role in the rate-limiting step if D_i values are between 10^{-5} and 10^{-13} cm^2/s , then intraparticle diffusion plays a role in the rate-limiting step, especially for chemisorption systems. This is observed in composites and in CC, meanwhile D_i value for IO is out the range (Table 26).

On the other hand, the initial behavior of the triclosan adsorption process can be analyzed using the intraparticle diffusion (Ec. 21):

$$R_i = \frac{q_{ref} - C}{q_{ref}} \quad (21)$$

where R_i is the initial adsorption factor of the intraparticle diffusion model, C is the initial adsorption amount and q_{ref} is the final adsorption amount.

The R_i values were 0.96, 0.08, 0.76, 0.42, and 0.18 for the CC, IO, 1CC:1IO, 2CC:1IO, and 4CC:1IO, respectively. They were showed in Table 26. In the case of CC ($1 > R_i > 0.9$), there is a weak initial adsorption (zone 1), the 1CC:1IO composite has an initial intermediate adsorption (zone 2: $0.9 > R_i > 0.5$), the other two composites have a strong initial adsorption (zone 3: $0.5 > R_i > 0.1$) and the IO approaches complete initial adsorption (zone 4: $R_i < 0.1$). Therefore, the IO and the chemical modification that occurs in the impregnation process of the nanoparticles influence the surface adsorption of triclosan. Indeed, surface adsorption was dominant in the IO and composites. This is associated with the higher reactivity of the IO, which allows faster triclosan adsorption kinetics due to shorter diffusion paths within the adsorbents.

Moreover, the obtained data were fit to the Bangham diffusion model (Ec. 22):

$$\text{loglog} \left[\frac{C_0}{C_0 - q_t m} \right] = \log \left[\frac{k_0 m}{2.303V} \right] + \alpha \log t \quad (22)$$

where C_0 is the initial concentration of triclosan (mg/dm^3), V the volume of solution (dm^3), m the dose of adsorbents used per dm^3 of solution (g/dm^3), q_t the amount of triclosan retained at time t (mg/g), α (<1) and k_0 are constant.

The nonlinearity of the curves of the $\text{loglog} (C_0/(C_0 - q_t m))$ versus t plot (Figure 38) suggests that the diffusion of triclosan molecules into the pores of IO and composites only controls the rate. Meanwhile, the adsorption of triclosan on the CC does not fit this model. No trend is observed in the K_0 value with respect to the amount of impregnated IO, this could be related to the agglomeration of the nanoparticles.

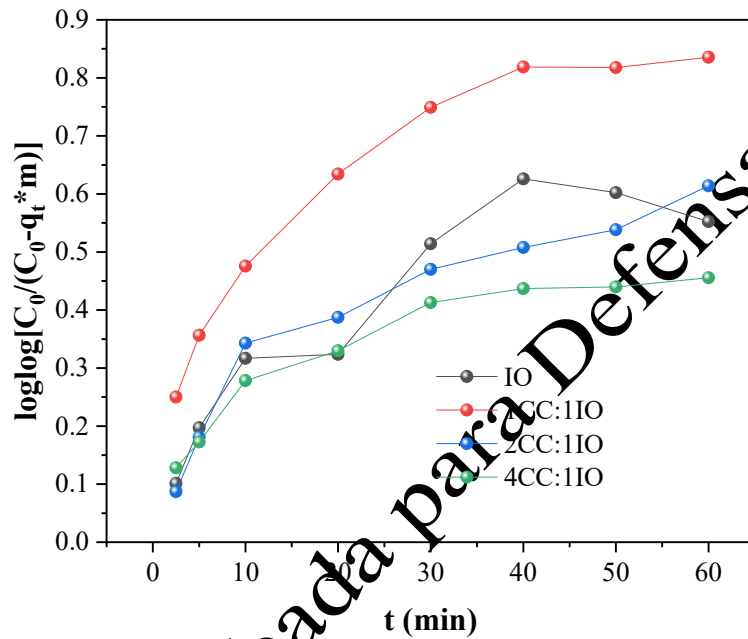


Figure 38. Bangham diffusion model for triclosan

On the other hand, intraparticle diffusion is controlled by both film and pore diffusion. The film diffusion coefficients can be calculated using the equation 23. It is assumed that the adsorbent has the shape of a sphere of radius a and that diffusion follows Fick's Law.

$$\frac{q_t}{q_e} = 6 \left[\frac{D_1}{\pi a^2} \right]^{0.5} t^{0.5} \quad (23)$$

The fractional uptake (q_t/q_e) of triclosan is suggested to be a function of the $t^{0.5}$ (Figure 39). The adsorbents exhibited swift initial triclosan adsorption, followed by slow adsorption into the pores. This trend is similar to that obtained in the intraparticle diffusion graph (Figure 37). Film diffusion is active in the triclosan adsorption mechanism in CC and composites, as the film diffusion coefficients are between 10^{-6} and 10^{-8} cm^2/s . While for the IO the diffusion of the film was not active in the triclosan adsorption mechanism.

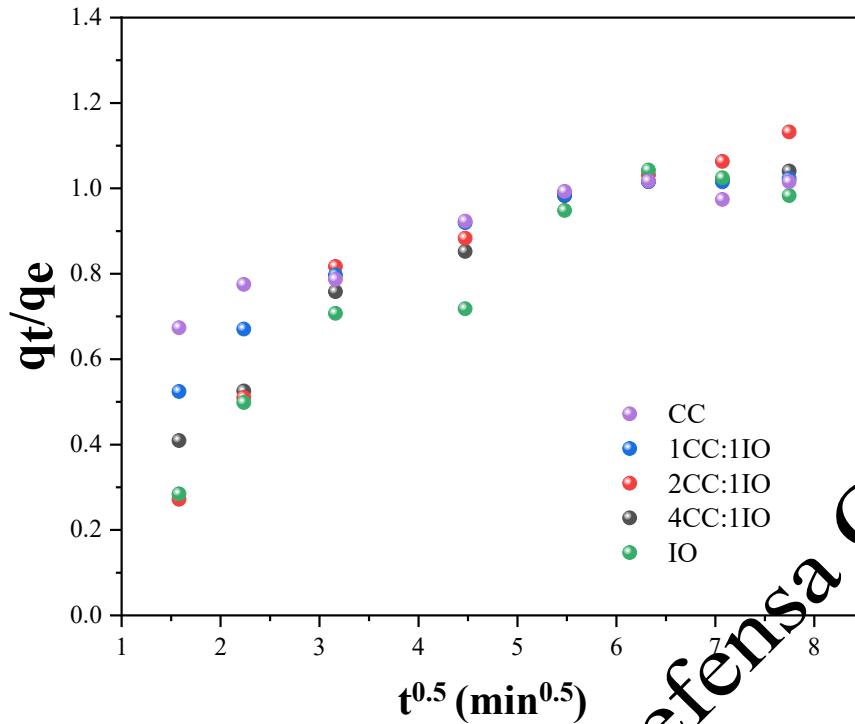


Figure 39. Fractional Uptake of triclosan in CC, composites and IO

For moderate and large times, the relation between weight uptake and diffusion equation is:

$$B_t = -0.4997 - \ln \left[1 - \frac{q_t}{q_e} \right] \quad (24)$$

where $B_t = D_2 \pi^2 / a^2$. The B_t vs t plot allows identifying whether external transport or interparticle diffusion controls the adsorption rate. The B_t vs t plots for triclosan adsorption (Figure 40) have a linear trend in the early stage of the adsorption process (up to 20 min). However, they do not pass through the origin, indicating that the external mass transfer of triclosan is rate-limiting in the early stages (Ofomaja 2011). The intercepts of the graphs intersect the y-axis at 0.45, -0.08, 0.06, -0.25, and -0.10 for the CC, IO, 1CC:1IO, 2CC:1IO, and 4CC:1IO, respectively. This indicates that the lines of the IO and the composites were closer to the origin than those of the CC. This suggests that there is a greater involvement of external mass transfer in the rate-determining step of IO and composites.

The values of the pore diffusion coefficient (D_2), for triclosan adsorption on the adsorbents, were calculated using the value of the slope (B) of the B_t vs t graph (Ec. 25). The D_2 values are presented in Table 26. An influence of the nanoparticles on the D_2 value concerning CC is not observed. The D_2 values for IO are very low compared to CC and composites. This suggests that there is a restriction of triclosan molecules on the inner surface of IO. Despite this, pore diffusion does not control the adsorption speed (D_2 outside the range of 10^{-7} - 10^{-13} cm²/s).

$$B = \pi^2 \frac{D_2}{r^2} \quad (25)$$

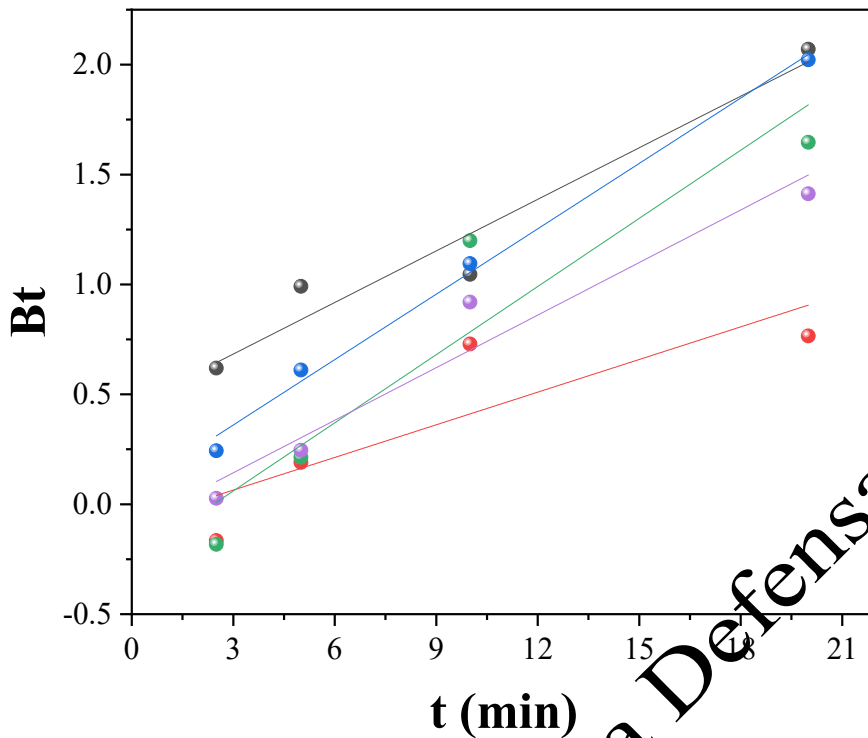


Figure 40. Boyd's diffusion of triclosan in CC, composites and IO

In this paper, the adsorbents show a good fit for both the pseudo-second-order and the intraparticle diffusion models. This suggests that the overall rate-determination step could be complex. Therefore, the empirical kinetic model of diffusion-chemisorption (non-linear) proposed by Sutherland (2004) was applied, Equation 26.

$$q_t = \frac{q_e K_{CD} t^{0.5}}{q_e + K_{CD}} \quad (25)$$

where q_t (mg/g) is the rate of change of concentration of the solid phase is equated to a function of the rate of mass transfer of triclosan from the liquid phase to the adsorption site, K_{CD} (mg/g \times min^{0.5}), and q_e (mg/g) is the equilibrium capacity.

The values of q_e , K_{CD} , and R^2 for triclosan adsorption are shown in Table 26. The R^2 values for the IO, 2CC:1IO, and 4CC:1IO were relatively high (0.52 - 0.74). While CC and 1CC:1IO present negative R^2 values. The results also show that the presence of nanoparticles increases the equilibrium capacities and the chemisorption-diffusion rate constant. An increase in the chemisorption-diffusion rate indicates that both diffusion and chemisorption processes become increasingly important in the rate-determining step.

3.4. Adsorption in fixed bed columns for triclosan/caffeine removal with CC and CC composites

The tests in the fixed-bed columns were carried out to determine the influence of the bed height and the hydraulic load on the removal of caffeine/triclosan using three particle sizes of CC and CC composite. The efficiencies in the removal of caffeine/triclosan achieved using the 4 and 5 cm heights did not show significant differences ($p > 0.05$) in the three CC and composite particle sizes. On the other hand, the hydraulic load = 4 m³/m²-day, produced clogging in the columns that used the small RH at 30 min of operation, so it was not possible to construct the breakthrough curve for this hydraulic load and establish its influence on the three particle sizes. The experimental breakthrough curves for the three CC particle sizes and composite using a bed height = 4 cm and a hydraulic load = 2 m³/m²-day are presented in Figure 41, and the main results are summarized in Table 27.

The size of the adsorbent particles is a very important parameter in the operation of fixed bed columns, since it defines the available surface area and the void fraction and the available path for the movement of wastewater (Sivarajasekar et al., 2018). An increase in particle size decreased the adsorption capacity at breakthrough time (q_b) and saturation time (q_s). However, this is not true for small CC (120 – 150 μm) particles, this may occur because over time there began to be clogging in the filter that used this particle size. But if it holds between medium (300 – 600 μm) and large particles (800 – 2,000 μm). The medium CC particles allow a shorter diffusion path for the caffeine/triclosan molecules. Therefore, the molecules of caffeine/triclosan will easily penetrate the pores of the CC, resulting in higher adsorption rate (A. Gupta & Garg, 2019; Sivarajasekar et al., 2018). The effect of particle size on adsorption capacity in both breakthrough time and saturation time is less for caffeine, probably due to its physicochemical characteristics (e.g., low water solubility, polarity and high hydrophobicity) (Álvarez-Torrellas et al., 2016; Rigueto et al., 2020). Something similar happens with the values of the breakthrough/saturation time. Therefore, an increase in CC particle size results in faster bed depletion and lower volume of treated water (Jaria et al., 2019; Peñafiel et al., 2021).

The medium CC particles also had lower h_{MTZ} than the large particles for both contaminants (caffeine/triclosan). A smaller particle size allows for a higher mass transfer rate and thus a smaller mass transfer zone (Gupta & Garg, 2019). Which indicates that the medium CC has better performance. A similar behavior was observed in cadmium adsorption when using date palm trunk fiber with size ranges of 250–355 and 560–630 μm (Al-Shawabkeh et al., 2021). A smaller mass transfer zone with a higher slope can also be identified on the C_f/C_o vs. t plot (Figure 41). Increasing h_{MTZ} in the larger RH reduced fractional bed utilization (FBU). The larger particles leave larger spaces between each other (the fraction of voids in the bed increases), so the contact time between the caffeine/triclosan and the CC particles decreases and this reduce de fraction of bed which is being effectively used (Sivarajasekar et al., 2018).

Moreover, with the data in Table 27, it can be seen that the presence of nanoparticles in the CC favors its performance as a filter material, since it increases the adsorption capacity, FBU and V_b and decreases the value of h_{MTZ} , this is true for caffeine and triclosan.

Table 27. Main results of adsorption experiments in fixed bed columns.

Contaminant	Adsorbent	Mass (g)	V_c (L)	EBTC (d)	FBU (%)	h_{MTZ} (cm)	C/C ₀ =0.1			C/C ₀ =0.9	
							t_b (min)	V_b (mL)	q_b (mg/g)	t_s (min)	q_s (mg/g)
Triclosan	CC(120 – 150 μm)	0.849	0.003	0.436	26.18	2.95	40	20	1.05	1400	4.01
	CC(300 – 600 μm)	1.001			58.32	1.67	100	15	1.87	1400	3.21
	CC(800 – 2,000 μm)	0.769			37.62	2.50	25	12.5	0.65	700	1.73
	4CC(800 – 2,000 μm):1IO	0.769			59.24	1.63	60	30	1.55	1250	2.62
Caffeine	CC(120 – 150 μm)	0.849			84.32	0.62	20	5	0.33	230	0.39
	CC(300 – 600 μm)	1.001			78.67	0.85	30	5	0.43	300	0.55
	CC(800 – 2,000 μm)	0.769			52.18	1.91	25	3.5	0.27	270	0.53
	4CC(800 – 2,000 μm):1IO	0.769			57.26	1.71	25	12.5	0.47	495	0.82

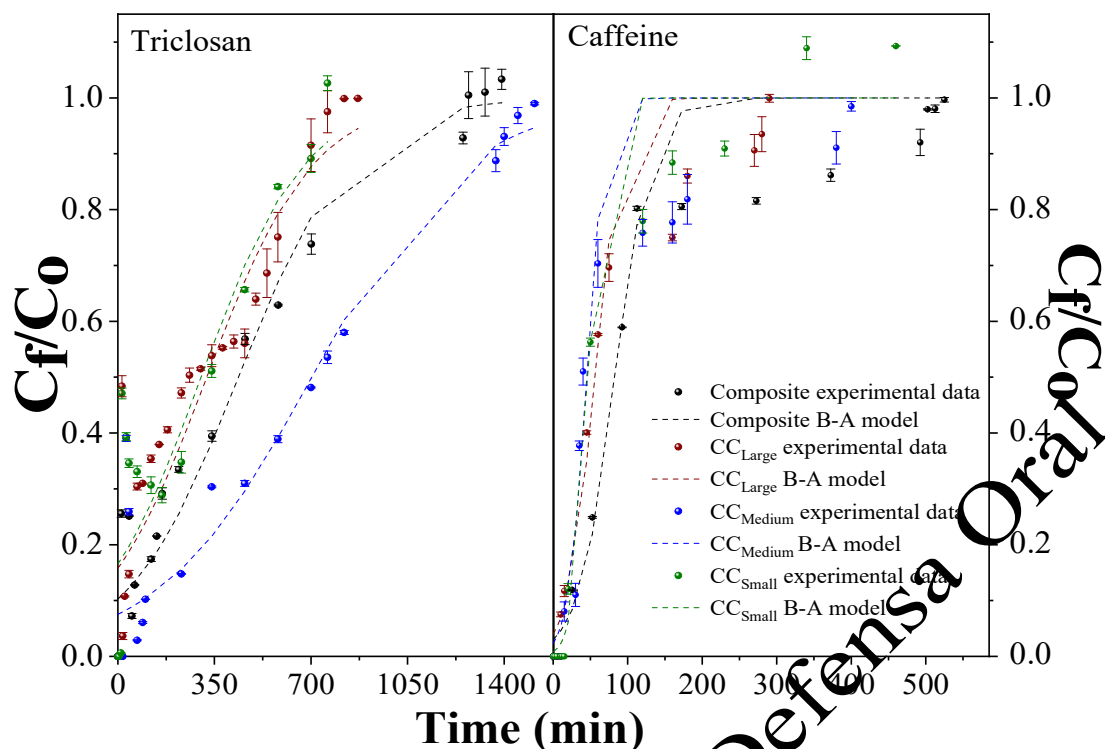


Figure 41. Effect of particle size and contaminant type on breakthrough curves.

Table 28 shows the results obtained by fitting the Bohart-Adams model to the experimental data of the adsorption process. This table shows the decrease in K_{AB} with increasing particle size, indicating that the process is dominated by external mass transfer. Likewise, it is observed that the composite has a higher adsorption capacity than CC alone.

Table 28. Bohart-Adams parameters for caffeine and triclosan adsorption.

Contaminant	Particle size	K_{AB} [L/(min*mg)]	N_0 [mg/L]	R^2	χ^2	SSE
Triclosan	CC(120 – 150 μ m)	1.197×10^{-4}	1911.214	0.814	0.046	0.294
	CC(300 – 600 μ m)	7.963×10^{-5}	4457.433	0.930	0.024	0.179
	CC(800 – 2,000 μ m)	1.160×10^{-4}	2042.210	0.980	0.002	0.002
Caffeine	4CC(800 – 2,000 μ m):1IO	1.106×10^{-4}	2772.448	0.934	0.019	0.121
	CC(120 – 150 μ m)	3.109×10^{-3}	216.254	0.977	0.016	0.093
	CC(300 – 600 μ m)	2.583×10^{-3}	203.457	0.999	2.27×10^{-4}	2.27×10^{-4}
	CC(800 – 2,000 μ m)	1.756×10^{-3}	255.427	0.960	0.003	0.002
	4CC(800 – 2,000 μ m):1IO	1.292×10^{-3}	378.748	0.964	0.011	0.100

N_0 = adsorption capacity, K_{BA} = Bohart-Adams constant

As with NH and PS, it was determined that the adsorption process is influenced by the composition of the adsorbent and its particle size. In this case, CC had a higher adsorption capacity (between 2.2 and 5.83 times) than CF. in the removal of triclosan. This is attributed to the higher concentration of extractives (3.2 times) that CF presents. Likewise, the smallest particles of the two residues (120 – 150 μ m) reached an adsorption capacity between 12.7 and 17.8 times greater than the larger sizes (300 – 600 and 800 – 2,000 μ m), due to the greater surface area and greater number of active sites. Since CC presented better adsorptive capacity than CF, it was chosen as the matrix of a magnetic composite (presence of iron oxide nanoparticles). The composites presented higher adsorption capacity (between 1058 and 1765.5 mg/g) than CC (16.5 mg/g) alone, due to their increased number of active sites and their greater diversity of functional groups. This indicates that CC composites are an alternative for the removal of ECs such as triclosan in batch adsorption processes.

Likewise, CC in its three particle sizes (120 – 150, 300 – 600 and 800 – 2,000 μ m) and the most efficient composite (weight ratio 4CC800 – 2,000 μ m) were used in tests of continuous adsorption processes

to remove caffeine and triclosan. In these processes, it was shown that although the smaller particles (120 – 150 μm) presented greater efficiency in the batch adsorption processes, they produced hydraulic problems in the continuous adsorption processes (clogging) while the operation time increased. This decreased the useful life of the filter bed, making it comparable to that of larger particles. Therefore, the medium particles presented better hydraulic performance, an equal saturation time (1400 min) for triclosan and longer for caffeine (70 min more) and an adsorption capacity compared to the medium particles. On the other hand, the composite, as in the batch tests, presented better adsorption capacity than the crude CC: 1.5 times for both contaminants. With which it is verified that the CC composite could be also used in continuous adsorption processes. However, using it on a larger scale is currently practically impossible. This is because the synthesis process used on a laboratory scale produces only small amounts of composite (about 3 g). Moreover, the washing of the composite to lower the pH (from 11 to 7) is not very efficient in terms of the amount of water consumed, around 5 L of distilled water were consumed by synthesis. Therefore, it is necessary to look for green synthesis processes that can be scaled to obtain a greater amount of composite and thus use it to treat larger volumes of wastewater. It is for this reason that in the following chapter only raw agro-industrial residues were used to remove contaminants present in the wastewater.

4. Conclusions

The CC in the three particle sizes used was more efficient than the CF for the removal of triclosan (up to 38.2%) in batch adsorption processes. On the other hand, the presence of nanoparticles impregnated in the CC favored the removal efficiency of triclosan. Being the 4CC:1MG composite the most efficient, no significant differences with the other composites was showed. The presence of nanoparticles decreased the dose (25 times) of adsorbent used. In terms of kinetics and isotherms, the experimental data for CC, small and medium CF, magnetite and composites fit the pseudo-second-order model and the Langmuir and Sips models. In fixed-bed columns, the particles 300-600 μm presented the best hydraulic behavior and the material was saturated at 1400 and 70 min for triclosan and caffeine, respectively. The composite, as in the batch tests, presented better adsorption capacity than the raw CC (1.5 times for both contaminants). The experimental data from the fixed bed columns fit the Bohart-Adams model well.

Conclusions of Chapter 3

Based on the outcomes detailed in this chapter, a compelling deduction can be drawn: the agro-industrial residues employed in the batch adsorption processes have proven to be notably effective in eliminating caffeine and triclosan. Indeed, one of the initial research hypotheses has been substantiated, corroborating the notion that the utilization of agro-industrial residues would yield heightened caffeine/triclosan removal rates. Moreover, it has been underscored that the incorporation of nanoparticles into the residues not only enhances the elimination of these contaminants (thereby reducing the required adsorbent dosage) but also facilitates their extraction from the aqueous milieu.

However, the inherent limitation of batch adsorption processes lies in their restricted capacity to handle modest volumes of wastewater, alongside the energy-intensive agitation demands. To surmount these challenges, the subsequent chapter proffers an innovative approach: the integration of agro-industrial residues within filtration/biofiltration technologies. It is important to note that experiments involving iron oxide nanoparticles and their composites have been excluded from consideration. The rationale behind this omission stems from the inefficient scaling up of nanoparticle and composite synthesis. To illustrate, the production of a mere 3g of composite on a laboratory scale necessitated an arduous 48-hour timeline and an astonishing 1.5 kg of packing material for a single column.

In essence, the pivotal conundrum concerning nanostructured materials revolves around the quest for viable alternatives that enable the large-scale and cost-effective production/synthesis of nanostructures and composites. This imperative pursuit is driven by the aspiration to subject such materials to rigorous testing in the treatment of substantially greater quantities of wastewater.

4. Optimization of operational parameters and configuration in continuous filtration processes used to remove contaminants from water

The United Nations has set forth ambitious sustainable development goals for 2030, including universal access to clean water and sanitation. Astonishingly, more than 3 billion people globally (approximately 42%) still lack access to fundamental sanitation services encompassing connection and treatment (Malik et al., 2015; Mateo-Sagasta et al., 2015). This glaring disparity has a direct nexus with poverty, significantly affecting developing nations (with a gross national income per capita range of \$1,035–\$12,615), where treatment and connection rates merely reach 30% and 50%, respectively. In stark contrast, developed countries (with a per capita income exceeding \$12,615) boast coverage exceeding 75% across both aspects (Malik et al., 2015).

Within municipal wastewater, domestic wastewater constitutes a substantial majority, accounting for over 80% of the total volume (Panikkar et al., 2010). Given its prodigious volume and the escalating global demand for water resources, domestic wastewater can be perceived as an unconventional yet potentially manageable water source. However, the volume (reaching up to 400 L hab⁻¹/day) and quality of domestic wastewater are contingent upon consumption patterns and income levels of the population (Villamar et al., 2018). The quality parameter encompasses factors such as solid content (100 – 350 mg TSS/L), organic matter (250 – 1600 mg COD/L, 110 – 800 mg BOD₅/L), nutrients (20 – 120 mg TN/L, 2 – 23 mg TP/L), pathogens (up to 10⁸ NPM/100 mL) (Villamar et al., 2018), as well as recently recognized emerging contaminants (e.g., pharmaceuticals and personal care products, each at levels below 1 mg/L) as previously indicated (Awfa et al., 2018). Consequently, discharge and regulatory constraints could impede the utilization of untreated domestic wastewater.

To address these challenges, treatment technologies encompassing conventional activated sludge systems and innovative passive options like biofiltration have emerged as potential avenues to enhance wastewater quality and enable efficient recyclability. The selection of the most suitable technology hinges on economic considerations, with a substantial portion of capital costs (approximately 80-90%) allocated to collection infrastructure (Libralato et al., 2012). While conventional methods such as activated sludge systems incur investment costs ranging from 65 to 200 USD per capita in centralized water resource recovery facilities catering to populations exceeding 2,000 individuals (Vera et al., 2016), non-conventional techniques like biofiltration may prove more suitable for decentralized contexts accommodating fewer than 2,000 inhabitants (Massoud et al., 2009). In fact, these non-conventional methods offer economic, social, and environmental advantages, potentially yielding investment costs between 35 and 630 USD per capita, along with reduced emissions by nearly 50%. For instance, the implantation area could be considered an influential factor within the wastewater technology investment costs. Biofiltration typologies (0.1–6 m² hab⁻¹) require higher surface area than centralized conventional technologies (activated sludge < 0.1 m² hab⁻¹) and result economically unfeasible for large populations (> 2,000 inhabitants), not only because of the required space but also due to the support material requirements (Arora & Kazmi, 2015; Kumar et al., 2015; Vera et al., 2016).

The realm of biofiltration boasts a diverse array of technologies employed for domestic wastewater treatment, as elaborated in section 1.3.2. Notably, hybrid biofilters integrating plants, earthworms, and microorganisms (referred to as HB) have gained prominence as a viable alternative (Samal et al., 2017b). These biofilters uniformly share a dual facet: a biotic element (plants/earthworms/microorganisms) and a supporting medium. This unique combination facilitates concurrent physical (sedimentation, precipitation), chemical (adsorption, ionic exchange), and biological (degradation, transformation, uptake) processes.

However, a crucial component in biofiltration—the support material—can comprise up to 50% of the total investment cost when utilizing conventional substrates such as gravel. Consequently, exploration of alternative materials becomes imperative. Non-conventional substances, including agro-industrial residues, chitosan, biochar, wood residue, and peat, among others, hold promise as viable alternatives for support purposes (Mohan et al., 2014; Zhou et al., 2015). Notably, organic materials like agro-industrial residues may cost up to 100 times less than traditional options (Gupta et al., 2009). The selection of an organic support material hinges not only on its availability but also its inherent properties, encompassing physicochemical stability (lignin/hemicellulose content), surface area (at least 80 m²/g), pore diameter (at least 20 Å), functional group presence (phenolic hydroxyls, methoxyl, carboxylic), and adsorption capacity (Almeida-Naranjo et al., 2021a; Tejedor et al., 2020). Moreover, many agro-industrial residues exhibit compatibility with biotic components, although certain degradation byproducts of lignin degradation have demonstrated toxicity in earthworms like *Eisenia foetida* (Savigny) (LC₅₀ of 0.6 and 0.7 µg/cm³ for 2,4-dinitrophenol and 4-nitrophenol, respectively) (Neuhauser et al., 1985). Additionally, most agro-industrial residues are also non-toxic (compatible) to biotic component, even though some of the products of the incomplete degradation of lignin have shown high toxicity levels in earthworms such as *Eisenia foetida* (Savigny) (Neuhauser et al., 1985). For instance, the reduction in survival (< 46.7%) and weight (< 32.1%) of *Eisenia foetida* (Savigny) in vermifilters has been attributed to bed filter material composition (100% v/v of peanut shells) and its hydrolysis (Tejedor et al., 2020).

Despite their tremendous potential as bed support in biofilters targeting contaminant removal from wastewater, widely available materials such as rice husk, peanut shells, corn cob, and coconut fiber have yet to undergo exhaustive exploration (Anastopoulos et al., 2020). For instance, while activated carbon/biochar derived from corn cob have exhibited relative efficiency in batch adsorption processes for ciprofloxacin (74%) (El-Bendary et al., 2021) and chlortetracycline (60%) (L. Zhang et al., 2018), the raw corn cob itself remains largely unstudied for emerging contaminants removal.

The forthcoming chapter endeavors to bridge the knowledge gap by elucidating the optimization of operating parameters and configurations within continuous filtration processes tailored for contaminant removal from water. Initial focus centers on assessing the efficiency of caffeine and triclosan removal using corn cob-based filter media in continuous filtration systems. Subsequently, the study explores the viability of rice husk, peanut shells, corn cob, and coconut fiber as potential mediums for vermifiltration technologies, anchored in their caffeine removal efficiency and affinity with the *Eisenia foetida* (Savigny) species. Caffeine serves as the model contaminant due to its intricate removal characteristics (high water solubility and polarity) compared to other pollutants. Lastly, the chapter delves into a mesocosm-scale study involving diverse biofilter types for the removal of macro-contaminants from synthetic wastewater. The materials employed in these biofilters are subjected to comprehensive physical-chemical and morphological characterizations, thus unraveling the intricate interplay between material properties and contaminant removal efficacy, including toxicity considerations. This comprehensive endeavor holds the potential to shed light on the intricate relationship between bed support material attributes and the removal of both macro and emerging contaminants within biofiltration systems, thereby elevating their overall performance.

Article 5. Caffeine and triclosan removal using corn cob biofilters (large columns)

ABSTRACT

The support material is extremely important in a biofilter, since it directly impacts the efficiency, operation and cost of the treatment. In this research, corn cob of different granulometry was used as filter support material: small particle (SPF= 0.8 – 2.0 cm), medium particle (MPF= 2.0 – 3.5 cm), large particle (LPF= 3.5 – 5.7 cm) and mixed particle (MxPF) (SPF+MPF+LPF). The filters were evaluated to remove caffeine and triclosan from 30 mg/L aqueous solutions. For this, 28 filters were operated in parallel under three nominal hydraulic flows (HRL= 1, 2 and 4 m³/m²-day) with intermittent feed (6 h/day). The corn cob was characterized at the beginning and at the saturation of the filters. The results showed that the corn cob presents good adsorbent properties, reaching efficiencies of up to 98.5% and 99.0% for caffeine and triclosan, respectively. Higher efficiencies (SPF > MPF ≥ MxPF > LPF) and low clogging are observed at lower hydraulic velocities, attributed to a smaller particle size ($p \leq 0.05$, only between the LPF and the others, operating with HLR= 2 m³/m²-d) and longer contact times. The hydraulic conductivity for all had values between 48.3 and 185.1 mm/h. Mixing the different particle sizes (MxPF) increased the removal of caffeine and triclosan compared to the MPF and LPF filters, but did not improve the hydraulic performance of the filter or the saturation time of the material. The filters that operated with triclosan (MPF) presented a longer saturation time (1.6 times) than caffeine, the same behavior was observed with the degradation of the material.

1. Introduction

The need to satisfy some human requirements in terms of food, health, personal care, among others, has led to the use/consumption of different products. The residues of these products (pharmaceuticals, personal care products, pesticides, hormones, plasticizers, etc.) are known as emerging contaminants (EC) and have been found in wastewater and in different bodies of water (Almeida-Naranjo et al., 2021b). This presence in the aquatic environment has generated several adverse effects (e.g., chronic toxicity, endocrine disruption and development of resistance to pathogens) on the biota, despite the low concentrations (ng/L-mg/L). Among the EC commonly found are caffeine and triclosan (Quadra et al., 2019; Triwiswara et al., 2020a).

Caffeine is an alkaloid from the methylxanthine family, generally used as a stimulant. It is characterized by its high solubility (21.6 g/L at 25 °C) and relatively low toxicity ($\log K_{ow} = 0.5$) (Rigueto et al., 2020). It has been found worldwide in wastewater (e.g., Singapore= 3.6 mg/L), surface waters (e.g., Costa Rica= 1.1 mg/L) and even in aquatic organisms (1.6 – 344.9 ng/g) (Quadra et al., 2019). Because of high consumption worldwide, mainly in coffee (10-58848 mg/person-day) (Korekar et al., 2019; Quadra et al., 2019). The presence of caffeine in the environment has caused negative effects, on aquatic organisms and terrestrial insects, such as: lethality, decrease in general stress, affect energy reserves and metabolic activity (oxidative stress/lipid peroxidation), affect reproduction and development (neurotoxic effects) (Li et al., 2020).

On the other hand, triclosan is a commonly used antibacterial (world production = 1500 tons/year) in mouthwashes, toothpastes, disinfectants, deodorants, clothing, textiles and furniture, etc. It is characterized by its high capacity for bioaccumulation ($\log K_{ow} = 4.3$), low solubility in water (10 mg/L at 25°C) (Kaur et al., 2018) and for being an endocrine disruptor (Triwiswara et al., 2020a). It has also been found in various water resources (river water= 6×10^{-5} – 74.3 µg/L, seawater= up to 58.3 ng/L, groundwater= up to 13.1 ng/L, drinking water= up to 9.74 ng/L) and in tributaries of WRRF (e.g., Brazil=1.3 µg/L, China=0.06 – 2.9 µg/L, Chile=0.2 ng/L) (Triwiswara et al., 2020a; Yin et al., 2022). However, the COVID-19 pandemic has increased its level (Milanović et al., 2021; Yin et al., 2022). Triclosan has caused reproductive effects in aquatic organisms (invertebrates, fish, amphibians, algae, and plants). In addition, it has been linked to health problems in humans (antibiotic resistance, skin irritation, endocrine disruption, prevalence of allergies, etc.) (Triwiswara et al., 2020).

The effects of both ECs make their removal essential. Therefore, technologies such as membrane reactors (removal: caffeine= 93.7%, triclosan= 89.7%), Photo (UVC)-Fenton (pZVI) (caffeine=99.5% and

triclosan= 100%) (Li et al., 2022), activated sludge systems (caffeine=98.5%, triclosan= 89.5%) (Chtourou et al., 2018), were used efficiently. Despite their performance, these technologies/processes are characterized by being expensive. A low-cost alternative to remove caffeine/triclosan is batch adsorption process and the technologies where this process occurs (filtration: trickling filters, and biofiltration: constructed wetlands, biofilters, vermifilters) (Tejedor et al., 2020). In a constructed wetland with horizontal subsurface flow, efficiencies of 91.9% and 94.5% were reached for caffeine and triclosan, respectively (Chtourou et al., 2018). Meanwhile, in biofilters the performance achieved was caffeine= 50 – 100% and triclosan= 22 – 99% (Devault et al., 2021).

The filter bed material plays a fundamental role in the operation and efficiency of biofiltration technologies. The commonly used materials are sand, gravel, anthracite and granular activated carbon (Loh et al., 2021). However, these materials represent more than 50% of the investment costs, so alternative materials are continually being sought. Agro-industrial, industrial and forestry residues can be an alternative due to their high availability and good adsorptive characteristics. Presenting high efficiencies in the removal of organic matter and nitrogen (> 80%) (Almeida-Naranjo et al., 2021a; Tejedor et al., 2020). However, its research/application is still limited for ECs.

Corn cobs are a very abundant residue worldwide (158.1 million tons/year) (Bergonzoli et al., 2020), so it could be an alternative to be used as filter beds. Furthermore, it was used in batch adsorption processes, demonstrating high efficiency in the removal of other ECs such as sulfamethoxazole (around 80%) (Juela, 2022). Therefore, the objective of this research was to determine the efficiency in the removal of caffeine and triclosan in biofilters that have corn cob as filter bed. The influence of the particle size, the combinations and the hydraulic load on the removal of both ECs was investigated.

2. Materials and Methods

2.1. Corn cob conditioning and characterization

Corn cob (CC) is the same that was used in Article 4. CC was cleaned to remove the remains of corn and washed. To reduce the amount of energy consumed in the drying process of the CC, this time they were first ground using a Thomas knife mill and dried at 80 °C for around 12 h. The corn cob particles were sieved and classified in three different size groups: 0.8-2.0 mm (small), 2.0-3.5 mm (medium) and 3.5-5.7 mm (large). Small CC was selected because it was worked with in Article 3 and it was necessary to know how it works in larger-scale systems. It has also been used in previous studies showing good results (Kandra et al., 2014; Tejedor et al., 2020; Tosuner et al., 2019). The other two sizes were chosen because it is necessary to use larger particles when using full-scale filtration systems, in previous studies using same size or even whole CCs (Ali et al., 2014; Arsalan et al., 2021).

Later they were characterized as the same performed in the Article 1 and 2. Corn cob was stored in bags at room temperature.

2.2. Experimental Model

2.2.1. Physical characteristics

The experimental model consisted on 28 columns made of acrylic (diameter=12, height= 100 cm). The support medium was composed of two layers: 15 cm of support layer (gravel, $\phi = 10 - 25$ mm) and 75 cm of active layer (CC of different particle size). Considering the particle size of the corn cob, 4 types of filters were used: small particle (SPF, $\phi = 0.8-2.0$ cm), medium particle (MPF, $\phi = 2.0-3.5$ cm), large particle (LPF, $\phi = 3.5 -5.7$ cm) and mixed particle (MxPF). The active layer of mixed particle filters was composed of three sublayers of 25 cm each, described from bottom to top as follows: active layer 3 ($\phi = 3.5 -5.7$ cm), active layer 2 ($\phi = 2.0-3.5$ cm) and active layer 1 ($\phi = 0.8-2.0$ cm). Figure 42 details the biofiltration typologies scheme. In the placement of the filter medium inside the columns, no compaction was performed. The tests were carried out inside a greenhouse.

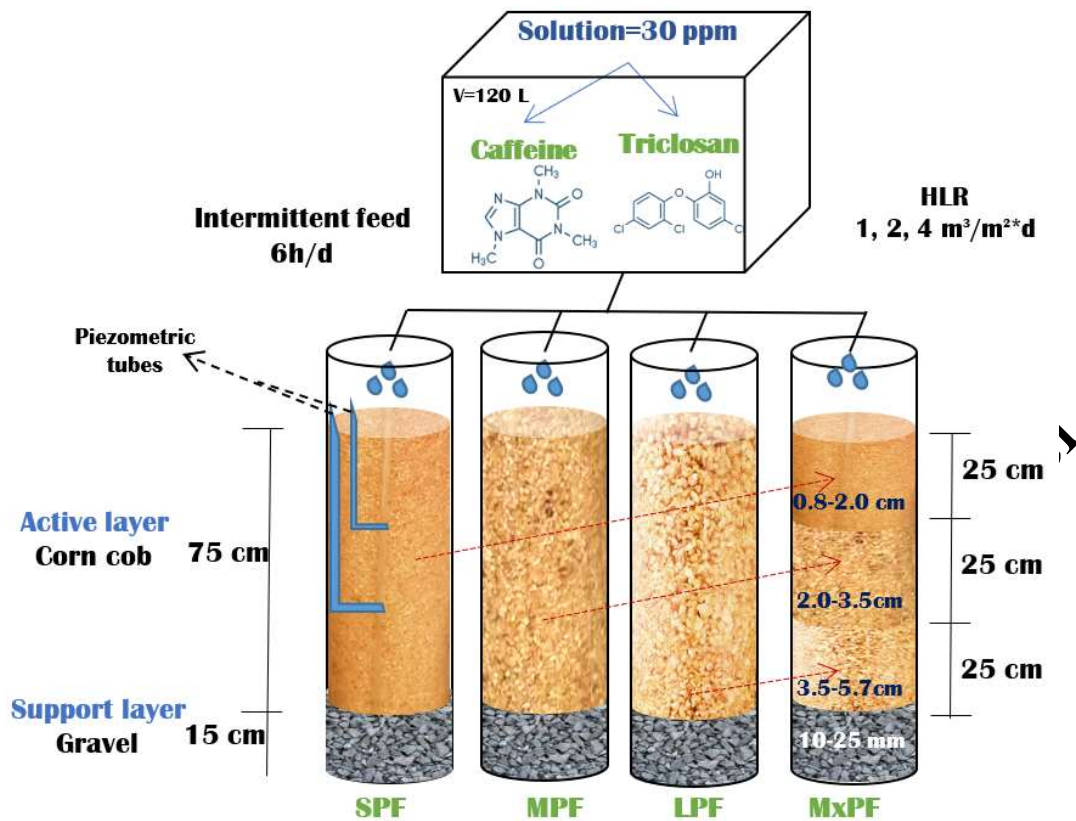


Figure 42. Filtration typologies scheme

2.2.2. Operational strategy

At the first stage, each filter worked in parallel using three different nominal hydraulic load rates (HLR=1, 2 and 4 m³/m²-d). These hydraulic loads were used because they are inside the range of loads used in a low rate filter (up to 4 m³/m²-d) (Chengero et al., 2020). Moreover, Tejedor et al., (2020) used loads of up to 1.5 m³/m²-d using peanut shell (0.8-2.0 cm), to remove macro contaminants from synthetic wastewater. Considering this, it was assumed that using higher loads with caffeine and triclosan solutions would allow determining the effect of this operating parameter in the removal of them. Filters were fed with caffeine solutions (30 mg/L, pH=7.08±0.18) from a 120 L elevated tank. During the first 10 days of operation, the material was washed using drinking water at a flow rate of 5 mL/min. On the other hand, to determine the hydraulic retention time (HRT), after the filter washing process, 5 L of drinking water was passed through them and the time it took for the first drop of water to come out was taken. HRTs achieved were 19.6 (±5.9), 9.8 (±2.7) and 4.9 (±2.1) h for HLR of 1, 2 and 4 m³/m²-d respectively.

The filters were operated until the material presented saturation (removal = 0%). The following days, the caffeine solution was drip-fed and the flow rates (around 5, 10 and 20 mL/min) were controlled with a LongerPump peristaltic pump model BT100-1L. Intermittent feed of 6 h/day were used. This intermittent feeding was used because it is in the range used by Chicaiza et al., (2020) (4 – 24 h/d). In this study, it was determined that a feeding of 8 h/d is more efficient, but they worked with vermifilters and earthworms prevent them from clogging. Since the filters in this study only have filter material, then, as a precaution, a lower feed was used. When the optimal operating conditions for caffeine removal (optimal nominal hydraulic head rate and particle size) were determined, the second stage was started. In this stage, the filters were operated with the optimized parameters to remove triclosan present in solutions of 30 mg/L and pH=7.87 (±0.92). Caffeine was initially used because by optimizing the configuration and operation parameters for this removal, these conditions would surely also be favorable for triclosan, since caffeine is more difficult to remove than triclosan due to the high polarity. The caffeine/triclosan solutions were prepared with drinking water (pH= 6.74 ± 0.20)/NaOH solution 0.01M, respectively. The tests in the two stages were carried out in duplicate, and a filter that functioned as a control fed with drinking water was placed. Environmental conditions (humidity and temperature) were measured twice a day. The maximum values of temperature and humidity were 50 °C and 99%, and the minimum 11.1 °C and 10 %, respectively.

2.3. Analytical methods

2.3.1. Influent/effluent monitoring

The concentrations of triclosan/caffeine in the influent and effluent were daily measured using a Horiba Analytik Jena Sperscord 210 Plus UV-VIS spectrophotometer at 294/287 nm, respectively. Furthermore, hydraulic conductivity and head loss were daily monitored with a manual piezometer located 25 and 50 cm below the upper level of each filter.

2.3.2. Support material characterization

Physical-chemical characterization and instrumental (FTIR and BET) analysis (used in Articles 1, 2 and 3) were performed to characterize corn cob. FTIR analysis was performed before and after (in the corn cob that shows more visible changes) the caffeine/triclosan removal. Moreover, SEM analysis was performed in a Phenom ProX scanning electron microscope equipped with an EDX-detector operating at 10 kV and ProSuite-EDS software.

2.4. Statistical analysis

Statistical analysis of significant differences between filter particle size (SPF, MPPF, LPF, MxPF), hydraulic loading rates (1.0, 2.0 and 4.0 m³/m²-d) and performance were analyzed by one-way analysis of variance (ANOVA). A significance level of 0.05 was defined. Parametric variance analysis was used for normal datasets (Tukey test), while non-parametric variance analysis (Kruskal-Wallis) was used for non-normal distributions. The software used was OriginPro version 2019.

3. Results and discussion

3.1. Corn cob characterization

Figure 43 shows the CC particles that were used in the different filter media, their shape and size can be distinguished.

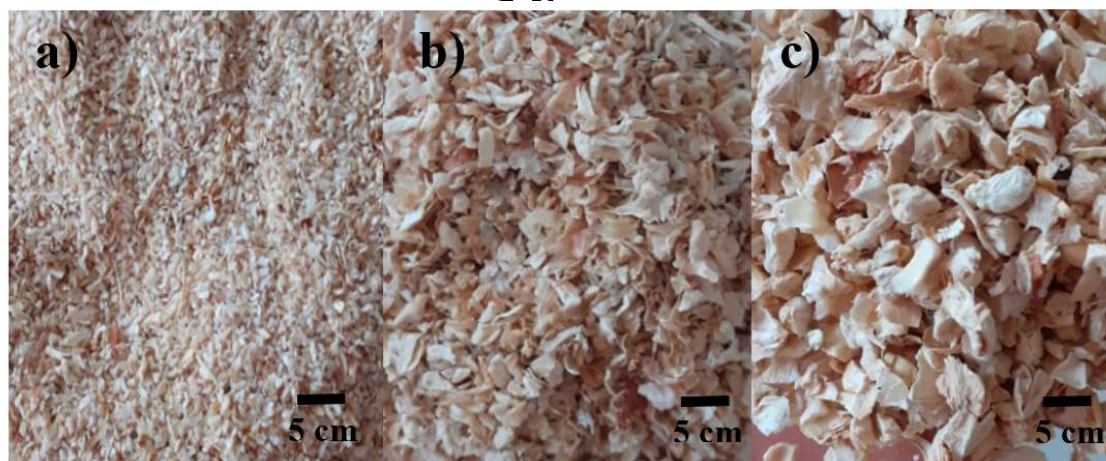


Figure 43. Raw corn cob particles by size. a) Small CC (0.8-2.0 cm), b) Medium CC (2.0-3.5 cm), c) Large CC (3.5-5.7 cm) used in filters.

3.1.1. Physical-chemical characterization

Table 29 shows the results of the physical chemical characterization of the corn cob. A high content of cellulose, hemicellulose and lignin is observed. Lignocellulosic materials have a high density of functional groups mainly hydroxyl and carbonyl, which impart good adsorptive properties to the adsorbent (León et al., 2019). The functional groups are responsible for attracting contaminants to the surface of the adsorbent through different mechanisms (e.g., chemical bonds, attraction forces, ion exchange, etc.) (Almeida-Naranjo et al., 2021a). Meanwhile, the total concentration of extractives (2.7 w/w%), both those soluble in water and those soluble in ethanol-toluene mixtures, are low compared to other residues (e.g., coconut fiber, orange peel) (Almeida-Naranjo et al., 2021a; Castro et al., 2021).

Higher extractive concentrations reduce the active sites of the residues and consequently their adsorption capacity decreases (Chowdhury et al., 2011). Therefore, this suggests that CC could remove efficiently triclosan/caffeine from wastewater through adsorption mechanism produced in filtration systems.

The humidity of the CC is within the range presented by other authors (3.1-10.2 w/w%) (Miranda et al., 2018; Sulaiman & Adetifa, 2019). The low humidity of the CC facilitates its drying process. If it is desired to dry large amounts of CC for use in large-scale filtration systems, the CC can be dried in environmental conditions, thus saving energy and avoiding the environmental impact generated by this use. On the other hand, the volatile solids concentration where there is the presence of lignin, cellulose, and hemicellulose was 91.53 (± 0.05) w/w.%; while that, of ashes was 1.41 (± 0.09) w/w.%. Volatile solids concentrations above 60% and low ash concentrations favor the adsorbent properties of the materials (Mussatto et al., 2010).

Table 29. Physicochemical characteristics of corn cob

Parameter	Unit	Value		
pH	--	5.87	\pm	0.03
Lignin	w/w.%	15.37	\pm	0.48
Hemicellulose	w/w.%	33.34	\pm	0.79
Cellulose	w/w.%	45.51	\pm	0.99
Ethanol – toluene extractives	w/w.%	1.13	\pm	0.05
Water extractives	w/w.%	1.57	\pm	0.15
Total extractives	w/w.%	2.70	\pm	0.17
*Humidity	w/w.%	5.19	\pm	0.15
Ashes	w/w.%	1.41	\pm	0.09
Volatile material	w/w.%	91.53	\pm	0.05
Fixed coal	w/w.%	1.87	\pm	0.08

*Parameter defined on a wet basis, without *: parameter defined on a dry basis

3.1.2. FTIR, SEM and BET characterization

Figure 44 shows the FTIR spectra obtained before and after caffeine adsorption. The material analyzed was CC of the small particle filter (SPF) that operated with an HLR= 1 m³/m²-d since it was the one that presented the greatest macroscopic changes. In the raw CC (black line), bands around 3300 and 2900 cm⁻¹ are present, these correspond to the vibrations of the OH- group and the C-H bond, respectively. The bands near 1700 cm⁻¹ and 1600 cm⁻¹ are related to the presence of the double bond between C and O (carbonyl group). Between 1250-1200 cm⁻¹ and around 1375 cm⁻¹ the bending of the C-H group is reported. Both the C-H and C-O groups are characteristic of cellulose and hemicellulose. While the presence of lignin is evidenced by the bands around 1600, 1500, 1400 and 1300 cm⁻¹. The bands around 1160 cm⁻¹ are characteristic of the C-O-C bond present in cellulose. The bands between 1000 and 1300 cm⁻¹ appear due to the vibration of the stretching of the C=O bond of the carboxylic and alcohol groups (Beltrame et al., 2016; Zhang et al., 2015). FTIR analysis showed that CC contains several functional groups (mainly carboxyl and hydroxyl) that could be the ones that attract caffeine and triclosan molecules.

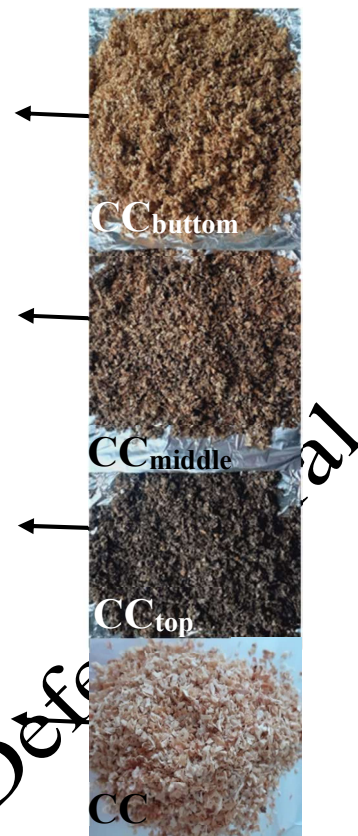


Figure 44. FTIR and photography of CC before and after caffeine removal. The CC subscripts represent the location of that material inside the filter.

Figure 45 shows the SEM and BET results. The SEM image of CC (Figure 45a) shows a porous and rough surface with the presence of protrusions and pockets, characteristics that coincide with those presented by Ji et al. (2015) and other agro-industrial residues. On the other hand, the BET analysis indicates that the residues have a low surface area, which is also characteristic of agro-industrial residues. The value of surface area ($0.42 \text{ m}^2/\text{g}$) coincides with the study by F Yu et al., (2014) ($< 0.7 \text{ m}^2/\text{g}$). However is less than that found by Wanitwattananarumlug et al., (2012) ($3.9 \text{ m}^2/\text{g}$). These differences are mainly due to the different species of corn cob that exist, maturity of the corn, place of origin, type of conditioning, among others (Daffalla et al., 2020; Ji et al., 2015; Wanitwattananarumlug et al., 2012; Yu et al., 2014). Moreover, they differ highly from that obtained by Ji et al., (2015), which presents a surface area ($87.4 \text{ m}^2/\text{g}$) that is not common for this type of material.

The pore volume and pore diameter determined by the Barrett-Joyner-Halenda (BJH) method were $0.001 \text{ cm}^3/\text{g}$ and 3.41 nm , respectively. According to the IUPAC standard, a pore diameter between 2 and 50 nm is characteristic of mesoporous materials (Beltrame et al., 2018). Figure 45b shows the nitrogen adsorption-desorption isotherm for CC. This is a type III isotherm, according to the Brunauer, Deming, Deming and Teller (BDDT) classification, and corresponds to a microporous or non-porous material with little affinity between the adsorbate and the adsorbent. So once the molecule is adsorbed, it acts as if it is free to adsorb another molecule; thus some parts act as monolayers and some others as multilayers (Sultan et al., 2018)

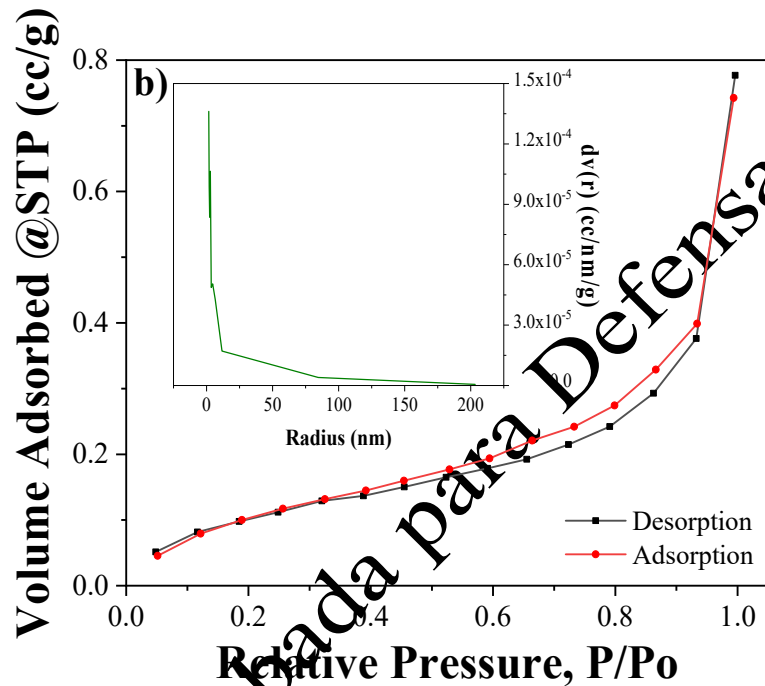
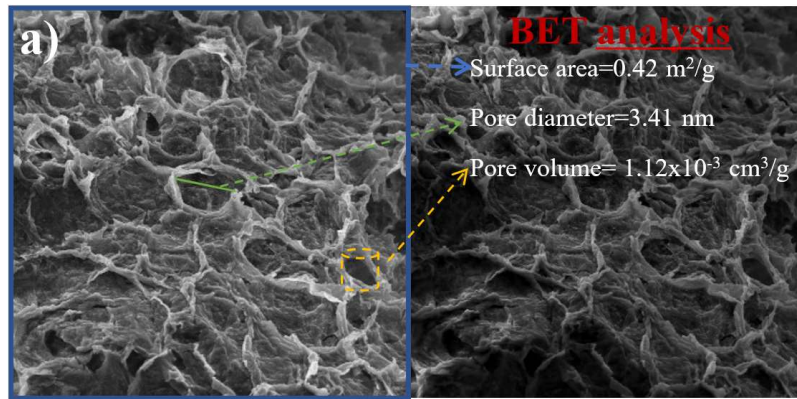


Figure 45. a) SEM image and results of BET analysis, b) nitrogen adsorption-desorption isotherm and pore size distribution (inset) for the CC particles (0.8-2.0 cm).

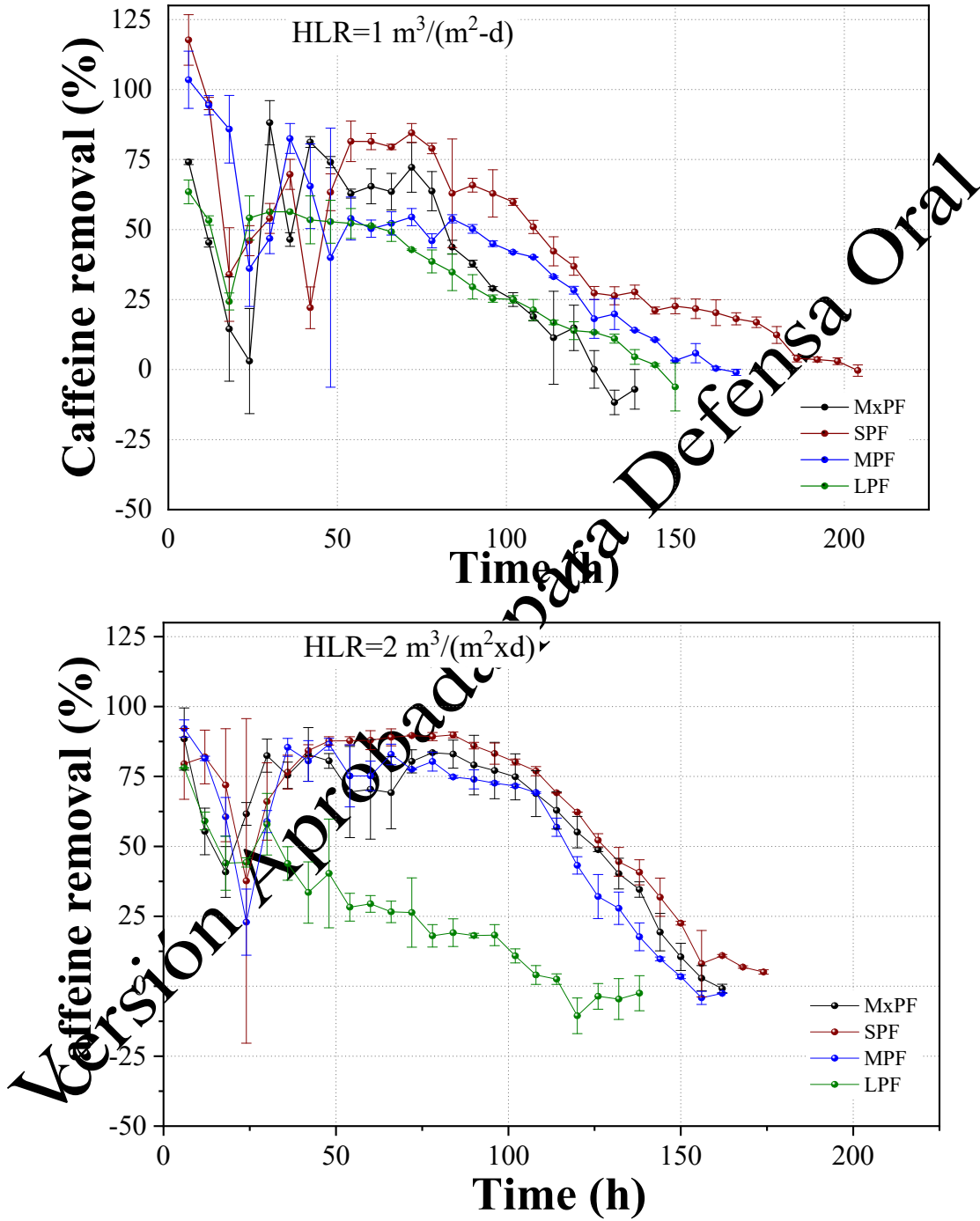
3.2. Filter performance

3.2.1. Caffeine removal

The results of the caffeine removal of caffeine are presented in Figure 46. The efficiencies achieved were high (up to 98.5%), however they were decreasing relatively fast as function of operating time. In the initial stage of the operation (up to 24 h) sudden increases and decreases in the caffeine removal efficiency was observed, this is probably since the filters were stabilizing. Later, the filter behavior shows changes with a defined trend. Moreover, at some points, there are large deviations from the caffeine removal (up to 46.2%). This is attributed to the heterogeneity that the CC particles present and to the difference in compaction that could exist when filling the columns (Kandra et al., 2014).

With the three HLRs, it is observed that the caffeine removal trend as follows: SPF > MPF ≥ MxPF > LPF. Thus, maximum efficiencies reached between 89.9 – 98.5%, 85.60 – 94.4%, 84.1 – 88.1% and 47.0 – 63.5.0%, for saturation times (removal= 0%) between 156 – 204 h, 126 – 168 h, 96 – 156 h and 120 – 150 h, respectively. As the particle size decreases, an increase in the removal of caffeine and in the saturation time of the filters is observed, this occurs due to the fact that the smaller particles present a greater surface area (greater active sites) for the caffeine to interact with the CC particles, thus favoring the adsorption capacity and prolonging the useful life (Iheanacho et al., 2021). Another factor that influences the contaminants removal is the shape of the material used in the filter bed. As can be seen in Figure 43, small (0.8 – 2.0 cm) and medium (2.0 – 3.5 cm) particles have irregular shapes, while larger particles (3.5 – 5.7 cm) have more homogeneous shapes. It has been shown that particles with irregular

and angular shapes present greater contaminants removal than more homogeneous particles (Kandra et al., 2014). However, only significant differences ($p \leq 0.05$) were found between the LPF and the other filters that operated with HLR= 2 m³/m²-d. The influence of particle size was not significant ($p > 0.05$) in the filters that operated with HLR of 1 and 4 m³/m²-d (Figure 46).



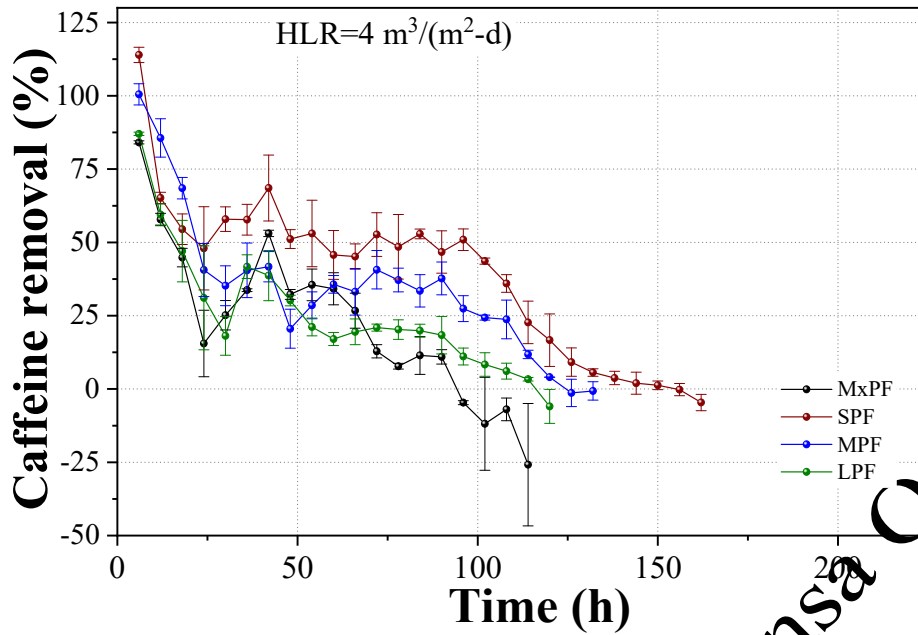


Figure 46. Filter performance in the removal of caffeine function of time.

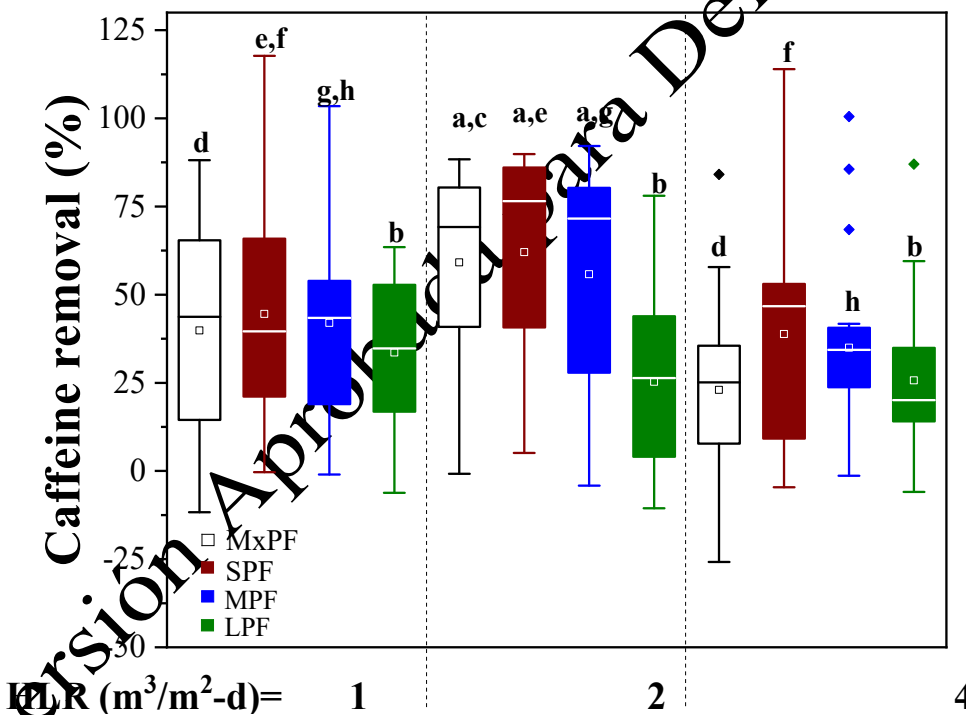


Figure 47. Filter performance in the removal of caffeine. Means with a common letter are not significantly different ($p < 0.05$).

Furthermore, it is observed that the removal efficiency of caffeine is also related to the HLR (Figure 46 and 47). This is evident when comparing the HLR= 1 and 2 $\text{m}^3/\text{m}^2\text{-d}$ with the HLR= 4 $\text{m}^3/\text{m}^2\text{-d}$. An increase in HLR produces a decrease in the removal efficiency. This behavior occurs because a high HLR reduces the hydraulic retention time (HRT) or the contact time of wastewater inside the filter bed, that is, the caffeine solution leaving the filter probably does not reach the adsorption equilibrium and this results in lower removal efficiency. Meanwhile, lower HLRs increase the contact time between caffeine and CC, this increases mass transfer and diffusion between CC particles (Iheanacho et al., 2021), thus increasing removal efficiency around 0.1 – 6.0% and 1.8 – 26.3% for HLR=1 $\text{m}^3/\text{m}^2\text{-d}$ and HLR=2 $\text{m}^3/\text{m}^2\text{-d}$, respectively. Something similar happened in the study by Arsalan et al., (2021), when CC (length= 5 cm,

$\phi = 2.5$ cm) was used in the organic matter removal, an increase in the HRL from 27 to 71 $\text{m}^3/\text{m}^2\text{-d}$ produced about 12.5% decrease in the removal. Likewise, Katam et al., (2020), found a decrease from 96 to 86% in the caffeine removal by reducing the HRT from 12 to 8 h, respectively. In this study, polyurethane foam sponge cubes ($2 \times 2 \times 2$ cm) were used as the filter bed.

In spite of this phenomenon is not observed when the HLR is increased from 1 to 2 $\text{m}^3/\text{m}^2\text{-d}$, since the highest caffeine removal efficiencies are achieved when operating with an HRL=2 $\text{m}^3/\text{m}^2\text{-d}$. This could be since in filters that operate with HRL=1 $\text{m}^3/\text{m}^2\text{-d}$, caffeine desorption increases, which increases the concentration in the effluent reducing the efficiency of the filtering systems. The separation of the contaminant from the CC can be a product of the material degradation. The degradation of the material was perceptible in all filters since changes in the organoleptic properties (color and smell) were observed (Figure 48). However, only the filters that operated with an HRL= 1 $\text{m}^3/\text{m}^2\text{-d}$ generated unpleasant odor (characteristic of degradation processes). Also, mosquitoes were found on top of the filters. pH is another parameter that evidenced the material degradation.

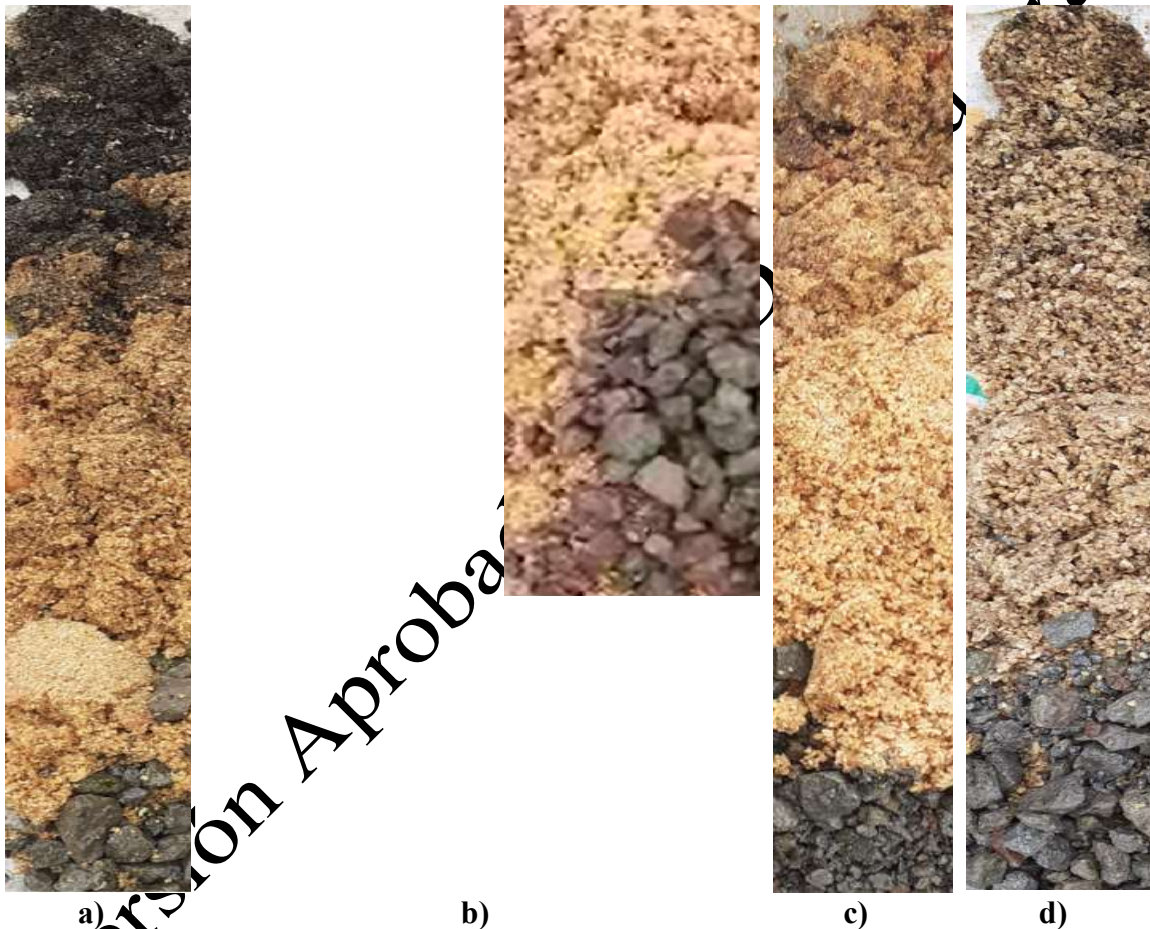


Figure 48. CC at the saturation with caffeine using an HRL=1 $\text{m}^3/\text{m}^2\text{-d}$. a) SPF (204 h), b) MPF (168 h), c) MxPF (138 h) and d) LPF (150 h).

The pH changes as function of time are shown in Figure 49. It is observed that the SPF, MxPF, MPF and LPF that worked with lower HLR presented a greater pH variation (up to 2.3, 2.0, 2.1 and 1.6, respectively) with respect to the filters that work with the highest loads (up to 2.0, 1.4, 1.6, 0.9, respectively). Different microorganisms can have different optimal pH values, and there is not a certain optimal range for all strains, many times changes in pH do not affect the microorganisms, but they can affect their efficiency in removing contaminants. In the removal of chromium (VI), pH changes of up to 2 units were reported, the more acidic pH favored the denitrification process. However, there were no significant differences in the chromium removal when the most basic pH values were reached (H. Wang et al., 2018).

Furthermore, initially there is a decrease in pH and later the pH stabilizes or begins to increase. In the degradation of organic matter, ammonium and acid ions are produced. If acids (carboxylic, phenolic and humic acids) are generated during the degradation, the pH decreases, and if ammonium ions are generated, the pH increases (Sharma & Garg, 2019). Material degradation is produced by the bacteria presence. According to Arora et al. (2014), the material degradation is due to the presence of microbial communities. Microbes generate extracellular enzymes that are capable of breaking down cellulose, proteins, starch, sugars, and phenolic compounds that are present in the material. The decomposition processes are linked to changes in pH and these in turn can modify the adsorption/precipitation of contaminants in the filter bed (Arora et al., 2014). In addition, in previous studies such as the one carried out by Tejedor et al. (2020), it has been verified that HLRs close to $1 \text{ m}^3/\text{m}^2\text{-d}$ (between 0.5 and $1.5 \text{ m}^3/\text{m}^2\text{-d}$) in biofilters favor a greater growth of microorganisms. On the other hand, the environmental conditions of the filters are suitable for the development of bacteria, since mesophilic conditions ($15 - 40 \text{ }^\circ\text{C}$), presence of water, pH between 4.5 and 8.5 and availability of food (in this case the material and caffeine) (Baltrėnas & Baltrėnaitė, 2020).

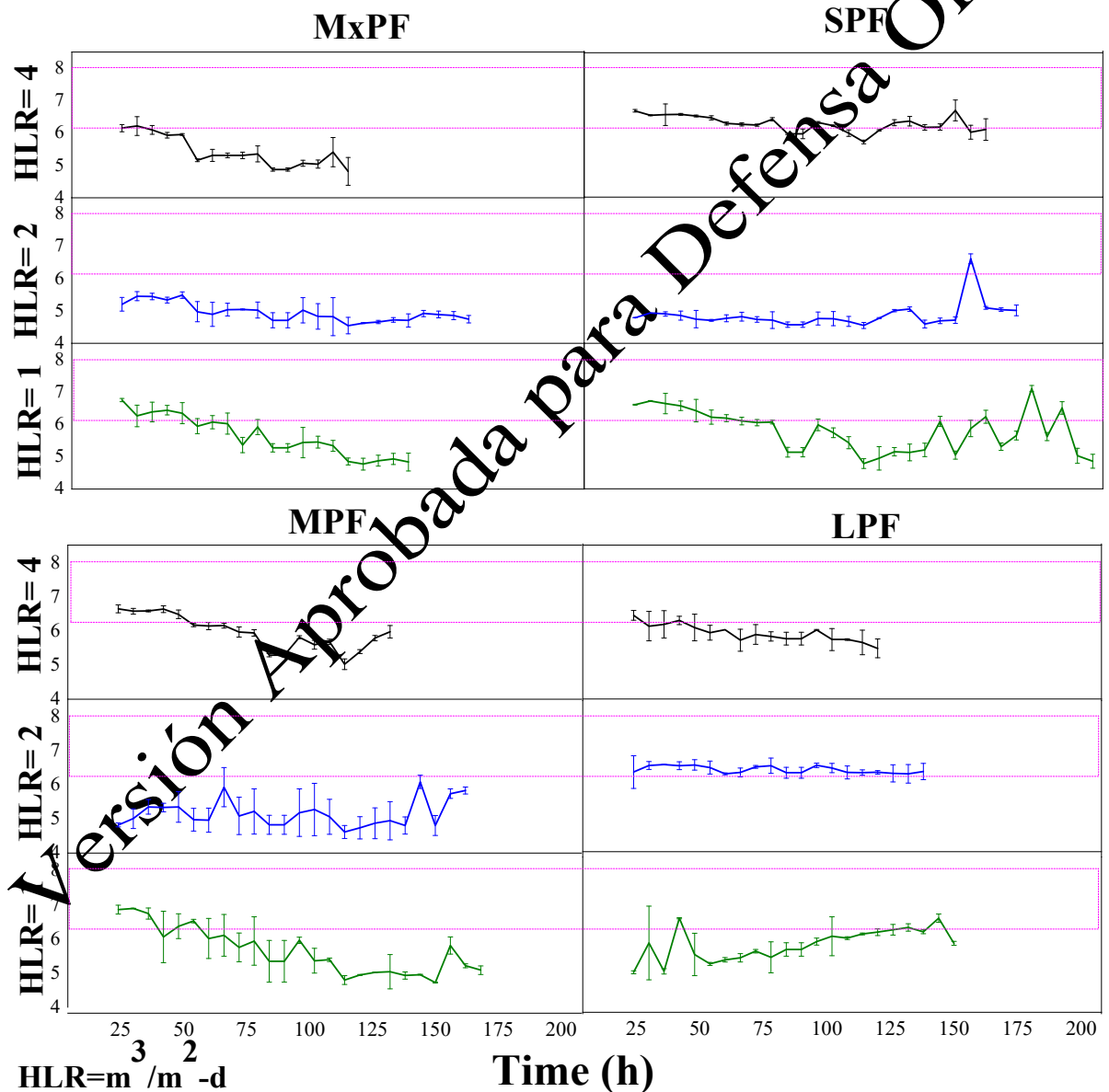


Figure 49. pH performance in the removal of caffeine by particle size. Dot fuchsia lines= optimal pH range to the microorganism development.

The degradation of the material was verified with the result of the FTIR analysis (Figure 44). In the saturated SPF (material after caffeine removal), three samples of material located at different heights of the column were taken: top=CC_{top}, middle=CC_{middle}, and bottom=CC_{bottom}. This was done because different changes in the CC color was observed within the filter, as shown by the photos in Figure 48. Macroscopic changes could be associated with the longer operating time (204 h) of SPF compared to the other filters. Nevertheless, the FTIR spectrum does not show significant changes between the different saturated CC and the raw CC; but they are more noticeable in the CC_{top}. Changes are observed in the bands around 2900 (CH₃, CH₂, O-CH₃ groups) and 1600 cm⁻¹ (C=C groups); these could be associated with the degradation of the aliphatic structure and the humification of lignin, respectively. There are also changes in the band around 1100 cm⁻¹ (C-OH and C-O groups), which indicates that the carbohydrates and polysaccharides were degraded (Hu et al., 2011).

On the other hand, in the CC_{top} the presence of bands around 3700 and 2300 cm⁻¹ can also be observed, which are characteristic bands of caffeine. The change in the intensity of the bands near 3300 (OH groups) and 1750 cm⁻¹ (C=O groups) can also be associated with the presence of caffeine in the CC (Paradkar & Irudaryaraj, 2002).

So far, it has been determined that the removal of caffeine is favored by decreasing the HLR and the particle size. However, it is necessary to determine if the particle sizes favor the hydraulic operation of the filter. The hydraulic operation of the filters in the removal of caffeine is shown in Figure 50. Hydraulic conductivity values varied between 48.3 and 185.1 mm/h. While the head losses values were between -3.0 and 4.8 cm water. The SPF, MPF, MxPF and LPF filters, when operated with HLR=1 and 2m³/m²-d, presented hydraulic conductivities lower than 100 mm/h. Being the SPF and MxPF the ones that presented the lowest conductivity values (around 50 mm/h). While with an HRL= 4 m³/m²-d, all filters presented a hydraulic conductivity greater than 100 mm/h. However, the LPF presented the highest hydraulic conductivity (between 118.3 and 185.1 mm/h). It is observed that both the hydraulic conductivity and the head losses are related to the characteristics of the CC (size and shape) and to the HLR. A smaller CC size decreases hydraulic conductivity and increases head losses. The mixture of the different sizes of CC did not favor the hydraulic operation of the filters, this occurs because the small material presented greater compaction over time and modified the wastewater flow (Le et al., 2020). This same phenomenon was observed in the SPF. Likewise, the irregular shape of the CC negatively influences the hydraulic operation of the filter, even though it benefited the caffeine removal. Because of irregular particles reduce the porosity of the bed and increases the specific surface area available for biofilm growth (Kandra et al., 2014). Moreover, hydraulic conductivities below 100 mm/h are not favorable since they could cause the accumulation of sediments and clogging. While hydraulic conductivities greater than 400 mm/h reduce the contaminant removal (Payne et al., 2015; Tejedor et al., 2020). Therefore, the LPF working with HLR= 4 m³/m²-d shows the best hydraulic operation.

The hydraulic conductivity values are low compared to those obtained by Tejedor et al., (2020). This is probably due to the fact that in that study only a fraction of the active layer (25%, height= 30 cm) had the same size as the one investigated (0.8 – 2.0 cm) and the rest was larger chips. The smaller particles leave smaller spaces between them that, over time, become clogged and hinder the passage of wastewater (Le et al., 2020). Therefore, the systems studied are probably not efficient when treating domestic wastewater, since their efficiency in hydraulic terms may be lower, that is, the filters may clog in shorter times.

Although the MPF is susceptible to clogging (hydraulic conductivity less than 200 mm/h), it did not happen during the operation of the filters as in the case of the SPF. In addition, this filter has the second-best caffeine removal efficiencies, and considering that the optimal HLR for these systems was 2, it was decided that the triclosan removal would be done under these operating parameters. The triclosan removal is presented as following.

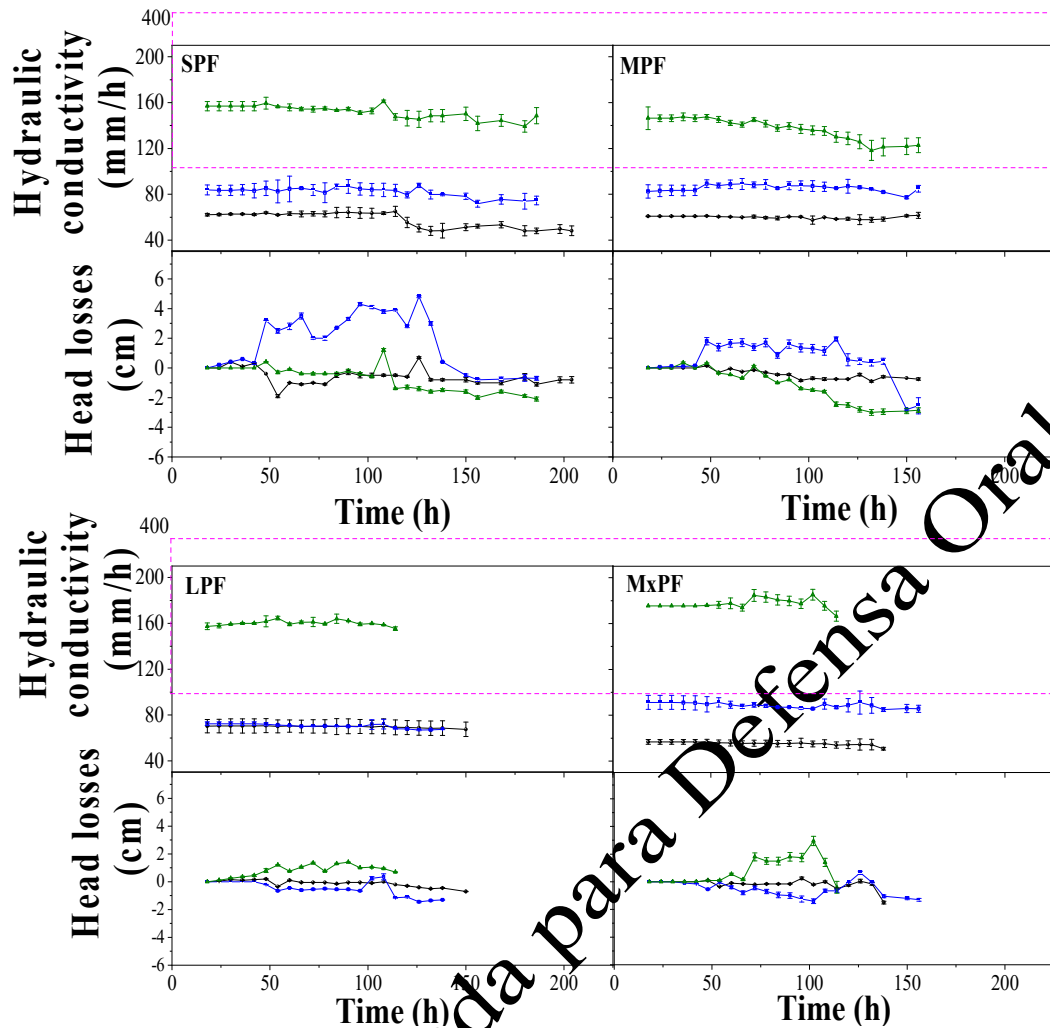


Figure 50. Hydraulic conductivity and head losses in the removal of caffeine. Black line= $1 \text{ m}^3/\text{m}^2\text{-d}$, blue line= $2 \text{ m}^3/\text{m}^2\text{-d}$, green line= $4 \text{ m}^3/\text{m}^2\text{-d}$. Dot fuchsia lines= optimal range of hydraulic conductivity to avoid clogging.

3.2.2. Triclosan removal

Figure 51 shows the triclosan removal in the MPF. Like caffeine, there are sudden changes at the beginning of the operation, which could be associated with the stabilization process of the filters. Efficiencies between $92.96 (\pm 0.10)$ and $91.57 (\pm 1.10)\%$ were maintained for a period of 84 h of operation. That is, the material presents a certain stability in the triclosan removal during this time and later the efficiency begins to decrease slowly until the CC reaches saturation at 246h of operation. The decrease in the removal of both caffeine and triclosan occurs because over time the active sites of the material are occupied with the contaminants, this occurs until all the sites are occupied (Almeida-Naranjo et al., 2021a).

The behavior observed is different from that of caffeine since this stability period does not occur. Moreover, their removal and the saturation time of their filters are shorter (9.49% and 48h, respectively). These differences are produced by the different physical-chemical characteristics that caffeine and triclosan have. Triclosan's lower water solubility/high hydrophobicity compared to caffeine allows it to be more rapidly adsorbed. Likewise, the high K_{ow} value results in a greater affinity of triclosan with organic matter, which is why it adheres easily to the surface of the CC (Montaseri & Forbes, 2016).

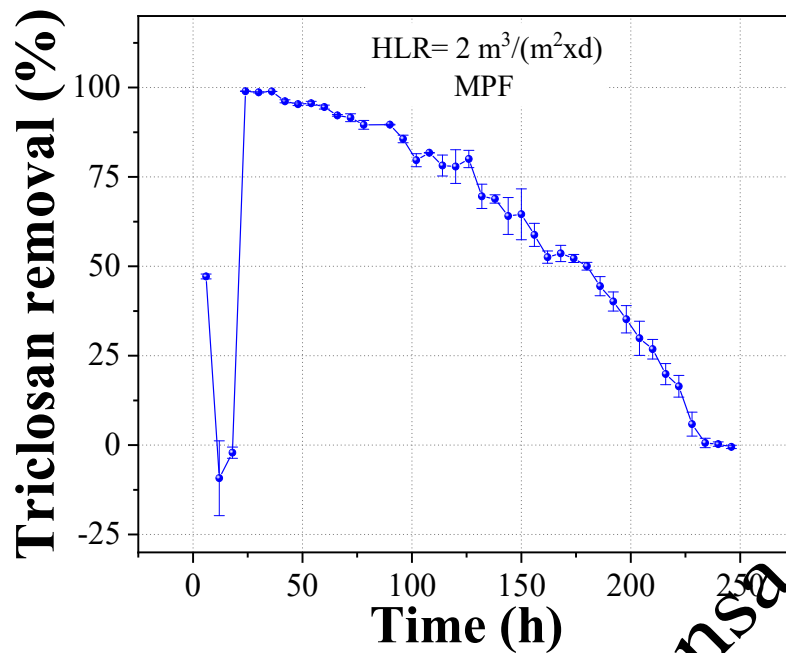


Figure 51. Filter performance in the removal of triclosan

On the other hand, the pH of the filter was maintained between 5.12 and 7.36 (Figure 52). The pH was higher than pH of filters used in the caffeine removal because the triclosan was prepared with 0.1 M NaOH solutions. However, triclosan filters also show pH changes, it would also indicate that the material is degrading. In Figure 53, a photograph of MPF that was fed with triclosan and the control filter that was used in this stage of operation is presented. As can be seen, the control filter material is more degraded than the one adsorbing triclosan even though the control operated with drinking water. This probably occurs because triclosan has some degree of toxicity to bacteria. Triclosan can alter the structure or function of microorganisms both in the environment and in engineered systems. For example, at concentrations between 0.02-4.0 mg/L, triclosan can decrease the abundance and diversity of denitrifiers in aged biosolids from activated sludge systems (Gao et al., 2019). Furthermore, triclosan can interfere with the stability and topology of protein structures of viruses and bacteria due to its hydrophobicity (low K_{ow}), inhibiting their biological function (Shrestha et al., 2020).

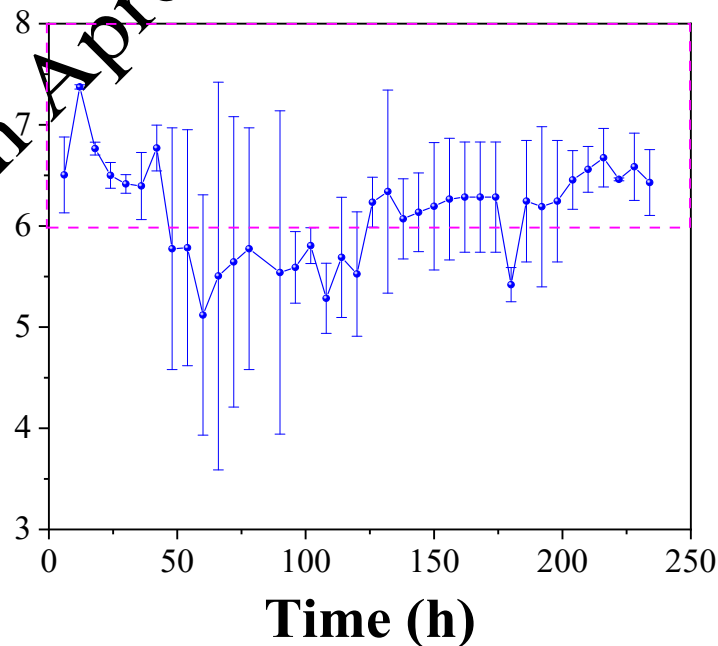


Figure 52. pH performance in the removal of triclosan. Dot fuchsia lines= optimal pH range to the microorganism development.



Figure 53. a) Control: MPF feed with drinking water b) MPF at the saturation with triclosan c) MPF duplicated. HRL=2 m³/m²-d.

On the other hand, the hydraulic behavior of the MPF filter that operated with triclosan present hydraulic conductivity between 78.6 mm/h (at the beginning) to 62.1 mm/h (at the end). This is more stable over time than the one that worked with caffeine, as can be seen in Figure 54. This suggests that triclosan has an effect on the bacteria deposited in the material, in such a way that large changes in the filter system are avoided. A similar behavior is showed in the head losses. The head losses in the MPFs that operated with triclosan was lower (between -0.2 and -4.4 cm of water) than in the caffeine MPFs (between -2.8 and 2.0 cm of water), in spite of the MPFs with triclosan worked for a longer time. Moreover, the head losses in triclosan have a definite trend, this may also be related to triclosan toxicity.

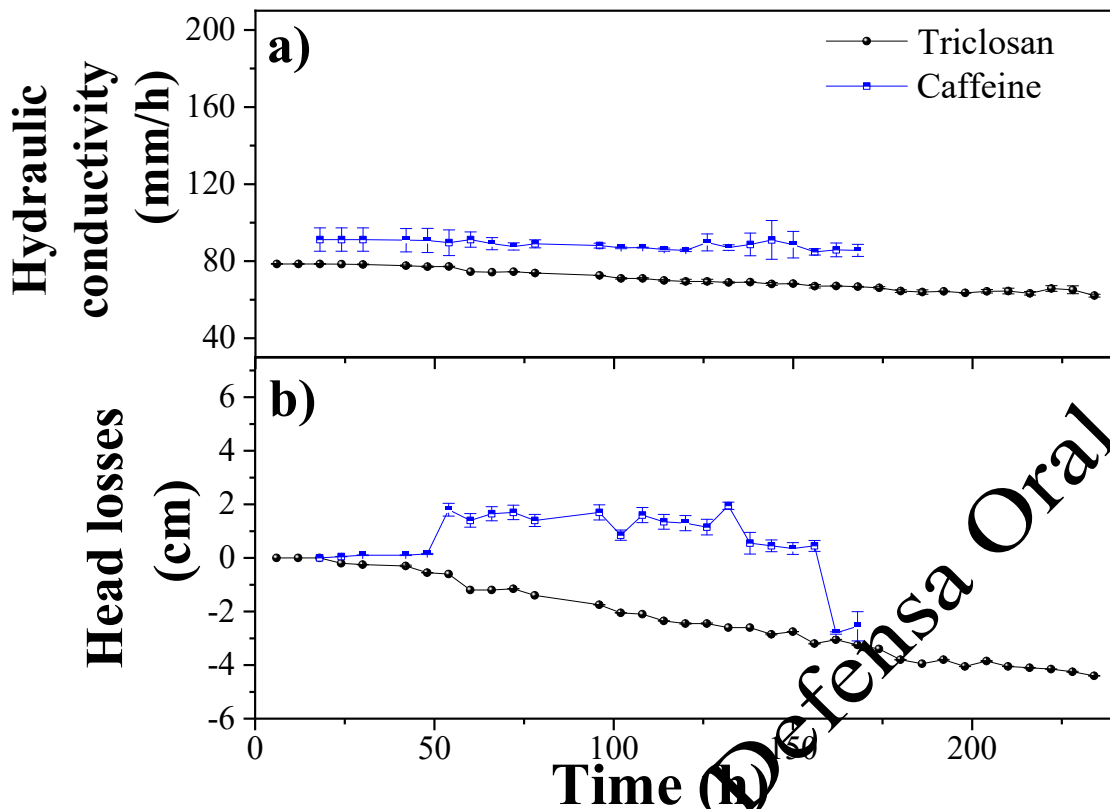


Figure 54. a) Hydraulic conductivity and b) head losses in the removal of caffeine and triclosan. Particle size= medium and HLR= $2 \text{ m}^3/\text{m}^2\text{-d}$

The CC removed caffeine and triclosan efficiently. It was evidenced that the particle size of the CC and the HLR influence it. The small particles (0.8-2.0 cm) operating with HRL= $2 \text{ m}^3/\text{m}^2\text{-d}$ were the optimum configuration and operating conditions for caffeine removal, respectively. However, in hydraulic terms, small particles are not a good alternative since they caused clogging. Therefore, medium particles (2.0-3.5 cm) were used in the triclosan removal. The removal efficiency of triclosan was higher for more time (>90% for 84 h) than that of caffeine, this is because caffeine has high water solubility/polarity and low K_{ow} compared to triclosan. Furthermore, the filters that operated with triclosan presented a better hydraulic behavior, this is associated with the fact that triclosan could have a control effect on microorganisms due to its toxicity, this prevents/decreases the paths through which the solution circulates from being clogged by formation of biofilm. Thus, this section shows that agro-industrial residues can be efficient in the removal of emerging contaminants such as caffeine and triclosan. However, certain disadvantages of the material are also observed, such as its susceptibility to degradation and clogging of filters. Therefore, it is necessary to continue investigating the possibility of improving this type of system. One of the alternatives is to combine them with living beings, such as plants and earthworms, or mix them with other materials (e.g., raw, treated, composites) to improve their properties. Likewise, it is important to define the behavior that the filtering systems will have if they are feed with wastewater. It is for this reason that the following sections present the results of works related to these topics.

4. Conclusions

Filters ($h=90 \text{ cm}$ and $\phi=10 \text{ cm}$) with ground corn cobs as bed material are an alternative to remove caffeine and triclosan, using hydraulic heads of up to $2 \text{ m}^3/\text{m}^2\text{-d}$ and intermittent feed of 6 h/d. The filters that used material between 2.0 and 3.5 cm were the most efficient in terms of caffeine and triclosan removal (85.6-94.4% and 91.6-99.0%, respectively). While in the largest particles they presented the best hydraulic behavior (greater than 180 mm/h). Triclosan was more easily removed than caffeine, taking almost twice the time to saturate corn cob. However, degradation was observed in the superficial layer of the columns. Although the filter in which the mixture of CC particle sizes was used was not efficient in

terms of hydraulics or material degradation, the results obtained are a premise to continue studying other filter configurations.

Although in this part of the investigation it was shown that corn cobs are an alternative to remove caffeine/triclosan in filtration technologies, it is important to determine their biocompatibility, as well as that of other residues. This in order to use biofiltration technologies in order to prolong, for example, the saturation time of the residue, its hydraulic behavior and reduce its degradation (hydrolysis). Well, this last problem could increase the content of organic matter in the treated water (effluent). Therefore, in the following section a study of the toxicity of rice husk, peanut shell, corn cob and coconut fiber is carried out, this test is complemented with the adsorptive capacity of these materials to remove caffeine.

Versión Aprobada para Defensa Oral

Article 6. Caffeine adsorptive performance and compatibility characteristics (Eisenia foetida (Savigny)) of agro-industrial residues potentially suitable for vermifilter beds

Almeida-Naranjo, C. E., Frutos, M., Tejedor, J., Cuestas, J., Valenzuela, F., Rivadeneira, M. I., Villamar C.A. & Guerrero, V. H. (2021). Caffeine adsorptive performance and compatibility characteristics (Eisenia foetida (Savigny)) of agro-industrial residues potentially suitable for vermifilter beds. *Science of The Total Environment*, 801, 149666.

ABSTRACT

The caffeine adsorptive performance and ecotoxicological characteristics (*Eisenia foetida (Savigny)*) of rice husk, peanut shell, corn cob and coconut fiber were studied, aiming to assess the suitability of these residues for vermifilter beds. For this purpose, the agro-industrial residues were characterized and the *E. foetida Savigny* toxicity was determined by acute and chronic toxicity tests. Batch adsorption tests were performed using caffeine solutions. Optimal adsorption conditions, kinetic models, isotherm type and the influence of three particle sizes (120 – 150, 300 – 600, 800 – 2,000 μm) in the caffeine removal were determined. Coconut fiber (120 – 150 μm) proved to be the most efficient residue for the caffeine removal (94.2%), requiring 4 g/L for 30 minutes. However, coconut fiber was the most toxic for earthworms (14d-LC₅₀= 82%). The results obtained allow to define adequate strategies (e.g., mixing highly adsorptive residues with the less toxic ones) to choose the most effective materials for vermifiltration technologies.

1. Introduction

The negative impacts associated to wastewater production (4,600 km³/year) have rapidly increased during the last decades (Singh et al., 2019). Therefore, one key challenge is to remove contaminants, many of them persistent and very toxic, before water is used. For this reason, intense research is focused on developing materials and technologies to remove water contaminants (Ishaq et al., 2020).

Pharmaceuticals and personal care products (PPCPs) are among the relatively new and concerning contaminants detected around the world. Caffeine (1,3,7-trimethylxanthine, CAF) is one of the most common PPCPs, found mainly in common drinks (cola drinks, tea, coffee, energy drinks), achieving an average daily consumption worldwide of 170-199 mg/(inhab day) (Anastopoulos et al., 2020b; Korekar et al., 2019). Furthermore, during the confinement due to the SARS-CoV-2 pandemic, the consumption of energizers, coffee and tea has increased (Abbas & Kamel, 2020). After it is consumed, CAF becomes a contaminant which is found in groundwater (0.02 – 23.97 $\mu\text{g/L}$), surface water (753.5 – 1,100 $\mu\text{g/L}$), rain water (0.18 $\mu\text{g/L}$), drinking water (0.5 – 5.0 $\mu\text{g/L}$), and wastewater treatment plant (WWTP) discharges (up to 303.6 $\mu\text{g/L}$). These concentrations are higher than those of other PPCPs (Korekar et al., 2019). Regarding toxicity, CAF concentrations up to 200 mg/L do not produce human health effects. Nevertheless, CAF evidences chronic toxicity on aquatic organisms, such as zebra fish, decreasing the growth rate on fish embryo development at concentrations greater than 2.6 $\mu\text{g/L}$ (Korekar et al., 2019). While in aquatic organisms such as *Mytilus californianus*, *Ruditapes philippinarum* and *Carcinusmaenas*, CAF produces cellular stress (Anastopoulos et al., 2020a).

PPCP removal in WWTPs is variable and depends on their physicochemical characteristics and the technology used. However, conventional WWTPs have relatively high implementation and operation costs (e.g., activated sludge system: 65 – 200 USD/inhab) and could not be applicable in decentralized contexts (< 2,000 habitants) (Tejedor et al., 2020). Non-conventional technologies as vermifiltration are an adaptable alternative for communities with < 2,000 habitants, and have been successfully used in the removal of PPCPs such as sulfamethoxazole, ciprofloxacin, tetracycline, ofloxacin, among others, reaching removals between 30 and 97% (Shokouhi et al., 2019).

Vermifiltration is also interesting because of a series of advantageous features such as easy operation, minimal sludge generation and energy consumption (up to 80% less) (Chicaiza et al., 2020). The removal efficiency of vermifilters showed also greater stability than that of activated sludge systems. In addition, vermifilters reduce the PPCP toxicity because earthworms contribute to their mineralization (Shokouhi et al., 2019).

The vermifilter performance in PPCP removal is a function of the symbiotic relationships between a biotic component (earthworms + microorganisms) and a non-biotic component (bed filter material) (Chicaiza et al., 2020). Conventional materials such as wood chip, gravel and sand, combined by layer, have been used as bed filter material. However, their use represents around 50% of the investment cost (Zhou et al., 2015). Therefore, one of the key challenges to improve the feasibility, usability and performance of vermifilters lies on the selection and use of inexpensive and adequate bed filter materials. These materials should be widely available, easy to process, durable, high-performing, and easy to dispose (Tejedor et al., 2020). Non-conventional materials such as agro-industrial residues represent promising alternatives (Adugna et al., 2019; Tejedor et al., 2020).

Agro-industrial residues are widely available; for instance, rice husk and coconut fiber achieved an annual generation of up to 150 and 57 million tons, respectively (Lin and Cramon-Taubadel, 2019; Pode, 2016). These residues have a relatively high specific surface area (0.034 – 120 m²/g), simple processing (washing, drying, grinding), and low or no costs (e.g., rice husk: 25.0 – 48.5 USD/ton) (Anastopoulos et al., 2020a; 2020b; Mo et al., 2018; Ngoc et al., 2018). Their high content of lignin (20 – 30%), cellulose (35 – 50%) and hemicellulose (15 – 30%), the presence of active surface functional groups (OH-, COOH-, C₆H₆O, CH₃O-) and their good chemical/mechanical stability, make them good adsorbents (Mo et al., 2018; Pode, 2016). Additionally, most agro-industrial residues are also non-toxic to earthworms, even though some of the products of the incomplete degradation of lignin have shown high toxicity levels in earthworms such as *Eisenia foetida* (Savigny) (LC₅₀ of 0.6 and 0.7 µg/cm² for 2,4-dinitrophenol and 4-nitrophenol, respectively) (Neuhauser et al., 1985). For instance, the reduction in survival (< 46.7%) and weight (< 32.1%) of *Eisenia foetida* (Savigny) in vermifilters has been attributed to bed filter material composition (100% v/v of peanut shells) and its hydrolysis (Tejedor et al., 2020).

Despite their great potential as bed support in vermifilters intended to remove emerging contaminants, widely available materials such as rice husk, peanut shells, corn cob, and coconut fiber have not been sufficiently studied (Anastopoulos, et al., 2020b). Therefore, the aim of this work was to characterize the physicochemical properties of these residues, and to evaluate their caffeine adsorptive performance and ecotoxicological characteristics (*Eisenia foetida* (Savigny)), to assess their potential use for vermifilter beds. This could contribute to elucidate the relationship between the properties of bed support materials and the removal of PPCPs in vermifilters, and to improve their performance.

2. Materials and Methods

2.1. Agro-industrial residues conditioning

This study was carried out in Ecuador, where rice husk (RH), peanut shells (PS), corn cob (CC), and coconut fiber (CF) were obtained from Bucay city (location S 2°11'23.1", W 79°09'49.6"W), Loja city (location S 3° 59' 35.3", W 78° 12' 15.2"), Saquisilí city (location S 0° 50', W 78° 40'), and Lomas de Sargentillo city (location S 1° 53' 00", W 80° 05' 00"), respectively. The residues were washed and dried at 80 °C for around 24 h. Then, they were ground using a Thomas knife mill and the adsorbent particles were sieved and classified in three different size groups: 120 – 150 µm (small), 300 – 600 µm (medium) and 800 – 2,000 µm (large), and later they were characterized as detailed.

2.2. Experimental assays

2.2.1. Batch adsorption tests

The solutions used in batch adsorption were prepared from the dilution of a 100.0 ppm standard solution prepared with ReagentPlus® caffeine, 99.0% pure, from Sigma-Aldrich. The adsorption batch tests were performed using 100 mL beakers at room temperature, in dark conditions to avoid photo-degradation and stirring at 150 rpm. About 20 mL of CAF solution of 30 ppm was placed in each beaker, setting an adsorbent dose according to the particle size and type (RH, PS, CC or CF). The adsorbent dose used was between 1 and 50 g/L. Each test was performed in triplicate and distilled water was used as control system.

The optimal dose for adsorption was determined for each adsorbent and for each particle size. For this purpose, the adsorbent was placed in contact with the CAF solution for 180 min. The optimal contact time was determined by placing the optimal adsorbent dose in contact with the CAF solution for up to 300 min.

Adsorption kinetic and adsorption equilibrium isotherm studies were performed according to the optimal dose and contact time for each residue and particle size. In the adsorption kinetic tests, caffeine solutions of 30 ppm and in the isothermal ones, with concentrations of 10, 20, 30, 40, 50 and 60 ppm were used. Data collected were fitted to the pseudo-first and pseudo-second-order kinetic models and to the Langmuir and Freundlich isotherm models. These classical models have shown good fitting to the equilibrium models (R^2 close to 1) described by agro-industrial residues in the removal of several contaminants (Anastopoulos et al., 2015).

2.2.2. Compatibility tests: acute and chronic bioassays

The earthworm's tolerance (*Eisenia foetida* (Savigny)) to RH, PS, CC and CF were driven by acute and chronic compatibility studies. *Eisenia foetida* (Savigny) species was analyzed because it is considered a representative species of the earthworms' soil fauna (OECD, 2015). The earthworms were obtained from a peri-urban farm located near Quito city. The species was verified by taxonomic records of ITIS (2020).

The method OECD (2015) modified was used for compatibility tests. Initially, acute assays were carried out with concentrations of 1.5, 3.0, 6.5, 12.5 and 25% v/v for the four residues. However, the results did not show significant differences ($p > 0.05$), mainly RH respect to the control (residues= 0% v/v), so that higher concentrations were used in the definitive assays. Before each compatibility assay, intestinal contents from *Eisenia foetida* (Savigny) individuals were purged. Individuals were placed for three hours on moistened cellulose paper and washed with deionized water. The acute and chronic compatibility tests using RH, PS, CC and CF were carried out in triplicate under optimal environmental conditions (20 ± 2 °C, pH 5 – 9, humidity 55 – 95%). The acute compatibility tests were carried out for 14 days. Ten clitiated two-month-old individuals with live weight from 0.25 to 0.65 g were placed in each container (V = 1.98 L). In the acute tests, for PS, CC and CF four different agro-industrial residue concentrations (control= 0, 25, 50 and 100% v/v) mixed with artificial soil (10% peat, 20% kaolin clay, 70% quartz sand) were evaluated. For RH three different concentrations (control= 0, 50 and 100% v/v) mixed with artificial soil were used. The lethal concentration (LC_{50}) was determined as a function of mortality or non-mobility of 50% or more of the exposed *Eisenia foetida* (Savigny) individuals. The earthworm chronic effects tests were carried out between 28 and 35 days under the same acute assays' conditions (OECD, 2015).

2.3. Analytical and instrumental methods

Composition of agro-industrial residues were determined according to the ASTM standards detailed before. The determination of total organic carbon and total nitrogen were carried out, using the wet digestion with sulfuric acid/potassium dichromate and Kjeldahl methods, respectively.

The surface morphology of RH, PS, CC and CF particles, their functional groups and their surface area/pore size/pore volume were analyzed with the same equipment of Articles 1 and 2. CAF concentrations in the batch adsorption tests were determined using an Analytik Jena Sperscord 210 Plus UV-VIS spectrophotometer at 287 nm.

2.4. Data analysis

2.4.1. Adsorption batch tests

Optimal dose and contact time were determined by performing an analysis of variance (ANOVA) with the CAF removal data obtained for each adsorbent particle size (large, medium, and small). Previously, normality was evaluated using Anderson Darling test. ANOVA parametric analysis was established using Tukey's test with a significance level of 0.05. The software used was Minitab 18 version 1.0. Moreover, the optimal adsorbent particle size was determined using OriginPro version 8.5 and comparing the adsorption efficiency with the adsorbent dose.

2.4.2. Compatibility tests: acute and chronic bioassays

Acute toxicity (LC_{50}) was determined using Probit (normal distribution) or Spearman-Kärber (non-normal distribution) tests. Chronic toxicity (NOEC) was determined using analysis of variance (ANOVA) with a significance level of 0.05. The Chi-square and Barlett tests were previously used to determine normality and variance homogeneity, respectively. Dunnett's test (normal distribution) and/or Kruskal-Wallis test

(non-normal distribution) were performed. The statistical programs were Toxtat (version 2.1), EPAProbit (version 1.5) and Spearman-Karber (version 1.5).

3. Results and discussion

3.1. Adsorbent's characterization

3.1.1. Physical-chemical characterization and proximal analysis

Figure 55 summarizes the physicochemical characterization and proximal analysis of the agro-industrial residues. Results evidenced that CF ($40.5 \pm 0.5\%$ w/w) and PS ($36.2 \pm 4.4\%$ w/w) had the highest lignin content. CC ($45.5 \pm 1.0\%$ w/w) and PS ($19.4 \pm 5.9\%$ w/w) reported the highest and the lowest cellulose content, respectively. Meanwhile, CC ($33.3 \pm 0.8\%$ w/w) and CF ($19.8 \pm 0.3\%$ w/w) reported the highest and the lowest hemicellulose content, respectively. Lignocellulosic compounds, mainly lignin, from agro-industrial residues generate a fibrous and porous structure with several functional groups (e.g., methoxy, methyl, hydroxyl, phenolic, ether and carboxyl) (Mo et al., 2018; Pode, 2016).

Volatile solids showed concentrations with mean values between $63.5 (\pm 2.4)$ and $91.5 (\pm 10.0)\%$ w/w. High values ($\geq 60\%$) of volatile solids from agro-industrial residues are characteristic of better adsorption properties, due to lignin, cellulose and hemicellulose presence (Mussatto et al., 2010). On the other hand, ash content was relatively low in the studied residues, whose values were between $1.4 (\pm 0.1)$ and $18.2 (\pm 4.6)\%$ w/w. RH contains the highest ash percentage, probably due to the silica presence in form of silicon-cellulose (Chowdhury et al., 2011; Eliche-Quesada et al., 2017). Silica acts as a barrier between the functional groups present on the RH surface and the contaminants. Therefore, it can be expected that CF and PS will have higher CAF adsorption capacity than RH and CC since they have the highest lignin concentration. However, the adsorption capacity of CF and PS could be affected by the extractive presence because extractives reduce the active sites of the residues (Chowdhury et al., 2011).

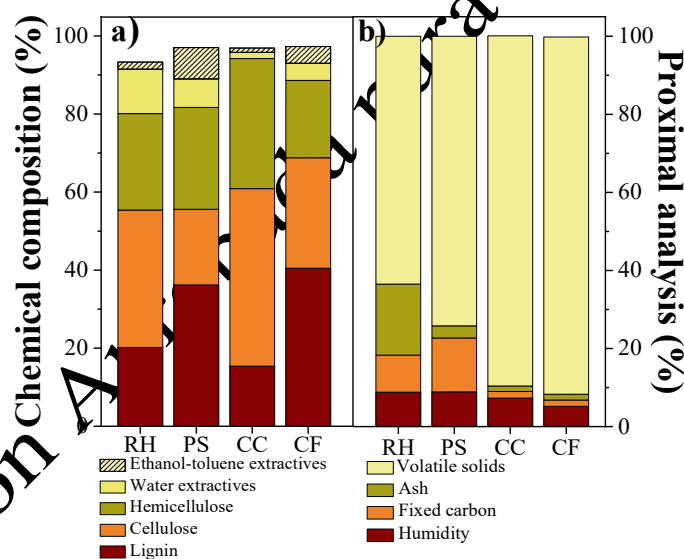


Figure 55.

a) Physicochemical composition and b) proximal analysis of agro-industrial residues.

3.1.2. FTIR, SEM and BET analyses

Figure 56 shows the FTIR spectra obtained before and after CAF adsorption, and SEM images before the CAF adsorption, corresponding to the more efficient particle sizes (small) for RH, PS, CC and CF. The bands around 3300 and 2900 cm^{-1} correspond to the stretching vibrations of the OH- group and C-H bond, respectively. The bands between 1700 cm^{-1} and 1600 cm^{-1} correspond to the C=O bonds; while the bands between $1259\text{-}1216\text{ cm}^{-1}$ and $1375\text{-}1362\text{ cm}^{-1}$ are due to the C-H bending, both functional groups are present in the cellulose and hemicellulose. The vibration of the lignin aromatic ring is represented by several groups of bands (around 1600 , 1500 , 1400 and 1300 cm^{-1}). The bands around 1160 cm^{-1} represented the antisymmetric stretching of the C-O-C bond of the cellulose. The bands between 1000 and 1300 cm^{-1} appeared due to the vibration of the C=O bond stretch of the carboxylic and alcohol groups (Beltrame et al., 2018; Zhang et al., 2015). The FTIR analysis showed the presence of several functional

groups in agro-industrial residues (mainly carboxyl and hydroxyl) that could be the main adsorption sites for the CAF removal.

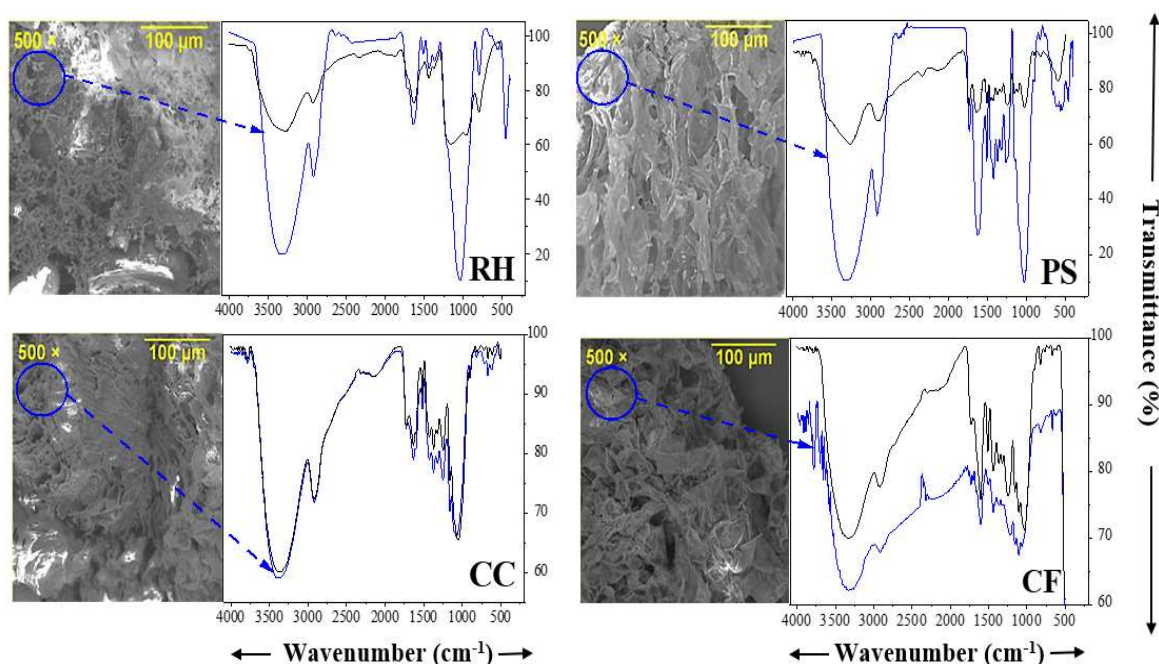


Figure 56. SEM images before CAF adsorption, and FTIR spectra before (blue line) and after CAF adsorption (black line) by agro-industrial residues (small particle size).

On the other hand, SEM images show that residues have an uneven surface where contaminants could be deposited. RH evidences an irregular surface with cavities and grooves and PS showed a compact and ordered porous surface. The CC exhibits a heterogeneous surface, characteristic of lignocellulosic materials. In the case of the CF surface, we observe a folding layer whose openings give rise to the pores (de Franco et al., 2017; Wang & Li, 2015). Therefore, agro-industrial residues show an irregular morphology with the presence of pores. These surface characteristics would facilitate the retention of CAF molecules. However, the medium (300 – 600 μm) and large (800 – 2,000 μm) particle sizes compared with the small particles showed less irregularity in their surface, so small particles could remove more CAF (Liu et al., 2016).

Table 30 shows the parameters of BET analysis for agro-industrial residues. The surface area (SA) of agro-industrial residues is relatively low (1.12 – 1.80 m^2/g) with minimal differences between them, being SACF > SAPS > SAPE > SACC. The values obtained are within the range of the SAs obtained in other studies. The ranges of SAs were very wide (between 0.1 and > 7.0 m^2/g) due to the different species existing in each residue (Daffalla et al., 2020; Kolar & Jin, 2019; Messina et al., 2015). The pore diameters of the four residues were between 2 and 50 nm, which according to the IUPAC is characteristic of mesoporous materials (Beltrame et al., 2018).

Table 30. Surface area, pore volume and pore diameter of agro-industrial residues.

Agro-industrial residue	Surface area (m^2/g)	Pore volume* 10^{-3} (cm^3/g)	Pore diameter (nm)
RH	1.18	6.36	9.95
PS	1.73	4.84	3.15
CC	1.12	4.20	4.12
CF	1.80	4.08	3.44

3.2. Adsorption optimization

Figure 57 shows the influence of the adsorbent dose and contact time on the CAF adsorption. An increase in the dose and contact time favors the CAF removal, reaching efficiencies between 51.9% and 96.4%. This is because increasing the amount of the adsorbents, increases the number of active sites and the surface area (Żółtowska-Aksamitowska et al., 2018). However, a higher dose than the optimal (7 – 16 g/L) does not produce a significant difference ($p > 0.05$) in the CAF removal using PS and CF. On the

other hand, the CAF removal efficiency decreased after the optimal dose was surpassed in the cases of RH (20 – 30%) and CC (10 – 30%). An excess of RH and CC could generate agglutination and the decrease of the surface that will be in contact with CAF (Noreen et al., 2013).

The optimal contact time for the small, medium, and large particles of RH, PS and CC was 180 min. For CF, the optimal contact time was shorter for the small (30 min), medium (45 min) and large (60 min) particles. The highest removal percentage was achieved at 180 min for RH and CC (Figures 46e and 46g). Once that optimal time had elapsed, the efficiency decreased (0.03 – 0.10%/min) as the contact time increased. This decrease could occur because active sites of the agro-industrial residues were saturated. Moreover, the aggregates formed by RH and CC particles suggest an increase in the required contact times (Noreen et al., 2013; Żółtowska-Aksamitowska et al., 2018).

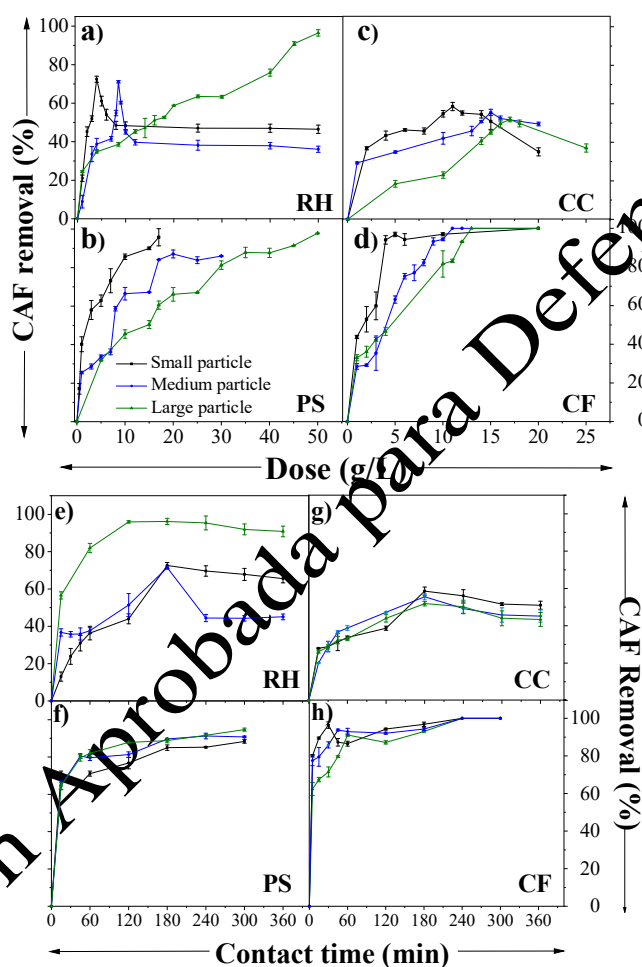


Figure 57. a) – d) Effect of the agro-industrial residue dose and contact time on the CAF adsorption by agro-industrial residue. e) – h) Contact time of the optimal dose = 180 min. Optimal timing dose = optimal dose.

Figure 58 shows the efficiencies achieved with the optimal dose and contact time for each particle size of the agro-industrial residues studied. The CF achieved the highest CAF removal efficiency (92.9 – 94.3%) using the least amount of residue, with mean doses of 4, 10 and 12 g/L for small, medium, and large particles, respectively. The higher CAF removal efficiency of CF, compared to the other residues, is related to its composition (lignin and volatile material) (Mo et al., 2018). However, the efficiency also depends on the presence of extractives. For instance, PS reports the second-highest lignin content (36.2%), but also the highest extractives content (15.3%); this limits its CAF removal efficiency, particularly for small particle sizes. In general, the CAF removal efficiency of agro-industrial residues showed direct linear relationships with the lignin/cellulose/hemicellulose content ($R^2 = 0.76 - 0.89$; $p < 0.05$) and their granulometry ($R^2 = 0.97$; $p < 0.05$). As previously mentioned, CF exhibited the best

adsorption performance considering the doses (4 – 12 g/L) and contact times (30 – 60 min) required, regardless of the particle size. In particular, the small CF particles showed higher CAF removals (10.5 – 24.9%, at 30 min) than medium and large particles, due to their higher porosity. This was consistent with the results of the FTIR analysis (Figure 56). After CAF adsorption, the spectra of the four residues showed modifications for the three particle sizes. However, these changes were greater for the small particles, due to the higher CAF concentration (between 2.6 and 35.2%) in them. The intensity of the carbonyl group (1632 cm^{-1}) and the bands related to lignin, cellulose and hemicellulose ($2900 - 3200$, $1500 - 1180\text{ cm}^{-1}$) decreased after CAF adsorption. The band intensity reductions suggest an interaction/bond between the functional groups of the residues and the CAF functional groups. The spectra of RH, PS and CF show more noticeable changes than the CC spectra, probably because the three residues have a greater capacity to have CAF on their surface than CC (Noreen et al., 2013).

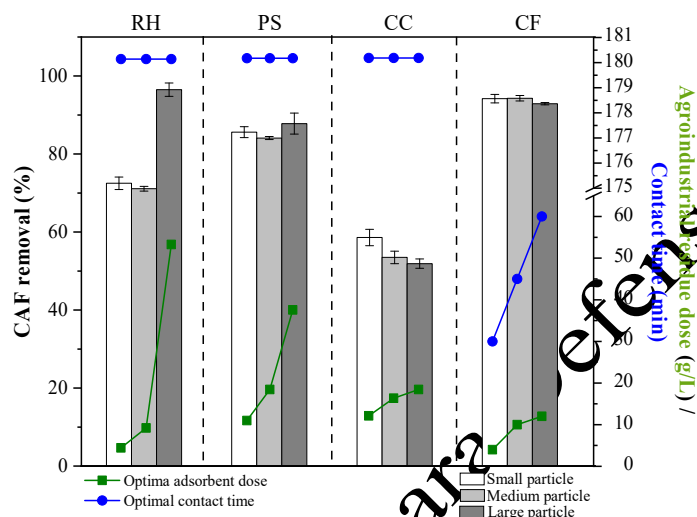


Figure 58. Comparison of CAF removal efficiency using optimal conditions of agro-industrial residue dose and contact time.

3.3. Adsorption kinetics

Table 31 shows the fittings for pseudo-first and second-order models used to describe the experimental adsorption kinetics data. The maximum CAF adsorption capacities obtained for small particles of RH, PS, CC, and CF were 6.3, 3.0, 1.4 and 7.0 mg/g, respectively. The kinetics data for RH, PS, CC and CF in the three particle sizes are better fitted to the pseudo-second-order model ($R^2 = 0.957 - 0.999$). This, combined with changes in the FTIR spectra of agro-industrial residues after CAF adsorption, suggests that chemisorption controls the CAF adsorption, and there is electron sharing between CAF and the functional groups on the residues surface (Beltrame et al., 2018; Castro et al., 2021).

The adsorption using small RH particles was better fitted to the pseudo-second-order kinetics model ($R^2 = 0.973$). However, its experimental q_e value (6.3 mg/g) is closer to the q_e obtained in the pseudo-first-order model (7.7 mg/g), which shows a good fitting ($R^2 = 0.959$). Furthermore, the q_e of the pseudo-first-order model is closer to the equilibrium adsorption capacity of the Langmuir isotherm ($q_e = 6.5\text{ mg/g}$). Other studies have also fitted to pseudo-first-order kinetics models ($q_e = 5.4 - 6.5\text{ mg/g}$), as in the case of oxidized biochar obtained from pine needles (Anastopoulos et al., 2020b).

Table 31. Kinetic parameters for the pseudo-first-order and pseudo-second-order on CAF

Agro-industrial residue	Particle size	q_e exp. [mg/g]	Pseudo-first-order			Pseudo-second-order			Pseudo-second-order fit Q_t [mg/g] vs. t [h] Black line: small particle Blue line: medium particle Green line: large particle
			q_e [mg/g]	K_1 [h ⁻¹]	R^2	q_e [mg/g]	K_2 [g/(mg h)]	R^2	
RH	Small	6.29	6.72	0.85	0.959	7.71	0.10	0.973	
	Medium	2.27	0.83	0.23	0.813	1.91	6.84	0.998	
	Large	0.72	0.56	1.34	0.976	0.74	5.96	0.994	
PS	Small	3.04	1.54	1.01	0.889	3.16	1.92	0.996	
	Medium	1.88	0.87	1.13	0.886	1.92	4.58	0.998	
	Large	0.94	0.42	1.12	0.909	0.96	10.09	0.999	
CC	Small	1.42	0.69	0.35	0.891	1.66	1.10	0.957	
	Medium	1.03	0.81	1.51	0.884	1.16	2.67	0.982	
	Large	0.84	2.12	3.58	0.885	0.97	3.18	0.976	
CF	Small	7.02	1.38	0.33	0.564	7.09	1.46	0.999	
	Medium	3.17	0.71	0.14	0.494	3.18	3.95	0.998	
	Large	2.69	0.85	0.53	0.743	2.75	20.39	0.997	

$C_0 = 30$ mg/L, RH dose = 4.0, 8.5 and 50 g/L, PS dose = 10, 17 and 35 g/L, CC dose = 11, 15 and 17 g/L, CF dose = 4, 10 and 12 g/L, for small, medium, and large particles, respectively

3.4. Adsorption equilibrium

The adsorption isotherm models evaluate the contaminant distribution on adsorbent surfaces, estimating the adsorbent adsorption capacity. Table 32 shows the parameters of Langmuir and Freundlich isotherm models fitted to the experimental data. The CAF adsorption for small size particles of RH, PS, CC and CF, for medium size particles of RH and CC and for large size particles of CF were best fitted to the Langmuir model. This model indicates a homogeneous adsorption with a monolayer surface coverage without interaction between the adsorbed molecules (Beltrame et al., 2018). On the other hand, the regression coefficients for the Langmuir and Freundlich models applied to large particles of RH and CC and medium particles of CF are very similar. This could mean that initially only monolayer adsorption occurs (chemisorption, Langmuir) and subsequently CAF is deposited to form multilayers (physisorption, Freundlich). This behavior is common for other adsorbents, such as hyacinth biochar, sepiolite, tea leaves, among others (Anastopoulos et al., 2020b). Finally, the Freundlich model was fitted to the CAF adsorption for the medium particle sizes of PS. The results of the isotherm models could be favorable as it indicates that residues bind to CAF through different mechanisms such as ion exchange, ion pairing, electrostatic attraction, hydrophobic bonding, hydrogen bonding and dispersion forces (Oliveira et al., 2019). This would suggest that they can be efficient in removing other contaminant types.

Regarding the adsorption capacities, CF show the highest ones, being 8.7, 5.4 and 4.4 mg/g for the small, medium, and large particle sizes, respectively. The adsorption capacity is related to the adsorbent size, adsorbent nature (functional groups/physicochemical properties), surface area and the adsorption type (physic/chemisorption) (Luo et al., 2018). The adsorption capacities (mg/g) for small/medium/large particles of RH (6.5/3.9/0.6), PS (3.9/3.2/1.2) and CC (2.3/2.3/0.12) were variable. These adsorption capacities are comparable to those found for hyacinth biochar (2.49 mg/g), commercial multi-walled carbon nanotubes (4.18 mg/g), oxidized pine needles biochar (5.35 mg/g), and bagasse biochar (3.52 – 4.53 mg/g) (Anastopoulos et al., 2020). On the other hand, the surface area of agro-industrial residues, in

spite of be low (1.18 – 1.80 m²/g) are comparable with the adsorption capacity of pyrolyzed *Gliricidia sepium* biochar at 300 °C (4 mg CAF/g), the material presented a similar surface (1.02 m²/g) to that obtained (Keerthan, et al., 2020b). There are other adsorbents, such as activated carbon, modified residues, and modified clay, with greater adsorption capacity for CAF (> 700 mg/g). These materials are generally subjected to physical or chemical modifications (Anastopoulos, et al., 2020; Oliveira et al., 2019). In these cases, it is important to consider that modified residues can generate by-products more toxic than CAF. For instance, TiO₂ nanoparticles have been impregnated in organic residues to provide them photocatalytic properties and remove emerging contaminants (León et al., 2020). However, the TiO₂ nanoparticles have produced effects in aquatic biota at the molecular level (Mahaye et al., 2017). This is relevant, if materials are used in filter beds in biofiltration technologies, where earthworms and microorganisms coexist. Such materials are also required to be compatible.

Table 32. Isotherm parameters for the Langmuir and Freundlich models on CAF adsorption at different dose of agro-industrial residues (C0= 30 mg/L, RH dose= 4.0, 8.5 and 50 g/L, PS dose= 10, 17 and 35 g/L, CC dose= 11, 15 and 17 g/L, CF dose= 4, 10 and 12 g/L, for small, medium, and large particles, respectively).

Agro-industrial residue	Particle size	Langmuir isotherm			Freundlich isotherm		
		q _{max} (mg/g)	K _L (L/mg)	R ²	K _F ((mg/g) (L/mg) ^{1/n})	n	R ²
RH	Small	6.49	0.49	0.962	2.09	2.62	0.991
	Medium	3.87	0.24	0.949	0.88	2.11	0.874
	Large	0.59	1.09	0.981	0.28	2.94	0.987
PS	Small	3.88	1.28	0.987	2.39	5.86	0.978
	Medium	3.15	0.29	0.992	0.75	1.86	0.982
	Large	1.16	0.23	0.963	0.22	1.71	0.997
CC	Small	2.29	0.16	0.953	0.65	3.11	0.596
	Medium	2.27	0.06	0.903	0.25	1.87	0.823
	Large	2.57	0.04	0.918	0.12	1.26	0.915
CF	Small	8.74	1.94	0.976	5.50	5.93	0.930
	Medium	5.47	0.55	0.961	2.21	2.99	0.964
	Large	4.43	0.44	0.996	1.60	2.66	0.936

3.5. Ecotoxicology characteristics

Figures 59 and 60 summarize the compatibility results of agro-industrial residues on *Eisenia foetida* (*Savigny*) individuals. The acute toxicity tests (Figure 59a) show that the concentration of PS and CF (% v/v) that produced mortality (14 d LC₅₀) of the earthworms was 97 and 82%, respectively. Meanwhile RH and CC did not report acute toxicity. Earthworm mortality is a bioindicator of the palatability and suitability of the foods to which they are exposed (González-Moreno et al., 2020). On the other hand, chronic toxicity effects were determined with the individual growth and their reproduction. Reproduction was affected but not significantly (p > 0.05) at concentrations of 50 and 100%, v/v for PS and CC, respectively. Moreover, earthworm growth did not show significant negative effects (p > 0.05) for all residues. However, CC showed an increase in weight of 40.0 and 4.0% at concentrations of 25 and 50%, v/v compared to control (CC= 0%, v/v). Meanwhile, CF and PS at 100% v/v concentrations showed earthworm weight losses of 82.0 and 32.2%, respectively. On the contrary, RH at 50%, v/v showed an increase (0.1 g) in the earthworm weight; the other concentrations showed a decrease between 0.05 and 0.92 g. Thus, both CF and PS are more incompatible with earthworms.

Figure 59b showed that RH favored the production of cocoons in all concentrations (25, 50 and 100%, v/v), the highest production was at 50%, v/v (1.85 cocoons/earthworm). CC in concentrations between 25 and 50%, v/v registered a cocoons production (0.64 – 0.86 cocoons/earthworm), like the control (0.71 cocoons/earthworm). However, CC at 100%, v/v decreased the cocoons production per individual (0.19 cocoons/earthworm). PS presented an increase in the cocoons production (0.35 – 0.41 cocoons/earthworm) at concentrations of 25, 50 and 100%, v/v, which is compared to the control (0.10 cocoons/earthworm). On the other hand, CF did not show a cocoons production per earthworm at concentration of 100%, v/v.

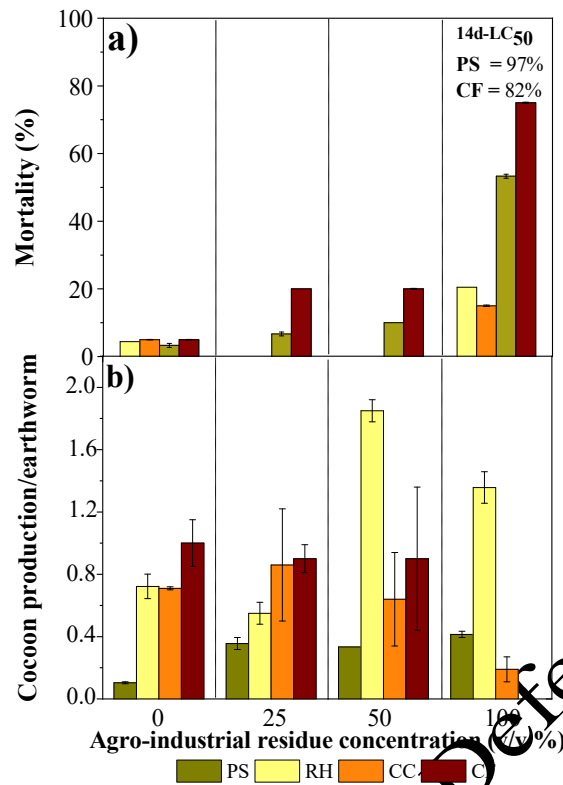


Figure 59. Mortality of *Eisenia foetida* by each agro-industrial residue.

The nature and composition of the filter bed material play a very important role in the earthworm behavior. The earthworms are the main drivers of the filter bed decomposition because they favor the fractionation by enzymatic and microbial enrichment, accelerating the degradation and mineralization of the residue (Chen et al., 2015). These microbial communities generate extracellular enzymes that degrade cellulose, proteins, starch, sugars and phenolic compounds, which favor the material degradation or change the pH due to the contaminant adsorption/precipitation (Arora et al., 2014). The initial pH of the agro-industrial residues was in a range between 6.1 and 6.6, while at the end of the toxicity tests the pH varied from 6.9 and 7.2 (Adugna et al., 2019). The increase in pH could be related with the ammonium ions generation. Despite this, the pH of agro-industrial residues is favorable for the earthworms because they could survive at pH range between 6.2 and 9.7 (Suthar, 2010). Therefore, gaseous pollutants were not development on our assays. Indeed, the compost production (> 2 months) within vermifilters generate CO₂, NH₄ and NO₂, produced by the humic acids total degradation, which could influence on the filter bed pH (Sharma & Garg, 2019). Incomplete humic acids degradation by carbon source recalcitrant (e.g., lignin) generates the ammonium production, modifying slight changes in pH. Effectively, microbial/earthworm degradation of lignocellulosic residues takes longer times due to the complex structure of polysaccharides (Sharma & Garg, 2019). For instance, residues with lignin concentrations higher than 35% showed a low residue degradation during the first 30 days and only after 60 days a mature compost was obtained. Residues with lignin percentages around 25% decreased the maturation time to 50 days (Gong et al., 2018; Wang et al., 2014).

C/N ratio for RH, PS, CC and CF were 31.1: 1, 41.4: 1, 83.2: 1, 57.7: 1, respectively. The optimal C/N ratio for vermicomposting is between 25:1 and 30:1 (Wang et al., 2014). Despite this, it is observed that CC does not present adverse effects in earthworms, that is, it does not present a nutritional deficit in the test time. This suggests that the incompatibility effect of CF on *Eisenia foetida Savigni* individuals is related to the low carbon source availability, due to the lignin is more difficult to degrade than cellulose and hemicellulose (Biruntha et al., 2019). Therefore, the agro-industrial residues compatibility was mainly caused by their composition.

3.6. Agro-industrial residues as filter bed within vermifilters

The agro-industrial residue decomposition, offers nutrients for earthworms and microorganisms (Singh et al., 2017). The content of cellulose, hemicellulose and lignin indicates the presence of sugars, which are glucose components (glucan and xylan). Glucose favors the microorganism growth, which works in symbiotic relationship with earthworms (Saha, 2003). However, high concentrations of lignin (recalcitrant compound) in raw agro-industrial residues, make it difficult for microorganisms to access cellulose and hemicellulose, slowing down the availability of food for microorganisms and earthworms (Gong et al., 2018). Moreover, the presence of lignocellulosic materials (formed by phenolic compounds) and the extractives (formed by phenolic, aromatic, lipid, fat, terpene, etc.) cause negative effects in earthworms because they produce adverse effects on their growth and reproduction (Garg & Gupta, 2009; Z. Li et al., 2016; Pholosi et al., 2013; Saha, 2003). *Lumbricus terrestris* was exposed to oil mill residues/modified soil (40/60 and 80/20% w/w) embedded with a total soluble polyphenols concentration of 873 (\pm 55) mg/kg, reporting mortality at concentrations of 100.0 and 53.3% for 2 and 4 weeks of exposure, respectively (Sanchez-Hernandez et al., 2020). In our study, CF (14d-LC₅₀: 82.0%) is the less compatible with *Eisenia foetida* (Savigny), as shown in Figure 60; this is due to its higher extractives content (2.5 and 3.3% for RH and CC) and the highest lignin concentration (4.3 – 25.1%, w/w). On the other hand, as previously mentioned, the ashes of the residues represent their silica content (Eliche-Quesada et al., 2017). Silica is not toxic to earthworms, and they can even weather it due to the microorganisms they contain in their gut (Georgiadis et al., 2019).

The compatibility studies on agro-industrial residues are limited because most of them are considered compatible or less suitable for detritivore species. However, few compatibility studies show that agro-industrial residues have negative effects on the growth, reproduction, and mortality of earthworms. Organic residues can change the medium pH, being also nutritionally unbalanced by-products during its degradation that ultimately lead to toxicity. Indeed, to reduce these effects, organic residues have been mixed with others (Gong et al., 2018; Ramnarain et al., 2019). González-Moreno et al. (2020) studied the feasibility of using different residues proportions from coffee industries mixed with mature horse manure during vermicomposting using *Eisenia andrei*. In fact, 100% v/v coffee residues produced a mortality between 87.5 and 100%; while that, residues/horse manure mixtures with ratios of 75/25, 50/50 and 25/75 produced a mortality between 8.3 and 30%. Likewise, these mixtures favored the earthworms' growth (1.01 – 4.39 mg/earthworm/day) and their reproduction (0.05 – 0.35 cocoons/g/week). On the other hand, the addition of the bamboo biochar to green waste with *Eisenia foetida* had the same effect. In this study, an increase in pH (0.6 – 0.8) was initially observed (30-40 days) and when the mature compost obtained (50 – 60 days) a decrease in pH (0.5 – 0.8), both changes are related to the degradation products of green waste. Thus, bamboo biochar at 8% w/w concentrations favored their growth (15.9 mg/earthworm/day) and reproduction (8.3 cocoons/g/day) (Gong et al., 2018). Both studies indicate that incompatibility effects are associated with the residue composition.

The SEM images (Figure 56) of the four residues studied show porous structures, without sharp edges. That suggests that the materials favor the earthworm and microorganism's development (Singh et al., 2017, 2019). Likewise, earthworms could increase the material porosity in their ingestion-excretion process. In this way, the surface area would be increased between 4 and 10 times, increasing the adsorption capacity (Singh et al., 2019; Wang et al., 2010). This happened with the removal of sulfamethoxazole, trimethoprim and metronidazole, producing an increase around 9.0, 10.5 and 10.1%, respectively (Shokouhi et al., 2019).

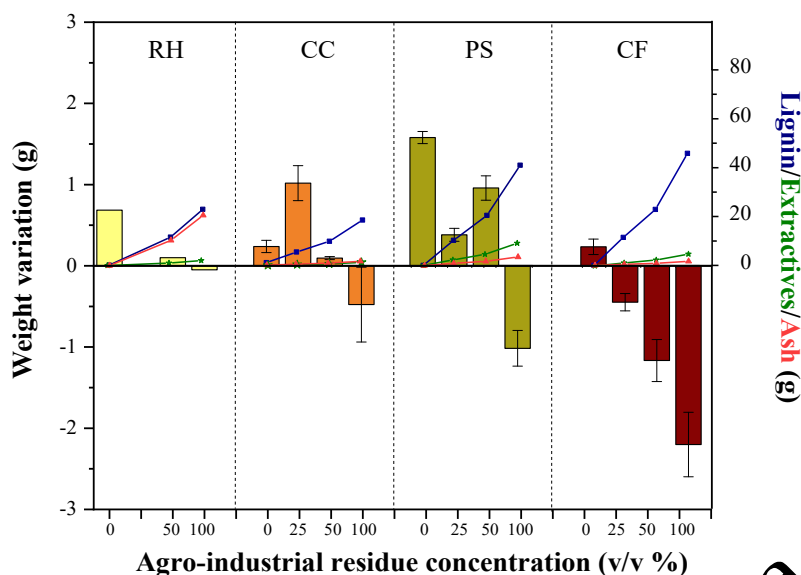


Figure 60. Influence of components from each agro-industrial residue on the *Eisenia foetida* growth.

The vermifilter performance could be improved by analyzing the adsorption capacity of the filter bed material and its compatibility. If the bed material by itself (100%, v/v residue) is not friendly to living beings, such as CF, it can be mixed with other materials in suitable proportions as has already been done in previous studies. In this sense, river bed was mixed with vermicompost, sawdust with soil, and sludge with vermicompost, reaching organic matter removal efficiencies (COD) between 64 and 86%. Tahir and Hamid (2012) used CF mixed with goat manure under different proportions (100:0, 70:30 and 50:50%, v/v). Indeed, their study determined that CF: goat manure (100:0) was the material that showed the highest earthworm death rate (40%) (Tahir & Hamid, 2012). Something similar happens with RH and PS; using only RH, the lowest earthworm growth was achieved (9.29 ± 5.06 mg/earthworm/day) compared to RH mixed with fruit (banana, honeydew, papaya) residues at 50:50%, v/v (Lim et al., 2012). Meanwhile, Romero et al. (2018) indicated that the adult earthworm survival decreased by more than 50% using only PS. On the other hand, CC in this same study have not showed incompatible effects on earthworms (Lim et al., 2012; Romero et al., 2018). Therefore, the physicochemical, morphological and particle size characteristics of the bed filter material should favor the adsorption process and contribute to the development/reproduction of earthworms and microorganisms, making it more efficient. In addition, the results allow us to suppose that if the agro-industrial residues studied are combined in the appropriate proportions (good adsorption + compatibility), they can be used in vermifiltration at industrial scale. The future challenge would be to determine this proportions and the optimal hydraulic conditions for each material.

4. Conclusion

The adsorption capacity of low-cost adsorbents such as rice husks, peanut shells, corn cob and coconut fiber in the caffeine removal was determined. Likewise, the compatibility of these residues on *Eisenia foetida* (Savigny) organisms was determined. The lats, in order to determine the possible application of these agro-industrial residues within vermifiltration processes. The composition (lignin/extractives/ash) and the size of the agro-industrial residues notably influenced the caffeine removal. Caffeine removal improves as particle size decreases. The small (120 – 150 μm) particles of coconut fiber showed the best performance during caffeine adsorptive removal (94.2%/8.7 mg/g), requiring the shortest contact time (30 minutes) and lowest dose (4 g/L). However, this was also the most incompatible residue (14d-LC₅₀= 82%) for *Eisenia foetida* (Savigny). Therefore, bed material composition also influences its compatibility. In this case, coconut fiber could be mixed in suitable proportions with less toxic and high adsorption residues, such as corn cob or rice husk, to obtain a friendlier filter bed material for the earthworms. This strategy could help improving the performance of vermifiltration technologies during emerging contaminant removal.

With the results of Article 6, it was shown that residues alone (PS, RH and CC) or mixed (CF+CC) can be compatible with *Eisenia foetida* (Savigny) and that they are also efficient in removing caffeine. This

information is very important as it guarantees that the materials will allow the development of organisms in biofiltration technologies. However, it is considered necessary to first know how different biofiltration technologies (mesocosm scale) behave with synthetic wastewater. This is because the information found in the literature is very limited when using this type of filter materials to remove caffeine, triclosan and other ECs in different types of biofilters; which would make it difficult to justify the results obtained. In addition, the biota of biofilters requires a C/N ratio, the same that could not be obtained from caffeine/triclosan solutions. Nor will synthetic wastewater enriched with caffeine/triclosan be used because it is necessary to know the behavior of technologies with only synthetic wastewater; because it is still unknown if the presence of organic matter will have an effect on the caffeine/triclosan removal. Another unknown parameter when working with agro-industrial residues as a biofilter filter bed is the hydraulic behavior when wastewater is fed, since corn cob filters only worked with caffeine/triclosan solutions and previous studies carried out similar investigations. Nevertheless, the results of this part of this study will be an important premise for further studies. Therefore, for the last part of the research, a conventional material (wood chips) was partially replaced by PS, which was improved in different types of biofiltration (biofilters, constructed wetlands, vermifilters, and hybrid biofilters) and fed with synthetic wastewater.

Versión Aprobada para Defensa Oral

Article 7. Performance of wood chips/peanut shells biofilters used to remove organic matter from domestic wastewater

Tejedor, J., Córdor, V., Almeida-Naranjo, C. E., Guerrero, V. H., & Villamar, C. A. (2020). Performance of wood chips/peanut shells biofilters used to remove organic matter from domestic wastewater. *Science of The Total Environment*, 738, 139589.

ABSTRACT

A continuously increasing global population and industrialization drives a rapidly growing clean water demand. Biofiltration is one of the main alternatives developed to improve wastewater quality and increase its recyclability. Support materials are extremely important when using this technology since they impact the cost of the treatment. In this work, we study the use of wood chips/peanut shell as support medium within biofilters incorporating microorganisms (BM), plants and microorganisms (RPM), earthworms and microorganisms (BEM) and plants, earthworms and microorganisms (hybrid biofilters, HB). These typologies were evaluated to remove organic matter from domestic wastewater. For this purpose, twelve biofilters were operated in parallel, feeding them with synthetic domestic wastewater under three different nominal hydraulic rates (0.5, 1 and 1.5 m³/m²-d). Previously, support materials were individually characterized and acute/chronic toxicity tests on plants (*Schoenoplectus californicus*) and earthworms (*Eisenia foetida*) were driven. Results showed that both materials have good adsorbent properties, providing adequate environmental conditions for biofiltration. Moreover, non toxicological response was reported when a 25 v/v% peanut shell fraction was selected. With this fraction used in every biofilter studied, the average hydraulic conductivity was between 321 and 502 mm/h, reaching organic matter removal efficiencies close to 80% (measured as COD), and between 40 and 63% (measured as VS). Higher efficiencies, attributed to the longer contact times, and lower clogging were observed at lower hydraulic rates. The incorporation of earthworms and plants improved the solids removal and reduced clogging. The statistical analysis indicated that the results obtained for biofilters operating at 0.5 m³/m²-d showed significant differences ($p < 0.05$) with respect to those achieved with the other two hydraulic rates. In terms of typology, the results for BEM were the ones that presented significant differences. As a conclusion, low-cost organic materials (wood chip/peanut shell mix) can be successfully used as support medium, since they provide adequate environmental conditions for plants and earthworms, improving the operation and maintaining contaminant (organic matter) removal within biofiltration typologies.

1. Introduction

Access to clean water and sanitation is one of the sustainable development goals committed by the United Nations for 2030. However, more than 3 billion of the world population (approx. 42%) lack access to basic sanitation (connection, treatment) (Malik et al., 2015; Mateo-Sagasta et al., 2015) and this has been directly related to poverty. Developing countries (\$ 1,035 – 12,615 per capita gross national income) only reach 30 and 50% of treatment and connection, respectively. Meanwhile, developed countries (> \$ 12,615 per capita) exceed 75% coverage in both (Malik et al., 2015).

Domestic wastewater is the most important fraction (> 80% v/v) of the municipal wastewater (Panikkar et al., 2010). Given the large amount generated, and the continuously rising water demand, domestic wastewater can also be considered as an unconventional water resource that could be properly managed. However, its quantity (up to 400 L hab⁻¹-/day) and quality depend on the consumption habits and income of the population (Villamar et al., 2018). The quality refers to the presence of solids (100 – 350 mg TSS/L), organic matter (250 – 1600 mg COD/L, 110 – 800 mg BOD₅/L), nutrients (20 – 120 mg TN/L, 2 – 23 mg TP/L), pathogens (up to 10⁸ NPM/100 mL), and micro pollutants (e.g., pharmaceuticals and personal care products < 1 mg/L) (Villamar et al., 2018). Thus, both discharge and legislation could limit the use of domestic wastewater without adequate treatment.

Treatment technologies, including those based on activated sludge systems or the ones related to passive technologies (e.g., biofiltration), represent alternatives to improve wastewater quality, increasing its recyclability. Decision making regarding the most convenient technology to be used depends on economic escalation (e.g., 80 – 90% of collection capital costs) (Libralato et al., 2012). Conventional

technologies (activated sludge systems) reach investment costs between 65 and 200 USD hab⁻¹ under centralized wastewater treatment plants (WWTPs) operating for more than 2,000 habitants (Vera et al., 2016). Meanwhile, non-conventional technologies (biofiltration) could be more adequate in decentralized contexts (< 2,000 habitants) (Massoud et al., 2009). In fact, economic (investment cost: 35 – 630 USD/hab), social (appropriate technologies) and environmental (approx. 50% less emissions) attributes could be valued. For instance, the implantation area could be considered an influential factor within the wastewater technology investment costs. Biofiltration typologies (0.1 – 6 m² hab⁻¹) require higher surface area than centralized conventional technologies (activated sludge < 0.1 m² hab⁻¹) and result economically unfeasible for large populations (> 2,000 habitants), not only because of the required space but also due to the support material requirements (Arora and Kazmi, 2015; Kumar et al., 2015; Vera et al., 2016).

There is a variety of technologies that are based on biofiltration for the domestic wastewater treatment. These technologies include trickling filters or biofilters based on autochthonous microorganisms (ABM), vertical subsurface constructed wetlands or biofilters based on plants and microorganisms (BPM) and vermifilters or biofilters based on earthworms and microorganisms (BEM). Moreover, emergent hybrid biofilters based on plants, earthworms and microorganisms (HB) (Samal et al., 2017b) are also an option. The common feature between these biofilters is the presence of a biotic component (plants/earthworms/microorganisms) and a support medium. This dual condition favours simultaneous processes: physical (sedimentation, precipitation), chemical (adsorption, ionic exchange), and biological (degradation, transformation, uptake).

The support material costs can reach up to 50% of the investment costs when using conventional materials (gravel). Therefore, it is necessary to think about alternative materials. Non-conventional materials that could be used for support purposes include agricultural byproducts, chitosan, biochar, wood residue and peat, among others (Mohan et al., 2014; Zhou et al., 2015). Moreover, organic material costs (e.g., agricultural byproducts) could be up to 100 times lower than conventional materials (Gupta et al., 2009). The choice of an organic support material for biofiltration depends not only on its availability but also on its properties. In fact, organic support materials are characterized by their physicochemical stability (lignin/hemicellulose content), surface area (80 m² g⁻¹ at least), pore diameter (20 Å at least), presence of functional groups (phenolic hydroxyls, methoxyl, carboxylic), non-toxicity (pH 6, non-extractives) and adsorption capacity (Ramírez-López et al., 2003; Gupta et al., 2009; Bhatnagar et al., 2015; Zhou et al., 2015; Quesada et al., 2019).

Peanut shells are agro-industrial residues that have usually no cost, being also abundant (up to 30 million ton/year) worldwide (Sawe, 2018). This agro-industrial residue is characterized by its content of lignin (41%), cellulose (37%) and hemicelluloses (9%) (Anike & Isikhuemhen, 2016). In addition, peanut shells report pH values close to 6.8, adequate surface area (at least 260 m²/m³) and porosity (at least 115 Å, 74%) (Ramírez-López et al., 2003). Thermally or chemically modified peanut shells have been mainly evaluated in adsorption batch tests to remove organic (e.g., dyes) contaminants, achieving performances greater than 60% (Dicit et al., 2019). On the other hand, wood chips are an abundant, inexpensive and durable organic sawmill residue, which has been used mainly as active layer in vermifilters (BEMs) at industrial scale (S. Li et al., 2007). In fact, wood byproducts have good adsorptive properties, due to their content of lignin (18–35%), cellulose (42%), hemicelluloses (33%), and extractives (< 5%). Additionally, their use as adsorbents would also benefit the environment since it would contribute to eliminate a disposal problem and could help to obtain clean water (Shukla et al., 2002). Wood chips generate adequate biotic environments (pH 6 – 8), having surface area up to 20,000 m²/m³ and an adequate porosity (75%) (Foo & Hameed, 2012; Shukla et al., 2002). Previous studies have reported the development of suitable environmental conditions for the operation of BEM, reaching organic matter removal greater than 90% as COD (T. Kumar et al., 2015). Moreover, chips chemical/thermally modified have demonstrated to remove inorganic (e.g., metals) and organic contaminants (e.g., emerging contaminants) with adsorption performance between 30 and 80% (Alidadi et al., 2018; Mohan et al., 2014).

Using mixed organic materials within different biofiltration typologies has not been reported. Few studies have evaluated the use of organic material within constructed wetlands, reporting an organic matter (BOD₅) removal up to 93% (de Rozari et al., 2018). Therefore, the work aim was to compare the

performance of different biofiltration typologies using an appropriate wood chip/peanut shell support medium for organic matter removal from domestic wastewater.

2. Materials and Methods

2.1. Wastewater characterization

The synthetic domestic wastewater was prepared following the method defined by Almeida-Naranjo et al., (2017). The wastewater was prepared daily, to preserve its characteristics. Table 33 summarizes the physicochemical characteristics of the synthetic wastewater, where the results resemble medium intensity real domestic wastewater (Villamar et al., 2018).

Table 33. Synthetic domestic wastewater physicochemical characteristics

Parameter	Symbol	Unit	Value	
			Mean	Range
Temperature	T	°C	19.10	18.70–25.00
pH	--	--	7.20	6.80 – 7.60
Chemical Oxygen Demand	COD	mg O ₂ /L	543.30	409.20–716.70
Ammonium	NH ₄ ⁺	mg N-NH ₄ ⁺ /L	22.50	18.90–26.00
Nitrite	NO ₂ ⁻	mg N-NO ₂ ⁻ /L	0.01	0.01 – 0.05
Nitrate	NO ₃ ⁻	mg N-NO ₃ ⁻ /L	3.30	0.01 – 6.8
Phosphates	PO ₄ ⁻³	mg/L	9.30	8.00 – 10.80
Total Solids	TS	mg/L	370.00	340.00–420.00
Volatile Solids	VS	mg/L	345.80	240.0 – 496.00

2.2. Support material conditioning: wood chips/peanut shells

Peanut shells were obtained in the city of Loja (southern Ecuador; location S 3° 59' 35.3", W 79° 12' 15.2") and wood chips (coming from laurel) were obtained from a sawmill located in the city of Quito (northern Ecuador; location S 0° 13' 47.5", W 78° 31' 28.8"). Samples of both residues were subsequently stored at 4 °C under dark conditions.

Peanut shells and wood chips were conditioned in stages of washing with deionized water and drying at 105 °C for 24 hours. Specifically, peanut shells were sieved (No. 10 – 20 meshes) to obtain a particle size between 850 µm and 2 mm. Both conditioned residues were stored in sterile bags at room temperature.

2.3. Compatibility tests: acute and chronic bioassays

Acute and chronic toxicity tests were performed to determine the tolerance of the individuals involved (*Eisenia foetida* and *Schoenoplectus californicus*) to peanut shells using the methods described by (C. Brami et al., 2017; OECD, 2015). Prior to testing, *Eisenia foetida* individuals were kept in moistened filter paper for three hours to purge their intestinal contents and washed with deionized water. Earthworm acute assays were driven in triplicate at optimum environmental conditions (20 ± 2 °C, pH 5 – 9, moisture 55 – 95%) for 14 days. Ten clutiated individuals (> 2 months old) were placed in each container (15 cm x 22 cm x 6 cm). Acute assays evaluated five different peanut shell concentrations (control, 12.5, 25, 50 and 100 v/v%) mixed with artificial soil (10% humus, 20% clay, 70% sand). Lethal Concentration (LC₅₀) as a function of mortality and non-mobility of 50% or higher of the exposed earthworms was measured. Earthworm chronic effect tests were driven under the same conditions (environment and procedure) used for the acute assays, but for 28 days. Live weight (g) and density (individuals' m³) of adults, juveniles and cocoons were reported as No Observed Effect Concentration (NOEC) (OECD, 2015).

Schoenoplectus californicus seedlings were washed with distilled water and transplanted to the support medium (Park et al., 2015). Acute and chronic assays were driven for 7 and 56 days, respectively. All bioassays were carried out in duplicate at optimum environmental conditions (20 ± 2 °C, pH 6 – 9). Two individuals (> 1 month old) were placed in each container (5 L volume). Five concentrations (control, 12.5, 25.0, 50.0 and 100.0 v/v%) of peanut shells/gravel (φ = 1.0 – 2.5 cm) were evaluated. Steinberg solution was weekly added to seedlings for supplying nutrients. Allometric measurement, such as: relative abundance (individual's/m²), apical height (cm), basal diameter (cm), number of leaves (# leaves/

individual) and chlorophyll a/b (g/g) were monitored. LC₅₀ and NOEC were also determined (OECD, 2002).

2.4. Experimental Model

2.4.1. Physical characteristics

The experimental model consisted on twelve biofilters made of recycled polyethylene terephthalate (12 x 90 cm). Four typologies were studied: biofilters (support medium + microorganisms, BM), vertical flow constructed wetlands (plants + support medium + microorganisms, BPM), vermifilter (support medium + earthworms + microorganisms, BEM) and hybrid biofilters (plants + support medium + earthworms + microorganisms, HB). The support medium was composed of three layers of 30 cm each one being described from bottom-up as follows: support layer (gravel, $\phi = 10 - 25$ mm), middle layer (sand, $\phi = 1 - 2$ mm) and active layer (25% peanut shells, 75% wood chips). Finally, the earthworm population density (10,000 individuals' m³) and plants relative abundance (100 plants/m²) for the corresponding typology were defined (Kumar et al., 2015; Samal et al., 2017a). Figure 61 details the biofiltration typologies scheme.

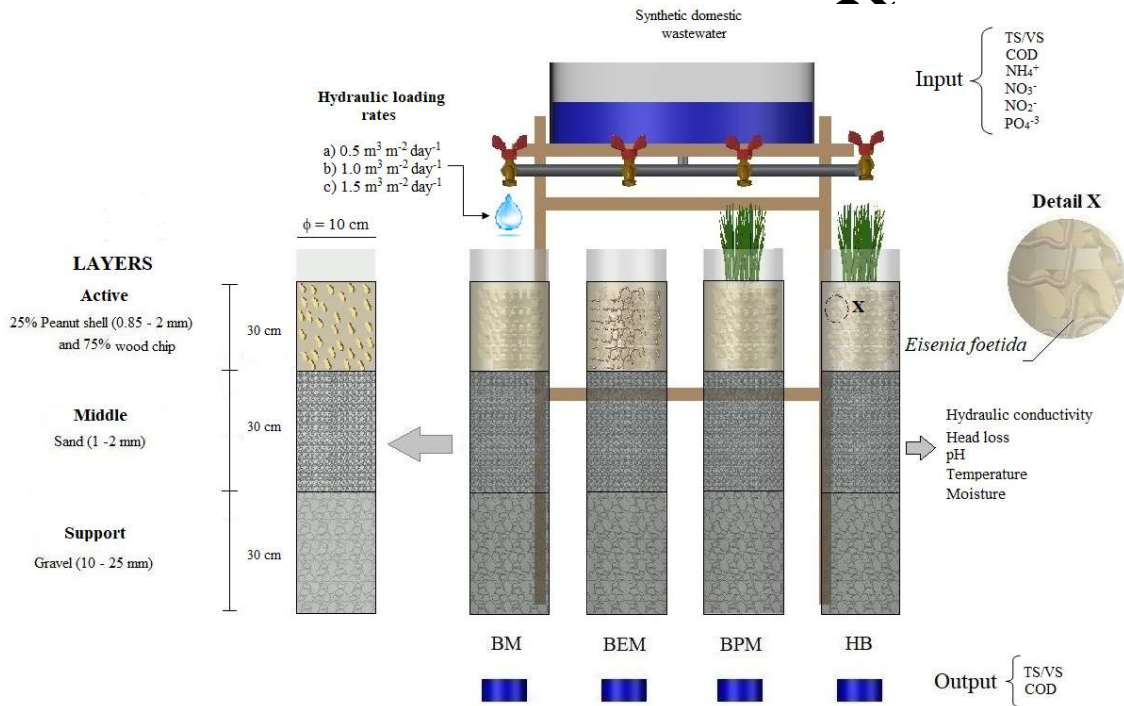


Figure 61. Experimental scheme. BM = Biofilter with microorganisms, BEM = Biofilter with microorganisms and *Eisenia foetida*, BPM = Biofilter with microorganisms and *Schoenoplectus californicus*, HB = Biofilter with microorganisms, *Eisenia foetida* and *Schoenoplectus californicus*.

2.4.2. Operational strategy

Each biofilter type operated in parallel using three different nominal hydraulic loading rates (0.5, 1 and 1.5 m³/m²-d). The wastewater feed was carried out through a 75 L elevated tank. The biofilters were operated for 67 days. The first week, the support medium conditioning was carried out using synthetic wastewater with a flow rate of 5 mL/min. The plants and earthworms conditioning were carried out within 10 days later, using 800 mL/day of residual water. The next 50 days, the biofilter operation was carried out in trickling mode using intermittent hydraulic rates of 8 h/day. The optimal conditions, such as humidity (70–89%), temperature (~ 21 °C) and neutral pH were monitored and controlled three times a day. The number of measurements of flow rate and hydraulic rate were 200 and 50, respectively. On the

other hand, 150 data points were taken for pH, temperature and humidity. Details of the operation of each typology are summarized in Table 34. Biofiltration typology (BM, BPM, BEM, HB) and a subscript corresponding to monitored hydraulic rate (0.5, 1.0, 1.5) was assigned to each biofilter.

Table 34. Operational strategy for each biofilter. The biofiltration typology (BM, BPM, BEM, HB) and a subscript corresponding to the nominal hydraulic loading rate (0.5, 1.0, 1.5 m³/m²-d) were used to identify each biofilter.

Biofilter	Parameter (Mean ± Standard Deviation)				
	Flow [cm ³ /min]	Hydraulic rate [m ³ m ⁻² /day]	pH	Moisture [%]	Temperature [°C]
BM _{0.5}	3.65 ± 0.21	0.46 ± 0.01	7.30 ± 0.20	80.12 ± 7.40	21.04 ± 1.60
BM _{1.0}	7.38 ± 0.38	0.94 ± 0.02	7.40 ± 0.20	78.88 ± 7.40	21.09 ± 1.60
BM _{1.5}	11.16 ± 0.50	1.42 ± 0.05	7.20 ± 0.20	81.43 ± 8.40	21.05 ± 1.50
BPM _{0.5}	3.61 ± 0.24	0.46 ± 0.02	7.40 ± 0.20	69.63 ± 5.70	21.11 ± 1.50
BPM _{1.0}	7.38 ± 0.41	0.94 ± 0.01	7.40 ± 0.20	69.78 ± 6.40	21.20 ± 1.70
BPM _{1.5}	11.13 ± 0.50	1.42 ± 0.03	7.40 ± 0.20	69.61 ± 5.20	21.04 ± 1.80
BEM _{0.5}	3.65 ± 0.28	0.46 ± 0.02	7.20 ± 0.10	80.64 ± 8.10	21.31 ± 1.70
BEM _{1.0}	7.41 ± 0.32	0.94 ± 0.02	7.30 ± 0.10	88.00 ± 7.80	21.28 ± 1.70
BEM _{1.5}	11.31 ± 0.40	1.44 ± 0.02	7.20 ± 0.10	89.48 ± 7.00	20.99 ± 1.80
HB _{0.5}	3.64 ± 0.22	0.46 ± 0.02	7.30 ± 0.20	75.30 ± 5.80	21.39 ± 1.80
HB _{1.0}	7.46 ± 0.32	0.95 ± 0.02	7.30 ± 0.20	80.31 ± 6.60	21.52 ± 1.80
HB _{1.5}	11.07 ± 0.40	1.41 ± 0.03	7.30 ± 0.20	79.01 ± 6.80	21.40 ± 1.77

2.5. Analytical methods

2.5.1. Influent/effluent and biotic monitoring

Influent and effluent were weekly characterized by Total Volatile Solids (TS/VS; method: 2540B), Chemical Oxygen Demand (COD; method: 5220) and phenol compounds (method: 5530), which were measured according to APHA-AWWA-WPCF, (2005). For the influent, the NH₄⁺, NO₃⁻, NO₂⁻ and PO₄⁻³ concentrations were quantified using HACH methods. The Nessler Hach 8038 Method (Range 0.02 to mg NH₃-N/L), the Hach 8039 Cadmium Reduction Method (Range: 0.3 to 30.0 mg NO₃⁻/L), the Diazotination Hach Method 8507 (Range 0.02 to 0.3 mg NO₂⁻/L) and the PhosVer 3 with digestion with ascorbic acid Hach Method 8048 (Range: from 0.02 to 1.10 mg PO₄⁻³/L), were used for the NH₄⁺, NO₃⁻, NO₂⁻, PO₄⁻³, respectively. In addition, hydraulic conductivity and head loss were daily monitored with a manual piezometer located 30 cm below the upper level of each biofilter column. Meanwhile, humidity and soil temperature were monitored by using XH300 Wireless equipment and pH was monitored by using a digital pH 6000 potentiometer.

Biofilm was evaluated extracting a 15 cm depth support material samples (up to 200 g), which were suspended in buffer solution (7.47 g K₂HPO₄/L, 1.43 g KH₂PO₄/L), sonicated (BRANSON 1800 ultrasound, 20 min) and used to quantify as Volatile Solids per area (American Public Health Association et al., 2017; Caselles-Osorio et al., 2007). Plants' allometric measures/chlorophyll was weekly monitored. Meanwhile, earthworm allometric measurements were carried out at the beginning and at the end of the experiments as described by Schuldt et al., (2005). Moreover, spectrophotometric equations (wavelength: 648.6 – 664.2 nm) are detailed by Porra, (2002). Steinberg growth medium was weekly prepared according to the procedure described by Park et al. (2015).

2.5.2. Support material characterization

Peanut shells and wood chips were characterized by lignin, hemicellulose and cellulose (method: D1106-96, D1109-84), extractives (methods: D1107-96, D1110-84), moisture content (method: D4442-16), ash (method: D1102-84), volatile matter (method: E872-82) and pH (method: D4972-13) tests, according to ASTM (1998, 2001, 2003, 2013).

2.6. Statistical analysis

2.6.1. Compatibility tests

Acute toxicity (LC₅₀) was determined using Probit analysis or the Spearman-Kärber method, when the dataset had a normal or non-normal distribution, respectively. NOEC (chronic effects) values were obtained using analysis of variance (ANOVA). The significance level was 0.05, while normality (Chi-square test) and variance homogeneity (Bartlett's tests) were previously verified. Parametric variance analysis was used for normal datasets (Dunnett test), while non-parametric variance analysis (Kruskal-Wallis) was used for non-normal distributions. The statistical programs used were Toxtat (version 2.1), EPA-Probit (version 1.5) and Spearman-Kärber (version 1.5).

2.6.2. Biofilter performance

Significant differences between typologies (BM, BPM, BEM, HB), hydraulic loading rates (0.5, 1.0, 1.5 m³ m⁻² d⁻¹) and performance (organic matter removal, hydraulic conductivity) were analyzed by multivariate analysis of variance (MANOVA). A significance level of 0.05 was defined. Normality (Shapiro Wilks) and homogeneity (Levene) were previously tested. The statistical software used was Infostat (version 2017).

3. Results and discussion

3.1. Conditioning phase

3.1.1. Material characterization

Table 35 details the organic support material physicochemical characteristics (% w/w) related to the environmental and adsorption properties. Peanut shells reported 31.7% lignin, 28.6% cellulose, and 24.5% hemicelluloses. Meanwhile, wood chips registered average percentages of 32.5% lignin, 49.7% cellulose, and 12.8% hemicellulose. According to León et al. (2020), the presence of polar functional groups (such as OH⁻) from the chemical structure of lignin, cellulose, and hemicellulose structures could favor the adsorption capacity of organic materials. These functional groups would participate in chemical binding through the cation exchange, influencing the contaminants adsorption (Gisi et al., 2016). Therefore, peanut shells and wood chips could strengthen the removal of dissolved organic matter via adsorption. Indeed, peanut shells and wood chips have been used separately to remove dissolved organic compounds (emerging contaminants), reaching up to 80% removal using particle size less than micron and depending on contaminant type (Alidadi et al., 2018; Duc et al., 2019; Mohan et al., 2014). However, both materials in this study were operated at particle size less than 2 mm, being likely that this size affects the optimal adsorption mentioned above, but the mix of materials within each biofiltration typology could diversify their adsorbent capacity.

Environmental conditions are favored mainly by the pH of the material. Thus, average pH values of peanut shells and wood chips were 6.2 and 5.9, respectively. These values are within or close to the range (6.0 to 8.0) that favors bioturbation processes and the development of microbial and biota population (OECD, 2002; OECD, 2015; Ramírez-López et al., 2003).

Table 35. Organic support material physicochemical characteristics

Parameter	Unit	Mean ± Standard Deviation			
		Peanut shells		Wood chips	
		Mean	SD	Mean	SD
pH	--	6.19	± 0.014	5.89	± 0.018
Lignin	%	31.71	± 0.53	32.54	± 0.17
Hemicellulose	%	24.45	± 0.50	12.75	± 0.04
Cellulose	%	28.57	± 0.72	49.73	± 0.69
Ethanol – toluene extractives	%	6.14	± 0.01	4.99	± 0.21
Water extractives	%	9.15	± 0.32	--	--
Total extractives	%	15.29	± 0.31	--	--
Humidity	%	9.94	± 0.40	9.58	± 0.10
Ashes	%	3.81	± 0.67	1.38	± 0.02
Volatile material	%	79.74	± 0.48	71.06	± 0.12
Fixed coal	%	6.75	± 1.14	17.99	± 0.52
Nitrogen	%	0.71	± 0.02	0.18	± 0.05

3.1.2. Compatibility tests

Table 36 summarizes compatibility tests (acute and chronic toxicity) of peanut shells on *Schoenoplectus californicus* and *Eisenia foetida*. Wood chips have been shown not to affect biota within biofiltration

systems (e.g., vermifilters or BEMs). However, peanut shells have never been used as support medium within biofilters, and there is a risk of compatibility with biota.

The peanut shells concentration (v/v,%) that produces mortality (LC₅₀) on 50% or more of *Schoenoplectus californicus* and *Eisenia foetida* population was 79 and 97%, respectively. Chronic effects were also measured in both species. Chronic toxicity on *Schoenoplectus californicus* measured as apical growth and basal diameter reported no significant ($p > 0.05$) negative effects at peanut shells concentrations more than 25%. Meanwhile, chlorophyll a and b showed significant negative effects ($p < 0.05$) for concentrations more than 12.5%. Chronic toxicity on *Eisenia foetida* was measured in growth (live growth) and reproductive (# cocoons, cocoons per individual) parameters. The individual reproduction (cocoons per individuals) was affected, but not significantly ($p > 0.05$) at concentrations more than 50%. Meanwhile, growth aspects (life weight) have not evidenced negative effects under no peanut shells concentration, increasing this parameter up to 40%.

The vegetative growth inhibition observed in *Schoenoplectus californicus* could be associated to chemical composition of the support medium, which can be slowly hydrolyzed generating aromatic compounds (e.g., phenol compounds). Some agricultural byproducts report presence of extractives compounds (up to 10 w/w%), which are rich in phenol structures (0.13–0.15 g/g) (Nepote et al., 2005; Anike et al., 2016). Chronic effects (vegetal metabolism) have been reported at phenol concentrations higher than 500 mg/L (Saleem et al., 2019). In our study, peanut shells reported extractives concentrations up to 5% (approx. 15 g/L) and *Schoenoplectus californicus* evidenced chronic effects (chlorophyll a) at concentrations higher than 12.5% peanut shells. Therefore, phenol compounds could be responsible for the decrease in vegetal photosynthetic capacity, being recommended and safe to work within biofilters with peanut shell concentrations less than or equal to 12.5%.

Table 36. Compatibility evaluation of peanut shells on *Eisenia foetida* and *Schoenoplectus californicus*

Species	Assay	Exposure time [days]	Response	Parameter	Dose [v/v%]	95% Confidence range [v/v%]
<i>Eisenia foetida</i>	Acute	14	Mortality	LC ₅₀	97.0 *	74.2–127.7
	Chronic	35	Live weight	NOEC	50.0	
			Cocoons per individual	NOEC	50.0	
<i>Schoenoplectus californicus</i>	Acute	7	Mortality	EC ₅₀	78.7 *	58.9–115
	Chronic	30	Chlorophyll a	NOEC	12.5 *	
			Chlorophyll b	NOEC	12.5 *	
			Apical height	NOEC	25.0	
			Basal diameter	NOEC	25.0	

3.2. Biofilter performance

Figure 62 summarizes the COD effluent concentrations and the organic matter removal in the biofilters studied. As can be observed, the COD efficiencies of the biofilters studied are relatively high and close to 80%. The average efficiencies obtained in the BEM were higher than those observed in the HB, BPM and BM biofilters, except for the cases in which a 1.5 m³/m²-d hydraulic rate was used.

The COD removal in every biofilter studied was produced by different processes, among which we can mention the oxidative processes where the microorganism communities biochemically degrade organic compounds (Arora & Kazmi, 2015). These mechanisms are strengthened by the presence of macrophytes in the filter bed, because the roots provide a greater surface area for biofilm formation. In addition, they improve physical filtration processes and favor aerobic conditions by the inclusion of oxygen from the roots of *Schoenoplectus californicus* in BPM and HB biofilters (Samal et al., 2017b). The *Eisenia foetida* present in BEM and HB biofilters accelerates the degradation and stabilization of organic matter through fractionation, synthesis, enzymatic and microbial enrichment processes.

Regarding the influence of the hydraulic rate, for each biofilter type, the average COD efficiencies obtained using 0.5 and 1.0 m³/m²-d were similar and higher than the efficiencies calculated when 1.5 m³/m²-d was used. These results can be attributed to the longer contact times between the wastewater and the biofilter components, which allows the adsorption, transformation and reduction of the contaminants present in wastewater (Samal et al., 2017b).

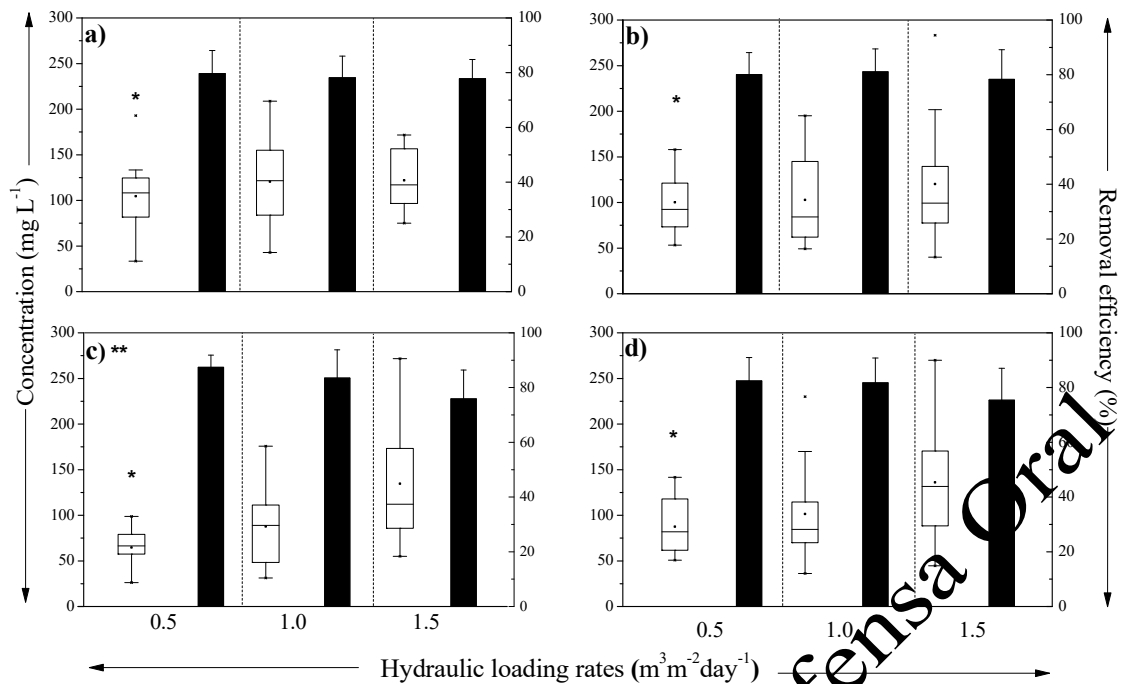


Figure 62. COD effluent concentrations (box-plot) and removal within biofilters (bar chart). a) BM, b) BPM, c) BEM and d) HB. * = Significant statistical differences between hydraulic rates, ** = Significant statistical differences between the biofilter type.

The VS average removal efficiencies observed in the biofilters studied are presented in Figure 63. These efficiencies were between 40 and 63%. The VS removal in MB and BPM biofilters is a consequence of mechanisms such as sedimentation, filtration through the *Schoenoplectus californicus* root system and biofilm adhesion that participates in aerobic and anaerobic degradation within the filter bed (Samal et al., 2017b). The incorporation of *Eisenia foetida* in HB and BEM biofilters increases the solid removal. These organisms consume the organic and inorganic particles retained in the filter and fragment them by muscular action in the digestive tract (Arora & Kazmi, 2015).

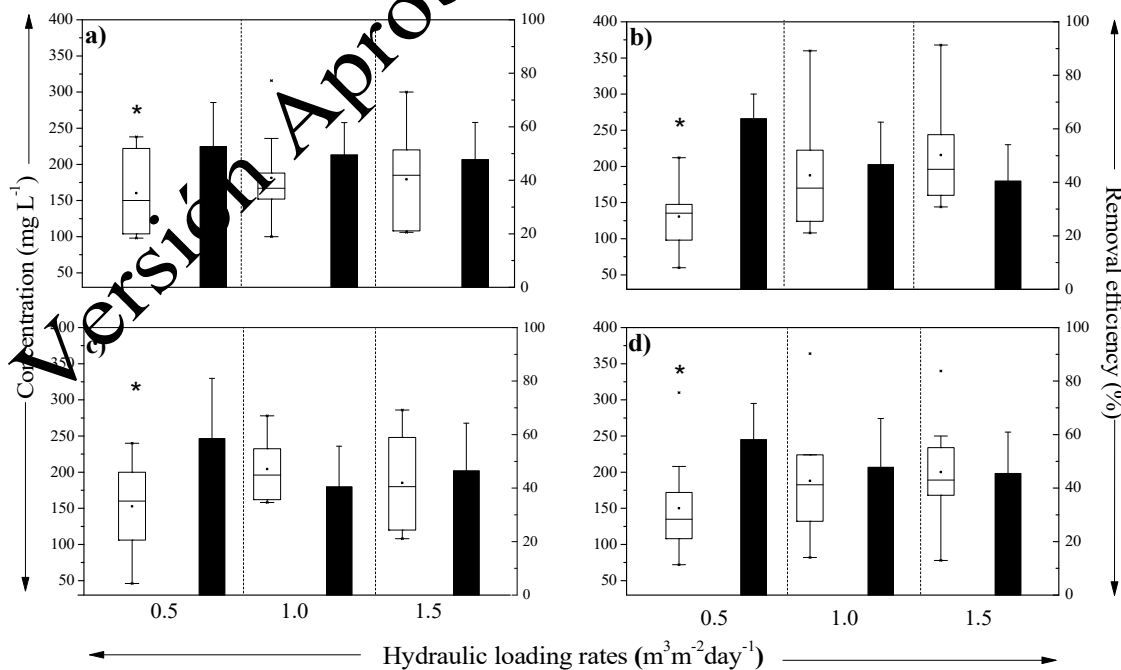


Figure 63. VS effluent concentrations (box-plot) and removal within biofilters (bar chart). a) BM, b) BPM, c) BEM and d) HB. * = Significant statistical differences between hydraulic rates.

3.3. Biota behavior

Figure 64 summarizes the biota behavior within biofilters. Biofilm (Figure 64a) located in the active layer (30 cm depth) reached values between 90 and 150 g VS/m², decreasing up to 1.7 times by a hydraulic rate increase from 0.5 to 1.5 m³/m²-d. Biodiverse biofilters (BPM, BEM, HB) showed greater biofilm and variability influenced by the hydraulic rate. The highest biofilm density (150 g VS/m²) was obtained within BPM at a 0.5 m³/m²-d hydraulic rate. This phenomenon could be related to the presence of root plants, which generate favorable microenvironments for growth of facultative microorganisms (Villamar et al., 2015). Moreover, earthworms graze some pathogenic bacteria, which could control the microbial population in HB and BEM (Arora & Kazmi, 2015). However, the successful biofilm growth achieved for all biofiltration typologies is favored by the composition of the organic support material, aspect that is mentioned by Ramirez-López et al. (2003). In addition, this fact highlights the importance of compatibility tests thanks to the symbiotic relationship of plants, earthworms and bacteria.

Earthworm growth (live growth, g/m²) (Fig 64b) ranged between 200 and 550 g/m², increasing up to 2.8 times by a hydraulic rate increase from 0.5 to 1.5 m³/m²-d. The highest live weight (550 g/m²) was reached by HB operating at a 1.5 m³/m²-d hydraulic rate. Thus, plants slightly favored the increasing of annelid weight up to 27%. Meanwhile, the growth of earthworm population (Figure 64c) showed values from 973 to 19,275 individual' m⁻², the earthworm population being up to 25% greater in HB than in BEM. Moreover, hydraulic rate increasing from 0.5 to 1.5 m³/m²-d favored up to 50% the growth population for HB. Adults, juvenile and cocoons were reported at the end of biofilter (BEM, HB) operation with a population average distribution of 13, 74 and 13%, respectively. In specific, juveniles increased 100% at the end of operation for both biofilters. In general, it was possible to see the success of the earthworm survival thanks to the control of optimal environmental conditions (20 °C, pH 7.2 – 7.4 and up to 89% moisture content), which are reported suitable by the bibliography (OECD, 2015). In fact, the population growth (up to 18,000 individuals m⁻²) obtained by all biofilters is within the range reported by bibliography (up to 20,000 individuals m⁻²) (Arora & Kazmi, 2015; Kumar et al., 2015; Li et al., 2007). Moreover, higher hydraulic rates (1.5 m³/m²-d) favored both individual and population growth thanks to the maintenance of higher, but adequate moisture contents (70 – 90%) (Kumar et al., 2015). The supremacy of juvenile individuals demonstrates success in the annelid reproduction under continuous operation conditions of biofiltration typologies. Finally, results evidenced that the biological diversity, specifically the presence of plants would favor earthworm growth. Indeed, Samal et al. (2017a) studying HB performance has reported earthworm population growth increasing up to 8%. Our work reported up to 3 times greater increase in annelid population perhaps favored also by support medium (Ramírez-López et al., 2003).

Plant growth measured as apical height/basal diameter and relative abundance (individual's/m²) was detailed in Figure 64d. Apical height varied between 25 and 51 cm, while basal diameter ranged from 4.9 to 16.5 cm, being maintained despite increases in the hydraulic rate. Meanwhile, relative abundance ranged between 358 and 2,829 individuals m⁻². This parameter increased within BPM up to 5.5 times, but it was decreased in HB up to 3 times by hydraulic rates increasing (1–1.5 m³ m⁻² d⁻¹). Results evidence that basal diameters are not influenced by the biofiltration typology or hydraulic rate, but the apical height increases slightly (up to 22%) in HB. Xu et al., (2013) report the apical height increasing of *P. australis*, *T. augustifolia* and *C. indica* within HB at percentages of 23%, 15% and 61%, respectively. Meanwhile, Samal et al., (2017b) attribute the plant height increasing to the earthworm action, because they improve the soil porosity and hence providing an adequate environment for root growth. On the other hand, BPM showed greater plant relative abundance (up to 7 times) than HB. This phenomenon could be explained by competition for nutrients with earthworms.

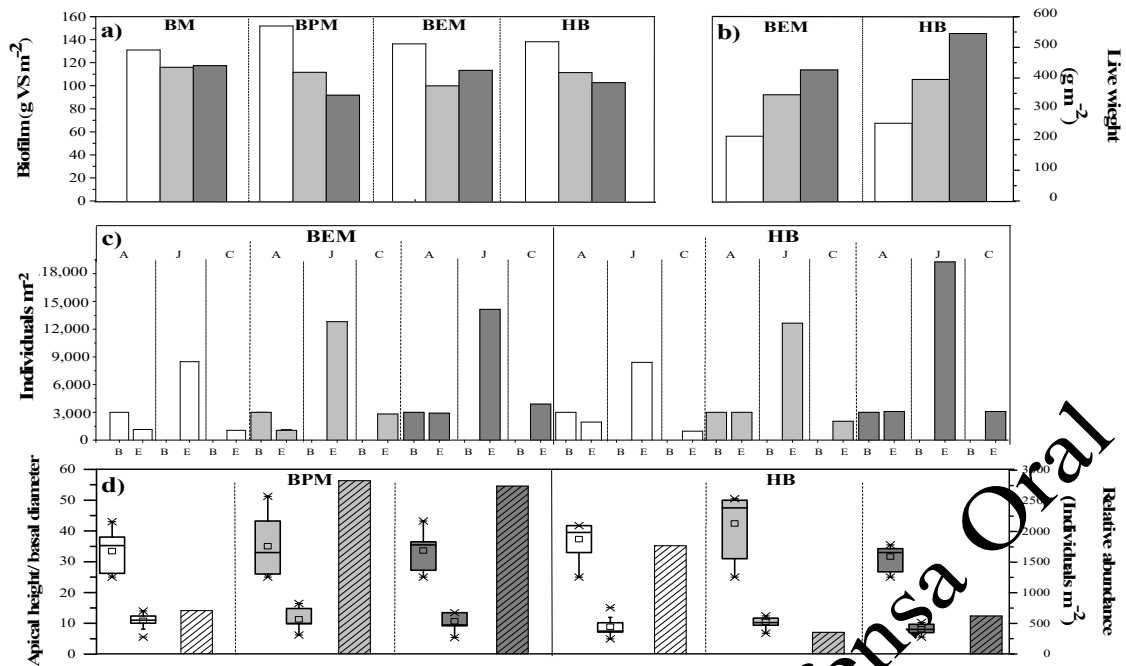


Figure 64. Biofilm, earthworm behavior and allometric measurements within BEMs. a) Biofilm, white box = 0.5 m³/m²-d, light grey box = 1.0 m³/m²-d and grey box = 1.5 m³/m²-d; b) Live weigh, white box = 0.5 m³/m²-d, light grey box = 1.0 m³/m²-d and grey box = 1.5 m³/m²-d; c) Individuals number per age, white box = 0.5 m³/m²-d, light grey box = 1.0 m³/m²-d and grey box = 1.5 m³/m²-d. A= adult earthworms, J = juvenile earthworms, C = cocoons. In the X axis, B= individuals quantity before operation, E= individuals quantity at the end of operation; d) Apical height, white box = 0.5 m³/m²-d, light grey box = 1.0 m³/m²-d and grey box = 1.5 m³/m²-d. Basal diameter, striped white box = 0.5 m³/m²-d, striped light grey box = 1.0 m³/m²-d, striped light grey box = 1.5 m³/m²-d and relative abundance, striped white bar = 0.5 m³/m²-d, striped light grey bar = 1.0 m³/m²-d, striped light grey bar = 1.5 m³/m²-d.

Figure 65 shows relation between effluent phenols concentrations and allometric measurements. In general, the average phenolic content varied between 10 and 187 mg/L, which were lower generally when a 0.5 m³ m²/day hydraulic rate was used. This may be associated with a reduction in the shear effect on the biofilter surface and less organic material detachment. On the other hand, Spearman's correlation results showed a direct relationship ($R^2 = 0.2 - 0.8$, $p < 0.05$) between the *Schoenoplectus californicus* allometric measurements and the phenol compounds content in the BPM and HB biofilter effluents. Indeed, studies reported that phenol compounds are regulators of gene expression in plan-microbe interactions (Saleem et al., 2018).

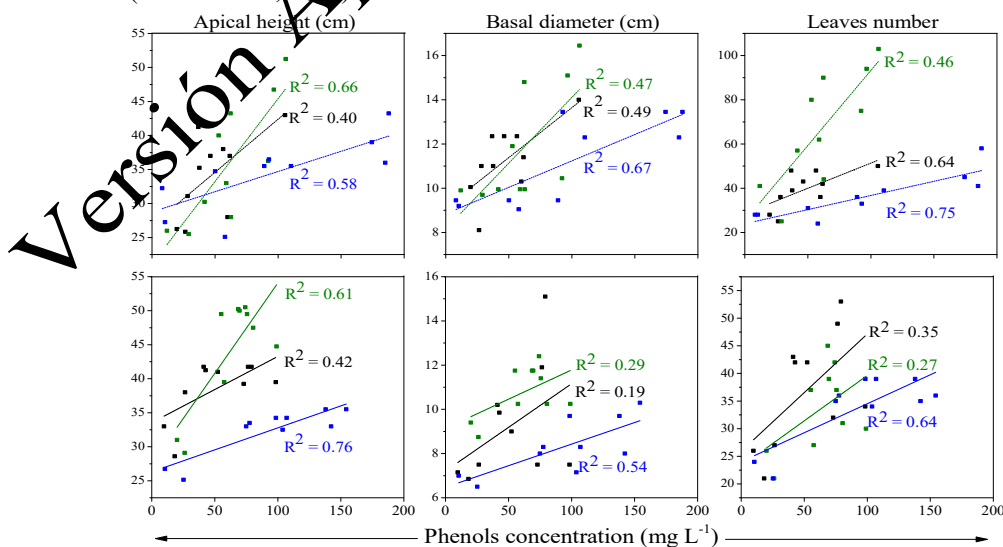


Figure 65. Phenols concentration vs. allometric measurements. a) BPM apical height, b) BPM basal diameter, c) BPM leaves number, d) HB apical height, e) HB basal diameter and f) HB leaves number.

Hydraulic operation (hydraulic conductivity, head losses) from biofiltration typologies are detailed in Figure 66. Hydraulic conductivity values varied between 250 and 700 mm/h. Meanwhile, head losses ranged from -1.4 to 8.3 cm of water column. The lowest hydraulic conductivity (250 mm/h) and the highest head losses (-1.4 cm water column) was reached by BM. The best hydraulic performance was reached by HB with average hydraulic conductivity close to 400 mm/h and head losses 0.1 cm of water column. Payne et al. (2015) mentioned that hydraulic conductivities below 100 mm/h should not be allowed, to avoid sediment accumulation and clogging. Meanwhile, hydraulic conductivities above 400 mm/h reduce contaminant removal operational efficiencies. All biofiltration typologies studied were above 100 mm/h, but under hydraulic rates more than 1 m³/m²-d they exceed the maximum hydraulic conductivities suggested. However, positive head losses were only reported between 25 (BM) and 6 (HB)% of the operation time, being the rest of the time close to 0 cm of water column for all biofilters. Definitely, hydraulic parameters can be controlled or improved by the presence of earthworms and root plants, which mix the support medium avoiding clogging (Payne et al., 2015; Samal et al., 2017b).

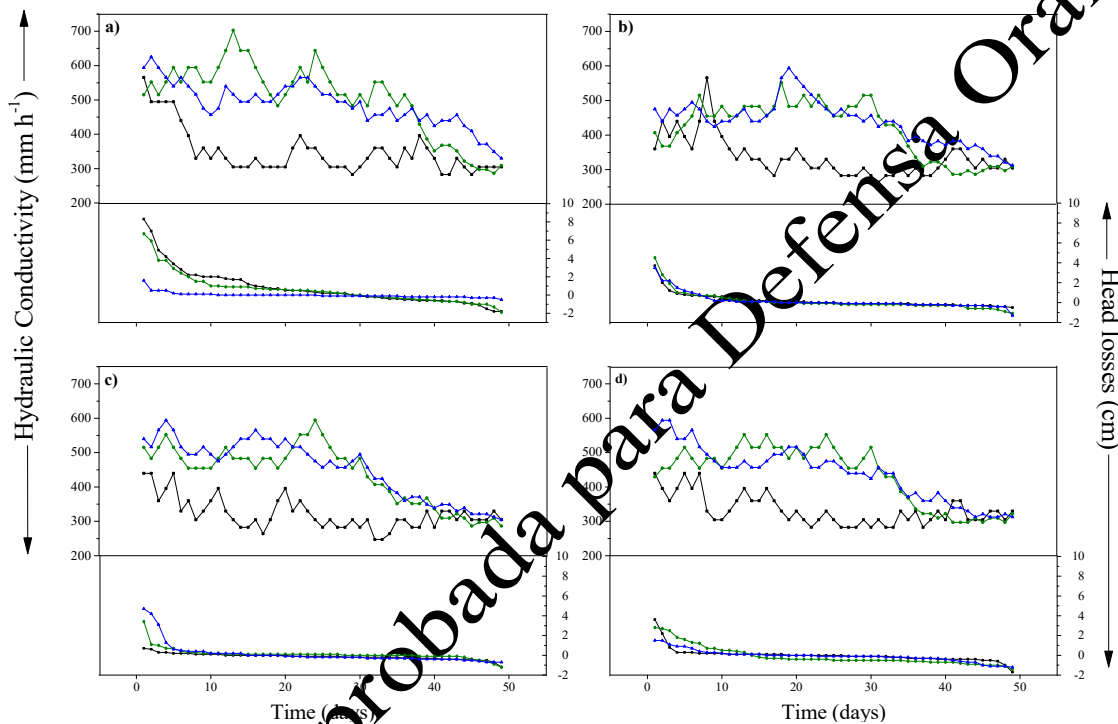


Figure 66. Hydraulic conductivity and head losses. a) BM, b) BPM, c) BEM and d) HB. Black line = 0.5 m³/m²-d Hydraulic loading rate, green line = 1.0 m³/m²-d Hydraulic loading rate and blue line = 1.5 m³/m²-d Hydraulic loading rate.

4. Conclusion

Wood chips/peanut shells are an adequate and inexpensive support material for biofiltration typologies (BM, BPM, BEM, HB) treating domestic wastewater to remove organic matter. On the one hand, separately wood chips and peanut shells show good adsorbent properties (lignin/cellulose > 29%), providing adequate conditions (pH close to 6) for the growth of plants, earthworms and associated microorganisms. However, peanut shell extractive contents (< 5%) could be toxic. Thus, a concentration of 25 v/v% peanut shells demonstrated that would not generate acute or chronic effects on plants (*Schoenoplectus californicus*) and earthworms (*Eisenia foetida*). Different types of biofilters (BM, BPM, BEM, HB) using organic support material (wood chips/peanut shells) and operating hydraulic rates of 0.5, 1.0 and 1.5 m³/m²-d can reach efficiencies close to 80% as Chemical Oxygen Demand and between 40 and 63% as Volatile Solids. Lower hydraulic rates (0.5 m³/m²-d) incorporating plants and earthworms (HB) keep head losses close to 0.1 cm of water column with hydraulic conductivities below 400 mm/h. Therefore, the use of low-cost organic materials with adequate properties (adsorbent/environmental) and biological diversity would improve the operation and disposal of organic matter in biofiltration systems.

5. Conclusions and outlook

Low-cost adsorbents, such as rice husk, peanut shells, corn cob, coconut fiber, and orange/banana peels, have demonstrated remarkable efficiencies ranging from 72.5% to 95.5% (3.5 mg/g to 15.2 mg/g) for caffeine removal, and 81.0% to 98.7% (96.9 mg/g to 285.6 mg/g) for triclosan removal. The removal of these emerging contaminants (ECs) has been significantly influenced by their underlying physicochemical properties. Similarly, the composition (lignin/extractives/ash) and size of the agro-industrial residues have played a substantial role in determining the removal and adsorption capacity for both caffeine and triclosan. Notably, orange peels and coconut fiber have proven to be more efficient than other residues in caffeine removal, achieving impressive adsorption capacities of approximately 15.2 mg/g and 7.0 mg/g, respectively. Meanwhile, corn cob has emerged as the superior residue for triclosan removal, displaying adsorption capacities of up to 286.0 mg/g. The incorporation of iron oxide nanoparticles has further enhanced the adsorption capacity of residues, resulting in a 1.7 and 4.8-fold increase in caffeine and triclosan adsorption, respectively.

While it's important to note that not all the studied residues, nanoparticles, and composites conformed uniformly to the same kinetic models and isotherms, there were instances where particle size exerted a discernible influence. Nevertheless, the kinetic and isothermal models predominantly aligned with the pseudo-second-order and Sips models, respectively. However, it must be acknowledged that despite the favorable fit with these models, the exact chemisorption/physisorption mechanism responsible for EC removal cannot be definitively guaranteed. Conversely, in the context of fixed bed columns, it was also observed that a smaller particle size (120 – 150 μm) exhibited superior adsorption capacity (up to 352.7 mg/L caffeine and 3797.2 mg/L triclosan), with a commendable fit to the Bohart-Adams model. However, these columns did encounter issues related to clogging.

Turning to the matter of toxicity, the findings indicate that coconut fiber (14d-LC₅₀= 82%) and peanut shells (14d-LC₅₀= 32%) are the most toxic to *Eisenia foetida* (Savignii), while rice husk and corn cob display no toxicity and even contribute positively to the development of earthworms. Despite this, the possibility of blending residues presents itself as a potential approach to mitigate toxicity and enhance overall efficiency.

Taking into consideration both adsorption capacity and toxicity, coconut fiber and peanut shells have been identified as the preferred options for utilization in filtration and biofiltration technologies. However, composites have not been included in this stage due to limitations stemming from laboratory capacity, reagent availability, and excessive water consumption, all of which hinder large-scale production. The utilization of coconut fiber as a filter bed in columns (with dimensions h= 75 cm coconut fiber + 15 cm gravel), operating at parameters of 2 m³/m²-d and 6h/d, has proven to be effective in achieving caffeine and triclosan removal rates surpassing 90%. Notably, the physicochemical attributes of ECs (saturation time: caffeine= 179 h, triclosan= 246 h) and particle size exerted a significant influence on performance. Particles ranging from 2.0 to 3.5 cm demonstrated superior efficiency not only in the removal of ECs but also in terms of hydraulic behavior (hydraulic conductivity < 100 mm/h). Furthermore, a combination of coconut fiber sizes yielded favorable caffeine/triclosan removal outcomes compared to using 2.0 – 3.5 cm and 3.5 – 5.7 cm particles. However, this did not translate to improvements in hydraulic conductivity (~50 mm/h). Likewise, peanut shell biofilters exhibited robust performance in the removal of organic matter (80%), and the presence of microorganisms, earthworms, and plants contributed positively to their hydraulic behavior. Importantly, the material of these filters did not exhibit degradation issues, a contrast to observations made with coconut fiber filters. Consequently, the utilization of agro-industrial residues presents itself as a viable and effective alternative for deployment in filtration/biofiltration technologies, particularly for the removal of various contaminants (characterized by differing physical-chemical properties) such as organic matter, caffeine, and triclosan. This efficacy stems from their strong adsorptive capacity, low toxicity, and abundant availability, positioning them as desirable adsorbents.

However, it is noteworthy that despite the commendable adsorbent characteristics of agro-industrial residues, their efficiencies remain slightly lower than those achieved by more expensive materials like activated carbon. The significance of this research is substantial, as it bridges the gap between controlled

laboratory studies and real-world application, which is often hindered by factors such as prohibitive costs, operational complexities, and limited practicality.

Certainly, it is unquestionably imperative to undertake forthcoming research endeavors that serve to complement and conclude the current study. In the context of batch adsorption processes, the determination of the isoelectric point of both the residues and the ECs holds utmost significance as it stands to optimize the removal process. Equally fundamental is the enhancement of composite synthesis methodologies, aimed at achieving a higher material yield within a shorter timeframe while generating reduced byproducts. This enhancement is vital to facilitate their application in continuous adsorption processes on a larger scale and, potentially, in filtration technologies. Additionally, a comprehensive evaluation of composite toxicity across diverse organism types (worms, macrophytes, microorganisms) is imperative, with the goal of facilitating their utilization in biofiltration technologies, either partially or as complete replacements for filter materials.

The assessment of the photocatalytic degradation capacity of iron oxide nanoparticles is another essential facet of this study, as it holds the potential to extend the operational lifespan of the composite. A more profound investigation into the removal mechanism observed in continuous adsorption processes is equally significant, warranting comprehensive exploration.

Furthermore, the blending of agro-industrial residue mixtures within filters and bioreactors will be carried out to ascertain potential enhancements in efficiency and reductions in toxicity. The configuration of filters will be systematically varied, incorporating parameters such as active layer height, particle sizes, and residue mixtures, all aimed at optimizing the removal of emerging contaminants. A thorough examination of filter behavior when subjected to real wastewater is indispensable, shedding light on the potential influence of organic matter presence on EC elimination. Moreover, the behavior of filters in scenarios involving multiple ECs in water will be scrutinized to establish potential interactions and outcomes.

Ultimately, a strategic approach will be devised to determine the most suitable application or management route for saturated residues, aimed at averting the transference of contaminants absorbed in filter material to other environmental matrices. Composting presents a viable alternative, particularly for residues with caffeine, given that the presence of caffeine at low concentrations favors the proliferation of microorganisms. The potential for reusing raw or heat-treated saturated materials in the removal of other contaminants will be rigorously analyzed. Furthermore, if the mechanical and chemical characteristics of these materials remain intact, they could be harnessed as reinforcements for composites. Similarly, the utilization of ashes derived from saturated materials as additives in blocks, adhesives, and cement presents yet another avenue for sustainable resource management.

Versión Aprobada para Defensa Oral

REFERENCES

- Aazza, M., Ahlafi, H., Moussout, H., & Maghat, H. (2017). Ortho-Nitro-Phenol adsorption onto alumina and surfactant modified alumina: Kinetic, isotherm and mechanism. *Journal of Environmental Chemical Engineering*, 5(4), 3418–3428. <https://doi.org/10.1016/j.jece.2017.06.051>
- Aazza, Mustapha, Ahla, H., Moussout, H., & Maghat, H. (2018). Adsorption of metha-nitrophenol onto alumina and HDTMA modified alumina: Kinetic, isotherm and mechanism investigations. 268, 587–597. <https://doi.org/10.1016/j.molliq.2018.07.095>
- Abbas, A. M., & Kamel, M. M. (2020). Dietary habits in adults during quarantine in the context of COVID-19 pandemic. *Obesity Medicine*, 19(April), 100254. <https://doi.org/10.1016/j.obmed.2020.100254>
- Abejón, A., Garea, A., & Irbaien, A. (2015). Arsenic removal from drinking water by reverse osmosis: Minimization of costs and energy consumption. *Separation and Purification Technology*, 144, 46–53. <https://doi.org/10.1016/j.seppur.2015.02.017>
- Abu, N., Sánchez-martín, M., M^a, R., & Valiente, M. (2018). Molecularly imprinted polymer for the removal of diclofenac from water: Synthesis and characterization. *Science of the Total Environment*, 631–632, 1534–1543. <https://doi.org/10.1016/j.scitotenv.2018.03.087>
- Adeel, M., Song, X., Wang, Y., Francis, D., & Yang, Y. (2017). Environmental impact of estrogens on human, animal and plant life: A critical review. *Environment International*, 99, 107–119. <https://doi.org/10.1016/j.envint.2016.12.010>
- Adeel, M., Yang, Y. S., Wang, Y. Y., Song, X. M., Ahmad, M. A., & Rogers, H. (2018). Uptake and transformation of steroid estrogens as emerging contaminants influence plant development. *Environmental Pollution*. <https://doi.org/10.1016/j.envpol.2018.09.016>
- Adugna, A. T., Andrianisa, H. A., Konate, Y., & Maiga, A. H. (2019). Fate of filter materials and microbial communities during vermifiltration process. *Journal of Environmental Management*, 242(February), 98–105. <https://doi.org/10.1016/j.jenvman.2019.04.076>
- Ahmad, J., Naeem, S., Ahmad, M., Usman, A. R. A., & Al-wabel, M. I. (2019). A critical review on organic micropollutants contamination in wastewater and removal through carbon nanotubes. *Journal of Environmental Management*, 246(September 2018), 214–228. <https://doi.org/10.1016/j.jenvman.2019.05.152>
- Ahmed, M. B., Zhou, J. L., Ngo, H. H., Guo, W., & Chen, M. (2016). Progress in the preparation and application of modified biochar for improved contaminant removal from water and wastewater. *Bioresource Technology*, 214, 836–851. <https://doi.org/10.1016/j.biortech.2016.05.057>
- Ahmed, M. B., Zhou, J. L., Ngo, H. H., Guo, W., Thomaidis, N. S., & Xu, J. (2016). Progress in the biological and chemical treatment technologies for emerging contaminant removal from wastewater: A critical review. *Journal of Hazardous Materials*, 323, 274–298. <https://doi.org/10.1016/j.jhazmat.2016.04.045>
- Ahmed, M. J., & Hameed, B. H. (2018). Removal of emerging pharmaceutical contaminants by adsorption in a fixed-bed column: A review. *Ecotoxicology and Environmental Safety*, 149(October 2017), 257–266. <https://doi.org/10.1016/j.ecoenv.2017.12.012>
- Ahmed, M., Mashkoo, F., & Nasar, A. (2020). Development, characterization, and utilization of magnetized orange peel waste as a novel adsorbent for the confiscation of crystal violet dye from aqueous solution. *Groundwater for Sustainable Development*, 100322. <https://doi.org/10.1016/j.gsd.2019.100322>
- Akhbarizadeh, R., Dobaradaran, S., Schmidt, T. C., Naeipour, I., & Spitz, J. (2020). Worldwide bottled water occurrence of emerging contaminants: A review of the recent scientific literature. *Journal of Hazardous Materials*. <https://doi.org/10.1016/j.jhazmat.2020.122271>
- Akhtar, J., Aishah, N., Amin, S., & Shahzad, K. (2015). A review on removal of pharmaceuticals from water by adsorption. *Desalination and Water Treatment*. <https://doi.org/10.1080/19443994.2015.1051121>
- Al-Ghouti, M. A., & Da, D. A. (2020). Guidelines for the use and interpretation of adsorption isotherm models: A review. *Journal of Hazardous Materials*, 393(February), 122383. <https://doi.org/10.1016/j.jhazmat.2020.122383>
- Al-Jabari, M. H., Sulaiman, S., Ali, S., Bakkat, R., Mubarak, A., & Khan, S. A. (2019). Adsorption study of levofloxacin on reusable magnetic nanoparticles: Kinetics and antibacterial activity. *Journal of Molecular Liquids*, 291, 111249. <https://doi.org/10.1016/j.molliq.2019.111249>
- Al-Qodah, Z., Yahya, M. A., & Al-Shannag, M. (2017). On the performance of bioadsorption processes for heavy metal ions removal by low-cost agricultural and natural by-products bioadsorbent: A review. *Desalination and Water Treatment*, 85(August), 329–347. <https://doi.org/10.5004/dwt.2017.21256>
- Al-shawabkeh, A. F., Omar, W., Haseine, A., & Al-amayreh, M. (2021). Experimental study of the application of date palm trunk fiber as biosorbent for removal cadmium using a fixed bed column: investigation of the influence of particle size. *Experimental study of the application of date palm trunk fiber as biosorbent for re. Desalination and Water Treatment, October*. <https://doi.org/10.5004/dwt.2021.27153>
- Alaa El-Din, G., Amer, A. A., Malsh, G., & Hussein, M. (2018). Study on the use of banana peels for oil spill removal. *Alexandria Engineering Journal*, 57(3), 2061–2068. <https://doi.org/10.1016/j.aej.2017.05.020>
- Alkessio, M. D., Yoneyama, B., Kirs, M., Kisand, V., & Ray, C. (2015). Pharmaceutically active compounds: Their removal during slow sand filtration and their impact on slow sand filtration bacterial removal. *Science of the Total Environment*, 524–525, 124–135. <https://doi.org/10.1016/j.scitotenv.2015.04.014>
- Ali, I., Asim, M., & Khan, T. A. (2012). Low cost adsorbents for the removal of organic pollutants from wastewater. *Journal of Environmental Management*, 113, 170–183. <https://doi.org/10.1016/j.jenvman.2012.08.028>
- Ali, I., Khan, Z. M., Ali, M., & Khan, M. (2014). Effect of Season and Organic Loading Variation on the Operation of an Indigenously Developed Maize Cobs Trickling Filter (MCTF). *International Journal of Engineering Works*, 1(3), 52–55. [http://www.kwpublisher.com/?paper=1-28-Effect-of-Season-and-Organic-Loading-Variation-on-the-Operation-of-an-Indigenously--Developed-Maize-Cobs-Trickling-Filter-\(MCTF\)](http://www.kwpublisher.com/?paper=1-28-Effect-of-Season-and-Organic-Loading-Variation-on-the-Operation-of-an-Indigenously--Developed-Maize-Cobs-Trickling-Filter-(MCTF))
- Alidadi, H., Dolatabadi, M., Davoudi, M., Askari, F. B., Farideh, J.-B., & Hosseinzadeh, A. (2018). Enhanced Removal of Tetracycline Using Modified Sawdust: Optimization, Isotherm, Kinetics, and Regeneration Studies. *Process Safety and Environmental Protection*. <https://doi.org/10.1016/j.psep.2018.04.007>
- Alizadeh Fard, M., & Barkdoll, B. (2018). Magnetic activated carbon as a sustainable solution for removal of micropollutants from water. *International Journal of Environmental Science and Technology*, 0123456789. <https://doi.org/10.1007/s13762-018-1809-5>
- Alizadeh, M., Vosough, A., Barkdoll, B., & Aminzadeh, B. (2017). Using polymer coated nanoparticles for adsorption of micropollutants from water. *Colloids and Surfaces A*, 531(August), 189–197. <https://doi.org/10.1016/j.colsurfa.2017.08.008>

- Almeida-Naranjo, C. E., Aldás, M. B., Cabrera, G., & Guerrero, V. H. (2021). Caffeine removal from synthetic wastewater using magnetic fruit peel composites: Material characterization, isotherm and kinetic studies. *Environmental Challenges*, 5(August), 100343. <https://doi.org/10.1016/j.envc.2021.100343>
- Almeida-Naranjo, C. E., Espinoza-Montero, P. J., Muñoz-Rodríguez, M. I., & Villamar-Ayala, C. A. (2017). Hydraulic Retention Time Influence on Improving Flocculation in the Activated Sludge Processes Through Polyelectrolytes. *Water Air Soil Pollut*, 1–9. <https://doi.org/10.1007/s11270-017-3427-0>
- Almeida-Naranjo, C. E., Frutos, M., Tejedor, J., Cuestas, J., Valenzuela, F., Rivadeneira, M. I., Villamar, C. A., & Guerrero, V. H. (2021). Caffeine adsorptive performance and compatibility characteristics (*Eisenia foetida* Savigny) of agro-industrial residues potentially suitable for vermifilter beds. *Science of The Total Environment*, 801, 149666. <https://doi.org/10.1016/j.scitotenv.2021.149666>
- Alsbaiee, A., Smith, B. J., Xiao, L., Ling, Y., Helbling, D. E., & Dichtel, W. R. (2016). Rapid removal of organic micropollutants from water by a porous β -cyclodextrin polymer. *Nature*, 529(7585), 190–194. <https://doi.org/10.1038/nature16185>
- Álvarez-Torrellas, S., Munoz, M., Gläsel, J., Pedro, Z. M. De, Domínguez, C. M., García, J., Etzold, B. J. M., & Casas, J. A. (2018). Highly efficient removal of pharmaceuticals from water by well-defined carbide-derived carbons. *Chemical Engineering Journal*, 347(April), 595–606. <https://doi.org/10.1016/j.cej.2018.04.127>
- Álvarez-Torrellas, S., Rodríguez, A., Ovejero, G., Gómez, J. M., & García, J. (2016). Removal of caffeine from pharmaceutical wastewater by adsorption: Influence of NOM, textural and chemical properties of the adsorbent. *Environmental Technology (United Kingdom)*, 37(13), 1618–1630. <https://doi.org/10.1080/09593330.2015.1122666>
- American Public Health Association, American Water Works Association, & Water Environment Federation. (2017). *Standard methods for the examination of water and wastewater*. <https://doi.org/10.2105/SMWW.2882.193>
- Anastopoulos, I., Katsouromalli, A., & Pashalidis, I. (2020). Oxidized biochar obtained from pine needles as a novel adsorbent to remove caffeine from aqueous solutions. *Journal of Molecular Liquids*, 304, 112661. <https://doi.org/10.1016/j.molliq.2020.112661>
- Anastopoulos, I., Massas, I., & Ehaliotis, C. (2015). Use of residues and by-products of the olive-oil production chain for the removal of pollutants from environmental media: A review of batch biosorption approaches Use of residues and by-products of the olive-oil production chain for the removal of pollut. *Journal of Environmental Science and Health, Part A*, April 2015, 37–41. <https://doi.org/10.1080/10934529.2015.1011964>
- Anastopoulos, I., Pashalidis, I., Orfanos, A. G., Manariotis, I. D., Tatarchuk, T., Sellaoui, I., Bonilla-Petriciolet, A., Mittal, A., & Núñez-Delgado, A. (2020). Removal of caffeine, nicotine and amoxicillin from (waste)waters by various adsorbents. A review. *Journal of Environmental Management*, 261(January). <https://doi.org/10.1016/j.jenvman.2020.110236>
- Anike FN, Y. M., & Isikhumhen, O. (2016). Co-Substrating of Peanut Shells with Cornstalks Enhances Biodegradation by *Pleurotus ostreatus*. *Journal of Bioremediation & Biodegradation*, 07(01), 1–7. <https://doi.org/10.4172/2155-6199.1000327>
- Arora, S., & Kazmi, A. A. (2015). The effect of seasonal temperature on pathogen removal efficacy of vermifilter for wastewater treatment. *Water Research*, 74, 88–99. <https://doi.org/10.1016/j.watres.2015.02.001>
- Arora, S., Rajpal, A., Bhargava, R., Pruthi, V., Bhatia, A., & Kazmi, A. A. (2019). Antibacterial and enzymatic activity of microbial community during wastewater treatment by pilot scale vermifiltration system. *Bioresource Technology*, 166, 132–141. <https://doi.org/10.1016/j.biortech.2014.05.041>
- Arora, S., Saraswat, S., Rajpal, A., Shringi, H., Mishra, R., Sethi, N., Rajvanshi, J., Nag, A., Saxena, S., & Kazmi, A. A. (2021). Effect of earthworms in reduction and fate of antibiotic resistant bacteria (ARB) and antibiotic resistant genes (ARGs) during clinical laboratory wastewater treatment by vermifiltration. *Science of the Total Environment*, 773, 145152. <https://doi.org/10.1016/j.scitotenv.2021.145152>
- Arsalan, M., Khan, Z. M., Sultan, M., Ali, I., Shakooba, M., Mahmood, M. H., Ahmad, M., Shamshiri, R. R., Imran, M. A., & Khalid, M. U. (2021). Experimental investigation of a wastewater treatment system utilizing maize cob as trickling filter media. *Fresenius Environmental Bulletin*, 30(1), 48–57.
- Ata, A., Nalcaci, O. O., & Ovez, B. (2012). Novel algae *Gracilaria verrucosa* as a biosorbent: A study of sorption mechanisms. *Algal Research*. <https://doi.org/10.1016/j.algal.2012.07.001>
- Ávila, C., García-galán, M. J., Borrego, M., Rodríguez-mozaz, S., García, J., & Barceló, D. (2021). New insights on the combined removal of antibiotics and ARGs in urban wastewater through the use of two configurations of vertical subsurface flow constructed wetland. *Science of the Total Environment*, 755, 142554. <https://doi.org/10.1016/j.scitotenv.2020.142554>
- Awfa, D., Ateia, M., Fujii, M., Johnson, M. S., & Yoshimura, C. (2018). Photodegradation of pharmaceuticals and personal care products in water treatment using carbonaceous-TiO₂ composites: A critical review of recent literature. *Water Research*, 142, 26–45. <https://doi.org/10.1016/j.watres.2018.05.036>
- Azhar, M. R., Abid, M. R., Periasamy, V., Sun, H., Tade, M. O., & Wang, S. (2017). Adsorptive removal of antibiotic sulfonamide by UiO-66 and ZIF-67 for wastewater treatment. *Journal of Colloid And Interface Science*. <https://doi.org/10.1016/j.jcis.2017.04.001>
- Bachmann, S., Calvete, T., & Féris, L. A. (2021). Caffeine removal from aqueous media by adsorption: An overview of adsorbents evolution and the kinetic, equilibrium and thermodynamic studies. *Science of the Total Environment*, 767, 144229. <https://doi.org/10.1016/j.scitotenv.2020.144229>
- Bagrlocher, C. (2007). Atlas of zeolite framework types [Book]. In *Atlas of zeolite framework types* (5th rev. ed. /). Elsevier.
- Bagneji, M., Ghaffari, E., & Aminzadeh, B. (2016). Removal of carbamazepine from municipal wastewater effluent using optimally synthesized magnetic activated carbon: Adsorption and sedimentation kinetic studies. *Journal of Environmental Chemical Engineering*. <https://doi.org/10.1016/j.jece.2016.06.034>
- Bahrami, M., Amiri, M. J., & Beigzadeh, B. (2018). Adsorption of 2,4-dichlorophenoxyacetic acid using rice husk biochar, granular activated carbon, and multi-walled carbon nanotubes in a fixed bed column system. *Water Science and Technology*, 1–10. <https://doi.org/10.2166/wst.2018.467>
- Baig, N., Sajid, M., & Saleh, A. (2019). Graphene-based adsorbents for the removal of toxic organic pollutants: A review. *Journal of Environmental Management*, 244(October 2018), 370–382. <https://doi.org/10.1016/j.jenvman.2019.05.047>
- Balarak, D., Mostafapour, F. K., Lee, S. M., & Jeon, C. (2019). Adsorption of bisphenol A using dried rice husk: Equilibrium, kinetic and thermodynamic studies. *Applied Chemistry for Engineering*. <https://doi.org/10.14478/ace.2019.1013>
- Balasubramani, K., Sivarajasekar, N., & Naushad, M. (2020). Effective adsorption of antidiabetic pharmaceutical (metformin) from aqueous medium using graphene oxide nanoparticles: Equilibrium and statistical modelling. *Journal of Molecular Liquids*, 112426. <https://doi.org/10.1016/j.molliq.2019.112426>
- Baltrėnas, P., & Baltrėnaitė, E. (2020). Natural and Inoculated Microorganisms as Important Component for Sustainability of Biofiltration System. In *Sustainable Environmental Protection Technologies* (pp. 433–482). Springer.
- Barka, N., Abdennouri, M., El, M., & Qourzal, S. (2013). Biosorption characteristics of cadmium and lead onto eco-friendly dried cactus (*Opuntia ficus indica*) cladodes. *Journal of Environmental Chemical Engineering*, 1(3), 144–149.

- <https://doi.org/10.1016/j.jece.2013.04.008>
- Bedia, J., Peñas-garz, M., Almudena, G., & Rodriguez, J. J. (2018). A Review on the Synthesis and Characterization of Biomass-Derived Carbons for Adsorption of Emerging Contaminants from Water. *Journal of Carbon Research*, 147(August 2017), 64–71. <https://doi.org/10.3390/c4040063>
- Beltrame, K. K., Cazetta, A. L., de Souza, P. S. C., Spessato, L., Silva, T. L., & Almeida, V. C. (2018). Adsorption of caffeine on mesoporous activated carbon fibers prepared from pineapple plant leaves. *Ecotoxicology and Environmental Safety*, 147(August 2017), 64–71. <https://doi.org/10.1016/j.ecoenv.2017.08.034>
- Beltrame, K. K., Cazetta, A. L., Souza, P. S. C. De, Spessato, L., Silva, T. L., & Almeida, V. C. (2018). Ecotoxicology and Environmental Safety Adsorption of caffeine on mesoporous activated carbon fibers prepared from pineapple plant leaves. *Ecotoxicology and Environmental Safety*, 147(August 2017), 64–71. <https://doi.org/10.1016/j.ecoenv.2017.08.034>
- Bergonzoli, S., Suardi, A., Rezaie, N., Alfano, V., & Pari, L. (2020). An innovative system for Maize Cob and wheat chaff harvesting: Simultaneous grain and residues collection. *Energies*, 13(5). <https://doi.org/10.3390/en13051265>
- Bernal, V., Giraldo, L., & Moreno-Piraján, J. C. (2020). Thermodynamic study of triclosan adsorption from aqueous solutions on activated carbon: Modelling of experimental adsorption isotherm and calorimetry data. *Journal of Thermal Analysis and Calorimetry*, 139(2), 913–921. <https://doi.org/10.1007/s10973-019-08474-4>
- Besharati, N., & Alizadeh, N. (2018). Adsorption of malachite green dye on different natural absorbents modified with magnetite nanoparticles. *Journal of Nanoanalysis*, 5(3), 143–155. <https://doi.org/10.22034/jna.2018.551649.1048>
- Bhat, S. A. (2020). *Earthworm Assisted Remediation of Effluents and Wastes Editors*.
- Bhatnagar, A. (2007). Removal of bromophenols from water using industrial wastes as low cost adsorbents. *Journal of Hazardous Materials*, 139, 93–102. <https://doi.org/10.1016/j.jhazmat.2006.06.139>
- Bhatnagar, A., Sillanpää, M., & Witek-krowiak, A. (2015). Agricultural waste peels as versatile biomass for water purification – A review. *Chemical Engineering Journal*, 270, 244–271. <https://doi.org/10.1016/j.cej.2015.01.135>
- Biruntha, M., Karmegam, N., Archana, J., Karunai Selvi, B., John Paul, J. A., Balamuralikrishnan, B., Chang, S. W., & Ravindran, B. (2019). Vermiconversion of biowastes with low-to-high C/N ratio into value added vermicompost. *Bioresource Technology*, 297, 122398. <https://doi.org/10.1016/j.biortech.2019.122398>
- Boretti, A., & Rosa, L. (2019). Reassessing the projections of the World Water Development Report. *Npj Clean Water*, June. <https://doi.org/10.1038/s41545-019-0039-9>
- Borthakur, P., Boruah, P. K., Das, M. R., Kulik, N., & Minofar, B. (2018). Adsorption of 17 α -ethynyl estradiol and β -estradiol on graphene oxide surface: An experimental and computational study. *Journal of Molecular Liquids*, #pagerange#. <https://doi.org/10.1016/j.molliq.2018.08.013>
- Boruah, P. K., Sharma, B., Hussain, N., & Das, M. R. (2016). Magnetically recoverable Fe₃O₄/graphene nanocomposite towards efficient removal of triazine pesticides from aqueous solution: Investigation of the adsorption phenomenon and specific ion effect. *Chemosphere*, 1–10. <https://doi.org/10.1016/j.chemosphere.2016.10.103>
- Boshir, M., Zhou, J. L., Hao, H., Guo, W., Thomaidis, N. S., & Xu, J. (2019). Progress in the biological and chemical treatment technologies for emerging contaminant removal from wastewater: A critical review. *Journal of Hazardous Materials*, 323, 274–298. <https://doi.org/10.1016/j.jhazmat.2016.04.045>
- Boudrahem, N., Delpeux-ouldriane, S., & Khenniche, L. (2017). Single and mixture adsorption of clofibrate, tetracycline and paracetamol onto Activated carbon developed from cotton linter residue. *Process Safety and Environmental Protection*, 111, 544–559. <https://doi.org/10.1016/j.psep.2017.08.025>
- Bouras, O., Bollinger, J. C., Baudu, M., & Khalaf, H. (2007). Adsorption of diuron and its degradation products from aqueous solution by surfactant-modified pillared clays. *Applied Clay Science*, 37(3–4), 240–250. <https://doi.org/10.1016/j.clay.2007.01.009>
- Brack, W., Altenburger, R., Schüürmann, G., Krauss, M., López Herráez, D., van Gils, J., Slobodnik, J., Munthe, J., Gawlik, B. M., van Wezel, A., Schriks, M., Hollender, J., Tol Jensen, K. E., Mekenyan, O., Dimitrov, S., Bunke, D., Cousins, I., Posthuma, L., van den Brink, P. J., ... de Aragão Albuquerque, G. (2015). The SOLUTIONS project: Challenges and responses for present and future emerging pollutants in land and water resources management. *Science of the Total Environment*. <https://doi.org/10.1016/j.scitotenv.2014.05.143>
- Brito Pires, C. I., Montes Candido, A. C., & de Oliveira, H. P. (2020). Adsorptive Removal of Crystal Violet from Water by Chemically Modified Coconut Shell. *Water Conservation Science and Engineering*.
- Brunner, A. M., Vughs, D., Siegers, W., Bertelkamp, C., Kolkman, A., & Laak, T. (2018). Monitoring transformation product formation in the drinking water treatments rapid sand filtration and ozonation. *Chemosphere*. <https://doi.org/10.1016/j.chemosphere.2018.09.140>
- Bui, T. X., & Choi, H. (2009). Adsorptive removal of selected pharmaceuticals by mesoporous silica SBA-15. 168, 602–608. <https://doi.org/10.1016/j.jhazmat.2009.02.072>
- Bundhoo, Z. M. A. (2019). Potential of bio-hydrogen production from dark fermentation of crop residues: A review. *International Journal of Hydrogen Energy*, 44(32), 17346–17362. <https://doi.org/10.1016/j.ijhydene.2018.11.098>
- C. Bрами, Glover, A. R., Butt, K. R., & Lowe, C. N. (2017). Avoidance, biomass and survival response of soil dwelling (endogeic) earthworms to OECD artificial soil: potential implications for earthworm ecotoxicology. *Ecotoxicology*, 576–579. <https://doi.org/10.1007/s10646-017-1788-1>
- Cao, Z., Liu, X., Xu, J., Zhang, J., Yang, Y., Zhou, J., Xu, X., & Lowry, G. V. (2017). Removal of Antibiotic Florfenicol by Sulfide-Modified Nanoscale Zero-Valent Iron. *Environmental Science and Technology*, 51(19), 11269–11277. <https://doi.org/10.1021/acs.est.7b02480>
- Caselles-Osorio, A., Puigagut, J., Segu, E., Garcá, D., & Garcá, J. (2007). Solids accumulation in six full-scale subsurface flow constructed wetlands. *Water Research*, 41, 1388–1398. <https://doi.org/10.1016/j.watres.2006.12.019>
- Castillo, N. E. T., Sierra, J. S. O., Oyervides-muñoz, M. A., Sosa-hernández, J. E., Iqbal, H. M. N., Parra-saldivar, R., & Elda, M. (2020). Exploring the potential of coffee husk as caffeine bio-adsorbent – a mini-review. *Case Studies in Chemical and Environmental Engineering*, 100070. <https://doi.org/10.1016/j.csee.2020.100070>
- Castro, D., Rosas-Laverde, N. M., Aldás, M. B., Almeida-naranjo, C., Guerrero, V. H., & Pruna, A. I. (2021). Chemical modification of agro-industrial waste-based bioadsorbents for enhanced removal of Zn(II) ions from aqueous solutions. *Materials*, under review, 1–17.
- Catherine, H. N., Ou, M.-H., Manu, B., & Shih, Y. (2018). Adsorption mechanism of emerging and conventional phenolic compounds on graphene oxide nano flakes in water. *Science of the Total Environment*, 635, 629–638. <https://doi.org/10.1016/j.scitotenv.2018.03.389>
- Çatıoğlu, F., Akay, S., Turunç, E., Gözmen, B., Anastopoulos, I., Kayan, B., & Kalderis, D. (2021). Preparation and application of Fe-modified banana peel in the adsorption of methylene blue: Process optimization using response surface methodology. *Environmental Nanotechnology, Monitoring and Management*, 16(April). <https://doi.org/10.1016/j.enmm.2021.100517>

- Çatlıoğlu, F. N., Akay, S., Gözmen, B., Turunc, E., Anastopoulos, I., Kayan, B., & Kalderis, D. (2020). Fe-modified hydrochar from orange peel as adsorbent of food colorant Brilliant Black: process optimization and kinetic studies. *International Journal of Environmental Science and Technology*, 17(4), 1975–1990. <https://doi.org/10.1007/s13762-019-02593-z>
- Chakraborty, S., Chowdhury, S., & Das Saha, P. (2011). Adsorption of Crystal Violet from aqueous solution onto NaOH-modified rice husk. *Carbohydrate Polymers*. <https://doi.org/10.1016/j.carbpol.2011.06.058>
- Chang, M., & Juang, R. (2005). Equilibrium and kinetic studies on the adsorption of surfactant, organic acids and dyes from water onto natural biopolymers. *Colloids and Surfaces A*, 269, 35–46. <https://doi.org/10.1016/j.colsurfa.2005.06.064>
- Chaukura, N., Gwenz, W., Tavengwa, N., & Manyuchi, M. M. (2016). Biosorbents for the removal of synthetic organics and emerging pollutants: Opportunities and challenges for developing countries. In *Environmental Development*. <https://doi.org/10.1016/j.envdev.2016.05.002>
- Chen, J., Deng, W., Liu, Y., Hu, L., He, L., Zhao, J., Wang, T., & Ying, G. (2019). Fate and removal of antibiotics and antibiotic resistance genes in hybrid constructed wetlands. *Environmental Pollution*. <https://doi.org/10.1016/j.envpol.2019.03.111>
- Chen, J., Liu, Y., Deng, W., & Ying, G. (2019). Removal of steroid hormones and biocides from rural wastewater by an integrated constructed wetland. *Science of the Total Environment*, 660, 358–365. <https://doi.org/10.1016/j.scitotenv.2019.01.049>
- Chen, K., Liu, L., & Chen, W. (2017). Adsorption of sulfamethoxazole and sulfapyridine antibiotics in high organic content soils. *Environmental Pollution*, 231, 1163–1171. <https://doi.org/10.1016/j.envpol.2017.08.011>
- Chen, W., Li, X., Pan, Z., Bao, Y., Ma, S., & Li, L. (2015). Efficient adsorption of Norfloxacin by Fe-MCM-41 molecular sieves: Kinetic, isotherm and thermodynamic studies. *CHEMICAL ENGINEERING JOURNAL*, 281, 397–403. <https://doi.org/10.1016/j.cej.2015.06.121>
- Chen, Z., Guo, J., Jiang, Y., & Shao, Y. (2021). High concentration and high dose of disinfectants and antibiotics used during the COVID-19 pandemic threaten human health. *Environmental Sciences Europe*. <https://doi.org/10.1186/s12502-021-00456-4>
- Chepngeno Ng'erechi, C., Njogu, P., Karanja, B., & Raude, J. M. (2020). Performance of a Modified Trickling Filter Packed with Different Substrates in Polishing Aquaculture Wastewater. *Journal of Environmental Science and Engineering*, 1–11. <https://doi.org/10.17265/2162-5263/2020.01.001>
- Chicaiza, C., Huaraca, L., Almeida-Naranjo, C. E., Guerrero, V. H., & Villamar, C. A. (2020). Improvement of organic matter and nutrient removal from domestic wastewater by using intermittent hydraulic rates on earthworm microorganism biofilters. *Water Science and Technology*, 1–11. <https://doi.org/10.2166/wst.2020.139>
- Cho, E. J., Kang, J. K., Moon, J. K., Um, B. H., Lee, C. G., Jeong, S., & Park, S. J. (2021). Removal of triclosan from aqueous solution via adsorption by kenaf-derived biochar: Its adsorption mechanism study via spectroscopic and experimental approaches. *Journal of Environmental Chemical Engineering*, 9(6), 106343. <https://doi.org/10.1016/j.jece.2021.106343>
- Choi, Y. K., Choi, T. R., Gurav, R., Bhatia, S. K., Park, Y. L., Kim, H. J., Kan, E., & Jang, Y. H. (2020). Adsorption behavior of tetracycline onto Spirulina sp. (microalgae)-derived biochars produced at different temperatures. *Science of the Total Environment*, 710, 136282. <https://doi.org/10.1016/j.scitotenv.2019.136282>
- Choong, C. E., Ibrahim, S., Yoon, Y., & Jang, M. (2018). Removal of lead and bisphenol A using magnesium silicate impregnated palm-shell waste powdered activated carbon: Comparative studies on single and binary pollutant adsorption. *Ecotoxicology and Environmental Safety*, 148(April 2017), 142–151. <https://doi.org/10.1016/j.ecoenv.2017.10.025>
- Choudhary, V., & Philip, L. (2022). Sustainability assessment of Cu-modified biochar as adsorbent for the removal of pharmaceuticals and personal care products from secondary treated wastewater. *Journal of Environmental Chemical Engineering*, 10(3), 107592. <https://doi.org/10.1016/j.jece.2022.107592>
- Chowdhury, S., Mishra, R., Saha, P., & Kushwaha, P. (2010). Adsorption thermodynamics, kinetics and isosteric heat of adsorption of malachite green onto chemically modified rice husk. *Desalination*, 265(1–3), 159–168. <https://doi.org/10.1016/j.desal.2010.07.047>
- Chtourou, M., Mallek, M., Dalmau, M., Mamo, J., Santos-Clotas, E., Salah, A. Ben, Walha, K., Salvadó, V., & Monclús, H. (2018). Triclosan, carbamazepine and caffeine removal by activated sludge system focusing on membrane bioreactor. *Process Safety and Environmental Protection*, 118, 1–8. <https://doi.org/10.1016/j.psep.2018.06.019>
- Couto, O. M., Matos, I., da Fonseca, I. M., Araújo, P. A., da Silva, E. A., & de Barros, M. A. S. D. (2015). Effect of solution pH and influence of water hardness on caffeine adsorption onto activated carbons. *Canadian Journal of Chemical Engineering*, 93(1), 68–77. <https://doi.org/10.1002/cjce.22104>
- Crane, R. A., & Scott, T. B. (2012). Nanoscale zero-valent iron: Future prospects for an emerging water treatment technology. *Journal of Hazardous Materials*, 211–212, 112–125. <https://doi.org/10.1016/j.jhazmat.2011.11.073>
- Crini, G., & Lichtfouse, E. (2018). Wastewater Treatment: An Overview. In *Green Adsorbents for Pollutant Removal*. <https://doi.org/10.1007/978-3-319-92111-2>
- Cusioli, L. F., Quesada, E. H., Barbosa de Andrade, M., Gutierrez Gomes, R., & Bergamasco, R. (2021). Microporous and Mesoporous Materials Application of a novel low-cost adsorbent functionalized with iron oxide nanoparticles for the removal of triclosan present in contaminated water. *Microporous and Mesoporous Materials*, 325(July). <https://doi.org/10.1016/j.micromeso.2021.111328>
- Czech, B., Koneczak, M., Rakowska, M., & Oleszczuk, P. (2021). Engineered biochars from organic wastes for the adsorption of diclofenac, naproxen and triclosan from water systems. *Journal of Cleaner Production*, 288. <https://doi.org/10.1016/j.jclepro.2020.125686>
- Danalioglu, S. B., Mukhtar, H., & Shaharun, M. S. (2020). Preparation and characterization of rice husk adsorbents for phenol removal from aqueous systems. *PLoS ONE*, 15(12 December), 1–8. <https://doi.org/https://doi.org/10.1371/journal.pone.0243540>
- Dafouz, R., Cáceres, N., Rodríguez-gil, J. L., Mastroianni, N., López, M., Alda, D., Barceló, D., Gil, Á., Miguel, D., & Valcárcel, Y. (2018). Science of the Total Environment Does the presence of caffeine in the marine environment represent an environmental risk? A regional and global study. *Science of the Total Environment*, 615, 632–642. <https://doi.org/10.1016/j.scitotenv.2017.09.155>
- Dafouz Ramírez, R., & Valcárcel Rivera, Y. (2017). Caffeína como contaminante ambiental. *Revista Mexicana de Fitopatología*, 34(2), 131–141. <https://doi.org/10.18781/R.MEX.FIT.1601-1>
- Dahiru, M., Zango, Z. U., & Haruna, M. A. (2018). Cationic Dyes Removal Using Low-Cost Banana Peel Biosorbent. *American Journal of Materials Science*, 8(2), 32–38. <https://doi.org/10.5923/j.materials.20180802.02>
- Danalioglu, S. T., Bayazit, S. S., Kuyumcu, Ö. K., & Salam, M. A. (2017). Efficient removal of antibiotics by a novel magnetic adsorbent: Magnetic activated carbon/chitosan (MACC) nanocomposite. *Journal of Molecular Liquids Journal*, 240, 589–596. <https://doi.org/10.1016/j.molliq.2017.05.131>
- Danis, T. G., Albanis, T. A., Petrakis, D. E., & Pomonis, P. J. (1998). Removal of chlorinated phenols from aqueous solutions by adsorption on alumina pillared clays and mesoporous alumina aluminum phosphates. *Water Research*, 32(2), 295–302. [https://doi.org/10.1016/S0043-1354\(97\)00206-6](https://doi.org/10.1016/S0043-1354(97)00206-6)
- Danish, M., Bimbach, J., Mohamad Ibrahim, M. N., & Hashim, R. (2020). Scavenging of caffeine from aqueous medium through

- optimized H3PO4-activated Acacia mangium wood activated carbon: Statistical data of optimization. *Data in Brief*, 28, 105045. <https://doi.org/10.1016/j.dib.2019.105045>
- Dann, A. B., & Hontela, A. (2011). Triclosan: Environmental exposure, toxicity and mechanisms of action. *Journal of Applied Toxicology*, 31(4), 285–311. <https://doi.org/10.1002/jat.1660>
- Dao, T. H., Vu, T. Q. M., Nguyen, N. T., Pham, T. T., Nguyen, T. L., Yusa, S. I., & Pham, T. D. (2020). Adsorption characteristics of synthesized polyelectrolytes onto alumina nanoparticles and their application in antibiotic removal. *Langmuir*, 36(43), 13001–13011. <https://doi.org/10.1021/acs.langmuir.0c02352>
- De Andrade, J. R., Oliveira, M. F., Da Silva, M. G. C., & Vieira, M. G. A. (2018). Adsorption of Pharmaceuticals from Water and Wastewater Using Nonconventional Low-Cost Materials: A Review. *Industrial and Engineering Chemistry Research*, 57(9), 3103–3127. <https://doi.org/10.1021/acs.iecr.7b05137>
- De Franco, M. A. E., de Carvalho, C. B., Bonetto, M. M., Soares, R. de P., & Féris, L. A. (2017). Removal of amoxicillin from water by adsorption onto activated carbon in batch process and fixed bed column: Kinetics, isotherms, experimental design and breakthrough curves modelling. *Journal of Cleaner Production*, 161, 947–956. <https://doi.org/10.1016/j.jclepro.2017.05.197>
- De Rozari, P., Greenway, M., & El Hanandeh, A. (2018). Nitrogen removal from sewage and septage in constructed wetland mesocosms using sand media amended with biochar. *Ecological Engineering*, 111, 1–10. <https://doi.org/10.1016/J.ECOLENG.2017.11.002>
- De Sousa, D. N. R., Insa, S., Mozeto, A. A., Petrovic, M., Chaves, T. F., & Fadini, P. S. (2018). Equilibrium and kinetic studies of the adsorption of antibiotics from aqueous solutions onto powdered zeolites. *Chemosphere*, 205, 135–146. <https://doi.org/10.1016/j.chemosphere.2018.04.085>
- De Sousa, P. A. R., Furtado, L. T., Neto, J. L. L., De Oliveira, F. M., Siqueira, J. G. M., Silva, L. F., & Coelho, R. M. (2019). Evaluation of the adsorption capacity of banana peel in the removal of emerging contaminants present in aqueous media - Study based on factorial design. *Brazilian Journal of Analytical Chemistry*, 6(22), 14–28. <https://doi.org/10.30744/brjac.2179-3425.AR.119-2018>
- Değermenci, G. D., Değermenci, N., Ayvaoglu, V., Durmaz, E., Çakır, D., & Akan, E. (2019). Adsorption of reactive dyes on lignocellulosic waste; characterization, equilibrium, kinetic and thermodynamic studies. *Journal of Cleaner Production*. <https://doi.org/10.1016/j.jclepro.2019.03.260>
- Delgado, N., Bermeo, L., Hoyos, D. A., Peñuela, G. A., Capparelli, A., Marino, D., Navarro, A., & Casas-zapata, J. C. (2020). Occurrence and removal of pharmaceutical and personal care products using subsurface horizontal flow constructed wetlands. *Water Research*, 187, 116448. <https://doi.org/10.1016/j.watres.2020.116448>
- Deng, Y., Ok, Y. S., Mohan, D., Pittman, C. U., & Dou, X. (2018). Carbamazepine removal from water by carbon dot- modified magnetic carbon nanotubes. *Environmental Research*. <https://doi.org/10.1016/j.envres.2018.11.035>
- Derylo-Marczewska, A., Blachnio, M., Marczewski, A. W., Seczkowska, M., & Jarasiuk, B. (2019). Phenoxyacid pesticide adsorption on activated carbon – Equilibrium and kinetics. *Chemosphere*, 214, 349–360. <https://doi.org/10.1016/j.chemosphere.2018.09.088>
- Devault, D. A., Amalric, L., Bristeau, S., Cruz, J., Tapie, N., Karolak, S., Buzinski, H., & Lévi, Y. (2021). Removal efficiency of emerging micropollutants in biofilter wastewater treatment plants in tropical areas. *Environmental Science and Pollution Research*, 28(9), 10940–10966. <https://doi.org/10.1007/s11266-020-10868-z>
- Devi, P., & Saroha, A. K. (2016). Utilization of sludge based adsorbents for the removal of various pollutants : A review. *Science of the Total Environment*. <https://doi.org/10.1016/j.scitotenv.2016.10.220>
- Dhillon, G. S., Kaur, S., Pulicharla, R., Brar, S. K., Cledón, M., Verma, M., & Surampalli, R. Y. (2015). Triclosan: Current status, occurrence, environmental risks and bioaccumulation potential. In *International Journal of Environmental Research and Public Health*. <https://doi.org/10.3390/ijerph12050657>
- Di Marcantonio, C., Bertelkamp, C., van Bel, M., Prank, T. E., Timmers, P. H. A., van der Wielen, P., & Brunner, A. M. (2020). Organic micropollutant removal in full-scale rapid sand filters used for drinking water treatment in The Netherlands and Belgium. *Chemosphere*, 260, 127630. <https://doi.org/10.1016/j.chemosphere.2020.127630>
- Diagboya, P. N. E., & Dikio, E. D. (2018). Silica-based mesoporous materials; emerging designer adsorbents for aqueous pollutants removal and water treatment. *Microbrous and Mesoporous Materials*. <https://doi.org/10.1016/j.micromeso.2018.03.008>
- Duan, W., Wang, N., Xiao, W., Zhao, Y., & Zheng, Y. (2018). Ciprofloxacin adsorption onto different micro-structured tourmaline, halloysite and biotite. *Journal of Molecular Liquids*, 269, 874–881. <https://doi.org/10.1016/j.molliq.2018.08.051>
- Duc, P. A., Dharanipriya, P., Velmurugan, B. K., & Shanmugavadiivu, M. (2019). Groundnut shell -a beneficial bio-waste. *Biocatalysis and Agricultural Biotechnology*, 20(June). <https://doi.org/10.1016/j.cbac.2019.101206>
- Edathil, A. A., Shittu, I., Yin, J. H., Banat, F., & Haija, M. A. (2018). Novel magnetic coffee waste nanocomposite as effective bioadsorbent for Pb(II) removal from aqueous solutions. *Environmental Chemical Engineering*, 1i. <https://doi.org/10.1016/j.jece.2018.03.041>
- Ejtahed, H. S., Hosseini-Ranjbar, S., Siadat, S. D., & Larijani, B. (2020). The most important challenges ahead of microbiome pattern in the post era of the COVID-19 pandemic. *Journal of Diabetes and Metabolic Disorders*, 10–12. <https://doi.org/10.1007/s40200-020-00579-0>
- El-Bendary, N., El-etriby, H. K., & Mahanna, H. (2021). Reuse of adsorption residuals for enhancing removal of ciprofloxacin from wastewater. *Environmental Technology*, 0(0), 1–17. <https://doi.org/10.1080/09593330.2021.1952310>
- El-bisi, H. E. E. M. K. (2014). *Merely Ag nanoparticles using different cellulose fibers as removable reductant*. 4219–4230. <https://doi.org/10.1007/s10570-014-0438-5>
- Eliche-Quesada, D., Felipe-Sesé, M. A., López-Pérez, J. A., & Infantes-Molina, A. (2017). Characterization and evaluation of rice husk ash and wood ash in sustainable clay matrix bricks. *Ceramics International*, 43(1), 463–475. <https://doi.org/10.1016/j.ceramint.2016.09.181>
- Espejo, W., Celis, J. E., Chiang, G., & Bahamonde, P. (2020). Environment and Covid-19: Pollutants, impacts, dissemination, management and recommendations for facing future epidemic threats. *Science of The Total Environment*, 747, 141314. <https://doi.org/https://doi.org/10.1016/j.scitotenv.2020.141314>
- Fakhri, A., & Behrouz, S. (2015). Comparison studies of adsorption properties of MgO nanoparticles and ZnO-MgO nanocomposites for linezolid antibiotic removal from aqueous solution using response surface methodology. *Process Safety and Environmental Protection*, 94(C), 37–43. <https://doi.org/10.1016/j.psep.2014.12.007>
- FAO. (2000). *Setting up fuel supply strategies for large - scale bio - energy projects using agricultural and forest residues* (M. Junginger (ed.); Issue 53).
- FAOSTAT Crops.FAOSTAT. (2018). *Agriculture Data*.
- Feitosa-Felizzola, J., Hanna, K., Chiron, S., & Poincare, H. (2009). Adsorption and transformation of selected human-used macrolide antibacterial agents with iron (III) and manganese (IV) oxides. *Environmental Pollution*, 157(4), 1317–1322.

- <https://doi.org/10.1016/j.envpol.2008.11.048>
- Feng, N. C., & Guo, X. Y. (2012). Characterization of adsorptive capacity and mechanisms on adsorption of copper, lead and zinc by modified orange peel. *Transactions of Nonferrous Metals Society of China (English Edition)*, 22(5), 1224–1231. [https://doi.org/10.1016/S1003-6326\(11\)61309-5](https://doi.org/10.1016/S1003-6326(11)61309-5)
- Feng, N. C., Guo, X. Y., & Liang, S. (2010). Enhanced Cu(II) adsorption by orange peel modified with sodium hydroxide. *Transactions of Nonferrous Metals Society of China (English Edition)*, 20(SUPPL.1), s146–s152. [https://doi.org/10.1016/S1003-6326\(10\)60030-1](https://doi.org/10.1016/S1003-6326(10)60030-1)
- Feng, N., Guo, X., & Liang, S. (2009). Adsorption study of copper (II) by chemically modified orange peel. *Journal of Hazardous Materials*, 164(2–3), 1286–1292. <https://doi.org/10.1016/j.jhazmat.2008.09.096>
- Fiol, N., & Villaescusa, I. (2009). Determination of sorbent point zero charge: usefulness in sorption studies. *Environmental Chemistry Letters*, 79–84. <https://doi.org/10.1007/s10311-008-0139-0>
- Flynn, D. O., Lawler, J., Yusuf, A., Parle-mcdermott, A., Harold, D., Cloughlin, M., & Holland, L. (2021). A review of pharmaceutical occurrence and pathways in the aquatic environment in the context of a changing climate and the COVID-19 pandemic Dylan. *Analytical Methods*, 575–594. <https://doi.org/10.1039/d0ay02098b>
- Foo, K. Y., & Hameed, B. H. (2012). Mesoporous activated carbon from wood sawdust by K₂CO₃ activation using microwave heating. *Bioresour Technol*, 111, 425–432. <https://doi.org/10.1016/j.biortech.2012.01.141>
- Forouzesh, M., Ebadi, A., & Aghaeinejad-meybodi, A. (2019). Separation and Purification Technology Degradation of metronidazole antibiotic in aqueous medium using activated carbon as a persulfate activator. *Separation and Purification Technology*, 210(July 2018), 145–151. <https://doi.org/10.1016/j.seppur.2018.07.066>
- Freitas, L. C., Barbosa, J. R., da Costa, A. L. C., Bezerra, F. W. F., Pinto, R. H. H., & Carvalho Junior, R. N. de. (2021). From waste to sustainable industry: How can agro-industrial wastes help in the development of new products? *Resources, Conservation and Recycling*, 169. <https://doi.org/10.1016/j.resconrec.2021.105466>
- Fuzimato, A. D., & Isidoro, C. (2020). The antiviral and coronavirus-host protein pathways inhibiting properties of herbs and natural compounds - Additional weapons in the fight against the COVID-19 pandemic? *Journal of Traditional and Complementary Medicine*, 10. <https://doi.org/10.1016/j.jtcme.2020.05.003>
- Gao, J., Liu, X., Fan, X., & Dai, H. (2019). Effects of triclosan on performance, microbial community and antibiotic resistance genes during partial denitrification in a sequencing moving bed biofilm reactor. *Bioresour Technol*, 281(January), 326–334. <https://doi.org/10.1016/j.biortech.2019.02.112>
- García-Mateos, F. J., Ruiz-Rosas, R., Marqués, M. D., Cotoruelo, L. M., Rodríguez-Mirasol, J., & Cordero, T. (2015). Removal of paracetamol on biomass-derived activated carbon: Modeling the fixed bed breakthrough curves using batch adsorption experiments. *Chemical Engineering Journal*, 279, 18–30. <https://doi.org/10.1016/j.cej.2015.04.144>
- Garg, V., & Gupta, R. (2009). Vermicomposting of Agro-Industrial Processing Waste. In *Biotechnology for Agro-Industrial Residues Utilisation* (pp. 431–456). <https://doi.org/10.1007/978-1-4020-9942-7>
- Gautam, P. K., Singh, A., Misra, K., Sahoo, A. K., & Samanta, S. K. (2019). Synthesis and applications of biogenic nanomaterials in drinking and wastewater treatment. *Journal of Environmental Management*, 231(October 2018), 734–748. <https://doi.org/10.1016/j.jenvman.2018.10.104>
- Gavrilescu, M., Demerová, K., Amand, J., Agathos, S., & Fava, F. (2015). Emerging pollutants in the environment: Present and future challenges in biomonitoring, ecological risks and bioremediation. *New Biotechnology*, 32(1), 147–156. <https://doi.org/10.1016/j.nbt.2014.01.001>
- Georgiadis, A., Marhan, S., Lattacher, A., Mäder, P., & Benner, J. (2019). *Pedobiologia - Journal of Soil Ecology Do earthworms affect the fractionation of silicon in soil? 75*(December 2018), 1–7. <https://doi.org/10.1016/j.pedobi.2019.05.001>
- Ghauch, A., Tuqan, A. M., & Kibbi, N. (2012). Ibutoprolol removal by heated persulfate in aqueous solution: A kinetics study. *Chemical Engineering Journal*, 197, 483–492. <https://doi.org/10.1016/j.cej.2012.05.051>
- Gil, A., Taoufik, N., García, A. M., & Korili, S. G. (2018). Comparative removal of emerging contaminants from aqueous solution by adsorption on an activated carbon. *Environmental Technology*, 3330. <https://doi.org/10.1080/09593330.2018.1464066>
- Gisi, S. De, Lofrano, G., Grassi, M., & Nocercola, M. (2016). Characteristics and adsorption capacities of low-cost sorbents for wastewater treatment: A review. *SUSMAT*, 9, 10–40. <https://doi.org/10.1016/j.susmat.2016.06.002>
- Gong, X., Cai, L., Li, S., Chang, S. X., Sun, X., & An, Z. (2018). Bamboo biochar amendment improves the growth and reproduction of *Eisenia fetida* and the quality of green waste vermicompost. *Ecotoxicology and Environmental Safety*, 156(March), 197–204. <https://doi.org/10.1016/j.ecoenv.2018.03.023>
- González-Moreno, M. A., García Cracianteparaluceta, B., Marcelino Sádaba, S., Zaratiegui Urdin, J., Robles Domínguez, E., Pérez Ezcurdia, M. A., & Saco Meneses, A. (2020). Feasibility of vermicomposting of spent coffee grounds and silverskin from coffee industry: A laboratory study. *Agronomy*, 10(8), 1–15. <https://doi.org/10.3390/agronomy10081125>
- Gorito, A. M., Ribeiro, A. R., & Almeida, C. M. R. (2017). A review on the application of constructed wetlands for the removal of priority substances and contaminants of emerging concern listed in recently launched EU legislation *. *Environmental Pollution*, 227, 428–443. <https://doi.org/10.1016/j.envpol.2017.04.060>
- Grassi, M., Kaykioglu, G., Belgiorno, V., & Lofrano, G. (2012). Removal of Emerging Contaminants from Water and Wastewater by Adsorption Process. In *Emerging Compounds Removal from Wastewater* (Vol. 7, Issue 1, pp. 45–48). https://doi.org/https://doi.org/10.1007/978-94-007-3916-1_2
- Grassi, Mariangela, Kaykioglu, G., Belgiorno, V., & Lofrano, G. (2012). Emerging Compounds Removal from Wastewater. In *Springer Briefs in Molecular Science Green Chemistry for Sustainability*. <http://link.springer.com/10.1007/978-94-007-2409-9>
- Greenstein, K. E., Lew, J., Dickenson, E. R. V., & Wert, E. C. (2018). Investigation of biotransformation, sorption, and desorption of multiple chemical contaminants in pilot-scale drinking water biofilters. *Chemosphere*, 200, 248–256. <https://doi.org/10.1016/j.chemosphere.2018.02.107>
- Guerranti, C., Martellini, T., Fortunati, A., Scodellini, R., & Cincinelli, A. (2019). ScienceDirect Environmental pollution from plasticiser compounds: Do we know enough about atmospheric levels and their contribution to human exposure in Europe? *Current Opinion in Environmental Science & Health*, 8, 1–5. <https://doi.org/10.1016/j.coesh.2018.10.004>
- Gupta, A., & Garg, A. (2019). Adsorption and oxidation of ciprofloxacin in a fixed bed column using activated sludge derived activated carbon. *Journal of Environmental Management*, 250(August), 109474. <https://doi.org/10.1016/j.jenvman.2019.109474>
- Gupta, V. K., Carrott, P. J. M., Ribeiro Carrott, M. M. L., & Suhas. (2009). Low-Cost adsorbents: Growing approach to wastewater treatmenta review. *Critical Reviews in Environmental Science and Technology*, 39(10), 783–842. <https://doi.org/10.1080/10643380801977610>
- Gupta, V. K., & Nayak, A. (2012). Cadmium removal and recovery from aqueous solutions by novel adsorbents prepared from orange peel and Fe 2O 3 nanoparticles. *Chemical Engineering Journal*, 180, 81–90.

- <https://doi.org/10.1016/j.ccej.2011.11.006>
- Gupta, V. K., & Suhas. (2009). Application of low-cost adsorbents for dye removal - A review. *Journal of Environmental Management*, 90(8), 2313–2342. <https://doi.org/10.1016/j.jenvman.2008.11.017>
- Gupta, Vinod K, Ali, I., & Saini, V. K. (2006). Adsorption of 2, 4-D and carbofuran pesticides using fertilizer and steel industry wastes. 299, 556–563. <https://doi.org/10.1016/j.jcis.2006.02.017>
- Gupta, Vinod Kumar, Kumar, R., Nayak, A., Saleh, T. A., & Barakart, M. A. (2013). Adsorptive removal of dyes from aqueous solution onto carbon nanotubes: A review. *Advances in Colloid and Interface Science*. <https://doi.org/10.1016/j.cis.2013.03.003>
- Hamdy, A., Mostafa, M. K., & Nasr, M. (2018). Zero-valent iron nanoparticles for methylene blue removal from aqueous solutions and textile wastewater treatment, with cost estimation. *Water Science and Technology*, 78(2), 367–378. <https://doi.org/10.2166/wst.2018.306>
- Hamid, H., & Eskicioglu, C. (2012). Fate of estrogenic hormones in wastewater and sludge treatment : A review of properties and analytical detection techniques in sludge matrix. *Water Research*, 46(18), 5813–5833. <https://doi.org/10.1016/j.watres.2012.08.002>
- Hedegaard, M. J., & Albrechtsen, H. (2014). Microbial pesticide removal in rapid sand filters for drinking water treatment e Potential and kinetics. *Water Research*, 48, 71–81. <https://doi.org/10.1016/j.watres.2013.09.024>
- Hedegaard, M. J., & Albrechtsen, H. (2017). Corrigendum to “ Microbial pesticide removal in rapid sand filters for drinking water treatment e Potential and kinetics .” *Water Research*, 122, 708–713. <https://doi.org/10.1016/j.watres.2017.05.071>
- Hedegaard, M. J., Prasse, C., & Albrechtsen, H.-J. (2019). Microbial degradation pathways of the herbicide bentazone in white sand used for drinking water treatment. *Environmental Science Water Research and Technology*. <https://doi.org/10.1039/c8ew00790j>
- Hiew, B. Y. Z., Lee, L. Y., Lee, X. J., Gan, S., Thangalazhy-Gopakumar, S., Lim, S. S., Pan, G. T., & Yang, T. C. K. (2018). Adsorptive removal of diclofenac by graphene oxide: Optimization, equilibrium, kinetic and thermodynamic studies. *Journal of the Taiwan Institute of Chemical Engineers*, 0, 1–13. <https://doi.org/10.1016/j.jtice.2018.07.024>
- Hoang, L. P., Van, H. T., Nguyen, H., & Mac, D. (2019). Removal of Cr (VI) from aqueous solution using magnetic modified biochar derived from raw corncob. *New Journal of Chemistry*, 18663–18672. <https://doi.org/10.1039/c9nj02661d>
- Honorio, J. F., Veit, M. T., Ramos, P. Y., Coldebella, P. F., Rigobello, E. S., & Regina, C. (2018). Adsorption of natural hormones estrone, 17 β -estradiol and estril by rice husk: monocomponent and multicomponent kinetics and equilibrium. *Environmental Technology*, 0(0), 1–33. <https://doi.org/10.1080/09593330.2018.1521472>
- Horton, A. A., Walton, A., Spurgeon, D. J., Lahive, E., & Svendsen, C. (2017). Microplastics in freshwater and terrestrial environments: Evaluating the current understanding to identify the knowledge gaps and future research priorities. *Science of the Total Environment*, 586, 127–141. <https://doi.org/10.1016/j.scitotenv.2017.01.090>
- Hossein, M., Mohammadirad, M., Shemirani, F., & Akbar, A. (2017). Magnetic cellulose ionomer/layered double hydroxide: An efficient anion exchange platform with enhanced diclofenac adsorption property. *Carbohydrate Polymers*, 157, 438–446. <https://doi.org/10.1016/j.carbpol.2016.10.017>
- Hu, J., Tong, Z., Hu, Z., Chen, G., & Chen, T. (2012). Adsorption of oxy-sone from aqueous solution by multi-walled carbon nanotubes. *Journal of Colloid And Interface Science*, 377(1), 355–361. <https://doi.org/10.1016/j.jcis.2012.03.064>
- Hu, X., & Cheng, Z. (2015). Removal of diclofenac from aqueous solution with multi-walled carbon nanotubes modified by nitric acid. *Chinese Journal of Chemical Engineering*. <https://doi.org/10.1016/j.cjche.2015.06.010>
- Hu, Z., Liu, Y., Chen, G., Gui, X., Chen, T., & Zhan, X. (2017). Characterization of organic matter degradation during composting of manure + straw mixtures spiked with tetracyclines. *Bioresource Technology*, 102(15), 7329–7334. <https://doi.org/10.1016/j.biortech.2011.05.003>
- Iheanacho, O. C., Nwabanne, J. T., Obi, C. C., & Otu, C. E. (2021). Packed bed column adsorption of phenol onto corn cob activated carbon: linear and nonlinear kinetics modeling. *South African Journal of Chemical Engineering*, 36(December 2020), 80–93. <https://doi.org/10.1016/j.sajce.2021.02.003>
- Ilyas, H., & Hullebusch, E. D. Van. (2020). A review on the occurrence, fate and removal of steroidal hormones during treatment with different types of constructed wetlands. *Journal of Environmental Chemical Engineering*, 8(3), 103793. <https://doi.org/10.1016/j.jece.2020.103793>
- Ishaq, A., Din, M. U., Ahmad, R., Singh, P., Singh, K., & Ahmad, S. (2020). Prospectives and challenges of wastewater treatment technologies to combat contaminants of emerging concerns. *Ecological Engineering*, 152(April), 105882. <https://doi.org/10.1016/j.ecoleng.2020.105882>
- Islam, M. A., Morton, D. N., Johnson, B. B., Mainali, B., & Angove, M. J. (2018). Manganese oxides and their application to metal ion and contaminant removal from wastewater. *Journal of Water Process Engineering*, 26(October), 264–280. <https://doi.org/10.1016/j.jwpe.2018.10.018>
- Ivanković, T., & Hrenović, J. (2010). Surfactants in the environment. *Journal of Surfactants in the Environment*, 1, 95–110. <https://doi.org/10.2478/10004-1254-61-2010-1943>
- Jaria, G., Calvo, V., Silva, C. P., Gil, M. V., Otero, M., & Esteves, V. I. (2019). Fixed-bed performance of a waste-derived granular activated carbon for the removal of micropollutants from municipal wastewater. *Science of the Total Environment*, 683, 699–708. <https://doi.org/10.1016/j.scitotenv.2019.05.198>
- Ji, Z., Jin, H., Chen, Y., Dong, Y., & Imran, M. (2015). Corn cob modified by lauric acid and ethanediol for emulsified oil adsorption. *Journal of Central South University*, 22, 2096–2105. <https://doi.org/10.1007/s11771-015-2734-0>
- Jiang, F., Dinh, D. M., & Hsieh, Y. Lo. (2017). Adsorption and desorption of cationic malachite green dye on cellulose nanofibril aerogels. *Carbohydrate Polymers*. <https://doi.org/10.1016/j.carbpol.2017.05.097>
- Jiang, J., Zhou, Z., & Sharma, V. K. (2013). SC. *Microchemical Journal*. <https://doi.org/10.1016/j.microc.2013.04.014>
- Jiang, N., Erdős, M., Moulton, O. A., Shang, R., Vlugt, T. J. H., Heijman, S. G. J., & Rietveld, L. C. (2020). The adsorption mechanisms of organic micropollutants on high-silica zeolites causing S-shaped adsorption isotherms: An experimental and Monte Carlo simulation study. *Chemical Engineering Journal*, 389(November 2019), 123968. <https://doi.org/10.1016/j.ccej.2019.123968>
- Jiang, N., Shang, R., Heijman, S. G. J., & Rietveld, L. C. (2018). High-silica zeolites for adsorption of organic micro-pollutants in water treatment: A review. *Water Research*, 144, 145–161. <https://doi.org/10.1016/j.watres.2018.07.017>
- Jing, X. R., Wang, Y. Y., Liu, W. J., Wang, Y. K., & Jiang, H. (2014). Enhanced adsorption performance of tetracycline in aqueous solutions by methanol-modified biochar. *Chemical Engineering Journal*, 248, 168–174. <https://doi.org/10.1016/j.ccej.2014.03.006>
- Joseph, L., Heo, J., Park, Y., Flora, J. R. V., & Yoon, Y. (2011). Adsorption of bisphenol A and 17 α -ethinyl estradiol on single walled carbon nanotubes from seawater and brackish water. *Desalination*, 281, 68–74. <https://doi.org/10.1016/j.desal.2011.07.044>

- Juela, D. M. (2022). Promising adsorptive materials derived from agricultural and industrial wastes for antibiotic removal: A comprehensive review. *Separation and Purification Technology*, 284(November 2021), 120286. <https://doi.org/10.1016/j.seppur.2021.120286>
- Käfferlein, H. U., Göen, T., & Angerer, J. (1998). Musk xylene: Analysis, occurrence, kinetics, and toxicology. *Critical Reviews in Toxicology*, 28(5), 431–476. <https://doi.org/10.1080/10408449891344245>
- Kammerer, D. R., Kammerer, J., & Carle, R. (2019). Adsorption and Ion Exchange for the Recovery and Fractionation of Polyphenols: Principles and Applications. In *Polyphenols in Plants* (2nd ed.). Elsevier Inc. <https://doi.org/10.1016/B978-0-12-813768-0.00018-9>
- Kamsonlian, S., Suresh, S., Majumder, C. B., & Chand, S. (2011). Characterization of Banana and Orange Peels: Biosorption Mechanism. *International Journal of Science Technology & Management*, 2(4), 1–7.
- Kandra, H. S., Mccarthy, D., Fletcher, T. D., & Deletic, A. (2014). Assessment of clogging phenomena in granular filter media used for stormwater treatment. *Journal of Hydrology*, 512, 518–527. <https://doi.org/10.1016/j.jhydrol.2014.03.009>
- Kapur, M., & Mondal, M. K. (2016). Magnetized sawdust for removal of Cu (II) and Ni (II) from aqueous solutions. *Desalination and Water Treatment*, 57(27), 12620–12631. <https://doi.org/10.1080/19443994.2015.1049962>
- Kasprzyk-Hordern, B. (2004). *Chemistry of alumina, reactions in aqueous solution and its application in water treatment*. 110, 19–48. <https://doi.org/10.1016/j.cis.2004.02.002>
- Katam, K., Shimizu, T., Soda, S., & Bhattacharyya, D. (2020). Performance evaluation of two trickling filters removing LAS and caffeine from wastewater: Light reactor (algal-bacterial consortium) vs dark reactor (bacterial consortium). *Science of the Total Environment*, 707, 135987. <https://doi.org/10.1016/j.scitotenv.2019.135987>
- Kaur, H., Bansawal, A., Hippargi, G., & Pophali, G. R. (2017). Effect of hydrophobicity of pharmaceuticals and personal care products for adsorption on activated carbon: Adsorption isotherms, kinetics and mechanism. *Environmental Science and Pollution Research*, 1–13. <https://doi.org/10.1007/s11356-017-0054-7>
- Kaur, H., Hippargi, G., Pophali, G. R., & Bansawal, A. (2019). Biomimetic lipophilic activated carbon for enhanced removal of triclosan from water. *Journal of Colloid And Interface Science*, 535, 111–121. <https://doi.org/10.1016/j.jcis.2018.09.093>
- Kaur, I., Gaba, S., Kaur, S., Kumar, R., & Chawla, J. (2018). Spectrophotometric determination of triclosan based on diazotization reaction: Response surface optimization using box-behnken design. *Water Science and Technology*. <https://doi.org/10.2166/wst.2018.123>
- Kaur, P., Kaur, P., & Kaur, K. (2020). Adsorptive removal of imazethapyr and imazamox from aqueous solution using modified rice husk. *Journal of Cleaner Production*, 244, 118699. <https://doi.org/10.1016/j.jclepro.2019.118699>
- Kaur, Y., Bhatia, Y., Chaudhary, S., & Chaudhary, G. R. (2017). Comparative performance of bare and functionalize ZnO nanoadsorbents for pesticide removal from aqueous solution. *Journal of Molecular Liquids*, 234, 94–103. <https://doi.org/10.1016/j.molliq.2017.03.069>
- Keerthanam, S., Bhatnagar, A., Mahatantila, K., & Jayasinghe, C. (2020). Engineered tea-waste biochar for the removal of caffeine, a model compound in pharmaceuticals and personal care products (PPCPs), from aqueous media. *Environmental Technology & Innovation*, 19, 100847. <https://doi.org/10.1016/j.eti.2020.100847>
- Keerthanam, S., Rajapaksha, S. M., Trakal, L., & Vithanage, M. (2020). Caffeine removal by *Gliricidia sepium* biochar: Influence of pyrolysis temperature and physicochemical properties. In *Environmental Research*. Elsevier Inc. <https://doi.org/10.1016/j.envres.2020.109865>
- Kestemont, P., & Depiereux, S. (2013). Sewage Treatment Plant Effluents and Endocrine Disruption Issues. In *Encyclopedia of Aquatic Ecotoxicology* (pp. 1047–1058). <https://doi.org/10.1007/978-94-007-5704-2>
- Khaleque, A., Alam, M. M., Hoque, M., Mondal, S., Haider, Bin, Xu, B., Johir, M. A. H., Karmakar, A. K., Zhou, J. L., Ahmed, M. B., & Moni, M. A. (2020). Zeolite synthesis from low-cost materials and environmental applications: A review. *Environmental Advances*, 2(August). <https://doi.org/10.1016/j.envadv.2020.100019>
- Khan, H., Gul, K., Ara, B., Khan, A., Ali, N., Rafiq, S., & Bilal, M. (2020). Adsorptive removal of acrylic acid from the aqueous environment using raw and chemically modified alumina: Batch adsorption, kinetic, equilibrium and thermodynamic studies. *Journal of Environmental Chemical Engineering*, 8(4), 103927. <https://doi.org/10.1016/j.jece.2020.103927>
- Khan, N. A., Khan, S. U., Ahmed, S., Farooqi, I. H., Yousefi, M., Mohammadi, A. A., & Changani, F. (2020). Recent trends in disposal and treatment technologies of emerging-pollutants- A critical review. In *TrAC - Trends in Analytical Chemistry* (Vol. 122, p. 115744). Elsevier B.V. <https://doi.org/10.1016/j.trac.2019.115744>
- Khezami, L., Chetouani, A., Taouk, B., & Capart, R. (2005). Production and characterisation of activated carbon from wood components in powder: Cellulose, lignin, xylan. *Powder Technology*, 157(1–3), 48–56. <https://doi.org/10.1016/j.powtec.2005.05.009>
- Khorishi, N., Mohd, F., & Hadibarata, T. (2018). Triclosan removal by adsorption using activated carbon derived from waste biomass: Isotherms and kinetic studies. *Journal of the Chemical Society, Dalton Transactions*, November 2017, 1–9. <https://doi.org/10.1002/jccs.201700427>
- Kim, E., Jung, C., Han, J., Her, N., Park, C., Jang, M., Son, A., & Yoon, Y. (2016). Sorptive removal of selected emerging contaminants using biochar in aqueous solution. *Journal of Industrial and Engineering Chemistry*. <https://doi.org/10.1016/j.jiec.2016.03.004>
- Kim, H., Hwang, Y. S., & Sharma, V. K. (2014). Adsorption of antibiotics and iopromide onto single-walled and multi-walled carbon nanotubes. *Chemical Engineering Journal*, 255, 23–27. <https://doi.org/10.1016/j.cej.2014.06.035>
- Kolar, P., & Jin, H. (2019). Baseline characterization data for raw rice husk. *Data in Brief*, 25, 104219. <https://doi.org/10.1016/j.dib.2019.104219>
- Korekar, G., Kumar, A., & Ugale, C. (2019). Occurrence, fate, persistence and remediation of caffeine: a review. *Environmental Science and Pollution Research*. <https://doi.org/10.1007/s11356-019-06998-8>
- Kot-Wasik, A., Jakimska, A., & Śliwka-Kaszyńska, M. (2016). Occurrence and seasonal variations of 25 pharmaceutical residues in wastewater and drinking water treatment plants. *Environmental Monitoring and Assessment*, 188(12). <https://doi.org/10.1007/s10661-016-5637-0>
- Kumar, B., Smita, K., Cumbal, L., Debut, A., Galeas, S., & Guerrero, V. H. (2016). Phytosynthesis and photocatalytic activity of magnetite (Fe₃O₄) nanoparticles using the Andean blackberry leaf. *Materials Chemistry and Physics*, 179, 310–315. <https://doi.org/10.1016/j.matchemphys.2016.05.045>
- Kumar, K. S. (2005). Fluorinated Organic Chemicals: A Review. *Research Journal of Chemistry and Environment*, 9(50).
- Kumar, T., Rajpal, A., Arora, S., Bhargava, R., Hari Prasad, K. S., & Kazmi, A. A. (2015). A comparative study on vermifiltration using epigeic earthworm *Eisenia fetida* and *Eudrilus eugeniae*. *Desalination and Water Treatment*, 57(14), 6347–6354. <https://doi.org/10.1080/19443994.2015.1010230>
- Kunduru, K. R., Nazarkovsky, M., Farah, S., Pawar, R. P., Basu, A., & Domb, A. J. (2017). Nanotechnology for water purification: applications of nanotechnology methods in wastewater treatment. In *Water Purification* (pp. 33–74). Elsevier Inc.

- <https://doi.org/10.1016/B978-0-12-804300-4/00002-2>
- Kyzas, G. Z., Bikiaris, D. N., & Lambropoulou, D. A. (2017). Effect of humic acid on pharmaceuticals adsorption using sulfonic acid grafted chitosan. *Journal of Molecular Liquids*, 230, 1–5. <https://doi.org/10.1016/j.molliq.2017.01.015>
- Kyzas, G. Z., Kostoglou, M., Lazaridis, N. K., Lambropoulou, D. A., & Bikiaris, D. N. (2013). Environmental friendly technology for the removal of pharmaceutical contaminants from wastewaters using modified chitosan adsorbents. *Chemical Engineering Journal*, 222, 248–258. <https://doi.org/10.1016/j.cej.2013.02.048>
- Lapworth, D. J., Baran, N., Stuart, M. E., & Ward, R. S. (2012). Emerging organic contaminants in groundwater: A review of sources , fate and occurrence. *Environmental Pollution*, 163, 287–303. <https://doi.org/10.1016/j.envpol.2011.12.034>
- Larous, S., & Meniai, A.-H. (2012). The use of sawdust as by product adsorbent of organic pollutant from wastewater: adsorption of phenol. *Energy Procedia*, 18, 905–914. <https://doi.org/10.1016/j.egypro.2012.05.105>
- Le, H., Valenca, R., Ravi, S., Stenstrom, M. K., & Mohanty, S. K. (2020). Size-dependent biochar breaking under compaction: Implications on clogging and pathogen removal in biofilters. *Environmental Pollution*, 266, 115195. <https://doi.org/10.1016/j.envpol.2020.115195>
- León, G. R., Aldás, M. B., Guerrero, V. H., Landázuri, A. C., & Almeida-Naranjo, C. E. (2019). Caffeine and irgasan removal from water using bamboo, laurel and moringa residues impregnated with commercial TiO₂ nanoparticles . *MRS Advances*, 4(64), 3553–3567. <https://doi.org/10.1557/adv.2020.33>
- León, H., Almeida-Naranjo, C., Aldás, M. B., & Guerrero, V. H. (2021). Methomyl removal from synthetic water using natural and modified bentonite clays. *IOP Conference Series: Earth and Environmental Science*, 776(1), 1–8. <https://doi.org/10.1088/1755-1315/776/1/012002>
- Leone, V. O., Pereira, M. C., Aquino, S., Oliveira, L., Correa, S., Ramalho, T. C., Gurgel, L., & da Silva, A. C. (2017). Adsorption of diclofenac on a magnetic adsorbent based on maghemite: experimental and theoretical studies. *New Journal of Chemistry*. <https://doi.org/10.1039/C7NJ03214E>
- Lessa, E. F., Nunes, M. L., & Fajardo, A. R. (2018). Chitosan/waste coffee-grounds composite: An efficient and eco-friendly adsorbent for removal of pharmaceutical contaminants from water. *Carbohydrate Polymers*. <https://doi.org/10.1016/j.carbpol.2018.02.018>
- Li, H., Fu, Z., Yan, C., Huang, J., Liu, Y.-N., & Kirin, S. I. (2016). Hydrophobic – hydrophilic post-crosslinked polystyrene / poly (methyl acryloyl diethylenetriamine) interpenetrating polymer networks and its adsorption properties. *Journal of Colloid and Interface Science*, 463, 61–68. <https://doi.org/10.1016/j.jcis.2015.10.044>
- Li, Jianan, Li, C., Oliveira, N. De, Teixeira, L. A. C., & Campos, L. C. (2022). Journal of Water Process Engineering Removal of diethyltoluamide , paracetamol , caffeine and triclosan from natural water by photo-Fenton process using powdered zero-valent iron. *Journal of Water Process Engineering*, 48(March), 102907. <https://doi.org/10.1016/j.jwpe.2022.102907>
- Li, Jianan, Zhou, Q., & Campos, L. C. (2018). The application of GAC sandwich slow sand filtration to remove pharmaceutical and personal care products. *Science of the Total Environment*, 635, 1182–1190. <https://doi.org/10.1016/j.scitotenv.2018.04.198>
- Li, Jingyi, Liu, H., & Paul Chen, J. (2018). Microplastics in freshwater systems: A review on occurrence, environmental effects, and methods for microplastics detection. *Water Research*, 137, 362–374. <https://doi.org/10.1016/j.watres.2017.12.056>
- Li, L., Zou, D., Xiao, Z., Zeng, X., Zhang, L., Jiang, L., Wang, A., Ge, D., Zhang, G., & Liu, F. (2018). Biochar as a sorbent for emerging contaminants enables improvements in waste management and sustainable resource use. *Journal of Cleaner Production*. <https://doi.org/10.1016/j.jclepro.2018.11.087>
- Li, M., Liu, Y., Zeng, G., Liu, N., & Liu, S. (2019). Graphene and graphene-based nanocomposites used for antibiotics removal in water treatment : A review. *Chemosphere*. <https://doi.org/10.1016/j.chemosphere.2019.03.117>
- Li, R., Zhang, Y., Chu, W., Chen, Z., & Wang, J. (2018). Adsorptive removal of antibiotics from water using peanut shells from agricultural waste. *RSC Advances*, 8(24), 13546–13555. <https://doi.org/10.1039/c7ra11796e>
- Li, S., He, B., Wang, J., Liu, J., & Hu, X. (2020). Risks of caffeine residues in the environment: Necessity for a targeted ecopharmacovigilance program. *Chemosphere*, 243, 125343. <https://doi.org/10.1016/j.chemosphere.2019.125343>
- Li, X., Zhou, M., Jia, J., Ma, J., & Jia, Q. (2018a). Design of a hyper-crosslinked B-cyclodextrin porous polymer for highly efficient removal toward bisphenol A from water. *Separation and Purification Technology*, 195, 130–137. <https://doi.org/10.1016/j.seppur.2017.12.007>
- Li, X., Zhou, M., Jia, J., Ma, J., & Jia, Q. (2018b). Separation and Purification Technology Design of a hyper-crosslinked β - cyclodextrin porous polymer for highly efficient removal toward bisphenol from water. *Separation and Purification Technology*, 195(December 2017), 130–137. <https://doi.org/10.1016/j.seppur.2017.12.007>
- Li, Y. S., Robin, P., Cluzeau, D., & Bouch, M. (2007). Vermifiltration as a stage in reuse of swine wastewater : Monitoring methodology on an experimental farm. *Ecologi*, 2, 301–309. <https://doi.org/10.1016/j.ecoleng.2007.11.010>
- Li, Yandan, Li, M., Li, Y., Yang, L., & Liu, X. (2019). Effects of particle size and solution chemistry on Triclosan sorption on polystyrene microplastic. *Chemosphere*. <https://doi.org/10.1016/j.chemosphere.2019.05.116>
- Li, Yanxia, Zhang, H., Chen, Y., Huang, L., Lin, Z., & Cai, Z. (2019). Core-Shell Structured Magnetic Covalent Organic Framework Nanocomposites for Triclosan and Triclocarban Adsorption. *ACS Applied Materials and Interfaces*. <https://doi.org/10.1021/acsami.9b06953>
- Li, Yifei, Zhu, G., Jern, W., & Keat, S. (2014). A review on removing pharmaceutical contaminants from wastewater by constructed wetlands: Design , performance and mechanism. *Science of the Total Environment*, 468–469, 908–932. <https://doi.org/10.1016/j.scitotenv.2013.09.018>
- Li, Z., Yu, Y., Sun, J., Li, D., Huang, Y., & Feng, Y. (2016). Effect of extractives on digestibility of cellulose in corn stover with liquid hot water pretreatment. *BioResources*, 11(1), 54–70. <https://doi.org/10.15376/biores.11.1.54-70>
- Libralato, G., Volpi Ghirardini, A., & Avezzi, F. (2012). To centralise or to decentralise: An overview of the most recent trends in wastewater treatment management. *Journal of Environmental Management*, 94(1), 61–68. <https://doi.org/10.1016/j.jenvman.2011.07.010>
- Lim, L. S., Wang, Y., Yih, E., & Clarke, C. (2012). Biotransformation of rice husk into organic fertilizer through vermicomposting. *Ecological Engineering*, 41, 60–64. <https://doi.org/10.1016/j.ecoleng.2012.01.011>
- Lin, J., & Cramon-taubadel, S. Von. (2019). *The role of institutional quality on the performance in the export*. September, 237–258. <https://doi.org/10.1111/agec.12552>
- Lin, S. H., & Juang, R. S. (2009). Adsorption of phenol and its derivatives from water using synthetic resins and low-cost natural adsorbents: A review. *Journal of Environmental Management*, 90(3), 1336–1349. <https://doi.org/10.1016/j.jenvman.2008.09.003>
- Liu, J., Li, E., You, X., Hu, C., & Huang, Q. (2016). Adsorption of methylene blue on an agro-waste oiltea shell with and without fungal treatment. November, 1–11. <https://doi.org/10.1038/strep38450>
- Liu, M., Chen, C., Hu, J., Wu, X., & Wang, X. (2011). Synthesis of magnetite/graphene oxide composite and application for cobalt(II) removal. *Journal of Physical Chemistry C*, 115(51), 25234–25240. <https://doi.org/10.1021/jp208575m>

- Liu, S., Tang, W., & Yang, Y. (2018). Adsorption of nicotine in aqueous solution by a defective graphene oxide. *Science of the Total Environment*, 643, 507–515. <https://doi.org/10.1016/j.scitotenv.2018.06.205>
- Liu, W., Langenho, A. A. M., Sutton, N. B., & Rijnaarts, H. H. M. (2018). Application of manganese oxides under anoxic conditions to remove diclofenac from water. *Journal of Environmental Chemical Engineering*, 6(April), 5061–5068. <https://doi.org/10.1016/j.jece.2018.05.011>
- Liu, Y., Tourbin, M., Lachaize, S., & Guiraud, P. (2014). Nanoparticles in wastewaters: Hazards, fate and remediation. *Powder Technology*, 255, 149–156. <https://doi.org/10.1016/j.powtec.2013.08.025>
- Liu, Yingying, Blowes, D. W., Ptacek, C. J., & Groza, L. G. (2019). Removal of pharmaceutical compounds, artificial sweeteners, and perfluoroalkyl substances from water using a passive treatment system containing zero-valent iron and biochar. *Science of the Total Environment*, 691, 165–177. <https://doi.org/10.1016/j.scitotenv.2019.06.450>
- Liu, Yong, Sun, X., & Li, B. (2010). Adsorption of Hg²⁺ and Cd²⁺ by ethylenediamine modified peanut shells. *Carbohydrate Polymers*, 81(2), 335–339. <https://doi.org/10.1016/j.carbpol.2010.02.020>
- Liu, Yuchen, Zhu, X., Qian, F., Zhang, S., & Chen, J. (2014). Magnetic activated carbon prepared from rice straw-derived hydrochar for triclosan removal. *RSC Advances*, 4(109), 63620–63626. <https://doi.org/10.1039/c4ra11815d>
- Lochananon, W., & Chatsiriwech, D. (2008). Effect of phosphoric acid concentration on properties of peanut shell adsorbents. *Journal of Industrial and Engineering Chemistry*, 14(1), 84–88. <https://doi.org/10.1016/j.jiec.2007.09.001>
- Loh, Z. Z., Zaidi, N. S., Syafiuddin, A., Yong, E. L., Boopathy, R., Hong, A. B., & Prastyo, D. D. (2021). Shifting from conventional to organic filter media in wastewater biofiltration treatment: A review. *Applied Sciences*, 11(18), 1–17. <https://doi.org/10.3390/app11188650>
- Lompe, K. M., Vo Duy, S., Peldszus, S., Sauv e, S., & Barbeau, B. (2018). Removal of micropollutants by fresh and colonized magnetic powdered activated carbon. *Journal of Hazardous Materials*, 360, 349–355. <https://doi.org/10.1016/j.jhazmat.2018.07.072>
- Long, J., Yuvaraja, G., Zhou, S., Mo, J., Li, H., Luo, D., Chen, D. Y., Kong, L., Subbaiah, M. V., & Reddy, G. M. (2019). Inactive Fusarium Fungal strains (ZSY and MJY) isolation and application for the removal of Pb(II) ions from aqueous environment. *Journal of Industrial and Engineering Chemistry*, 72(Ii), 442–452. <https://doi.org/10.1016/j.jiec.2019.12.047>
- Lozano-Morales, V., Gardi, I., Nir, S., & Undabeytia, T. (2018). Removal of pharmaceuticals from water by clay-cationic starch sorbents. *Journal of Cleaner Production*, 190, 703–711. <https://doi.org/10.1016/j.jclepro.2018.04.174>
- Luo, J., Zhang, Q., Cao, M., Wu, L., Cao, J., Fang, F., & Li, C. (2019). Ecotoxicity and environmental fates of newly recognized contaminants-artificial sweeteners: A review. *Science of the Total Environment*, 653, 1149–1160. <https://doi.org/10.1016/j.scitotenv.2018.10.445>
- Luo, Yunhe, Jianqiu, C., Wu, C., Zhang, J., Tang, J., Shang, J., & Liao, Q. (2018). Effect of particle size on adsorption of norfloxacin and tetracycline onto suspended particulate matter in lake. *Environmental Pollution*. <https://doi.org/10.1016/j.envpol.2018.10.066>
- Luo, Yunlong, Guo, W., Ngo, H. H., Nghiem, L. D., Hai, F. I., Zhang, J., Dang, S., & Wang, X. C. (2014). A review on the occurrence of micropollutants in the aquatic environment and their fate and removal during wastewater treatment. *Science of the Total Environment*, 473–474, 619–641. <https://doi.org/10.1016/j.scitotenv.2013.12.065>
- Luo, Z., He, Y., Zhi, D., Luo, L., Sun, Y., Khan, E., Wang, L., Peng, Y., Zhou, Y., & Tsang, D. C. W. (2019). Current progress in treatment techniques of triclosan from wastewater: A review. *Science of the Total Environment*, 696, 133990. <https://doi.org/10.1016/j.scitotenv.2019.133990>
- Lye, J. W. P., Saman, N., Sharuddin, S. S. N., Othman, N. S., Mehtar, S. S., Noor, A. M. M., Buhari, J., Cheu, S. C., H., K., & Mat, H. (2017). Removal performance of tetracycline and oxytetracycline from aqueous solution via natural zeolites: An equilibrium and kinetic study. *CLEAN-Soil, Air, Water*, 45(10)(July 2017). <https://doi.org/10.1002/clen.201600260>
- Ma, B., Arnold, W. A., & Hozalski, R. M. (2018). The relative roles of sorption and biodegradation in the removal of contaminants of emerging concern (CECs) in GAC-sand biofilters. *Water Research*. <https://doi.org/10.1016/j.watres.2018.09.023>
- Ma, J., Zhao, J., Zhu, Z., Li, L., & Yu, F. (2019). Effect of microplastic size on the adsorption behavior and mechanism of triclosan on polyvinyl chloride. *Environmental Pollution*, 113104. <https://doi.org/10.1016/j.envpol.2019.113104>
- Ma, Y., Yang, L., Wu, L., Li, P., Qi, X., Fan, L., Cui, S., Ding, Y., & Zhang, Z. (2020). Carbon nanotube supported sludge biochar as an efficient adsorbent for low concentrations of sulfamethoxazole removal. <https://doi.org/10.1016/j.scitotenv.2020.137299>
- Mahaye, N., Thwala, M., Cowan, D. A., & Musee, N. (2017). Genotoxicity of metal based engineered nanoparticles in aquatic organisms: a review. *Mutation Research*. <https://doi.org/10.1016/j.mrrev.2017.05.004>
- Mahmood, T., Aslam, M., Ansem, A., & Ali, R. (2018). Equilibrium, kinetics, mechanism and thermodynamics studies of As (III) adsorption from aqueous solution using iron impregnated used tea Equilibrium, kinetics, mechanism and thermodynamics studies of As (III) adsorption from aqueous solution using. *Desalination and Water Treatment, January*. <https://doi.org/10.5004/dwt.2018.21855>
- Malakootian, M., Farsi, M., & Faraji, M. (2019). Removal of antibiotics from aqueous solutions by nanoparticles: a systematic review and meta-analysis. *Environmental Science and Pollution Research*, 26(9), 8444–8458. <https://doi.org/10.1007/s11356-019-04227-w>
- Malik, O. A., Hsu, A., Johnson, L. A., & de Sherbinin, A. (2015). A global indicator of wastewater treatment to inform the Sustainable Development Goals (SDGs). *Environmental Science and Policy*, 48, 172–185. <https://doi.org/10.1016/j.envsci.2015.01.005>
- Mallek, M., Chtourou, M., Portillo, M., Moncl us, H., Walha, K., & Salvad o, V. (2018). Granulated cork as biosorbent for the removal of phenol derivatives and emerging contaminants. *Journal of Environmental Management*, 223(December 2017), 576–585. <https://doi.org/10.1016/j.jenvman.2018.06.069>
- Man, Y. B., Chow, K. L., Cheng, Z., Kang, Y., & Wong, M. H. (2018). Profiles and removal efficiency of organochlorine pesticides with emphasis on DDTs and HCHs by two different sewage treatment works. *Environmental Technology and Innovation*, 9, 220–231. <https://doi.org/10.1016/j.eti.2017.12.004>
- Mansour, F., Al-Hindi, M., Yahfoufi, R., Ayoub, G. M., & Ahmad, M. N. (2018). The use of activated carbon for the removal of pharmaceuticals from aqueous solutions: a review. *Reviews in Environmental Science and Biotechnology*, 17(1), 109–145. <https://doi.org/10.1007/s11157-017-9456-8>
- Marcelo, L. R., Gois, J. S. De, Araujo, A., & Vargas, D. (2020). Synthesis of iron - based magnetic nanocomposites and applications in adsorption processes for water treatment: a review. *Environmental Chemistry Letters*, 0123456789. <https://doi.org/10.1007/s10311-020-01134-2>
- Martillo-Aseffe, J. A., Lesme-Ja n, R., & Oliva-Ru z, L. O. (2020). Estimaci n del potencial energ tico de la tusa en la provincia de los R os y Guayas, Ecuador. *Revista Centro Az car*, 11–21. http://centroazucar.uclv.edu.cu/index.php/centro_azucar
- Martinez-Ruano, J. A., Caballero-Galv n, A. S., Restrepo-Serna, D. L., & Cardona, C. A. (2018). Techno-economic and

- environmental assessment of biogas production from banana peel (*Musa paradisiaca*) in a biorefinery concept. *Environmental Science and Pollution Research*, 25(36), 35971–35980. <https://doi.org/10.1007/s11356-018-1848-y>
- Massoud, M. A., Tarhini, A., & Nasr, J. A. (2009). Decentralized approaches to wastewater treatment and management: Applicability in developing countries. *Journal of Environmental Management*, 90(1), 652–659. <https://doi.org/10.1016/j.jenvman.2008.07.001>
- Matamoros, V., Hijosa, M., & Bayona, J. M. (2009). Assessment of the pharmaceutical active compounds removal in wastewater treatment systems at enantiomeric level. Ibuprofen and naproxen. *Chemosphere*, 75(2), 200–205. <https://doi.org/10.1016/j.chemosphere.2008.12.008>
- Mateo-Sagasta, J., Raschid-sally, L., & Thebo, A. (2015). *Global Wastewater and Sludge Production, Treatment and Use*. 15–25. <https://doi.org/10.1007/978-94-017-9545-6>
- Mckelvie, J. R., Wolfe, D. M., Celejewski, M. A., Alae, M., Simpson, A. J., & Simpson, M. J. (2011). Metabolic responses of *Eisenia fetida* after sub-lethal exposure to organic contaminants with different toxic modes of action. *Environmental Pollution*, 159(12), 3620–3626. <https://doi.org/10.1016/j.envpol.2011.08.002>
- Medina, M., Tapia, J., Pacheco, S., Espinosa, M., & Rodriguez, R. (2010). Adsorption of lead ions in aqueous solution using silica-alumina nanoparticles. *Journal of Non-Crystalline Solids*, 356(6–8), 383–387. <https://doi.org/10.1016/j.jnoncrysol.2009.11.032>
- Meffe, R., & Bustamante, I. De. (2014). Science of the Total Environment Emerging organic contaminants in surface water and groundwater: A first overview of the situation in Italy. *Science of the Total Environment*, 481, 280–295. <https://doi.org/10.1016/j.scitotenv.2014.02.053>
- Messina, L. I. G., Bonelli, P. R., & Cukierman, A. L. (2015). Copyrolysis of peanut shells and cassava starch mixtures: Effect of the components proportion. *Journal of Analytical and Applied Pyrolysis*. <https://doi.org/10.1016/j.jaap.2015.05.017>
- Milanović, M., Đurić, L., Milošević, N., & Milić, N. (2021). Comprehensive insight into triclosan—from widespread occurrence to health outcomes. *Environmental Science and Pollution Research*, 0123456789. <https://doi.org/10.1007/s11356-021-17273-0>
- Minh, T. D., Lee, B. K., & Nguyen-Le, M. T. (2018). Methanol-dispersed of ternary Fe₃O₄@γ-AP50/graphene oxide-based nanohybrid for novel removal of benzotriazole from aqueous solution. *Journal of Environmental Management*, 209, 452–461. <https://doi.org/10.1016/j.jenvman.2017.12.085>
- Miranda, M. T., Septilveda, F. J., Arranz, J. I., Montero, I., & Rojas, C. V. (2018). Analysis of pelletizing from corn cob waste. *Journal of Environmental Management*, 228(February), 303–311. <https://doi.org/10.1016/j.jenvman.2018.08.105>
- Mo, J., Yang, Q., Zhang, N., Zhang, W., Zheng, Y., & Zhang, Z. (2018). A review on agro-industrial waste (AIW) derived adsorbents for water and wastewater treatment. *Journal of Environmental Management*, 227(August), 395–405. <https://doi.org/10.1016/j.jenvman.2018.08.069>
- Mohan, D., Sarswat, A., Ok, Y. S., & Pittman, C. U. (2014). Organic and inorganic contaminants removal from water with biochar, a renewable, low cost and sustainable adsorbent - A critical review. *Bioresource Technology*, 160, 191–202. <https://doi.org/10.1016/j.biortech.2014.01.120>
- Mohd Khori, N. K. E., Hadibarata, T., Elshikh, M. S., Al-Ghamdi, A. A., Sumiati, & Yusop, Z. (2018). Triclosan removal by adsorption using activated carbon derived from waste biomass: Isotherms and kinetic studies. *Journal of the Chinese Chemical Society*. <https://doi.org/10.1002/jccs.201700427>
- Montaseri, H., & Forbes, P. B. C. (2016). A review of monitoring methods for triclosan and its occurrence in aquatic environments. *TrAC - Trends in Analytical Chemistry*, 85, 221–231. <https://doi.org/10.1016/j.trac.2016.09.010>
- Moussavi, G., Hossaini, Z., & Pourakbar, M. (2016). High rate adsorption of acetaminophen from the contaminated water onto double-oxidized graphene oxide. *Chemical Engineering Journal*, 287, 665–673. <https://doi.org/10.1016/j.cej.2015.11.025>
- Mubarik, S., Saeed, A., Mehmood, Z., & Iqbal, M. (2012). Phenol adsorption by charred sawdust of sheesham (Indian rosewood ; Dalbergia sissoo) from single , binary and ternary contaminated solutions. *Journal of the Taiwan Institute of Chemical Engineers*, 43(6), 926–933. <https://doi.org/10.1016/j.jtice.2012.07.003>
- Muñoz-Peñuela, M., Moreira, R. G., Gomes, L. O., Tolussi, C. E., Branco, G. S., Pinheiro, J. P. S., Zampieri, R. A., & Lo Nostro, F. L. (2022). Neurotoxicity, biotransformation, oxidative stress and genotoxic effects in *Astyanax altiparanae* (Teleostei, Characiformes) males exposed to environmentally relevant concentrations of diclofenac and/or caffeine. *Environmental Toxicology and Pharmacology*, 91(January). <https://doi.org/10.1016/j.etap.2022.103821>
- Mussatto, S. I., Fernandes, M., Rocha, C. J. M., Orfão, J. J. M., Teixeira, J. A., & Roberto, I. C. (2010). Bioresource Technology Production , characterization and application of activated carbon from brewer ’ s spent grain lignin. *Bioresource Technology*, 101(7), 2450–2457. <https://doi.org/10.1016/j.biortech.2009.11.025>
- N’diaye, A. D., & Kankou, M. S. (2020). Sorption of Aspirin from Aqueous Solutions using Rice Husk as Low Cost Sorbent. *Journal of Environmental Treatment Techniques*, 8(1), 1–5.
- N’diaye, D. A., & Ahmed Kankou, M. S. (2019). Sorption of caffeine onto low-cost sorbent: Application of two and three-parameter isotherm models. *Applied Journal of Environmental Engineering Science*, 3, 263–272. <https://doi.org/10.48422/IMIST.PRSM/ajees-v5i3.17210>
- N diaye, A. D., & Ahmed Kankou, M. S. (2020). Modeling of Adsorption Isotherms of Caffeine onto Groundnut Shell as a Low Cost Adsorbent. *Journal of Environmental Treatment Techniques*, 8(3), 1191–1195. [https://doi.org/10.47277/JETT/8\(3\)1195](https://doi.org/10.47277/JETT/8(3)1195)
- Nasir, T., & Waseem, M. (2021). A comprehensive review on the role of some important nanocomposites for antimicrobial and wastewater applications. *International Journal of Environmental Science and Technology*, 0123456789. <https://doi.org/10.1007/s13762-021-03256-8>
- Nassar, M. M., Farrag, T. E., & Ahmed, M. H. (2012). Removal of an insecticide (methomyl) from aqueous solutions using natural clay. *Alexandria Engineering Journal*, 51(1), 11–18. <https://doi.org/10.1016/j.aej.2012.07.002>
- Nassar, M. Y., Ahmed, I. S., & Hendy, H. (2018). A facile one-pot hydrothermal synthesis of hematite (α-Fe₂O₃) nanostructures and cephalixin antibiotic sorptive removal from polluted aqueous media. *Journal of Molecular Liquids*, #page#.#. <https://doi.org/10.1016/j.molliq.2018.09.057>
- Neuhauser, E. F., Loehr, R. C., Malecki, M. R., Milligan, D. L., & Durkin, P. R. (1985). The Toxicity of Selected Organic Chemicals to the Earthworm *Eisenia fetida*. *Journal of Environmental Quality*, 14(3), 383–388. <https://doi.org/10.2134/jeq1985.00472425001400030015x>
- Ngigi, A. N., Ok, Y. S., & Thiele-Bruhn, S. (2018). Biochar-mediated sorption of antibiotics in pig manure. *Journal of Hazardous Materials*. <https://doi.org/10.1016/j.jhazmat.2018.10.045>
- Ngoc, T., Id, M., Xuan, T. D., & Ahmad, A. (2018). Efficacy from Different Extractions for Chemical Profile and Biological Activities of Rice Husk. *Sustainability*, 10(5), 1–15. <https://doi.org/10.3390/su10051356>
- Nguyen, L. H., Van, H. T., Chu, T. H. H., Nguyen, T. H. V., Nguyen, T. D., Hoang, L. P., & Hoang, V. H. (2021). Paper waste sludge-derived hydrochar modified by iron (III) chloride for enhancement of ammonium adsorption: An adsorption

- mechanism study. *Environmental Technology and Innovation*, 21(Iii), 101223. <https://doi.org/10.1016/j.eti.2020.101223>
- Nguyen, N. T., Dao, T. H., Truong, T. T., Minh, T., Nguyen, T., & Pham, T. D. (2020). Adsorption characteristic of ciprofloxacin antibiotic onto synthesized alpha nanoparticles with surface modification by polyanion. *Journal of Molecular Liquids*, 309, 113150. <https://doi.org/10.1016/j.molliq.2020.113150>
- Nie, Y., Deng, S., Wang, B., Huang, J., & Yu, G. (2014). Removal of clofibrac acid from aqueous solution by polyethylenimine-modified chitosan beads. *Frontiers of Environmental Science & Engineering*. <https://doi.org/10.1007/s11783-013-0622-0>
- Nielsen, L., & Bandosz, T. J. (2015). Analysis of the competitive adsorption of pharmaceuticals on waste derived materials. *Chemical Engineering Journal*, 287(November), 139–147. <https://doi.org/10.1016/j.cej.2015.11.016>
- Nielsen, L., & Bandosz, T. J. (2016). Analysis of sulfamethoxazole and trimethoprim adsorption on sewage sludge and fish waste derived adsorbents. *Microporous and Mesoporous Materials*, 220, 58–72. <https://doi.org/10.1016/j.micromeso.2015.08.025>
- Nizamuddin, S., Siddiqui, M. T. H., Baloch, H. A., Mubarak, N. M., Griffin, G., Madapusi, S., & Tanksale, A. (2018). Upgradation of chemical, fuel, thermal, and structural properties of rice husk through microwave-assisted hydrothermal carbonization. *Environmental Science and Pollution Research*, 25(18). <https://doi.org/10.1007/s11356-018-1876-7>
- Nopsa-Hernández, J. F. (2019). Situación del cultivo de maíz en Ecuador: investigación y desarrollo de tecnologías en el Inia. *Memorias Del IV Congreso de Semillas*.
- Noreen, S., Bhatti, H. N., Nausheen, S., Sadaf, S., & Ashfaq, M. (2013). Batch and fixed bed adsorption study for the removal of Drimarine Black CL-B dye from aqueous solution using a lignocellulosic waste: A cost affective adsorbent. *Industrial Crops and Products*, 50, 568–579. <https://doi.org/10.1016/j.indcrop.2013.07.065>
- Organization for Economic Co-operation and Development (OECD). (2015). Earthworm Reproduction Test (eisenia fetida/ Eisenia Andrei). In *OECD Guideline*. OECD Publishing.
- Organization for Economic Cooperation and Development (OECD), 2002. OECD-Guideline for the Testing of Chemicals, revised proposal for a new guideline No. 221. Lemna sp. Growth Inhibition Test. Paris.
- Organization for Economic Cooperation and Development (OECD), 2015. OECD-Guideline for the Testing of Chemicals, Draft updated TG No. 222 Earthworm Reproduction Test (Eisenia fetida/ Eisenia andrei), Paris.
- Orozco, R. S., Hernández, P. B., Morales, G. R., Núñez, F. U., Villafuerte, J. O., Lugo, V. L., Ramírez, J. F., Díaz, C. E. B., & Vázquez, P. C. (2014). Characterization of lignocellulosic fruit waste as an alternative feedstock for bioethanol production. *BioResources*, 9(2), 1873–1885.
- Ofomaja, A. E. (2011). Kinetics and pseudo-isotherm studies of 4-nitrophenol adsorption onto Manihot wood sawdust. *Industrial Crops & Products*, 33(2), 418–428. <https://doi.org/10.1016/j.indcrop.2010.10.036>
- Oliveira, M. De, Atalla, A. A., Emanuel, B., Frihling, F., Cavalheri, P. S., Migliolo, I., & Filho, F. J. C. M. (2019). Ibuprofen and caffeine removal in vertical flow and free-floating macrophyte constructed wetlands with Heliconia rostrata and Eichornia crassipes. *Chemical Engineering Journal*. <https://doi.org/10.1016/j.cej.2019.05.064>
- Oliveira, G., Calisto, V., Santos, S. M., Otero, M., & Esteves, V. I. (2018). Paper pulp-based adsorbents for the removal of pharmaceuticals from wastewater: A novel approach towards diversification. *Science of the Total Environment*, 631–632, 1018–1028. <https://doi.org/10.1016/j.scitotenv.2018.03.072>
- Oliveira, M. F., Silva, M. G. C., & Vieira, M. G. A. (2019). Equilibrium and kinetic studies of caffeine adsorption from aqueous solutions on thermally modified Verde-lodo bentonite. *Applied Clay Science*, 168(July 2018), 366–373. <https://doi.org/10.1016/j.clay.2018.12.011>
- Oliveira, R., Domingues, I., Grisolia, C. K., & Soares, A. M. V. M. (2009). Effects of triclosan on zebrafish early-life stages and adults. *Environmental Science and Pollution Research*, 16, 679–688. <https://doi.org/10.1007/s11356-009-0119-3>
- Oyekanmi, A. A., Ahmad, A., Hossain, K., & Id, M. R. (2019). Adsorption of Rhodamine B dye from aqueous solution onto acid treated banana peel: Response surface methodology, kinetics and isotherm studies. *PLoS ONE*, 1–20.
- Palčić, A., & Valtchev, V. (2020). Analysis and control of acid sites in zeolites. *Applied Catalysis A: General*, 606(May 2020), 117795. <https://doi.org/10.1016/j.apcata.2020.117795>
- Pallarés, J., González-Cencerrado, A., & Aranda, J. (2018). Production and characterization of activated carbon from barley straw by physical activation with carbon dioxide and steam. *Biomass and Bioenergy*, 115(April), 64–73. <https://doi.org/10.1016/j.biombioe.2018.04.015>
- Palmer, M., & Hatley, H. (2018). The role of surfactants in wastewater treatment: impact, removal and future techniques: A critical review. *Water Research*. <https://doi.org/10.1016/j.watres.2018.09.039>
- Pan, B., Zhang, W., Li, L., Zhang, Q., & Zheng, S. (2009). Development of polymeric and polymer-based hybrid adsorbents for pollutants removal from waters. *Chemical Engineering Journal*, 151, 19–29. <https://doi.org/10.1016/j.cej.2009.02.036>
- Panepinto, D., Fiore, S., Zappone, M., Genon, G., & Meucci, L. (2016). Evaluation of the energy efficiency of a large wastewater treatment plant in Italy. *Applied Energy*, 161, 404–411. <https://doi.org/10.1016/j.apenergy.2015.10.027>
- Panikkar, A. K., Okamoto, S. A., Riley, S. J., Shrestha, S. P., & Hung, Y. (2010). Total Treatment of Black and Grey Water for Rural Communities. In *Environmental Bioengineering* (Vol. 11). <https://doi.org/10.1007/978-1-60327-031-1>
- Panneerselvam, P., Morad, N., & Tan, K. A. (2011). Magnetic nanoparticle (F3O4) impregnated onto tea waste for the removal of nickel(II) from aqueous solution. *Journal of Hazardous Materials*, 186(1), 160–168. <https://doi.org/10.1016/j.jhazmat.2010.10.102>
- Papadimitrakou, A., Hedegaard, M. J., Musovic, S., & Smets, B. F. (2018). Methanotrophic contribution to biodegradation of phenoxy acids in cultures enriched from a groundwater-fed rapid sand filter.
- Paradkar, M. M., & Irudaryaraj, J. (2002). A Rapid FTIR Spectroscopic Method for Estimation of Caffeine in Soft Drinks and Total Methylxanthines in Tea and Coffee. *Journal of Food Science: Food Chemistry and Toxicology*, 67(7), 2507–2511. <https://doi.org/https://doi.org/10.1111/j.1365-2621.2002.tb08767.x>
- Paredes-Laverde, M., Silva-agredo, J., & Torres-palma, R. A. (2018). Removal of norfloxacin in deionized, municipal water and urine using rice (*Oryza sativa*) and coffee (*Coffea arabica*) husk wastes as natural adsorbents. *Journal of Environmental Management*, 213, 98–108.
- Parida, V. K., Saidulu, D., Majumder, A., Srivastava, A., Gupta, B., & Gupta, A. K. (2021). Emerging contaminants in wastewater: A critical review on occurrence, existing legislations, risk assessment, and sustainable treatment alternatives. In *Journal of Environmental Chemical Engineering* (Vol. 9, Issue 5). Elsevier Ltd. <https://doi.org/10.1016/j.jece.2021.105966>
- Park, J., Brown, M., & Han, T. (2015). The Lemna Toxicity Test : Guideline of a New Test System Based on Root. *Protoc. Exch.*, 2015–2017. https://doi.org/http://hdl.handle.net/10026.1/4396_10.1038/protex.2015.091
- Pathak, P. D., Mandavgane, S. A., & Kulkarni, B. D. (2017). Fruit peel waste: Characterization and its potential uses. *Current Science*, 113(3), 444–454. <https://doi.org/10.18520/cs/v113/i03/444-454>
- Patiño, Y., Díaz, E., Ordóñez, S., Gallegos-Suarez, E., Guerrero-Ruiz, A., & Rodríguez-Ramos, I. (2015). Adsorption of emerging pollutants on functionalized multiwall carbon nanotubes. *Chemosphere*, 136, 174–180.

- <https://doi.org/10.1016/j.chemosphere.2015.04.089>
- Payne, E., Hatt, B., Deletic, A., Dobbie, M., Mccarthy, D., & Chandrasena, G. (2015). *Adoption Guidelines for Stormwater Biofiltration Systems - Summary Report, Melbourne, Australia: Cooperative Research Centre for Water Sensitive Cities.*
- Peñafiel, M. E., Matesanz, J. M., Vanegas, E., Bernejo, D., Mosteo, R., & Ormad, M. P. (2021). Comparative adsorption of ciprofloxacin on sugarcane bagasse from Ecuador and on commercial powdered activated carbon. *Science of the Total Environment*, 750, 141498. <https://doi.org/10.1016/j.scitotenv.2020.141498>
- Peng, J., Wang, X., Yin, F., & Xu, G. (2019). Characterizing the removal routes of seven pharmaceuticals in the activated sludge process. *Science of the Total Environment*, 650, 2437–2445. <https://doi.org/10.1016/j.scitotenv.2018.10.004>
- Peng, X., Hu, F., Zhang, T., Qiu, F., & Dai, H. (2018). Amine-functionalized magnetic bamboo-based activated carbon adsorptive removal of ciprofloxacin and norfloxacin: A batch and fixed-bed column study. *Bioresource Technology*, 249(November 2017), 924–934. <https://doi.org/10.1016/j.biortech.2017.10.095>
- Pezhhanfar, S., Zarei, M., & Shekaari, T. (2021). Introduction of maize cob and husk for wastewater treatment; evaluation of isotherms and artificial neural network modeling. *Journal of the Iranian Chemical Society*. <https://doi.org/10.1007/s13738-021-02301-0>
- Pham, T. D., Vu, T. N., Nguyen, H. L., Le, P. H. P., & Hoang, T. S. (2020). Adsorptive removal of antibiotic ciprofloxacin from aqueous solution using protein-modified nanosilica. *Polymers*, 12(1). <https://doi.org/10.3390/polym12010057>
- Pholosi, A., Ofomaja, A. E., & Naidoo, E. B. (2013). Effect of chemical extractants on the biosorptive properties of pine cone powder: Influence on lead(II) removal mechanism. *Journal of Saudi Chemical Society*, 17(1), 77–86. <https://doi.org/10.1016/j.jscs.2011.10.017>
- Pode, R. (2016). Potential applications of rice husk ash waste from rice husk biomass power plant. *Renewable and Sustainable Energy Reviews*, 53, 1468–1485. <https://doi.org/10.1016/j.rser.2015.09.051>
- Pompei, C. M. E., Ciric, L., Canales, M., Karu, K., Vieira, E. M., & Campos, L. C. (2017). Influence of PPCPs on the performance of intermittently operated slow sand filters for household water purification. *Science of the Total Environment*, 1–12. <https://doi.org/10.1016/j.scitotenv.2016.12.091>
- Porra, R. J. (2002). The chequered history of the development and use of simultaneous equations for the accurate determination of chlorophylls a and b. *Photosynthesis Research*, 149–156.
- Portinho, R., Zanella, O., & Fêris, L. A. (2017). Grape stalk application for caffeine removal through adsorption. *Journal of Environmental Management*, 202, 178–187. <https://doi.org/10.1016/j.jenvman.2017.05.038>
- Praveena, S. M., Cheema, M. S., & Guo, H.-R. (2019). Non-nutritive artificial sweeteners as an emerging contaminant in environment: A global review and risks perspectives. *Ecotoxicology and Environmental Safety*, 170(December 2018), 699–707. <https://doi.org/10.1016/j.ecoenv.2018.12.048>
- Pukcothanung, Y., Siritanon, T., & Rangriwatananon, K. (2018). The efficiency of zeolite Y and surfactant-modified zeolite Y for removal of 2,4-dichlorophenoxyacetic acid and 1,1'-dimethyl-4,4'-bipyridinium ion. *Microporous and Mesoporous Materials*, 258, 131–140. <https://doi.org/10.1016/j.micromeso.2017.08.015>
- Qin, X., Liu, F., Wang, G., Weng, L., & Li, L. (2014). Adsorption of levofloxacin onto goethite: Effects of pH, calcium and phosphate. *Colloids and Surfaces B: Biointerfaces*, 116, 591–596. <https://doi.org/10.1016/j.colsurfb.2013.09.056>
- Quadra, G. R., Paranaíba, J. R., Vilas-Boas, J., Roland, F., Amado, A. M., Barros, N., Dias, R. J. P., & Cardoso, S. J. (2019). A global trend of caffeine consumption over time and related environmental impacts. *Environmental Pollution*, 256, 113343. <https://doi.org/10.1016/j.envpol.2019.113343>
- Quesada, H. B., Alves Baptista, A. T., Cusioli, L. F., Seibert, D., de Oliveira Bezerra, C., & Bergamasco, R. (2019). Surface water pollution by pharmaceuticals and an alternative for Removal by low-cost adsorbents: a review. *Chemosphere*. <https://doi.org/10.1016/j.chemosphere.2019.02.009>
- Rajendran, K., & Sen, S. (2018). Adsorptive removal of carbamazepine using biosynthesized hematite nanoparticles. *Environmental Nanotechnology, Monitoring and Management*. <https://doi.org/10.1016/j.enmm.2018.01.001>
- Rajput, S., Pittman, C. U., & Mohan, D. (2015). Magnetic magnetite (Fe₃O₄) nanoparticle synthesis and applications for lead (Pb²⁺) and chromium (Cr⁶⁺) removal from water. *Journal of Colloid and Interface Science*, 468, 334–346. <https://doi.org/10.1016/j.jcis.2015.12.008>
- Rakshit, S., Sarkar, D., Punamiya, A., & Datta, R. (2013). Kinetics of oxytetracycline sorption on magnetite nanoparticles. *International Journal of Environmental Science and Technology*, 11(5), 1207–1214. <https://doi.org/10.1007/s13762-013-0317-x>
- Ramírez-López, E., Corona-Hernández, J., Dendooven, L., Rangel, P., & Thalasso, F. (2003). Characterization of five agricultural by-products as potential biofilter carriers. *Bioresource Technology*, 88, 259–263. [https://doi.org/10.1016/S0960-8524\(02\)00316-2](https://doi.org/10.1016/S0960-8524(02)00316-2)
- Ramírez, J., & Enriquez, M. (2015). Remoción de plomo (II) usando lignina obtenida a partir del procesamiento del seudotallo de plátano. *Acta Agronomica*, 64(3), 209–213. <https://doi.org/10.15446/acag.v64n3.43488>
- Ramnarain, Y., Ansari, A. A., & Ori, L. (2019). Vermicomposting of different organic materials using the epigeic earthworm *Eisenia foetida*. *International Journal of Recycling of Organic Waste in Agriculture*, 8(1), 23–36. <https://doi.org/10.1007/s40093-018-0225-7>
- Rangabhashyam, S., & Balasubramanian, P. (2019). Industrial Crops & Products The potential of lignocellulosic biomass precursors for biochar production: Performance, mechanism and wastewater application — A review. *Industrial Crops & Products*, 128(November 2018), 405–423. <https://doi.org/10.1016/j.indcrop.2018.11.041>
- Rasamimanana, S., Mignard, S., & Batonneau-Gener, I. (2016). Hierarchical zeolites as adsorbents for mesosulfuron-methyl removal in aqueous phase. *Microporous and Mesoporous Materials*, 226, 153–161. <https://doi.org/10.1016/j.micromeso.2015.12.014>
- Reeve, P. J., & Fallow, H. J. (2018). Natural and surfactant modified zeolites: A review of their applications for water remediation with a focus on surfactant desorption and toxicity towards microorganisms. *Journal of Environmental Management*, 205. <https://doi.org/10.1016/j.jenvman.2017.09.077>
- Reguyal, F., & Sarmah, A. K. (2018). Site energy distribution analysis and influence of Fe₃O₄ nanoparticles on sulfamethoxazole sorption in aqueous solution by magnetic pine sawdust biochar. *Environmental Pollution*, 233, 510–519. <https://doi.org/10.1016/j.envpol.2017.09.076>
- Remucal, C. K., & Ginder-Vogel, M. (2014). A critical review of the reactivity of manganese oxides with organic contaminants. *Environmental Sciences: Processes and Impacts*, 16(6), 1247–1266. <https://doi.org/10.1039/c3em00703k>
- Rigueto, C. V. T., Nazari, M. T., De Souza, C. F., Cadore, J. S., Brião, V. B., & Piccin, J. S. (2020). Alternative techniques for caffeine removal from wastewater: An overview of opportunities and challenges. *Journal of Water Process Engineering*, 35(March). <https://doi.org/10.1016/j.jwpe.2020.101231>
- Rodríguez-Gil, J. L., Cáceres, N., Dafouz, R., & Valcárcel, Y. (2018). Caffeine and paraxanthine in aquatic systems: Global

- exposure distributions and probabilistic risk assessment. *Science of the Total Environment*. <https://doi.org/10.1016/j.scitotenv.2017.08.066>
- Rodríguez-Narvaez, O. M., Peralta-hernandez, J. M., Goonetilleke, A., & Bandala, E. R. (2017). Treatment technologies for emerging contaminants in water: A review. *Chemical Engineering Journal*, 323, 361–380. <https://doi.org/10.1016/j.cej.2017.04.106>
- Román, S., Ledesma, B., Álvarez, A., & Herdes, C. (2018). Towards sustainable micro-pollutants' removal from wastewaters: caffeine solubility, self-diffusion and adsorption studies from aqueous solutions into hydrochars. *Molecular Physics*, 116(15–16), 2129–2141. <https://doi.org/10.1080/00268976.2018.1487597>
- Romeo-Arroyo, E., Mora, M., & Vázquez-Araújo, L. (2020). Consumer behavior in confinement times: Food choice and cooking attitudes in Spain. *International Journal of Gastronomy and Food Science*, 21(June). <https://doi.org/10.1016/j.ijgfs.2020.100226>
- Romero, C., Ocampo, J., Sandoval, E., & Tobar, J. (2018). Substrates evaluation for the production of earthworm (*Eisenia foetida*). *Centro Agrícola*, 45(4), 68–74.
- Rout, J., Tripathy, S. S., Misra, S. K. N. M., & Mohanty, A. K. (2001). Scanning Electron Microscopy Study of Chemically Modified Coir Fibers. *Journal of Applied Polymer Science*.
- Rout, P. R., Zhang, T. C., Bhunia, P., & Surampalli, R. Y. (2021). Treatment technologies for emerging contaminants in wastewater treatment plants: A review. *Science of the Total Environment*, 753, 141990. <https://doi.org/10.1016/j.scitotenv.2020.141990>
- Rwiza, M. J., Oh, S. Y., Kim, K. W., & Kim, S. D. (2018). Comparative sorption isotherms and removal studies for Pb(II) by physical and thermochemical modification of low-cost agro-wastes from Tanzania. *Chemosphere*. <https://doi.org/10.1016/j.chemosphere.2017.12.043>
- S.D. Al-Ahmari, Watson, K., Fong, B. N., Ruyonga, R. M., & Ali, H. (2018). Adsorption Kinetics of 4-n-Nonylphenol on Hematite and Goethite. *Environmental Chemical Engineering*. <https://doi.org/10.1016/j.jece.2018.05.052>
- Sabogal-Paz, L. P., Cintra, L., Bogush, A., & Canales, M. (2020). Household slow sand filters in intermittent and continuous flows to treat water containing low mineral ion concentrations and Bisphenol A. *Science of the Total Environment*, 702, 135078. <https://doi.org/10.1016/j.scitotenv.2019.135078>
- Saha, B. C. (2003). Hemicellulose bioconversion. *Journal of Industrial Microbiology and Biotechnology*, 30(5), 279–291. <https://doi.org/10.1007/s10295-003-0049-x>
- Sahoo, T. R., & Prelot, B. (2020). Adsorption processes for the removal of contaminants from wastewater: the perspective role of nanomaterials and nanotechnology. In *Nanomaterials for the Detection and Removal of Wastewater Pollutants*. Elsevier Inc. <https://doi.org/10.1016/B978-0-12-818489-9.00007-4>
- Saleem, H., Arslan, M., Rehman, K., Tahseen, R., & Afzal, M. (2018). *Phragmites australis* — a helophytic grass — can establish successful partnership with phenol-degrading bacteria in a floating treatment wetland. *Saudi Journal of Biological Sciences*. <https://doi.org/10.1016/j.sjbs.2018.01.014>
- Samal, K., Dash, R. R., & Bhunia, P. (2017a). Performance assessment of a *Crotalaria indica* assisted vermifilter for synthetic dairy wastewater treatment. *Process Safety and Environmental Protection*. <https://doi.org/10.1016/j.psep.2017.07.027>
- Samal, K., Dash, R. R., & Bhunia, P. (2017b). Treatment of wastewater by vermifiltration integrated with macrophyte filter: A review. *Journal of Environmental Chemical Engineering*. <https://doi.org/10.1016/j.jece.2017.04.026>
- Sanchez-Hernandez, J. C., Sáez, J. A., Vico, A., Moreno, J., & Moral, R. (2020). Evaluating Earthworms' Potential for Remediating Soils Contaminated with Olive Mill Waste Sediments. *Applied Sciences*. <https://doi.org/https://doi.org/10.3390/app10072624>
- Sandoval, R., Cooper, A. M., Aymar, K., Jain, A., & Hristova, K. (2011). Removal of arsenic and methylene blue from water by granular activated carbon media impregnated with titanium dioxide nanoparticles. *Journal of Hazardous Materials*, 193, 296–303. <https://doi.org/10.1016/j.jhazmat.2010.09.061>
- Santaufemia, S., Abalde, J., & Torres, E. (2019). Eco-friendly rapid removal of triclosan from seawater using biomass of a microalgal species: Kinetic and equilibrium studies. *Journal of Hazardous Materials*, 369, 674–683. <https://doi.org/10.1016/j.jhazmat.2019.02.083>
- Sauvé, S., & Desrosiers, M. (2014). A review of what is an emerging contaminant. *Chemistry Central Journal*, 1–7.
- Sawe. (2018). *Where Are Peanuts Grown?* - WorldAtlas. <https://www.worldatlas.com/articles/top-peanut-groundnut-producing-countries.html>
- Schuldt, M., Rumi, A., & Gregoric, B. G. (2005). Determinación de “edades” (clases) en poblaciones de *Eisenia fetida* (Annelida: Lumbricidae) y sus implicancias reprobilógicas. *Miguel Schuldt Alejandra Rumi Diego E. Gutiérrez Gregoric*, 1–10.
- Sgroi, M., Pelissari, C., Roccaro, P., Sezerino, P. H., García, J., Vagliasindi, F. G. A., & Ávila, C. (2018). Removal of organic carbon, nitrogen, emerging contaminants and fluorescing organic matter in different constructed wetland configurations. *Chemical Engineering Journal*, 332, 619–627. <https://doi.org/10.1016/j.cej.2017.09.122>
- Shamsollahi, Z., & Nurgovinia, A. (2019). Recent advances on pollutants removal by rice husk as a bio-based adsorbent: A critical review. *Journal of Environmental Management*, 246(February), 314–323. <https://doi.org/10.1016/j.jenvman.2019.05.145>
- Sharif, A., Khanrasani, M., & Shemirani, F. (2018). Nanocomposite Bead (NCB) Based on Bio-polymer Alginate Caged Magnetic Graphene Oxide Synthesized for Adsorption and Preconcentration of Lead (II) and Copper (II) Ions from Urine, Saliva and Water Samples. *Journal of Inorganic and Organometallic Polymers and Materials*, 0(0), 0. <https://doi.org/10.1007/s10904-018-0900-1>
- Sharipova, A. A., Aidarova, S. B., Bekturganova, N. E., Tleuova, A., Schenderlein, M., Lygina, O., Lyubchik, S., & Miller, R. (2016). Triclosan as model system for the adsorption on recycled adsorbent materials. *Colloids and Surfaces A: Physicochemical and Engineering Aspects*, 505, 193–196. <https://doi.org/10.1016/j.colsurfa.2016.04.049>
- Sharma, K., & Garg, V. K. (2019). Recycling of lignocellulosic waste as vermicompost using earthworm *Eisenia fetida*. *Environmental Science and Pollution Research*.
- Sharma, S., Nandal, P., & Arora, A. (2018). Ethanol Production from NaOH Pretreated Rice Straw: a Cost Effective Option to Manage Rice Crop Residue. *Waste and Biomass Valorization*, 0(0), 0. <https://doi.org/10.1007/s12649-018-0360-4>
- Shebanova, O. N., & Lazor, P. (2003). Raman spectroscopic study of magnetite (FeFe₂O₄): A new assignment for the vibrational spectrum. *Journal of Solid State Chemistry*, 174(2), 424–430. [https://doi.org/10.1016/S0022-4596\(03\)00294-9](https://doi.org/10.1016/S0022-4596(03)00294-9)
- Shen, Z., Zhang, Y., McMillan, O., jin, F., & Al-Tabbaa, A. (2017). Characteristics and mechanisms of nickel adsorption on biochars produced from wheat straw pellets and rice husk. *Environmental Science and Pollution Research*. <https://doi.org/10.1007/s11356-017-8847-2>
- Shirvanimoghaddam, K., & Trojanowska, E. (2020). Sorption of pharmaceuticals and personal care products (PPCPs) onto a sustainable cotton based adsorbent. 18(July). <https://doi.org/10.1016/j.sep.2020.100324>
- Shoiful, A., Ueda, Y., Nugroho, R., & Honda, K. (2016). Degradation of organochlorine pesticides (OCPs) in water by iron (Fe)-based materials. *Journal of Water Process Engineering*, 11, 110–117. <https://doi.org/10.1016/j.jwpe.2016.02.011>

- Shokouhi, R., Ghobadi, N., Godini, K., Hadi, M., & Atashzaban, Z. (2019). Antibiotic detection in a hospital wastewater and comparison of their removal rate by activated sludge and earthworm-based vermifiltration: Environmental risk assessment. *Process Safety and Environmental Protection*, 134, 169–177. <https://doi.org/10.1016/j.psep.2019.10.020>
- Shrestha, P., Zhang, Y., Chen, W., & Wong, T. (2020). Triclosan: antimicrobial mechanisms, antibiotics interactions, clinical applications, and human health. *Journal of Environmental Science and Health, Part C*, 38(3), 245–268. <https://doi.org/10.1080/26896583.2020.1809286>
- Shukla, A., Zhang, Y. H., Dubey, P., Margrave, J. L., & Shukla, S. S. (2002). The role of sawdust in the removal of unwanted materials from water. *Journal of Hazardous Materials*, 95(1–2), 137–152. [https://doi.org/10.1016/S0304-3894\(02\)00089-4](https://doi.org/10.1016/S0304-3894(02)00089-4)
- Silva, C. P., Jaria, G., Otero, M., Esteves, V. I., & Calisto, V. (2017). Waste-based alternative adsorbents for the remediation of pharmaceutical contaminated waters: has a step forward already been taken? *Bioresource Technology*. <https://doi.org/10.1016/j.biortech.2017.11.102>
- Singh, M., Pawar, M., Bothra, A., & Choudhary, N. (2020). Overzealous hand hygiene during the COVID 19 pandemic causing an increased incidence of hand eczema among general population. *Journal of the American Academy of Dermatology*, 83(1), e37–e41. <https://doi.org/10.1016/j.jaad.2020.04.047>
- Singh, N. B., Nagpal, G., & Agrawal, S. (2018). Water purification by using Adsorbents : A Review. *Environmental Technology & Innovation*. <https://doi.org/10.1016/j.eti.2018.05.006>
- Singh, R., Bhunia, P., & Dash, R. R. (2017). A mechanistic review on vermifiltration of wastewater: Design, operation and performance. *Journal of Environmental Management*, 197, 656–672. <https://doi.org/10.1016/j.jenvman.2017.04.042>
- Singh, R., Samal, K., Dash, R. R., & Bhunia, P. (2019). Vermifiltration as a sustainable natural treatment technology for the treatment and reuse of wastewater: A review. *Journal of Environmental Management*, 247(June), 140–151. <https://doi.org/10.1016/j.jenvman.2019.06.075>
- Sivarajasekar, N., Mohanraj, N., Baskar, R., & Sivamani, S. (2018). Fixed-Bed Adsorption of Ranitidine Hydrochloride Onto Microwave Assisted—Activated Aegle marmelos Correa Fruit Shell: Statistical Optimization and Breakthrough Modelling. *Arabian Journal for Science and Engineering*, 43(5), 2205–2215. <https://doi.org/10.1007/s13369-016-2295-4>
- Sivaselvam, S., Premasudha, P., Viswanathan, C., & Ponpandian, N. (2020). Enhanced removal of emerging pharmaceutical contaminant ciprofloxacin and pathogen inactivation using morphologically tuned MgO nanostructures. In *Journal of Environmental Chemical Engineering* (Vol. 8, Issue 5). Elsevier B.V. <https://doi.org/10.1016/j.jece.2020.104256>
- Slavov, L., Abrashev, M. V., Merodiiska, T., Gelev, C., Vandenberghe, R. E., & Markova-Geneva, I. (2010). Raman spectroscopy investigation of magnetite nanoparticles in ferrofluids. *Journal of Magnetism and Magnetic Materials*, 322(14), 1904–1911. <https://doi.org/10.1016/j.jmmm.2010.01.005>
- Sophia A., C., & Lima, E. C. (2018). Removal of emerging contaminants from the environment by adsorption. *Ecotoxicology and Environmental Safety*, 150(December 2017), 1–17. <https://doi.org/10.1016/j.ecoenv.2017.12.026>
- Sotelo, J. L., Rodríguez, A., Álvarez, S., & García, J. (2012). Removal of caffeine and diclofenac on activated carbon in fixed bed column. *Chemical Engineering Research and Design*, 90(7), 967–974. <https://doi.org/10.1016/j.cherd.2011.10.012>
- Sotelo, José Luis, Ovejero, G., Rodríguez, A., Álvarez, S., Galán, J., & Gamfa, C. (2014). Competitive adsorption studies of caffeine and diclofenac aqueous solutions by activated carbon. *Chemical Engineering Journal*, 240, 443–453. <https://doi.org/10.1016/j.cej.2013.11.094>
- Sreejon Das, Nillohit Mitra Ray, J. W., Adnan Khan, T. C. and, R. J., M. B. (2017). Micropollutants in Wastewater: Fate and Removal Processes. In *Intech open* (Vol. 2, p. 64). <https://doi.org/10.5772/32009>
- Srinivasan, R. (2011). Advances in application of natural clay and its composites in removal of biological, organic, and inorganic contaminants from drinking water. *Advances in Materials Science and Engineering*, 2011. <https://doi.org/10.1155/2011/872531>
- Stavrinou, A., Aggelopoulos, C. A., & Tsakiroglou, C. D. (2018). Exploring the adsorption mechanisms of cationic and anionic dyes onto agricultural waste peels of banana, cucumber and potato: Adsorption Kinetics and Equilibrium Isotherms as a Tool. *Environmental Chemical Engineering*. <https://doi.org/10.1016/j.jece.2018.10.063>
- Stuart, M., & Lapworth, D. (2013). Emerging Organic Contaminants in Groundwater. In S. Mukhopadhyay & A. Mason (Eds.), *Smart Sensors, Measurement and Instrumentation* (pp. 259–284). Springer Berlin Heidelberg. https://doi.org/10.1007/978-3-642-37006-9_12
- Sulaiman, M. A., & Adetifa, B. O. (2019). Experimental Characterization of Maize Cob and Stalk Based Pellets for Energy Use. *Engineering Journal*, 23(6), 117–128. <https://doi.org/10.4186/ej.2019.23.6.117>
- Sultan, M., Miyazaki, T., & Koyama, S. (2018). Optimization of adsorption isotherm types for desiccant air-conditioning applications. *Renewable Energy*, 121, 441–450. <https://doi.org/10.1016/j.renene.2018.01.045>
- Sun, K., Shi, Y., Wang, X., & Li, Z. (2017). Sorption and retention of diclofenac on zeolite in the presence of cationic surfactant. *Journal of Hazardous Materials*, 323, 584–592. <https://doi.org/10.1016/j.jhazmat.2016.08.026>
- Suthar, S. (2010). Recycling of agro-industrial sludge through vermifiltration. *Ecological Engineering*, 36(8), 1028–1036. <https://doi.org/10.1016/j.ecoleng.2010.04.015>
- Taha, M. R., & Mobasser, S. (2015). Adsorption of DDT and PCB by nanomaterials from residual soil. *PLoS ONE*, 10(12), 1–16. <https://doi.org/10.1371/journal.pone.0144071>
- Tajir, A. A., & Hamid, F. S. (2012). Vermicomposting of two types of coconut wastes employing *Eudrilus eugeniae*: a comparative study. *International Journal of Recycling of Organic Waste in Agriculture*, 1–6. <https://doi.org/10.1186/2251-7715-1-7>
- Tanyildizi, M. S. (2011). Modeling of adsorption isotherms and kinetics of reactive dye from aqueous solution by peanut hull. *Chemical Engineering Journal*, 168(3), 1234–1240. <https://doi.org/10.1016/j.cej.2011.02.021>
- Tarasi, R., Alipour, M., Gorgannezhad, L., Imanparast, S., Yousefi-Ahmadipour, A., Ramezani, A., Ganjali, M. R., Shafiee, A., Faramarzi, M. A., & Khoobi, M. (2018). Laccase Immobilization onto Magnetic β -Cyclodextrin-Modified Chitosan: Improved Enzyme Stability and Efficient Performance for Phenolic Compounds Elimination. *Macromolecular Research*, 26(8), 755–762. <https://doi.org/10.1007/s13233-018-6095-z>
- Taşar, Ş., Kaya, F., & Özer, A. (2014). Biosorption of lead(II) ions from aqueous solution by peanut shells: Equilibrium, thermodynamic and kinetic studies. *Journal of Environmental Chemical Engineering*, 2, 1018–1026. <https://doi.org/10.1016/j.jece.2014.03.015>
- Tejedor, J., Cónor, V., Almeida-Naranjo, C. E., Guerrero, V. H., & Villamar, C. A. (2020). Performance of wood chips/peanut shells biofilters used to remove organic matter from domestic wastewater. *Science of the Total Environment*, 738, 139589. <https://doi.org/10.1016/j.scitotenv.2020.139589>
- Tejedor, Jennifer, Guerrero, V. H., Vizuete, K., & Debut, A. (2022). Environmentally friendly synthesis of silicon dioxide nanoparticles and their application for the removal of emerging contaminants in aqueous media. *Journal of Physics: Conference Series*. <https://doi.org/10.1088/1742-6596/2238/1/012005>

- Thiebault, T. (2019). Raw and modified clays and clay minerals for the removal of pharmaceutical products from aqueous solutions: State of the art and future perspectives. *Critical Reviews in Environmental Science and Technology*, 50(14), 1451–1514. <https://doi.org/10.1080/10643389.2019.1663065>
- Thiebault, T., Guégan, R., & Boussafir, M. (2015). Adsorption mechanisms of emerging micro-pollutants with a clay mineral : Case of tramadol and doxepine pharmaceutical products. *Journal of Colloid and Interface Science*, 453, 1–8. <https://doi.org/10.1016/j.jcis.2015.04.029>
- Thompson, K. A., Shimabuku, K. K., Kearns, J. P., Knappe, D. R. U., Summers, R. S., Cook, S. M., & Cook, S. M. (2016). Environmental Comparison of Biochar and Activated Carbon for Tertiary Wastewater Treatment Table of Content Art. *Environmental Science and Technology*.
- Thuptimdang, P., Siripattanakul-Ratpukdi, S. T. R., Youngwilai, A., & Khan, E. (2020). Biofiltration for Treatment of Recent Emerging Contaminants in Water: Current and Future Perspectives. *Water Environment Research*, 0–2. <https://doi.org/10.1002/wer.1493>
- Tomul, F., Arslan, Y., Kabak, B., Tran, H. N., & Chi, H. (2020). Adsorption process of naproxen onto peanut shells-derived biosorbent: Important role of n- π interaction and van der Waals force. *Journal of Chemical Technology & Biotechnology*, 0–1. <https://doi.org/10.1002/jctb.6613>
- Tonicioli Rigueto, V. C., Torres, M., Favretto, C., Stefanello, J., Barbosa, V., & Steffanelo, J. (2020). Alternative techniques for caffeine removal from wastewater : An overview of opportunities and challenges. *Journal of Water Process Engineering*, 35(February). <https://doi.org/10.1016/j.jwpe.2020.101231>
- Torrellas, S. Á., García Lovera, R., Escalona, N., Sepúlveda, C., Sotelo, J. L., & García, J. (2015). Chemical-activated carbon from peach stones for the adsorption of emerging contaminants in aqueous solutions. *Chemical Engineering Journal*, 279, 788–798. <https://doi.org/10.1016/j.cej.2015.05.104>
- Tosuner, Z. V., Taylan, G. G., & Özmişçi, S. (2019). Effects of rice husk particle size on biohydrogen production under solid state fermentation. *International Journal of Hydrogen Energy*, 44(34), 18785–18791. <https://doi.org/10.1016/j.ijhydene.2018.10.230>
- Tran, H. N., Nguyen, H. C., Woo, S. H., Nguyen, T. V., Vigneswaran, S., Hosseini-Bandegharai, A., Firdaube, J., Kumar Sarmah, A., Ivanets, A., Dotto, G. L., Bui, T. T., Juang, R. S., & Chao, H. P. (2019). Removal of various contaminants from water by renewable lignocellulose-derived biosorbents: a comprehensive and critical review. *Critical Reviews in Environmental Science and Technology*, 49(23), 2155–2219. <https://doi.org/10.1080/10643389.2019.1607444>
- Tran, H. N., You, S., Hosseini-bandegharai, A., & Chao, H. (2017). Mistakes and inconsistencies regarding adsorption of contaminants from aqueous solutions: A critical review. *Water Research*. <https://doi.org/10.1016/j.watres.2017.04.014>
- Tran, H., Reinhard, M., & Gin, K. Y. (2018). Occurrence and fate of emerging contaminants in municipal wastewater treatment plants from different geographical regions-a review. *Water Research*, 133, 182–207. <https://doi.org/10.1016/j.watres.2017.12.029>
- Tran, T. H. (2018). Adsorption and transformation of the anthelmintic drug ivermectin by manganese oxide. *Chemosphere*, 201, 425–431. <https://doi.org/10.1016/j.chemosphere.2018.03.021>
- Triwiswara, M., Kang, J. K., Moon, J. K., Lee, C. G., & Park, S. J. (2020). Removal of triclosan from aqueous solution using thermally treated rice husks. *Desalination and Water Treatment*, 202(November), 317–326. <https://doi.org/10.5004/dwt.2020.26161>
- Triwiswara, M., Lee, C. G., Moon, J. K., & Park, S. J. (2020). Adsorption of triclosan from aqueous solution onto char derived from palm kernel shell. *Desalination and Water Treatment*, 202(November), 71–79. <https://doi.org/10.5004/dwt.2020.24872>
- Turku, I., Sainio, T., & Paatero, E. (2007). Thermodynamic of tetracycline adsorption on silica. *Environmental Chemistry Letters*, 4, 225–228. <https://doi.org/10.1007/s10311-007-0106-6>
- Varsha, M., Kumar, P. S., & Rathi, B. S. (2022). A review on recent trends in the removal of emerging contaminants from aquatic environment using low-cost adsorbents. *Chemosphere*, 287(P3), 132270. <https://doi.org/10.1016/j.chemosphere.2021.132270>
- Vera, I., Jorquera, C., López, D., & Vidal, G. (2016). Humedales construidos para tratamiento y reúso de aguas servidas en Chile: Reflexiones. *Tecnología y Ciencias Del Agua*, 7(3), 19–35.
- Verma, S., Daverey, A., & Sharma, A. (2017). Slow sand filtration for water and wastewater treatment – a review. *Environmental Technology Reviews*, 25(1)(January), 1–10. <https://doi.org/10.1080/21622515.2016.1278278>
- Vieira, L. R., Soares, A. M. V. V., & Freitas, R. (2022). Caffeine as a contaminant of concern: A review on concentrations and impacts in marine coastal systems. *Chemosphere*, 286(P2), 131675. <https://doi.org/10.1016/j.chemosphere.2021.131675>
- Villamar-Ayala, C. A., Carrera-Cevallos, J. V., Espinoza-Montero, P. J., Alejandra, C., & Carrera-Cevallos, J. V. (2019). Technology Hurdles, ecotoxicological characteristics, and treatment processes applied to water polluted with glyphosate : A critical review. *Critical Reviews in Environmental Science and Technology*, 0(0), 1–39. <https://doi.org/10.1080/10643389.2019.1579627>
- Villamar, C. A., Vera, D., Neubauer, M. E., & Vidal, G. (2015). Nitrogen and phosphorus distribution in a constructed wetland fed with treated swine slurry from an anaerobic lagoon. *Journal of Environmental Science and Health - Part A Toxic/Hazardous Substances and Environmental Engineering*, 50(1), 60–71. <https://doi.org/10.1080/10934529.2015.964628>
- Villamar, C. A., Vera-Puerto, I., Rivera, D., & De la Hoz, F. D. (2018). Reuse and recycling of livestock and municipal wastewater in Chilean agriculture: A preliminary assessment. *Water (Switzerland)*, 10(6), 1–22. <https://doi.org/10.3390/w10060817>
- Wang, Baoxia, & Li, D. (2015). Strong and optically transparent biocomposites reinforced with cellulose nanofibers isolated from peanut shell. *COMPOSITES PART A*. <https://doi.org/10.1016/j.compositesa.2015.08.029>
- Wang, Bing, Wan, Y., Zheng, Y., Lee, X., Liu, T., Yu, Z., Huang, J., Ok, Y. S., Chen, J., Gao, B., Wang, B., Wan, Y., Zheng, Y., Lee, X., & Liu, T. (2018). Alginate-based composites for environmental applications : a critical review. *Critical Reviews in Environmental Science and Technology*, 0(0), 1–39. <https://doi.org/10.1080/10643389.2018.1547621>
- Wang, D., Zhang, Z., Li, X., Zheng, W., Ding, Y., Yang, B., Yang, Q., Zeng, T., Cao, J., & Yue, X. (2010). Effects of earthworms on surface clogging characteristics of intermittent sand filters. *Water Science and Technology*, 2881–2889. <https://doi.org/10.2166/wst.2010.180>
- Wang, F., Lu, X., Peng, W., Deng, Y., Zhang, T., Hu, Y., & Li, X. (2017). Sorption Behavior of Bisphenol A and Triclosan by Graphene: Comparison with Activated Carbon. *ACS Omega*. <https://doi.org/10.1021/acsomega.7b00616>
- Wang, F., Yang, B., Wang, H., Song, Q., Tan, F., & Cao, Y. (2016). Removal of ciprofloxacin from aqueous solution by a magnetic chitosan grafted graphene oxide composite. *Journal of Molecular Liquids*. <https://doi.org/10.1016/j.molliq.2016.07.037>
- Wang, H., Zhang, S., Wang, J., Song, Q., Zhang, W., He, Q., Song, J., & Ma, F. (2018). Comparison of performance and microbial communities in a bioelectrochemical system for simultaneous denitrification and chromium removal: Effects of pH. *Process Biochemistry*, 73(April), 154–161. <https://doi.org/10.1016/j.procbio.2018.08.007>
- Wang, Jianlong, & Guo, X. (2020). Adsorption kinetic models: Physical meanings, applications, and solving methods. *Journal of*

- Hazardous Materials*, 390(January), 122156. <https://doi.org/10.1016/j.jhazmat.2020.122156>
- Wang, Jianlong, & Wang, S. (2016). Removal of pharmaceuticals and personal care products (PPCPs) from wastewater: A review. *Journal of Environmental Management*, 182, 620–640. <https://doi.org/10.1016/j.jenvman.2016.07.049>
- Wang, Jianlong, & Wang, S. (2018). Activation of persulfate (PS) and peroxymonosulfate (PMS) and application for the degradation of emerging contaminants. *Chemical Engineering Journal*, 334, 1502–1517. <https://doi.org/10.1016/j.cej.2017.11.059>
- Wang, Jianlong, Zhuang, S., & Wang, J. (2018). Removal of various pollutants from water and wastewater by modified chitosan adsorbents. *Critical Reviews in Environmental Science and Technology*, 3389. <https://doi.org/10.1080/10643389.2017.1421845>
- Wang, Jinsong, Ridder, D. De, Wal, A. Van Der, Sutton, N. B., Wang, J., Ridder, D. De, Wal, A. Van Der, & Sutton, N. B. (2021). Technology Harnessing biodegradation potential of rapid sand filtration for organic micropollutant removal from drinking water: A review. *Critical Reviews in Environmental Science and Technology*, 51(18), 2086–2118. <https://doi.org/10.1080/10643389.2020.1771888>
- Wang, Jinzhi, Hu, Z., Xu, X., Jiang, X., Zheng, B., Liu, X., Pan, X., & Kardol, P. (2014). Emissions of ammonia and greenhouse gases during combined pre-composting and vermicomposting of duck manure. *Waste Management*. <https://doi.org/10.1016/j.wasman.2014.04.010>
- Wang, Q., Wei, W., Gong, Y., Yu, Q., Li, Q., Sun, J., & Yuan, Z. (2017). Technologies for reducing sludge production in wastewater treatment plants: State of the art. *Science of the Total Environment*. <https://doi.org/10.1016/j.scitotenv.2017.02.203>
- Wang, S., Nam, H., & Nam, H. (2020). Preparation of activated carbon from peanut shell with KOH activation and its application for H₂S adsorption in confined space. *Journal of Environmental Chemical Engineering*, 8(1), 103683. <https://doi.org/10.1016/j.jece.2020.103683>
- Wang, X., Yin, R., Zeng, L., & Zhu, M. (2019). A review of graphene-based nanomaterials for removal of antibiotics from aqueous environments. *Environmental Pollution*. <https://doi.org/10.1016/j.envpol.2019.06.067>
- Wang, Y., Chang, W., Wang, L., Zhang, Y., Zhang, Y., Wang, M., Wang, Y., & Li, P. (2019). A review on sources, multimedia distribution and health risks of novel fluorinated alternatives. *Ecotoxicology and Environmental Safety*, 182(May), 109402. <https://doi.org/10.1016/j.ecoenv.2019.109402>
- Wanitwattanarumlug, B., Luengnaruemitchai, A., & Wongkasemjit, S. (2012). Characterization of Corn Cobs from Microwave and Potassium Hydroxide Pretreatment. *International Journal of Chemical and Biological Engineering*, 6(January), 2–7.
- Wanjeri, V. W. O., Sheppard, C. J., Prinsloo, A. R. E., Ngila, J. C., & Ndungu, P. G. (2018). Isotherm and kinetic investigations on the adsorption of organophosphorus pesticides on graphene oxide based silica coated magnetic nanoparticles functionalized with 2-phenylethylamine. *Journal of Environmental Chemical Engineering*. <https://doi.org/10.1016/j.jece.2018.01.064>
- Wei, Q., Li, X., Zhang, J., Hu, B., Zhu, W., Liang, W., & Sun, K. (2019). Full-size pore structure characterization of deep-buried coals and its impact on methane adsorption capacity: A case study of the Shihzezi Formation coals from the Panji Deep Area in Huainan Coalfield, Southern North China. *Journal of Petroleum Science and Engineering*, 173. <https://doi.org/10.1016/j.petrol.2018.10.100>
- Wilkinson, J., Hooda, P. S., Barker, J., Barton, S., & Swinden, J. (2017). Occurrence, fate and transformation of emerging contaminants in water: An overarching review of the field. *Environmental Pollution*, 231, 954–970. <https://doi.org/10.1016/j.envpol.2017.08.032>
- Wilkinson, J. L., Hooda, P. S., Swinden, J., Barker, J., & Barton, S. (2018). Spatial (bio) accumulation of pharmaceuticals, illicit drugs, plasticisers, perfluorinated compounds and metabolites in river sediment, aquatic plants and benthic organisms*. *Environmental Pollution*, 234, 864–875. <https://doi.org/10.1016/j.envpol.2017.11.090>
- Wong, K. T., Yoon, Y., Snyder, S. A., & Jang, M. (2010). Phenyl-functionalized magnetic palm-based powdered activated carbon for the effective removal of selected pharmaceutical and endocrine-disruptive compounds. *Chemosphere*, 152, 71–80. <https://doi.org/10.1016/j.chemosphere.2010.02.090>
- Xu, D., Li, Y., Howard, A., & Guan, Y. (2013). Chemo sphere Effect of earthworm *Eisenia fetida* and wetland plants on nitrification and denitrification potentials in vertical flow constructed wetland. *Chemosphere*, 92(2), 201–206. <https://doi.org/10.1016/j.chemosphere.2013.03.016>
- Yang, Q., Wu, P., Liu, J., Rehman, S., Ahmed, Z., & Ruan, B. (2019). Batch interaction of emerging tetracycline contaminant with novel phosphoric acid activated corn straw porous carbon: Adsorption rate and nature of mechanism. *Environmental Research*, September, 108899. <https://doi.org/10.1016/j.envres.2019.108899>
- Yang, Y., Ok, Y. S., Kim, K. H., Kwon, E. E., & Tsang, Y. F. (2017). Occurrences and removal of pharmaceuticals and personal care products (PPCPs) in drinking water and water/sewage treatment plants: A review. *Science of the Total Environment*, 596–597, 303–320. <https://doi.org/10.1016/j.scitotenv.2017.04.102>
- Yin, R., Sun, J., Xiang, Y., & Shang, C. (2018). Recycling and Reuse of Rusted Iron Particles Containing Core-shell Fe-FeOOH for Ibuprofen Removal: Adsorption and Persulfate-Based Advanced Oxidation. *Journal of Cleaner Production*. <https://doi.org/10.1016/j.jclepro.2018.01.005>
- Yin, Yiran, Wu, H., Jiang, Z., Jiang, J., & Lu, Z. (2022). Degradation of Triclosan in the Water Environment by Microorganisms: A Review. *Microorganisms*, 10(9). <https://doi.org/10.3390/microorganisms10091713>
- Yin, Jingyuan, Guo, X., & Peng, D. (2018). Iron and manganese oxides modified maize straw to remove tylosin from aqueous solutions. *Chemosphere*. <https://doi.org/10.1016/j.chemosphere.2018.04.108>
- Ying, G., Kookana, R. S., & Ru, Y. (2002). Occurrence and fate of hormone steroids in the environment. *Environment International*, 28, 545–551.
- Yokoyama, J. T. C., Cazetta, A. L., Bedin, K. C., Spessato, L., Fonseca, J. M., Carraro, P. S., Ronix, A., Silva, M. C., & Silva, T. L. (2019). Stevia residue as new precursor of CO₂-activated carbon: Optimization of preparation condition and adsorption study of triclosan. *Ecotoxicology and Environmental Safety*, 172(December 2018), 403–410. <https://doi.org/10.1016/j.ecoenv.2019.01.096>
- Yu, F., Steele, P. H., & Ruan, E. R. (2014). Microwave Pyrolysis of Corn Cob and Characteristics of the Pyrolytic Chars. *Energy Sources, Part A: Recovery, Utilization and Environmental Effects*, November 2014, 37–41. <https://doi.org/10.1080/15567030802612440>
- Yu, Fei, Li, Y., Han, S., & Ma, J. (2016). Adsorptive removal of antibiotics from aqueous solution using carbon materials. *Chemosphere*, 153, 365–385. <https://doi.org/10.1016/j.chemosphere.2016.03.083>
- Yu, Fei, Ma, J., & Han, S. (2014). Adsorption of tetracycline from aqueous solutions onto multi-walled carbon nanotubes with different oxygen contents. *Scientific Reports*, 4, 1–8. <https://doi.org/10.1038/srep05326>
- Zaghouane-Boudiaf, H., & Boutahala, M. (2011). Preparation and characterization of organo-montmorillonites. Application in adsorption of the 2,4,5-trichlorophenol from aqueous solution. *Advanced Powder Technology*, 22(6), 735–740.

- <https://doi.org/10.1016/j.appt.2010.10.014>
- Zaheer, M., Sun, X., Liu, J., Song, C., Wang, S., & Javed, A. (2018). Enhancement of ciprofloxacin sorption on chitosan/biochar hydrogel beads. *Science of the Total Environment*, 639, 560–569. <https://doi.org/10.1016/j.scitotenv.2018.05.129>
- Zamora-Ledezma, C., Negrete-Bolagay, D., Figueroa, F., Zamora-Ledezma, E., Ni, M., Alexis, F., & Guerrero, V. H. (2021). Heavy metal water pollution: a fresh look about hazards, novel and conventional remediation methods. *In Press*.
- Zepon Tarpani, R. R., & Azapagic, A. (2018). Life cycle environmental impacts of advanced wastewater treatment techniques for removal of pharmaceuticals and personal care products (PPCPs). *Journal of Environmental Management*, 215, 258–272. <https://doi.org/10.1016/j.jenvman.2018.03.047>
- Zhai, X., Ren, Y., Wang, N., Guan, F., Agievich, M., Duan, J., & Hou, B. (2019). Microbial Corrosion Resistance and Antibacterial Property of Electrodeposited Zn–Ni–Chitosan Coatings. *Molecules*, 1–12.
- Zhang, H., Zeng, X., Xie, J., Li, Z., & Li, H. (2016). Study on the sorption process of triclosan on cationic microfibrillated cellulose and its antibacterial activity. *Carbohydrate Polymers*. <https://doi.org/10.1016/j.carbpol.2015.09.060>
- Zhang, Liang, Carvalho, P. N., Bollmann, U. E., Ei-taliawy, H., & Bester, K. (2019). Enhanced removal of pharmaceuticals in a biofilter: Effects of manipulating co-degradation by carbon feeding. *Chemosphere*. <https://doi.org/10.1016/j.chemosphere.2019.07.034>
- Zhang, Lin, Tong, L., Zhu, P., Huang, P., Tan, Z., Shi, W., Wang, M., Nie, H., & Yan, G. (2018). Adsorption of chlortetracycline onto biochar derived from corn cob and sugarcane bagasse. *Water Science and Technology*, October, 1–12. <https://doi.org/10.2166/wst.2018.407>
- Zhang, Lizhu, Ma, J., & Yu, M. (2008). The microtopography of manganese dioxide formed in situ and its adsorptive properties for organic micropollutants. *Solid State Sciences*, 10, 148–153. <https://doi.org/10.1016/j.solidstatesciences.2007.08.013>
- Zhang, P., Dong, S., Ma, H., Zhang, B., Wang, Y., & Hu, X. (2015). Fractionation of corn stover into cellulose, hemicellulose and lignin using a series of ionic liquids. *Industrial Crops & Products*, 76, 688–696. <https://doi.org/10.1016/j.indcrop.2015.07.037>
- Zhang, S., Courtois, S., Gitungo, S., Raczko, R. F., Dyksen, J. E., Li, M., & Axe, L. (2018). Microbial community analysis in biologically active filters exhibiting efficient removal of emerging contaminants and impact of operational conditions. *Science of the Total Environment*, 640–641, 1455–1464. <https://doi.org/10.1016/j.scitotenv.2018.06.027>
- Zhang, Yanyang, Wu, B., Xu, H., Liu, H., Wang, M., He, Y., & Pan, B. (2016). Nanomaterials-enabled water and wastewater treatment. *NanoImpact*, 3–4, 22–39. <https://doi.org/10.1016/j.impact.2016.09.004>
- Zhang, Yongjun, Zhu, H., Szwedzyk, U., Lübbecke, S., & Geissen, S. U. (2017). Removal of emerging organic contaminants with a pilot-scale biofilter packed with natural manganese oxides. *Chemical Engineering Journal*. <https://doi.org/10.1016/j.cej.2017.02.095>
- Zhao, F., Li, X., & Graham, N. (2012). Treatment of a model HA compound (resorcinol) by potassium manganate. *Separation and Purification Technology*, 91, 52–58. <https://doi.org/10.1016/j.seppur.2011.10.018>
- Zhao, L., Deng, J., Sun, P., Liu, J., Ji, Y., Nakada, N., Qiao, Z., Tanaka, T., & Yang, Y. (2018). Nanomaterials for treating emerging contaminants in water by adsorption and photocatalysis: Systematic review and bibliometric analysis. *Science of the Total Environment*, 627, 1253–1263. <https://doi.org/10.1016/j.scitotenv.2018.02.006>
- Zhao, Y., Liu, F., & Qin, X. (2017). Adsorption of diclofenac onto zeolite: Adsorption kinetics and effects of pH. *Chemosphere*. <https://doi.org/10.1016/j.chemosphere.2017.04.007>
- Zheng, C., Feng, S., Liu, P., Fries, E., Wang, Q., Shen, Z., Liu, H., & Zhang, T. (2016). Sorption of Organophosphate Flame Retardants on Pahokee Peat Soil. *CLEAN-Soil, Air, Water*, 44(9999), 1–11. <https://doi.org/10.1002/clel.201500807>
- Zheng, X., Wang, J., Xue, X., Liu, W., Kong, Y., Cheng, S., & Yuan, D. (2018). Facile synthesis of Fe₃O₄@MOF-100(Fe) magnetic microspheres for the adsorption of diclofenac sodium in aqueous solution. *Environmental Science and Pollution Research*, 25(31), 31705–31717. <https://doi.org/10.1007/s11356-018-3134-4>
- Zhou, A., Chen, W., Liao, L., Xie, P., Zhang, T., Liu, X., & Feng, X. (2019). Comparative adsorption of emerging contaminants in water by functional designed magnetic poly (N-isopropylacrylamide) / chitosan hydrogels. *Science of the Total Environment*, 671, 377–387. <https://doi.org/10.1016/j.scitotenv.2019.03.183>
- Zhou, L.-C., Meng, X., Fu, J., & Yang, Y. (2014). Highly efficient adsorption of chlorophenols onto chemically modified chitosan. *Applied Surface Science*, 292, 765–741. <https://doi.org/10.1016/j.apsusc.2013.12.041>
- Zhou, S., Shao, Y., Gao, N., Deng, J., Li, C., Reuse, R., & Reuse, R. (2013). Equilibrium, Kinetic, and Thermodynamic Studies on the Adsorption of Triclosan onto Multi-Walled Carbon Nanotubes. *CLEAN-Soil, Air, Water*, 41(6), 539–547. <https://doi.org/10.1002/clel.201200082>
- Zhou, Yanbo, Chen, L., Lu, J., Tang, X., & Lu, J. (2011). Removal of bisphenol A from aqueous solution using modified fibric peat as a novel biosorbent. *Separation and Purification Technology*, 81(2), 184–190. <https://doi.org/10.1016/j.seppur.2011.07.026>
- Zhou, Yanbo, Lu, J., & Lu, J. (2012). Application of natural biosorbent and modified peat for bisphenol a removal from aqueous solutions. *Carbohydrate Polymers*, 88(2), 502–508. <https://doi.org/10.1016/j.carbpol.2011.12.034>
- Zhou, Yong, Zhang, L., & Cheng, Z. (2015). Removal of organic pollutants from aqueous solution using agricultural wastes: A review. *Journal of Molecular Liquids*, 212, 739–762. <https://doi.org/10.1016/j.molliq.2015.10.023>
- Zhou, Yuzhou, Wang, T., Zhi, D., Guo, B., & Zhou, Y. (2019). Applications of nanoscale zero-valent iron and its composites to the removal of antibiotics: a review. *Journal of Materials Science*. <https://doi.org/10.1007/s10853-019-03606-5>
- Zhu, C. S., Wang, L. P., & Chen, W. bin. (2009). Removal of Cu(II) from aqueous solution by agricultural by-product: Peanut hull. *Journal of Hazardous Materials*, 168(2–3), 739–746. <https://doi.org/10.1016/j.jhazmat.2009.02.085>
- Żółtowska-Aksamitowska, S., Bartczak, P., Zembrzuska, J., & Jesionowski, T. (2018). Removal of hazardous non-steroidal anti-inflammatory drugs from aqueous solutions by biosorbent based on chitin and lignin. *Science of the Total Environment*, 612, 1223–1233. <https://doi.org/10.1016/j.scitotenv.2017.09.037>

Versión Aprobada para Defensa Oral